UNCLASSIFIED

AD NUMBER
AD890037
NEW LIMITATION CHANGE
TO Approved for public release, distribution unlimited
FROM Distribution authorized to U.S. Gov't. agencies only; Test and Evaluation; Aug 1971. Other requests shall be referred to Air Force Flight Dynamic Lab., Wright-Patterson AFB, OH 45433.
AUTHORITY
AFFDL ltr, 10 May 1976

THIS PAGE IS UNCLASSIFIED

AFFDL-TR-71-126

AD 890037

ADVANCED COMPOSITE JOINTS; DESIGN AND ACOUSTIC FATIGUE CHARACTERISTICS

W. J. JACOBSON

Northrop Corporation

Hawthorne, California

AD No.
DDC FILE COPY

TECHNICAL REPORT AFFDL-TR-71-126

D D C
DEC 27 1971

Air Force Flight Dynamics Laboratory
Air Force Systems Command
Wright-Patterson Air Force Base, Ohio

Distribution limited to U.S. Government agencies only; test and evaluation; statement applied August 1971. Other requests for this document must be referred to AF Flight Dynamic Laboratory, (FY) Wright-Patterson AFB, Ohio 45433.

B

NOTICE

When Government drawings, specifications, or other data are used for any purpose other than in connection with a definitely related Government procurement operation, the United States Government thereby incurs no responsibility nor any obligation whatsoever; and the fact that the Government may have formulated, furnished, or in any way supplied the said drawings, specifications, or other data, is not to be regarded by implication or otherwise as in any manner licensing the holder or any other person or corporation, or conveying any rights or permission to manufacture, use, or sell any patented invention that may in any way be related thereto.

Copies of this report should ~~not be~~ returned unless return is required by security considerations, contractual obligations, or notice on a specific document.

ADVANCED COMPOSITE JOINTS; DESIGN AND ACOUSTIC FATIGUE CHARACTERISTICS

W. J. JACOBSON

Northrop Corporation

Hawthorne, California

Air Force Flight Dynamics Laboratory
Air Force Systems Command
Wright-Patterson Air Force Base, Ohio

Distribution limited to U.S. Government agencies only; test and evaluation; statement applied August 1971. Other requests for this document must be referred to AF Flight Dynamic Laboratory, (FY) Wright-Patterson AFB, Ohio 45433.

FOREWORD

The research work reported herein was conducted by the Northrop Corporation, Aircraft Division, Hawthorne, California, for the Aero-Acoustics Branch, Vehicle Dynamics Division, Air Force Flight Dynamics Laboratory, Wright-Patterson Air Force Base, Ohio, under Contract F33615-70-C-1463. This research is a part of a continuing effort to establish tolerance levels and design criteria for acoustic fatigue prevention under the exploratory development program of the Air Force Systems Command. The effort was conducted under Project 1471 "Aero-Acoustic Problems in Air Force Flight Vehicles" Task 147101 "Sonic Fatigue of Structures in Air Force Flight Vehicles." Mr. E.A. Tolle was the Project Engineer. This study was performed during the period April 1970 to July 1971.

The manuscript was released by the author in July 1971 for publication, and assigned the Northrop number NOR 71-114.

The work was performed at Northrop with Dr. M.J. Jacobson serving as the Principal Investigator under the technical guidance of Dr. C. Hwang — both in the Structures Research and Technology Department — and under the supervision of Mr. C. Rosenkranz, Manager of the Structures Research and Technology Department, wherein the analysis and design were conducted. Major tasks were carried out under the direction of the following Northrop personnel: Mr. D.C. Skilling, who directed the acoustics and vibration test programs; Mr. G. Meuleman, who directed the metal fabrication, tooling fabrication and assembly, welding, riveting, and the manufacture of the advanced-composite I-beams, tee sections, and angle sections; Mr. W.M. Wochos, who directed the manufacture of the acoustic test panels, the layup and bonding of the advanced-composite laminates, and the manufacturing and tests for obtaining the mechanical and physical properties of the advanced-composite materials; Dr. W.S. Pi and Mr. J.R. Yamane, who directed the use of the dynamic stress analysis, finite element computer programs; and Dr. N.M. Bhatia who directed the use of the advanced-composite computer programs.

This technical report has been reviewed and is approved.

ABSTRACT

The results of an interrelated analytic investigation, acoustic test program, and shaker test program to develop information on the design and acoustic fatigue characteristics of joints with advanced-composite materials are presented. Three nine-bay, cross-stiffened, graphite-epoxy panels with a six-ply skin and a central bay with nominal dimensions of 10.0 x 7.0 x 0.03 inch were designed and manufactured. The panels were tested to obtain acoustic response and acoustic fatigue data. The final two of the three tested panels survived 100 hours (the planned runout time) of exposure in a broad-band 166 db SPL acoustic environment; the first panel experienced a premature acoustic fatigue failure that was attributed to a design and manufacturing deficiency that was corrected for the other two panels. A shaker test program was conducted to demonstrate that S-N data for acoustic fatigue predictions can be obtained in shaker specimen testing which is inexpensive relative to more costly acoustic panel tests. S-N data that were obtained in the shaker test program led to a prediction, which was subsequently confirmed by tests, that the joint assemblies of the flat, acoustic test panels would not experience an acoustic fatigue failure. In the shaker test program, six S-N curves were developed and included data obtained with two joint configurations, either bonded or riveted, and three material combinations with six-ply skins, namely, graphite-epoxy skin to a graphite-epoxy stiffener, boron-epoxy skin to a titanium alloy stiffener, and graphite-epoxy skin to a titanium alloy stiffener. The lamina stacking sequence was the same for all the shaker specimens. A simplified theory for hand calculation predictions of dynamic stresses in an unstiffened orthotropic plate subjected to a spatially uniform, white noise environment was developed and successfully applied in the dynamic analysis of the cross-stiffened, graphite-epoxy test panels. Other principal items in the analytic investigation included the use of a finite-element computer program for the prediction of the cross-stiffened panel response to acoustic excitation and another finite-element computer program for the static stress analysis of bonded-joint assemblies to determine the acoustic fatigue critical component of the joint assemblies. The effect of the experimental multimodal response of the acoustic test panels was considered in predicting the absence of an acoustic fatigue failure in the two acoustic test panels that survived the 100 hours of acoustic exposure.

PRECEDING PAGE BLANK-NOT FILMED.

CONTENTS

SECTION		PAGE
I	INTRODUCTION	1
II	GENERAL CONSIDERATIONS	3
	II.1 Analytical Methods	3
	II.2 S-N Curves for a Joint Assembly	3
	II.3 Characteristic of Dynamic Modes of Panels with Stiffeners	4
	II.4 Shaker Versus Acoustic Excitation	6
	II.5 Narrow-band Versus Broad-band Excitation	6
	II.6 Configurations and Materials	7
III	DESIGN AND MANUFACTURE OF ACOUSTIC PANELS AND SHAKER SPECIMENS	9
	III.1 Acoustic Panels	9
	III.1.(a) Manufacture of Panel A-GG-B-1	15
	III.1.(b) Plan for Manufacturing Panel A-GG-B-2	26
	III.1.(c) Manufacture of Panels A-GG-B-2 and A-GG-B-3	28
	III.2 Shaker Specimens	34
	III.2.(a) Initial Design	34
	III.2.(b) Final Specimen Design	47
	III.2.(c) Manufacture of Shaker Specimens	47
IV	APPROACH TO THE ACOUSTIC PROGRAM	53
	IV.1 Objective	53
	IV.2 Test Conditions	53
	IV.3 General Test Procedure	56
	IV.3.(a) Modal Surveys	56
	IV.3.(b) Damping Factors	56
	IV.3.(c) Response and Acoustic Fatigue Tests	56
	IV.3.(d) Failure Detection	56
	IV.3.(e) Noise Reduction	57
	IV.4 Test Instrumentation	57
	IV.4.(a) Location and Quantity of Strain Gages, Accelerometers, and Thermocouples	57
	IV.4.(b) Location of Microphones in the Acoustic Test Section	57

CONTENTS (Continued)

SECTION			PAGE
	IV.5	Test Facilities and Equipment	60
		IV.5.(a) Progressive Wave Test Chamber	60
		IV.5.(b) Test Equipment	60
	IV.6	Data Reduction and Analysis	60
V	DETAIL DESCRIPTION OF ACOUSTIC TESTS		63
	V.1	Test of Acoustic Panel A-GG-B-1	63
		V.1.(a) Modal Surveys	63
		V.1.(b) Damping Factors	68
		V.1.(c) Response to Acoustic Excitation	69
		V.1.(d) Acoustic Fatigue Test	71
		V.1.(e) Data Analysis	79
		V.1.(f) Discussion of Test Results	79
	V.2	Test of Acoustic Panel A-GG-B-2	86
		V.2.(a) Instrumentation and Assembly of the Panel to the Test Fixture	86
		V.2.(b) Modal Surveys	86
		V.2.(c) Damping Factors	92
		V.2.(d) Response to Acoustic Excitation	92
		V.2.(e) Noise Reduction	94
		V.2.(f) Acoustic Fatigue Test	95
		V.2.(g) Data Analysis	99
	V.3	Test of Acoustic Panel A-GG-B-3	113
		V.3.(a) Initial Modal Survey	113
		V.3.(b) Instrumentation, Damping Factors, and Repetition of Modal Survey	113
		V.3.(c) Response to Acoustic Excitation	117
		V.3.(d) Acoustic Fatigue Test	117
		V.3.(e) Data Analysis	119
	V.4	Acoustic Fatigue Life	133
	V.5	Acoustic Fatigue Prediction for Panel A-GG-B-3	134
	V.6	Conclusions from the Acoustic Test Program	136
VI	SHAKER TEST PROGRAM		137
	VI.1	Objective	137
	VI.2	General Information on Shaker Testing	137
		VI.2.(a) Vibration Input Spectrum	137
		VI.2.(b) Response Measurement Methods	137
		VI.2.(c) Strain Gage System	140
		VI.2.(d) Accelerometer System	141
		VI.2.(e) Displacement Probe	141

CONTENTS (Continued)

SECTION		PAGE
	VI.3 Final Establishment of the Specimen Length and End Conditions	141
	VI.4 Specimen Coding	143
	VI.5 Fatigue Failures	143
	VI.6 Computation of Cycles to Failure	147
	VI.7 Test Procedure in Individual Specimen Testing	148
	VI.8 Multiple Specimen Tests	148
	VI.9 Shaker S-N Data and Static Ultimate Tensile Strains	160
	VI.10 Test Equipment	160
	VI.11 Discussion of Shaker S-N Data	160
VII	THEORY OF ORTHOTROPIC PANEL RESPONSE TO ACOUSTIC EXCITATION	163
	VII.1 General Theory	163
	VII.1.(a) Equations of Motion	164
	VII.1.(b) Eigenvalue Solutions	164
	VII.1.(c) Modal Amplitudes	165
	VII.1.(d) Deflection Spectral Density	165
	VII.1.(e) Stresses Under Arbitrary Excitation	166
	VII.1.(f) Stresses Under White Noise Excitation	167
	VII.1.(g) Method of Applying the General Theory	168
	VII.2 Simplified Theory	168
	VII.3 Definitions of PSD	173
VIII	APPLICATIONS OF STRESS ANALYSIS METHODS	177
	VIII.1 Free Vibrations and Dynamic Stress Analysis of Isotropic Plates and Beams	177
	VIII.1.(a) Unstiffened Square Plate	178
	VIII.1.(b) Unstiffened Beam	182
	VIII.1.(c) Effect of Node Locations on Stress Predictions of Cross-Stiffened Panels	183
	VIII.1.(d) Warning on Use of Simplified Theory (of Section VII.2)	187
	VIII.1.(e) Effect of Flanges of Stiffeners on Dynamic Characteristics of Stiffened Panels	187
	VIII.2 Free Vibrations and Dynamic Stress Analysis of Advanced-Composite Panels	188
	VIII.2.(a) Material Properties	188
	VIII.2.(b) Unstiffened Plates	190
	VIII.2.(c) Cross-Stiffened Panels	192
	VIII.3 Detailed Stress Analysis of Bonded Joints	194
	VIII.3.(a) Analytic Approach	194
	VIII.3.(b) Elastic Constants	199

CONTENTS (Continued)

SECTION		PAGE
	VIII. 4 Supporting Calculations for the Design of Acoustic Panel A-GG-B-2	202
	VIII. 4. (a) Thermal Stress Analysis	202
	VIII. 4. (b) Critical Buckling Stresses	205
IX	SUMMARY AND CONCLUSIONS	207
	REFERENCES	211
APPENDIX A	ADVANCED COMPOSITE MATERIALS	A-1

ILLUSTRATIONS

FIGURE		PAGE
1	Simple, Idealized Mode Shapes	5
2	Modes with Significant Inertial Forces in Stiffeners	5
3	Panel A-GG-B-1	11
4	Panel A-GG-B-2	13
5	Cross-Stiffened Graphite-Epoxy Detail Including Two Each 6-Ply $[\pm 45/0]_S$ Fothergill/Harvey Courtaulds HT-S/4617 I-Beams and Tee Sections	16
6	Schematic of I-Beam Fabrication	17
7	Bonding Tool, MRD 70-64	19
8	6-Ply $[0/\pm 45]_S$, Fothergill/Harvey Courtaulds HT-S/4617 Graphite-Epoxy Skin and 13-Ply Narmco 500/1581 Glass Doubler	20
9	Bonding Tool with Glass Doubler in Place	21
10	Bonding Tool with Graphite-Epoxy Skin in Place on Top of Glass Doubler	22
11	6Al-4V Titanium Z and Angle Frame and Cross-Stiffened Graphite-Epoxy Detail	23
12	Bonding Tool with Titanium Frame in Place on Top of Graphite-Epoxy Skin and Glass Doubler	24
13	Bonding Tool with Cross-Stiffened Graphite-Epoxy Detail in Place Inside of Titanium Frame on Top of Graphite-Epoxy Skin and Glass Doubler	25
14	Graphite-Epoxy Doubler Cross Section to Replace Section H-H of Figure 3	27
15	View of Graphite-Epoxy Skin and Stepped Doubler of Bonded Subassembly	29
16	View of Cross-Stiffeners of Bonded Graphite-Epoxy Subassembly	30
17	Effect of Multi-Cure Cycles on Adhesive Strength	33
18	Panel A-GG-B-3 (Before Acoustic Test) with Peripheral Glass Reinforcement	35
19	Repair of a Web of an I-Beam Detail of Panel A-GG-B-3	36
20	Candidate A-1 Shaker Specimens	38
21	Candidate A-2 Shaker Specimens	39
22	Graphite-Epoxy Shaker Test Specimens (Bonded Specimens)	41
23	Graphite-Epoxy Shaker Test Specimens (Riveted Specimens)	43
24	Boron-Epoxy Shaker Test Specimens	45
25	Bonded Shaker Specimen	48
26	Upper Surface of a Riveted Shaker Specimen	50
27	Lower Surface of a Riveted Shaker Specimen	51
28	Schematic of Acoustic Test Panel and its Location in the Progressive Wave Test Cell	54
29	Progressive Wave Acoustic Test Chamber	55

ILLUSTRATIONS (Continued)

FIGURE		PAGE
30	Instrumentation — Schematic Diagram	58
31	Schematic of Strain Gage Locations for the Acoustic Panels	59
32	Panel A-GG-B-1 and Partial Assembly of Wood Filler Blocks	64
33	Assembly of Panel A-GG-B-1 and Wood Filler Blocks	65
34	Test Fixture in the 4 x 4 Foot Test Cell of the Progressive Wave Acoustic Test Chamber	66
35	Modal Surveys of Panel A-GG-B-1	67
36	Location of Accelerometers During Excitation in the Progressive Wave Chamber	71
37	Adhesive Failure at the Tee Section Separating Bays 4 and 7	73
38	Tee Section Failure Between Bays 2 and 5	74
39	Adhesive Failure at Tee Section Separating Bays 6 and 9	75
40	Separation of Skin at Bay 6 From Glass Doubler	76
41	Failure in Flange of I-Beam Between Bays 6 and 9	77
42	Damage (Enclosed at Several Locations) on Exposed Surface of Bay 5	78
43	Strain Gage No. 2 Response with Oil Canning at 148 db SPL	80
44	Strain Gage No. 2 Response without Oil Canning at 148 db SPL	81
45	Strain Gage No. 2 Response	82
46	Spectral Shape of Pressure During the 139 db SPL Run	83
47	Spectral Shape of Pressure During the 148 db SPL run	84
48	Panel A-GG-B-2 and Wood Blocks Attached to Test Fixture in Vertical Position	87
49	Location of Strain Gages on Panel A-GG-B-2	88
50	Quantitative Modal Surveys (Accelerometer Readings) of Panel A-GG-B-2	89
51	Nodal Lines Under Loudspeaker Excitation of Panel A-GG-B-2	90
52	Noise Reduction Through Panel A-GG-B-2	94
53	Adhesive Failure (Between Arrows) in Bay 4 of Panel A-GG-B-2	96
54	Doublers in Bays 4 and 6 Added to Panel A-GG-B-2	97
55	Frame Failure at the End of the Acoustic Test of Panel A-GG-B-2	100
56	Pressure Spectral Density	101
57	Pressure Spectral Density	102
58	Strain Spectral Density	103
59	Strain Spectral Density	104
60	Strain Spectral Density	105
61	Strain Spectral Density	106
62	Strain Spectral Density	107

ILLUSTRATIONS

FIGURE		PAGE
1	Simple, Idealized Mode Shapes	5
2	Modes with Significant Inertial Forces in Stiffeners	5
3	Panel A-GG-B-1	11
4	Panel A-GG-B-2	13
5	Cross-Stiffened Graphite-Epoxy Detail Including Two Each 6-Ply $[\pm 45/0]_S$ Fothergill/Harvey Courtaulds HT-S/4617 I-Beams and Tee Sections	16
6	Schematic of I-Beam Fabrication	17
7	Bonding Tool, MRD 70-64	19
8	6-Ply $[0/\pm 45]_S$, Fothergill/Harvey Courtaulds HT-S/4617 Graphite-Epoxy Skin and 13-Ply Narmco 500/1581 Glass Doubler	20
9	Bonding Tool with Glass Doubler in Place	21
10	Bonding Tool with Graphite-Epoxy Skin in Place on Top of Glass Doubler	22
11	6Al-4V Titanium Z and Angle Frame and Cross-Stiffened Graphite-Epoxy Detail	23
12	Bonding Tool with Titanium Frame in Place on Top of Graphite-Epoxy Skin and Glass Doubler	24
13	Bonding Tool with Cross-Stiffened Graphite-Epoxy Detail in Place Inside of Titanium Frame on Top of Graphite-Epoxy Skin and Glass Doubler	25
14	Graphite-Epoxy Doubler Cross Section to Replace Section H-H of Figure 3	27
15	View of Graphite-Epoxy Skin and Stepped Doubler of Bonded Subassembly	29
16	View of Cross-Stiffeners of Bonded Graphite-Epoxy Subassembly	30
17	Effect of Multi-Cure Cycles on Adhesive Strength	33
18	Panel A-GG-B-3 (Before Acoustic Test) with Peripheral Glass Reinforcement	35
19	Repair of a Web of an I-Beam Detail of Panel A-GG-B-3	36
20	Candidate A-1 Shaker Specimens	38
21	Candidate A-2 Shaker Specimens	39
22	Graphite-Epoxy Shaker Test Specimens (Bonded Specimens)	41
23	Graphite-Epoxy Shaker Test Specimens (Riveted Specimens)	43
24	Boron-Epoxy Shaker Test Specimens	45
25	Bonded Shaker Specimen	48
26	Upper Surface of a Riveted Shaker Specimen	50
27	Lower Surface of a Riveted Shaker Specimen	51
28	Schematic of Acoustic Test Panel and its Location in the Progressive Wave Test Cell	54
29	Progressive Wave Acoustic Test Chamber	55

ILLUSTRATIONS (Continued)

FIGURE		PAGE
30	Instrumentation — Schematic Diagram	58
31	Schematic of Strain Gage Locations for the Acoustic Panels	59
32	Panel A-GG-B-1 and Partial Assembly of Wood Filler Blocks	64
33	Assembly of Panel A-GG-B-1 and Wood Filler Blocks	65
34	Test Fixture in the 4 x 4 Foot Test Cell of the Progressive Wave Acoustic Test Chamber	66
35	Modal Surveys of Panel A-GG-B-1	67
36	Location of Accelerometers During Excitation in the Progressive Wave Chamber	71
37	Adhesive Failure at the Tee Section Separating Bays 4 and 7	73
38	Tee Section Failure Between Bays 2 and 5	74
39	Adhesive Failure at Tee Section Separating Bays 6 and 9	75
40	Separation of Skin at Bay 6 From Glass Doubler	76
41	Failure in Flange of I-Beam Between Bays 6 and 9	77
42	Damage (Enclosed at Several Locations) on Exposed Surface of Bay 5	78
43	Strain Gage No. 2 Response with Oil Canning at 148 db SPL	80
44	Strain Gage No. 2 Response without Oil Canning at 148 db SPL	81
45	Strain Gage No. 2 Response	82
46	Spectral Shape of Pressure During the 139 db SPL Run	83
47	Spectral Shape of Pressure During the 148 db SPL run	84
48	Panel A-GG-B-2 and Wood Blocks Attached to Test Fixture in Vertical Position	87
49	Location of Strain Gages on Panel A-GG-B-2	88
50	Quantitative Modal Surveys (Accelerometer Readings) of Panel A-GG-B-2	89
51	Nodal Lines Under Loudspeaker Excitation of Panel A-GG-B-2	90
52	Noise Reduction Through Panel A-GG-B-2	94
53	Adhesive Failure (Between Arrows) in Bay 4 of Panel A-GG-B-2	96
54	Doublers in Bays 4 and 6 Added to Panel A-GG-B-2	97
55	Frame Failure at the End of the Acoustic Test of Panel A-GG-B-2	100
56	Pressure Spectral Density	101
57	Pressure Spectral Density	102
58	Strain Spectral Density	103
59	Strain Spectral Density	104
60	Strain Spectral Density	105
61	Strain Spectral Density	106
62	Strain Spectral Density	107

ILLUSTRATIONS (Continued)

FIGURE		PAGE
63	Strain Spectral Density	108
64	Strain Spectral Density	109
65	Strain Spectral Density	110
66	Strain Spectral Density	111
67	Strain Spectral Density	112
68	Nodal Lines Under Loudspeaker Excitation of Panel A-GG-B-3	114
69	Model Survey of Panel A-GG-B-3 with Nodal Lines Estimated with Accelerometer Signals	116
70	Tee Section Damage During Acoustic Fatigue Test of Panel A-GG-B-3	120
71	Pressure Spectral Density	121
72	Pressure Spectral Density	122
73	Strain Spectral Density	123
74	Strain Spectral Density	124
75	Strain Spectral Density	125
76	Strain Spectral Density	126
77	Strain Spectral Density	127
78	Strain Spectral Density	128
79	Strain Spectral Density	129
80	Strain Spectral Density	130
81	Strain Spectral Density	131
82	Strain Spectral Density	132
83	Single Specimen Mounted for Shaker Fatigue Test	138
84	Three Specimens Mounted for Shaker Fatigue Tests	139
85	Strain Gage Locations on Shaker Specimens	140
86	Multiple Flash Exposure During a Shaker Specimen Fatigue Test	142
87	Skin Fatigue Failure (Between Arrows) of a Shaker Specimen with a Bonded Joint	144
88	Skin Fatigue Failure Across the Width of a Shaker Specimen with a Bonded Joint	145
89	Photomicrograph of Fatigue Failure of Vibration Specimen V-GT-R-2	146
90	Photomicrograph of Fatigue Failure of Vibration Specimen V-BT-R-2	146
91	Sine Sweep to Determine Natural Frequencies	149
92	Strain Response of Specimen V-GG-B-5 (5 g Run)	150
93	Strain Response of Specimen V-GG-B-5 (10 g Run)	151
94	Strain Response of Specimen V-GG-B-5 (20 g Run)	152
95	Base Acceleration of Specimen V-GG-B-5 (5 g Run)	153
96	Base Acceleration of Specimen V-GG-B-5 (10 g Run)	154
97	Base Acceleration of Specimen V-GG-B-5 (20 g Run)	155
98	Summary of Shaker S-N Data and Preliminary S-N Curves	162
99	Geometry and Coordinate System of Rectangular Plate	169
100	Finite Element Models	179
101	Mathematical Models	184

ILLUSTRATIONS (Continued)

FIGURE		PAGE
102	Finite Element Model M-3 Representing Lower Left Quadrant of Acoustic Test Panels A-GG-B-2 and A-GG-B-3	193
103	Cross Section Used for Stress Analysis	195
104	Finite Elements in Bonded Joint Analysis	196
105	Stresses in the Bonding Material and Individual Panel Plies for Case 1	197
106	Stresses in the Bonding Material and Individual Panel Plies for Case 2	198
107	Coordinate System for the Bonded Joint Analysis	200
108	Alternate Coordinate System for Bonded Joint Analysis	200
109	Schematic Drawing of Nine-Bay, Cross-Stiffened Panel A-GG-B-1	203
A-1	Longitudinal Tensile Stress-Strain Data	A-5
A-2	Transverse Tensile Stress-Strain Data	A-6
A-3	Longitudinal Compressive Stress-Strain Data	A-7
A-4	Transverse Compressive Stress-Strain Data	A-8
A-5	Rail Shear Stress-Strain Data	A-9
A-6	Longitudinal Tensile Stress-Strain Data	A-10
A-7	Longitudinal Tensile Stress-Strain Data	A-11
A-8	Transverse Tensile Stress-Strain Data	A-12
A-9	Longitudinal Tensile Stress-Strain Data	A-13
A-10	Transverse Tensile Stress-Strain Data	A-14

TABLES

NUMBER		PAGE
I	Types of Shaker Tests	34
II	Acceleration Peak Responses of Panel A-GG-B-1 Obtained Under Discrete Frequency Excitation	68
III	Damping Factors of Panel A-GG-B-1	69
IV	Strain Gage Response (Micro-inch/Inch-Rms) and Accelerometer Response (G's — rms) of Panel A-GG-B-1	70
V	Estimate of Rms Strains of Panel A-GG-B-1 at 165 db SPL	85
VI	Damping Factors of Panel A-GG-B-2	92
VII	Strain Gage Response (Micro-inch/Inch-Rms) of Panel A-GG-B-2	93
VIII	Strain Readings of Panel A-GG-B-2 at 166 db SPL	98
IX	Damping Factors of Panel A-GG-B-3	113
X	Strain Gage Response (Micro-inch/Inch-Rms) of Panel A-GG-B-3	118
XI	Cycles of Response of Panel A-GG-B-3 During 100 Hours of Acoustic Exposure	135
XII	Calculated Rms Strains of Panel A-GG-B-3	136
XIII	Sample Computation of Cycles to Failure	147
XIV	Summary of Shaker S-N Data	157
XV	Beam Functions and Second Derivatives at the Centers of the Edges	174
XVI	Fundamental Frequencies	179
XVII	Theoretical Mode Shapes	180
XVIII	Deflection and Stresses at the Center of the Plate	181
XIX	Theoretical Mode Shape	182
XX	Natural Frequency and Stress at the Center of Beam, Simply Supported at Both Ends	182
XXI	Model to Investigate the Effect of Node Locations	185
XXII	Natural Frequencies	186
XXIII	Theoretical Frequency and Response Data	186
XXIV	Comparison of Experimental Results of Cross-Stiffened Panels with Results Using the Simplified Theory	191
XXV	Comparison of Natural Frequencies and Strains of Cross-Stiffened, Graphite-Epoxy Panels Using Finite Element and Experimental Data	192
XXVI	Elastic Constants for Bonded Joint Analysis	199
XXVII	Data for Thermal Analysis	204
A-1	Location of Test Summaries	A-2
A-2	Six-Ply Specimen Uniaxial Test Results	A-3

PRECEDING PAGE BLANK-NOT FILMED.

SYMBOLS AND NORMAL UNITS

SYMBOLS		UNITS
$[A]$	Matrix of finite elements areas	$inch^2$
$[A]$	Matrix relating forces per unit length to strains	lb/inch
a	Edge (of rectangular plate) parallel to x-axis	inch
$[B]$	Matrix relating forces per unit length to curvatures	lb
$[B]$	Matrix relating stresses to deflections	$lb/inch^3$
b	Edge (of rectangular plate) parallel to y-axis	inch
$[C]$	Matrix of viscous damping factors	lb sec/inch
c.c.	(As subscript) complex conjugate	
$[D]$	Matrix relating moments per unit length to curvatures	lb inch
E	Young's modulus of isotropic material	psi
E_1	Young's modulus in the direction of the fibers of a unidirectional advanced-composite laminate	psi
E_2	Young's modulus (inplane) in the direction transverse to the fibers in a unidirectional laminate	psi
E_x, E_y	Young's modulus parallel to x and y axes, respectively, of an orthotropic laminate	psi
e, e_x, e_y	Extensional strain	inch/inch
$e_{\alpha n}, e_{1n}, e_{2n}$	Shear strains	inch/inch
e_1	Strain in y-direction at the center of a rectangular plate edge that is parallel to the x-axis	inch/inch

SYMBOLS AND NORMAL UNITS (Continued)

SYMBOLS		UNITS
e_2	Strain in x-direction at the center of a rectangular plate edge that is parallel to the y-axis	inch/inch
F	Temperature	degree F
$\{f(t)\}$	Matrix of nodal forces	lb
f	Frequency	Hz
G	Shear modulus of isotropic plate; inplane shear modulus of orthotropic plate	psi
G_{1n}, G_{2n}	Shear moduli including the direction normal to the plate	psi
g	Gravitational constant (386 inch/sec^2)	inch/sec^2
$H(\Omega_o)$	Nondimensional frequency response function	
H	Torsional rigidity ($H = D_{xy} + 2D_{zz}$)	lb inch
h	Plate thickness	inch
i	$\sqrt{-1}$	
$[K]$	Matrix with stiffness coefficients	lb/inch
K	Generalized stiffness in the fundamental mode	lb/inch
K_o	Constant in thermal analysis	inch/inch/F
L	Length of beam	inch
$[M]$	Matrix of (finite element) moments per unit length	lb inch/inch
$[M]$	Matrix of (finite element) forces per unit length	lb sec^2/inch
M	Generalized mass in the fundamental mode (when using the beam function approach)	lb sec^2/inch
$[M_i]$	Matrix of generalized masses in the i modes	lb sec^2 inch
M_i	Generalized mass in the ith mode	lb sec^2 inch
M_o	Mass per unit area of plate	lb sec^2/inch^3
$[N]$	Matrix of (finite element) forces per unit length	lb/inch

SYMBOLS AND NORMAL UNITS (Continued)

SYMBOLS		UNITS
N	Life	cycles
n	Coordinate normal to the plane of the plate	inch
$p(t)$	Pressure	psi
p_o	Amplitude of pressure	psi
$[Q]$	Matrix of eigenvectors	inch
$\{q^i\}$	Matrix of the ith eigenvector	inch
$R_{f_i f_j}$	Cross correlation function	lb^2
S	Strain	inch/inch
$\{S_d(w)\}$	Matrix of Fourier transforms of $\{d(t)\}$	inch sec
$\{S_f(w)\}$	Matrix of Fourier transforms of $\{f(t)\}$	lb sec
$\{S_\xi(w)\}$	Matrix of modal amplitudes in the frequency domain	rad/sec
S_p	Spectral density of pressure	psi^2 sec
S_w	Spectral density of deflection	$inch^2$ sec
s	Stress	psi
ΔT	Incremental temperature	degree F
T	Period	sec
t	Time	sec
w	Lateral deflection	inch
x, y, z	Orthogonal rectilinear coordinates	inch
$[Z]$	Matrix of modal impedances	rad/sec^2
α	Nondimensional beam function parameter	
α_i	Thermal coefficient of expansion of ith member	inch/inch/F
β	Beam function parameter	$inch^{-1}$
γ	Beam function parameter	$inch^{-1}$

SYMBOLS AND NORMAL UNITS (Continued)

SYMBOLS		UNITS
Γ	Participation factor	$inch^2$
γ_{xy}	Shear strain	inch/inch
γ_o	Density	lb/in^3
$[\gamma]$	Matrix of nondimensional viscous damping factors	
δ_i	Total expansion of ith member	inch
δ_i^T	Free thermal expansion of ith member	inch
$\{\epsilon\}$	Matrix of strains	inch/inch
ζ	Nondimensional viscous damping factor	
η	Generalized deflection coordinate	inch
θ	Nondimensional beam function parameter	
θ	Angular measure	degree
$\{\kappa\}$	Matrix of curvatures	$inch^{-1}$
ν	Poisson's ratio	
ν_1	Poisson's ratio (ratio of the induced strain in the 2-direction due to an applied strain in the 1-direction)	
ρ	Mass per unit volume	$lb\ sec^2/inch^4$
σ_1, σ_2	Ultimate strengths	psi
σ_{max}	Maximum stress	psi
σ_{yield}	Extensional yield stress	psi
τ	Time	sec
τ	Shear stress	psi
τ_{yield}	Shear yield stress	psi
ϕ	Clamped - clamped beam function	
$\phi_\sigma(\omega)$	Power spectral density of stress	$psi^2\ sec$

SYMBOLS AND NORMAL UNITS (Continued)

SYMBOLS		UNITS
$[\phi_d(\omega)]$	Matrix of cross-power spectral density of deflection	$inch^2$ sec
$[\phi_f(\omega)]$	Matrix of cross-power spectral density of forces	lb^2 sec
$[\phi_p(\omega)]$	Matrix of cross-power spectral density of pressure	psi^2 sec
$\phi_{d_i d_j}$	Cross-power spectral density of deflection	$inch^2$ sec
$\phi_{f_i f_j}$	Cross-power spectral density of forces	lb^2 sec
ψ	Clamped-clamped beam function	
Ω	Circular frequency	rad/sec
Ω_o	Discrete (driving) circular frequency	rad/sec
ω	Circular frequency	rad/sec
$\bar{\omega}_i$	Natural circular frequency	rad/sec
*	(As superscript) Fourier transform	
-	(Above a symbol to denote rms; for example, $\bar{s}$ means rms stress)	

I. INTRODUCTION

High modulus type fiber materials are under development for use on aircraft components such as skin panels, substructural parts, fairings, etc. Many of these components are exposed to high intensity noise fields generated by the aircraft propulsion system and are subject to acoustic fatigue. In order to develop acoustic fatigue design information on filament-type materials and structural configurations such as panels and joints, it is necessary to investigate typical configurations for various fiber reinforced materials and designs. For example, in the analytic and experimental program that was conducted under Contract F33615-67-C-1672 (Reference 1), it was demonstrated that honeycomb panels with cross-plied boron-epoxy facings (two plies per facing) resisted acoustic loading longer than equivalent-weight and -thickness honeycomb panels with aluminum alloy facings. However, there has been a scarcity of comprehensive investigations on the acoustic fatigue of structural elements with fiber reinforced components.

The objective of this program was to develop design information for filament type structural configurations employing advanced-composite materials that are projected for use in high noise level areas of the vehicle; and this effort concentrated on an analytical and experimental investigation of the dynamic and fatigue characteristics of joint assemblies (which are defined below) utilizing high strength fiber materials. Besides developing fatigue curves (S-N curves) for joint assemblies of two different configurations with varying composites of fiber materials, the program also included the acoustic fatigue life investigation of three larger cross-stiffened structural sections of projected aircraft structures characterized by minimum practical thickness composite materials as skin and utilizing joints. During the process, important parameters governing the acoustic designs have been established and documented.

The program followed a combined analytical and experimental approach to achieve broad applicability. The analysis was conducted to identify and determine numerically the design parameters. The test program covered experiments using both mechanical (shaker) and acoustic pressure field excitation. The test data were organized and evaluated to validate the analytical predictions. In order that the experiments would generate meaningful information for realistic aircraft application, careful attention was given to the design of the specimens, the fabrication methods, and the test procedures.

A joint assembly was defined for this program as encompassing the joint and the adjacent internal structure and skin. As distinct from internal structure, which by definition for this program comprises ribs, spars, stringers, etc., a joint has been defined for this program as a connection or intersection between two structural members — such as between the skin and a stringer, and between the skin and a rib or a spar — as considered for use in lightweight aircraft structure utilizing high-strength fiber materials. For skin-rib-stringer type structure with advanced-composite components, it is quite possible that in many instances the critical acoustic design item is at or close to the joint. Since an advanced-composite skin can be considered a layered assembly with interlaminar strength provided by the resin system, and since

it may be bonded or riveted to advanced-composite or metallic internal structure (with appropriate local reinforcements), the failure modes that are not expected when homogenous metal structures are used may be experienced at or near the joints.

Past acoustic fatigue investigations (for example, References 2, 3, 4) principally have been concerned with the design of skins of conventional (metallic) aircraft structure. A by-product of the analytic work conducted in this program is a method of analysis that is applicable in the design of conventional (metallic) panels.

This document summarizes the interrelated analytic investigation, acoustic test program, and shaker test program that were conducted to achieve the overall program objective with all of the contracted work conducted at the Northrop Corporation, Aircraft Division. In Section II is a discussion of several major items that were considered during the formulation of the program. A review of the design and manufacturing of the acoustic panels and shaker specimens for the test program is in Section III. The approach in conducting the acoustic test program is covered in Section IV. A detailed review of the acoustic tests of three large cross-stiffened panels and a discussion of acoustic fatigue life prediction are in Section V. The review of the shaker test program is in Section VI. In Section VII is the development of a simplified and a general stress analysis method, both of which were used in predicting the stress and/or strain response of the acoustic panels. In Section VIII are applications of theoretical stress analyses of joint assemblies. The summary and conclusions drawn at the end of the program are in Section IX. A detailed description of the advanced-composite materials used in the test program are in Appendix A.

II. GENERAL CONSIDERATIONS

Important items that were considered during the formulation and conduct of various phases of the program are discussed in this section.

II.1 ANALYTICAL METHODS

Considerable emphasis is placed on analytical methods in the establishment of the design of stiffened panels for service in acoustic environments. Emphasis is placed on analysis because it is impractical (especially in the case of the costly advanced-composite materials) to conduct a sufficient number of tests to generate enough empirical data for establishing acoustic design procedures for joints encompassing all of the many parameter variations that may exist in actual practice. Furthermore, in order to extract the maximum amount of information from a limited number of test specimens, a carefully conducted analytical effort is needed to guide and validate the soundness of the test approach throughout the program.

The use of advanced-composite materials at structural joints necessitates the application of more advanced analysis methods than in cases where metallic skin and internal structures are used. This necessity is due to the corresponding analytical complexities associated with material properties and variations in fiber orientation through the laminate thickness. Therefore, several available finite element computer programs that had been previously developed for the analysis of orthotropic structures were used extensively in the analytic investigations conducted to obtain theoretical data in this effort.

II.2 S-N CURVES FOR A JOINT ASSEMBLY

In Section I, joint, internal structure, and joint assembly were carefully defined. An acoustic failure of a joint assembly may occur in the skin, or in the internal structure, or in the joint (for example, in the adhesive of a bonded joint).

For an S-N curve of a joint assembly to have meaning, it is necessary to define S. In simple coupon fatigue tests of homogeneous materials, S is usually defined as the applied stress. However, for the joint assemblies of panels and beams such as were tested in this program under acoustic or shaker excitation, S is more difficult to define. For example, if failures occur in the skin, S should be related in some manner to the stress or strain in the skin; if failures occur in the adhesive, S should be related in some manner to the stress or strain in the adhesive. The generalization of this concept is that S should be related to the stress or strain in the fatigued component of the joint assembly.

The experimental fatigue failures in the shaker test program were instrumental in defining S as the strain in the outer fiber of the skin (where fatigue failures occurred) of the joint assembly.

The location of the initial failure in a joint assembly of an acoustically loaded panel can be estimated by first predicting (possibly with a finite element computer program) the stress or strain response at all reference points and comparing those stresses or strains with the known or assumed stress or strain states that produce failure at each point in order to predict the location of the weakest point in the joint assembly. For a point with a biaxial or triaxial stress state, the exact state of stress or strain that will produce failure has to be estimated until one has sufficient confidence in the material properties of the panel and in biaxial and triaxial strength theories. Finally, if satisfactory S-N data were available for the material at the location of failure, life could then be predicted. This two step method of first predicting strain and then predicting life was used in this program.

For the test program, strains were predicted at various locations of specimens under acoustic excitation. To obtain confidence in the validity of the theoretical predictions (especially when advanced-composite materials are considered), a portion of the acoustic test program was directed toward obtaining experimental strains to confirm the theoretical strains. In general, there is a problem in establishing the location of strain gages, since gage data are unreliable when the gages are in areas of rapidly varying stress, such as in areas of stress concentration where failures often occur. In view of the above considerations, some strain gages were at locations such as in the middle of bays and in stiff regions where it was expected that stress concentrations would be insignificant.

Furthermore, since the use of composite materials for the skin and/or stiffener may also lead to substantial stress concentrations that are of more importance than when the skin and stiffener are metallic, stress concentrations in the joint assembly were investigated. The stress concentration is a function principally of the ply layup, the transverse shear modulus and strength, and the extensional modulus and strength. For example, in uniaxial tensile coupons for which tests have been conducted with composite specimens featuring holes and reinforcing doublers, failures have occurred in the basic specimen because of the high stress concentration in transferring load from the specimen to the doubler.

II.3 CHARACTERISTICS OF DYNAMIC MODES OF PANELS WITH STIFFENERS

In the development of acoustic fatigue design information for the joints, a preliminary review of typical joint configurations of representative panels subjected to acoustic pressure was conducted. In addition, vibratory characteristics (in particular, the mode shapes and stresses) of beams and panels with the joints were considered. Some of the mode shapes that may occur are shown in Figure 1, where symmetry refers to the mode shape within a bay, and phase refers to the phase relationship of adjacent bays.

The symmetric, in-phase mode of a flat panel (Figure 1a) is apt to be excited when the stiffeners (stringers, ribs, or formers) have a high flexural rigidity and torsional rigidity; therefore, they do not bend or twist appreciably during excitation. The symmetric, out-of-phase mode (Figure 1b) is apt to be excited if the stiffeners have a high bending rigidity but low torsional rigidity. The intermediate mode (Figure 1c) is apt to be excited when the stiffeners have a low bending and torsional rigidities. These modes have also been reported elsewhere (e.g., Reference 5).

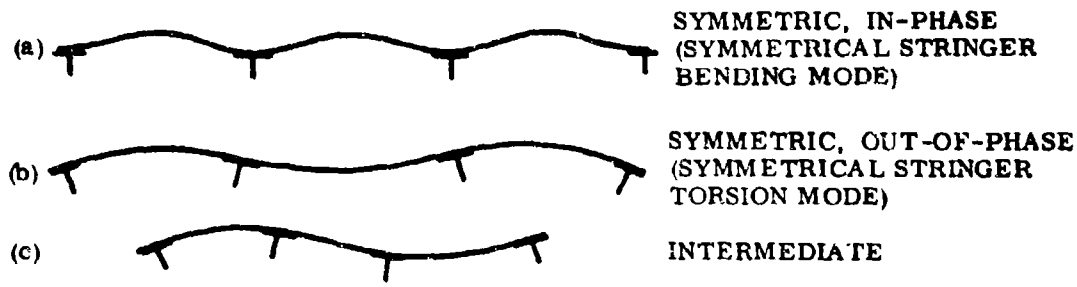

FIGURE 1. SIMPLE, IDEALIZED MODE SHAPES

When the stiffener bends or twists appreciably, the stiffener motion may introduce significant inertia forces in the joint. These inertia forces may play an important role in acoustic fatigue although they did not appear to be of primary importance in the test program. For example, when a stiffener rotates, the inertia forces may produce considerable bending stresses at the root of the stiffener web (Figure 2a). When the stiffener vibrates perpendicular to the plane of the skin, the inertia forces may exert a sizable bending in the skin at the joint extremities and consequently high shearing stresses may exist in the adhesive at the ends of the joint (Figure 2b). Additionally, the limited interlaminar strength of composites may induce local failures (for example, delaminations) that are not found in metal structure. It appears that finite element computer program analyses with programs such as SAAS-II can be conducted to predict when the inertia forces from the bending of a stiffener will be instrumental in producing fatigue failures in a joint assembly. SAAS-II was developed over a period of years with sponsors including NSF and NASA. The present version that was used in this program was developed by R. M. Jones and J. G. Crose at Aerospace Corporation and includes plane-stress and plane-strain options.

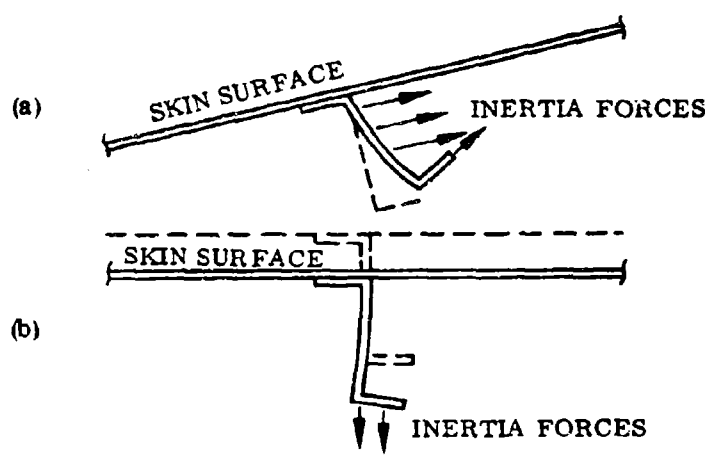

FIGURE 2. MODES WITH SIGNIFICANT INERTIAL FORCES IN THE STIFFENERS

II.4 SHAKER VERSUS ACOUSTIC EXCITATION

In order to conduct shaker tests to obtain acoustic design information, it is necessary to establish carefully the specimen design and test procedure for shaker excitation. The designs of the acoustic test specimens and the shaker test specimens were based on obtaining experimentally the same key parameters (including modes of failure) in acoustic test specimens as in shaker test specimens. By following this procedure, considerable acoustic design information has been obtained by conducting shaker tests to supplement the data generated in the acoustic tests.

There were more specimens for shaker tests than for acoustic tests in the test program, even though the ultimate program objective was to obtain acoustic fatigue design information. The reasons for this were as follows:

1. Less material is required in a shaker test program since specimens are smaller and less complex. This reduces costs appreciably since advanced-composite materials are rather expensive.

2. Less labor is required to fabricate the smaller and less complex specimens. This too reduces program costs.

3. Less labor is required in a test program which includes multiple-specimen shaker tests but individual acoustic tests.

4. Closer control of the planned excitation spectra is possible.

Since shaker test programs are less costly for a fixed number of test specimens and since shaker tests can provide stress or strain versus life data for a joint assembly that are applicable to joint assemblies in panels under acoustic loading, the use of shaker tests was employed to obtain S-N data for the joint assemblies.

II.5 NARROW-BAND VERSUS BROAD-BAND EXCITATION

The shaker tests were conducted under narrow-band excitation. The advantages of narrow-band excitation as opposed to broad-band excitation are as follows:

1. It takes less time, for a given power input, to produce a failure if the excitation frequency is at or close to the specimen's fundamental frequency.

2. It is easier to compare the fatigue life of the shaker test specimens with lives of coupons that have been tested under constant amplitude-constant frequency excitation, which is the more common method of excitation.

3. It is reasonable to expect the experimental strains to occur at essentially one response frequency. Hence a unique random S-N point is obtained in contrast to the situation of broad-band excitation with multi-modal response for which some average frequency must be defined.

The disadvantages of narrow-band excitation as opposed to broad-band excitation are:

1. Broad-band excitation is more typical of aircraft loading; however, in general it may be difficult or impossible to conduct the acoustic tests under an arbitrarily defined spectrum, whereas in shaker tests the load spectrum may be controlled in a more precise manner.

2. There is an additional task to convert, analytically or empirically, the S-N data obtained under narrow-band loading to S-N data under broad-band random loading.

3. Careful monitoring of the fundamental frequency is necessary, and if the fundamental frequency drifts during testing, either it must be restored to its initial value through manual adjustment, or the driving frequency must be adjusted to maintain excitation at the new fundamental frequency. The drift in fundamental frequency becomes more critical when specimens are tested simultaneously.

The shaker tests were conducted in the Northrop Vibration Test Laboratory under narrow-band excitation, since after careful consideration it was considered that the advantages outweighed the disadvantages.

The acoustic tests were conducted in the Northrop Progressive Wave Acoustic Test Chamber under broad-band excitation. Since the shaker tests were conducted under narrow-band excitation and the acoustic tests under broad-band excitation, the excitation spectra were recognized in the assessment of the experimental fatigue data.

II.6 CONFIGURATION AND MATERIALS

In the shaker test program, an adhesive-bonded joint was used for one joint configuration and a riveted joint for the other. These two configurations are typical of configurations projected for use in aircraft applications. In addition, the following material combinations ("stiffeners" refer to shaker specimen components that simulate either ribs, spars, or stringers, etc.) were used:

1. Graphite-epoxy skin to graphite-epoxy stiffeners.

2. Graphite-epoxy skin to titanium alloy stiffeners.

3. Boron-epoxy skin to titanium alloy stiffeners.

The use of either three-bay, stiffened panels (with two parallel stiffeners dividing the panel into three rectangular bays) or nine-bay, cross-stiffened panels was considered for the panels in the acoustic test program. The decision was made to fabricate and test the nine-bay, cross-stiffened panels since they were more representative of larger sections of aircraft structure.

The Fothergill/Harvey Courtaulds HT-S/4617 graphite-epoxy system and the Narmco 5505 boron-epoxy system were selected as the advanced-composite materials for the test program.

FM-123-2 adhesive (0.085 psf) was chosen for bonding the advanced-composite skins to the internal structure in joint assemblies of the acoustic panels and shaker

specimens. FM-123-2 was chosen because of its low modulus and relatively low curing temperature (250F).

EC 2216, a room temperature curing adhesive, was used in peripheral areas that were not part of the test sections of the acoustic panels and the shaker specimens. When the EC 2216 adhesive was used rather than FM-123-2 adhesive in the acoustic panels, it was chosen to avoid residual thermal stresses resulting from the cooling from an elevated bonding temperature. When the EC 2216 adhesive was used in shaker specimen assemblies, it was selected because of the ease in conducting the bonding operation.

III. DESIGN AND MANUFACTURE OF ACOUSTIC PANELS AND SHAKER SPECIMENS

III.1 ACOUSTIC PANELS

Three test panels were fabricated for the acoustic test program and they were identified as panels A-GG-B-1, A-GG-B-2, and A-GG-B-3. The letters in the panel identification are descriptive of the following: Acoustic panel with a Graphite-epoxy skin and Graphite-epoxy internal structure with Bonded joints. The number in the coding indicates the particular test panel; for example, panel A-GG-B-3 is the third of the three acoustic test panels. The design of the acoustic test panels is described below:

The three acoustic test panels were assembled with 6-ply $[0/\pm45]_S$ graphite-epoxy skin and 6-ply $[\pm45/0]_S$ graphite-epoxy I-beams and tee sections. In the assembled panel, the I-beams simulated ribs and the tee sections simulated stringers. The graphite-epoxy details that were chosen, as well as numerous detail variations of them, are expected to see considerable use in aircraft structure.

Adhesive-bonded skin/rib and skin/stringer joint configurations were chosen for the acoustic test panels, since the potential weight savings in using adhesive-bonded joints is attractive. It is anticipated that the design details discussed below will pertain to advanced-composite construction in lightly loaded and acoustic critical structural areas. As a matter of general policy, the internal structure must be designed carefully to avoid stress concentrations and early peeling and delamination of the joint assembly when the skin is subjected to acoustic loads in order to achieve the potential weight savings. Symmetric internal structural elements are used in service applications of metallic materials and are expected to be used in service applications of advanced-composite materials since the symmetry tends to decrease the nonsymmetric (torsional) loading at the joint, and, therefore, promotes longer life. The flanges of the internal structure may be scarfed to reduce the stress concentration at the edges of the flanges when the flanges are bonded to the skin, although the edges of the flanges were not scarfed in this program because of the thin flanges.

Each acoustic test panel was cross-stiffened and contained nine rectangular bays in a three by three array. Each acoustic test panel was said to have a test section and a fixture section, with the test section including the skin and joint assemblies enclosed by a rectangle drawn through the centers of the exterior eight bays. The fixture section included all of the panel area exterior to the panel test section.

The design of the initial test panel, A-GG-B-1, is given in Figure 3 (Drawing ACD-G-237). Panel A-GG-B-1 was manufactured and during the acoustic test experienced a premature acoustic fatigue failure. The panel design was then modified according to Drawing ACD-G-238 (Figure 4) and panels A-GG-B-2 and A-GG-B-3 were manufactured according to the modified design that is discussed in detail in Section III.1.(b). Panels A-GG-B-2 and A-GG-B-3 were subjected to approximately 10^8 cycles (the predetermined runout point) without experiencing an acoustic fatigue failure in a panel test section.

A description of the manufacturing of the three acoustic test panels follows.

PRECEDING PAGE BLANK-NOT FILMED.

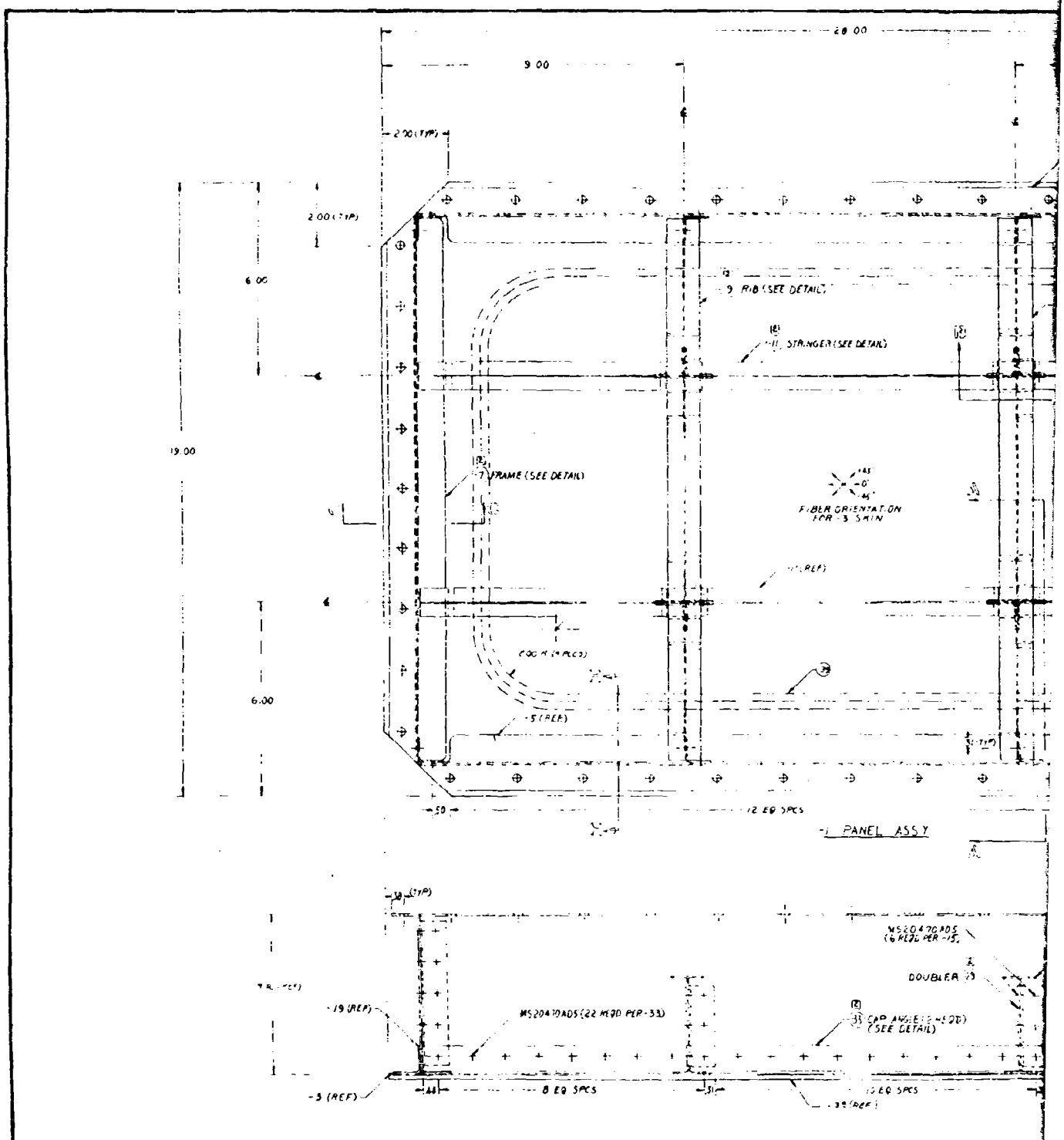

FIGURE 3. PANEL A-GG-B-1

PRECEDING PAGE BLANK-NOT FILMED.

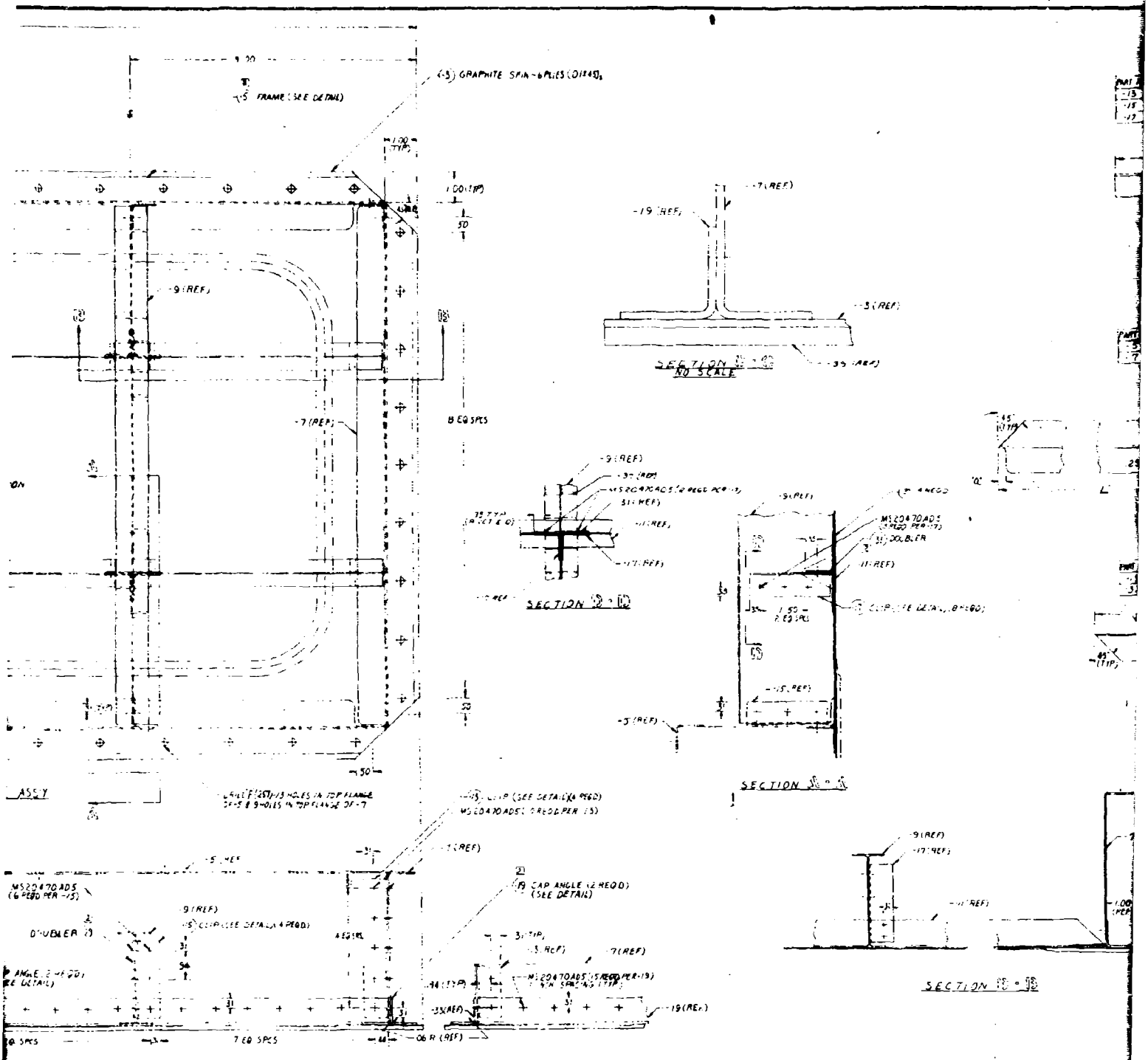

3

PRECEDING PAGE BLANK-NOT FILMED.

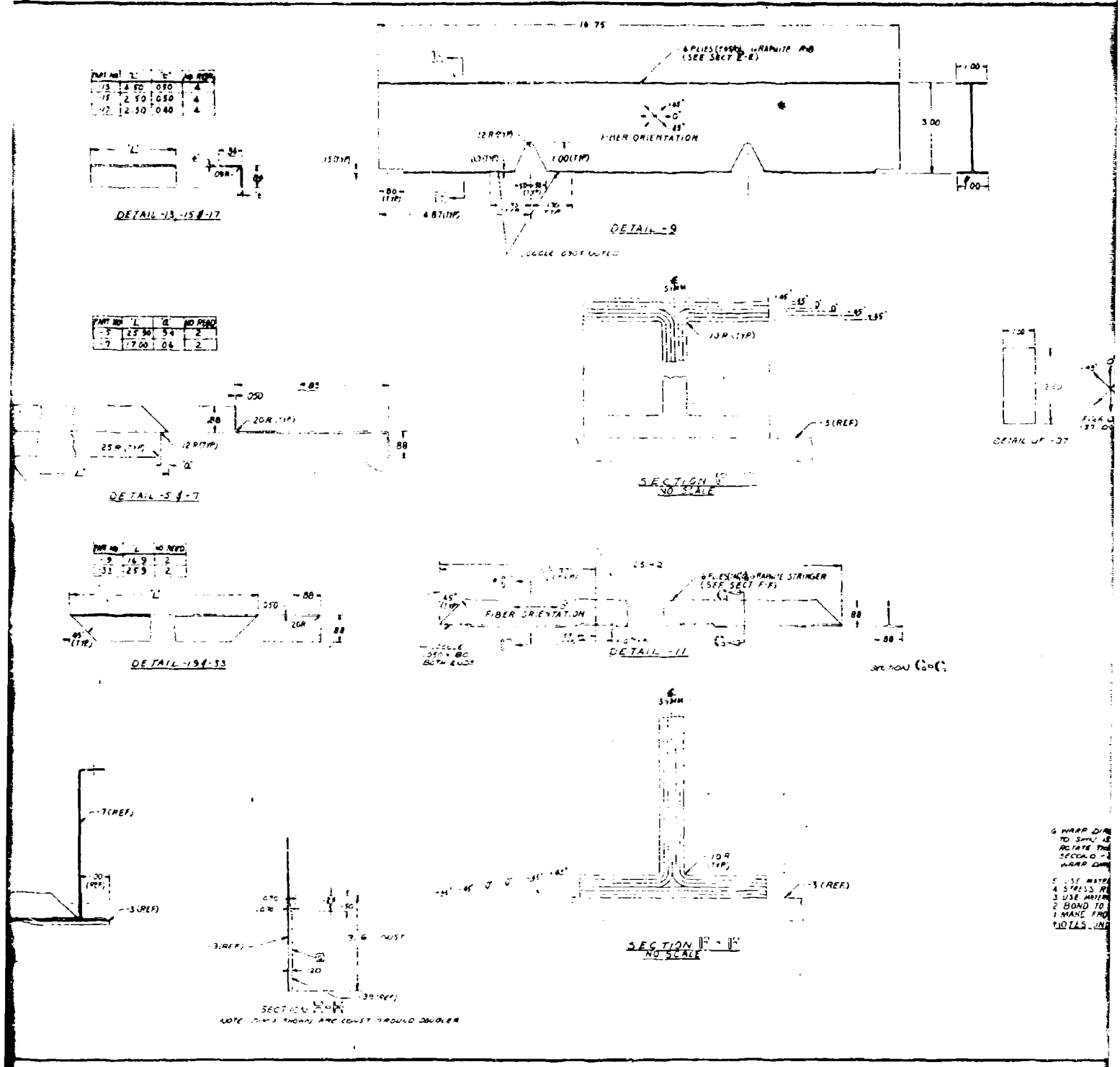

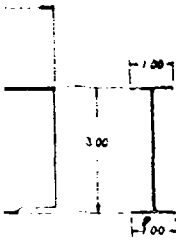

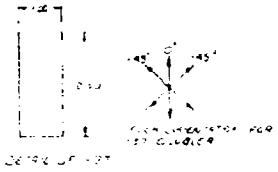

1	.39	1	DOUBLER	FIBERGLASS	[illegible]	.250x9.00 [illegible]
4	.37	1	DOUBLER	GRAPHITE COMPOSITE	[illegible]	.250x1.00 [illegible]
20		1	RIVET (PER NAS1204 GRADE 3)		5/32 DIA	
158			RIVET (PER NAS1204 GRADE 5)		5/32 DIA	
4	.35	3	DOUBLER	TIT (6AL-4V)	.040x1.22	MIL-T-9046
2	.35	3,4	ANGLE		.050x2x27	
4	.31	3	DOUBLER		.040x1.78	
4	.29	3	DOUBLER	TIT (6AL-4V)	.050x1.78	
16	.29	4	SPLICE PLATE		.040x2.8	
8	.25	3			.050x1.78	
8	.25	8			.050x1.78	
4	.24	4,8	SPLICE PLATE	TIT (6AL-4V)	.050x1.78	
2	.19	3,4	ANGLE	TIT (6AL-4V)	.040x1.8	MIL-T-9046
8	.17	5	CLIP	STEEL (AISI 1025)	.040x2x3	MIL-S-7952
4	.15	5	CLIP	STEEL (AISI 1025)	.050x2x3	MIL-S-7952
4	.15	5	CLIP	STEEL (AISI 1025)	.050x2x3	MIL-S-7952
2	.11	1	STRINGER	GRAPHITE COMPOSITE	6 PLIES (.25/PLY)	
2	.09	1	RIB	GRAPHITE COMPOSITE	6 PLIES (.25/PLY)	
2	.07		FRAME (SIDE)	TIT (6AL-4V)	.250x5.8	MIL-T-9046
2	.05		FRAME (FWD)	TIT (6AL-4V)	.050x8.2	MIL-T-9046
1	.3	1	SKIN	GRAPHITE COMPOSITE	6 PLIES 21x50	
	.1		PANEL ASSY			
PER						

PARTS LIST

ACOUSTIC TEST PANEL
GRAPHITE COMPOSITE

ACD-G-237

6 WARP DIRECTION OF THE FIRST .39 PLY ADJACENT TO SKIN IS PARALLEL TO PROC LENGTH OF SKIN. ROTATE THE WARP DIRECTION 90° FOR THE SECOND .39 PLY COMPOSITE ALTERNATING THE WARP DIRECTION OF EACH PLY IN THIS MANNER

5 USE MATERIAL IN COLD FINISHED CONDITION
4 SPECIAL REQUIREMENT AFTER FORMING
3 USE MATERIAL IN ANNEALED CONDITION NO HEAT TREAT REQD
2 BOND TO MATING SURFACE WITH FM-23-2 ADHESIVE
1 MADE FROM FETHERSTONE & HARVEY 40/60 COLORTRAVLOS HT-S

NOTES UNLESS OTHERWISE SPECIFIED:

4

PRECEDING PAGE BLANK-NOT FILMED.

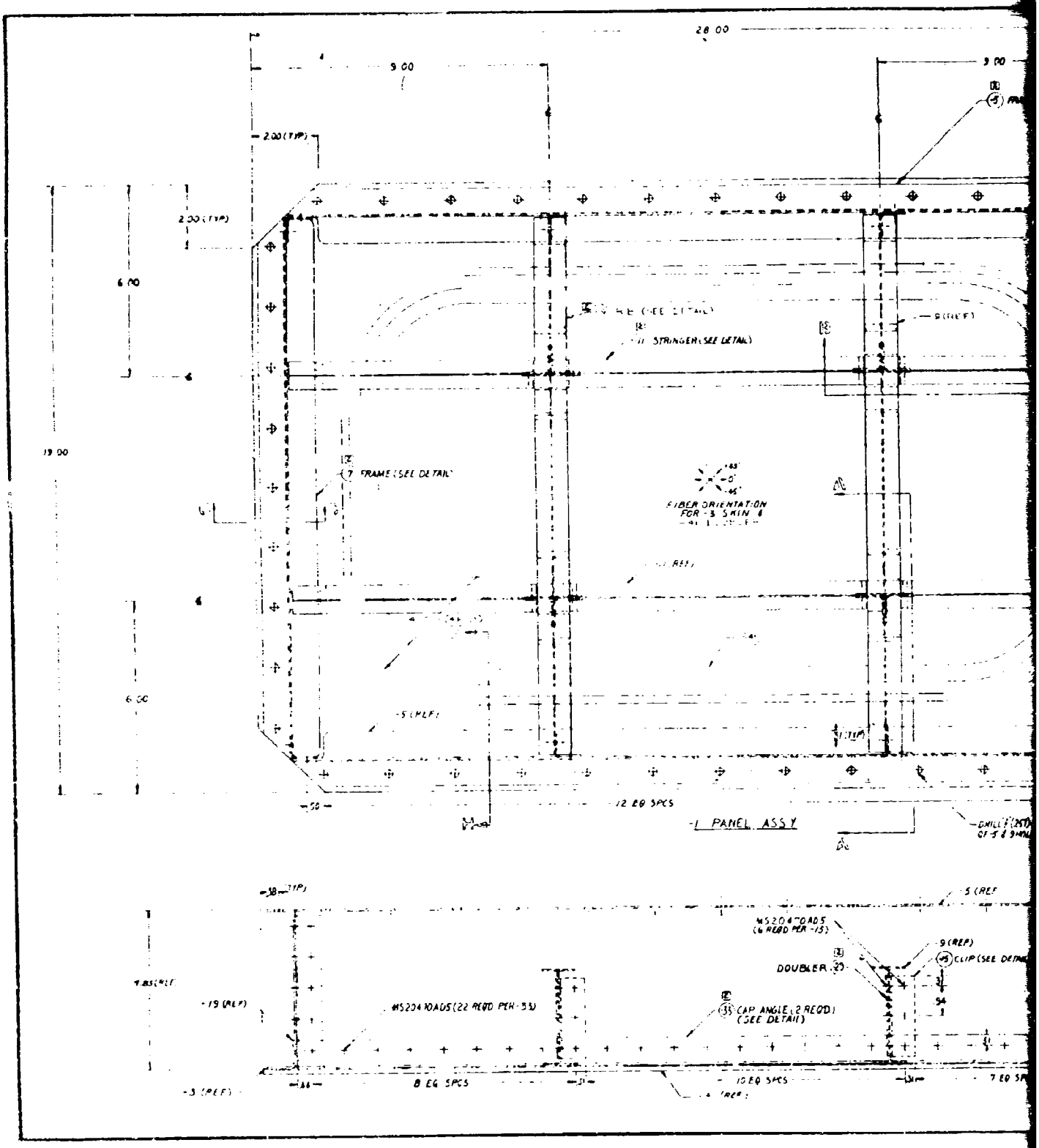

FIGURE 4. PANEL A-GG-B-2

PRECEDING PAGE BLANK-NOT FILMED.

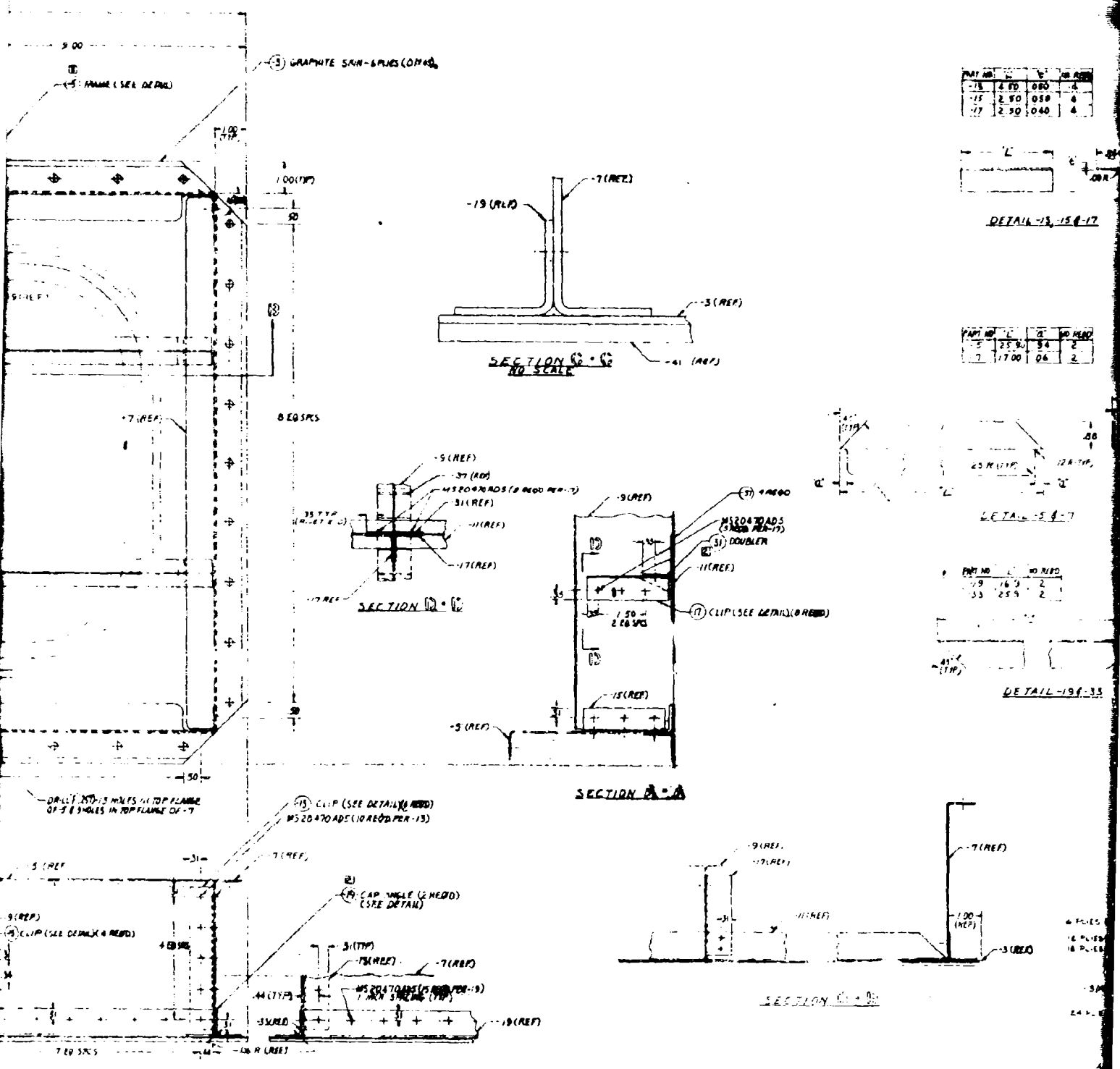

2

PRECEDING PAGE BLANK-NOT FILMED.

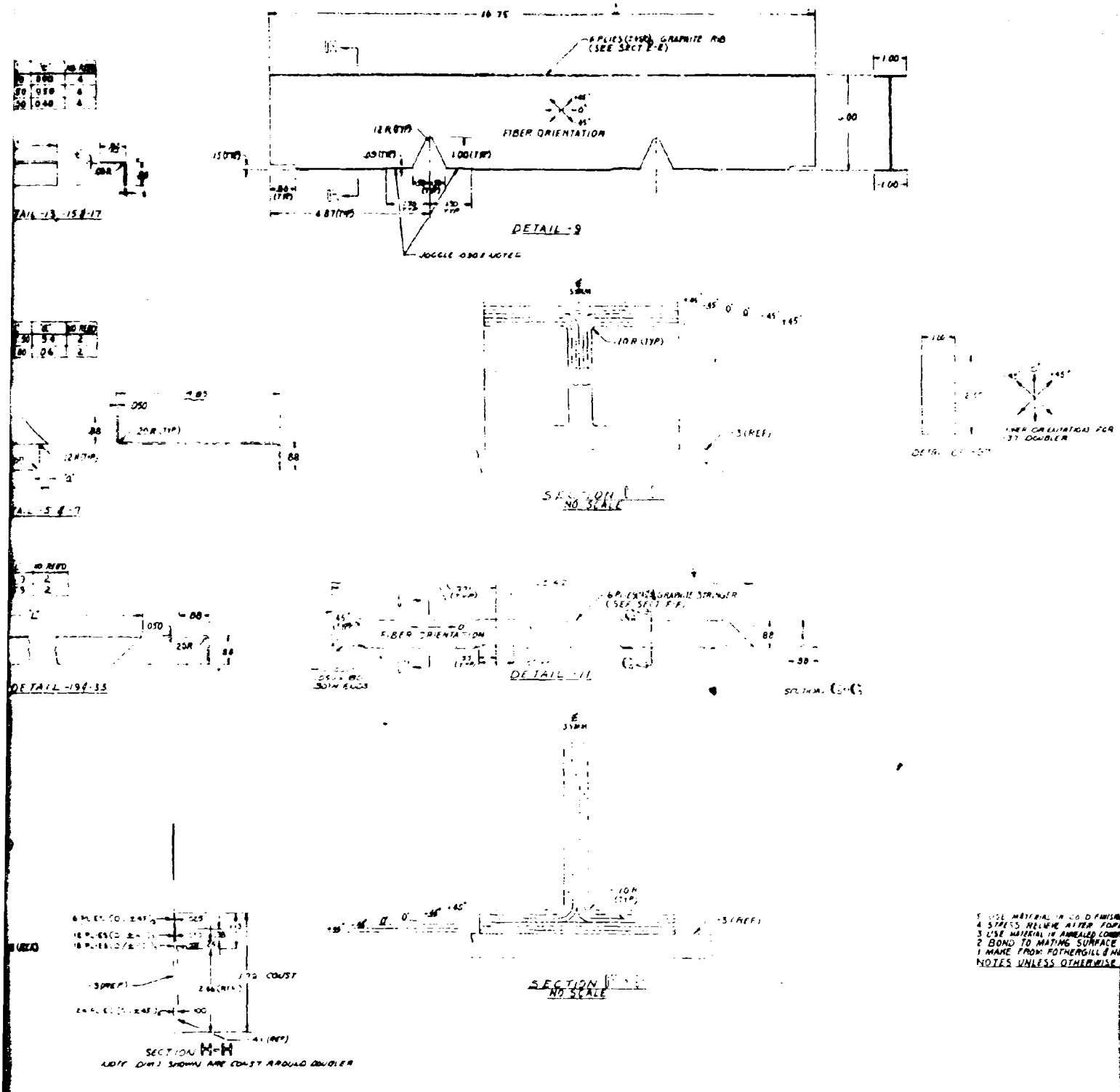

3

PRECEDING PAGE BLANK-NOT FILMED.

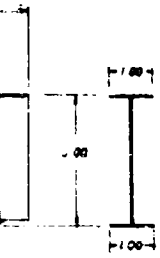

5 USE MATERIAL IN COLD FINISHED CONDITION
4 STRESS RELIEVE AFTER FORMING
3 USE MATERIAL IN ANNEALED CONDITION NO HEAT TREAT REQD
2 BOND TO MATING SURFACE WITH [illegible] 210 ADHESIVE
1 MADE FROM FOTHERGILL & HARVEY 4617/COURTAULDS HT-5
NOTES UNLESS OTHERWISE SPECIFIED:

PARTS LIST

NORTHROP

PANEL A-GG-B-2

ACD-G-238

PRECEDING PAGE BLANK-NOT FILMED.

III. 1. (a). Manufacture of Panel A-GG-B-1

TOOLING AND FIXTURES. Lay up tools were fabricated for use in manufacturing the I-beam and tee section components of the acoustic test panels and vibration specimens. An assembly jig and bonding tool were fabricated for the acoustic test panels.

FABRICATION OF THE GLASS DOUBLER. For panel A-GG-B-1, a 13-ply glass doubler (-39 detail of Figure 3) was fabricated using Narmco 500/1581 E glass. Thirteen plies were used rather than twelve plies of the -39 detail in order to use an existing flat plate as part of the bonding tool and to eliminate the possibility of introducing curvature in the bonding tool by machining 0.008 inch from the flat plate. Each glass ply was layed up in its flat sheet shape without overlaps or butt joints and with the appropriate center cutout for the -39 detail. A layer of Mil-Tex No. 3921 peel ply was applied to the bonding surface of the glass laminate to obtain a good bonding surface to the -3 graphite-epoxy skin. The glass laminate was bagged and autoclave cured for 90 minutes at 250F with 60 psi/vented vacuum. Upon completion of the cure, the doubler was trimmed to produce a hollow rectangle with each outer edge dimension two inches longer than the corresponding edges of the titanium frame detail.

FABRICATION OF THE GRAPHITE-EPOXY SKIN. A six-ply $[0/\pm 45]_S$, -3 detail skin was fabricated using the Fothergill/Harvey Courtaulds HT-S/4617 graphite-epoxy prepregged system to produce a 30 x 20-inch rectangular skin. The Mil-Tex No. 3921 peel ply was applied to obtain a good bonding surface to the titanium alloy frame and the cross-stiffened graphite-epoxy I-beams and tee sections. The skin was bagged and autoclave cured for three hours at 350F with 100 psi/vented vacuum. After cure, the skin was trimmed to produce a rectangle with each edge dimension two inches longer than the corresponding edges of the titanium frame detail. Four -37 details were machined out of the excess trim skin material.

FABRICATION OF THE GRAPHITE-EPOXY I-BEAMS AND TEE SECTIONS. The layup of the 6-ply graphite-epoxy I-beams and tee sections (-9 and -11 details) is shown in Figure 5. Note that in the layup of 6-ply I-beams, it is impossible to obtain simultaneously symmetry of layup about the center plane of the web and about the center plane of each of the flanges. Likewise in the layup of 6-ply tee sections, it is impossible to obtain simultaneously symmetry of layup about the center plane of the head of the tee and about the center plane of the leg of the tee.

A schematic drawing of the assembly of an I-beam is shown in Figure 6. The I-beams were fabricated in the following manner. Three plies each for the web and one-half of the flanges were laid up in the flat to the orientation shown in Figure 5. Each 3-ply layup was then formed about a silicone rubber plug. Three additional plies were then laid up to the required orientation and added (after filling the void at the center of the flanges with a small bundle of the 0° graphite-epoxy material) to the previous 3-ply layups on the silicone rubber plugs. The rubber plugs were then confined inside steel tooling, pressurized to 100 psi on the graphite-epoxy plies, heated to 350F, and cured for three hours to produce the I-beams. The fabrication of the tee sections was conducted in a like manner (except for the absence of a flange) to the fabrication of the I-beams. After cure the I-beams and tee sections were trimmed to size and assembled as the cross stiffened detail (Figure 5) in the assembly jig.

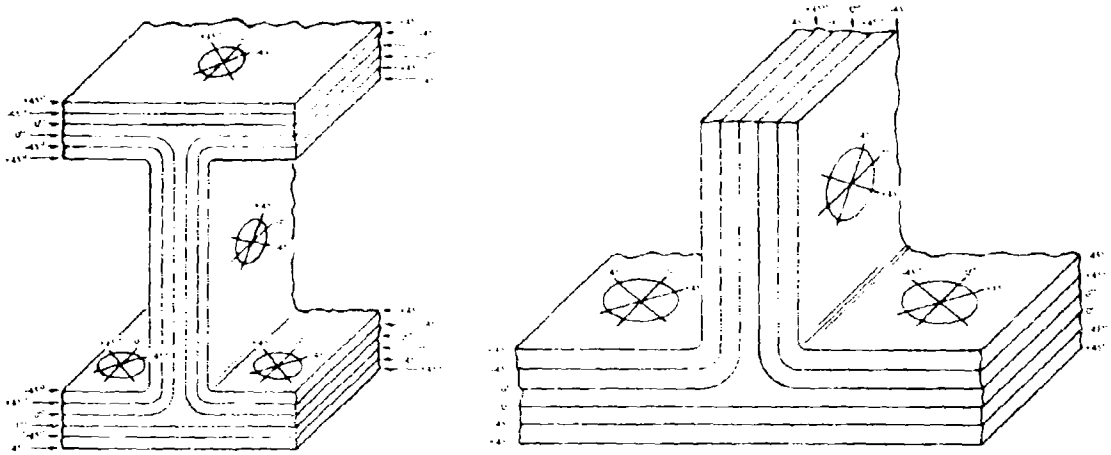

EACH VERTICAL PLY REMAINS CONTINUOUS WHEN BENT INTO A HORIZONTAL PLANE

SCHEMATIC LAYUP OF 6-PLY $[\pm 45/0]_S$ IN WEB FOTHERGILL/ HARVEY COURTAULDS HT-S/4617 GRAPHITE EPOXY I-BEAM

SCHEMATIC LAYUP OF 6-PLY $[\pm 45/0]_S$ IN VERTICAL LEG FOTHERGILL/HARVEY COURTAULDS HT-S/4617 GRAPHITE-EPOXY TEE SECTION

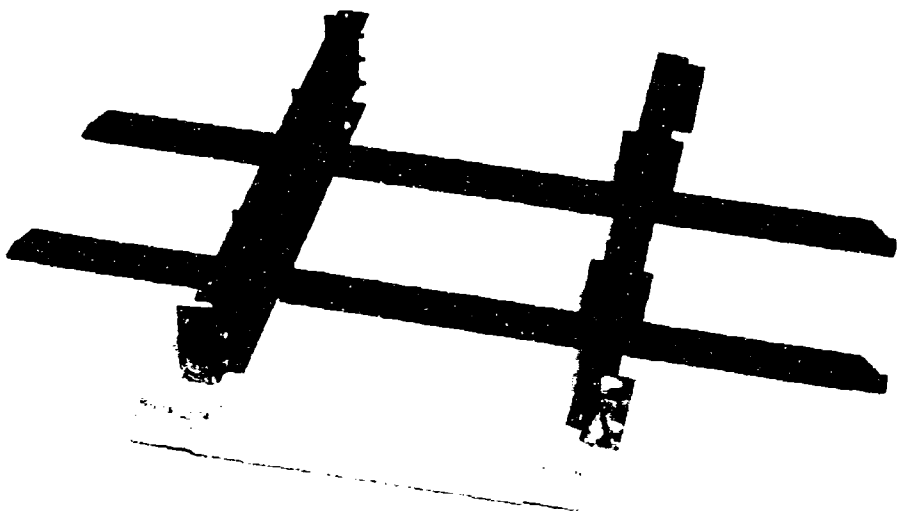

NO. 70-02820

FIGURE 5. CROSS-STIFFENED GRAPHITE-EPOXY DETAIL INCLUDING TWO EACH 6-PLY $[\pm 45/0]_S$ FOTHERGILL/HARVEY COURTAULDS HT-S/4617 I-BEAMS AND TEE SECTIONS

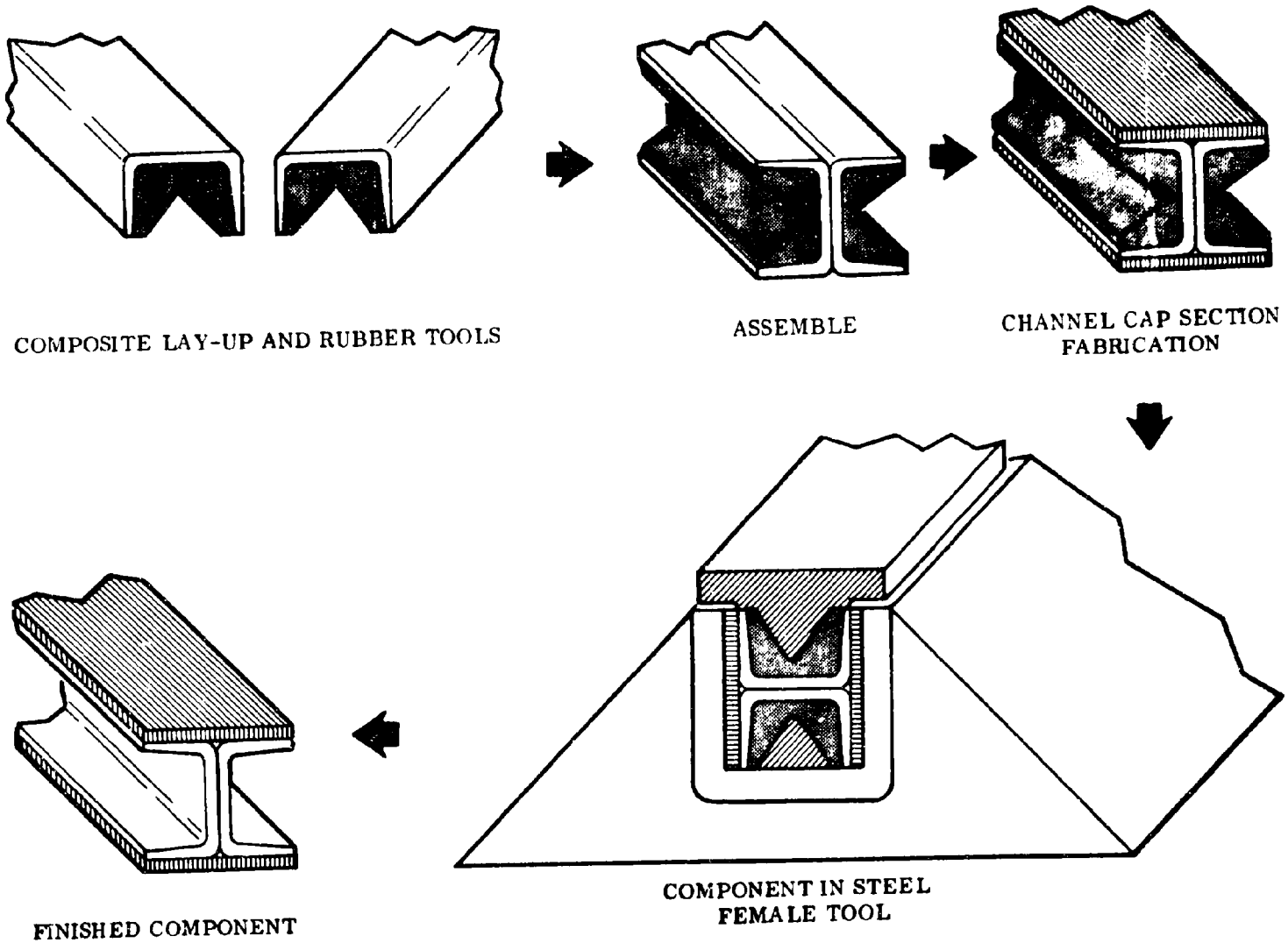

FIGURE 6. SCHEMATIC OF I-BEAM FABRICATION

FABRICATION OF ACOUSTIC TEST PANEL A-GG-B-1. Prior to bonding panel A-GG-B-1, all details were prefitted in the bonding tool to ensure good mating surfaces. All glass and graphite-epoxy bonding surfaces were stripped of their peel ply or sanded with 250 grit sand paper when there was no peel ply, and then wiped clean with M.E.K. The titanium alloy details were cleaned and phosphate coated prior to bonding. FM-123-2 adhesive film was applied to all bonding surfaces. The assembly and bonding procedure follows.

1. The base plate of the bonding tool, MRD 70-64 (Figure 7) was sprayed with MS-122 fluorocarbon release agent and covered with teflon glass coated cloth.

2. The fiberglass doubler (Figure 8) detail was aligned on the base of the bonding tool (Figure 9).

3. The graphite-epoxy skin (Figure 8) was aligned on top of the glass doubler in the bonding tool (Figure 10).

4. The titanium alloy Z and angle frame (Figure 11) was then placed on top of the graphite skin and aligned using the preset aligning bolts incorporated into the side plates of the bonding tool (Figure 12).

5. The self-aligning cross-stiffened graphite-epoxy detail (Figure 11) was then positioned into the titanium alloy frame. This completed the assembly (Figure 13) in the bonding tool.

6. The graphite-epoxy skin surface in the interior of the panel assembly was covered with teflon coated glass cloth. The assembly was then filled with glass impact beads and wood blocks to obtain positive pressure during cure.

7. Osnaburg cloth was used to pad the bead filled assembly prior to closing the assembly with a steel pressure plate.

8. The panel assembly and bonding tool were covered with Osnaburg cloth and bagged.

9. The final assembly was then autoclave cured for one hour at 250F with 35 psi/vented vacuum.

10. After completion of the cure and removal from the bonding tool, the final riveting and trimming operations were performed.

INSPECTION OF PANEL A-GG-B-1 AS MANUFACTURED. After the cure was completed, it was noted that the skin had a noticeable oil can in the center bay. The oil can was attributed to residual stresses resulting from the bonding operation.

FIGURE 7. BONDING TOOL, MRD 70-64

Number 70-02816

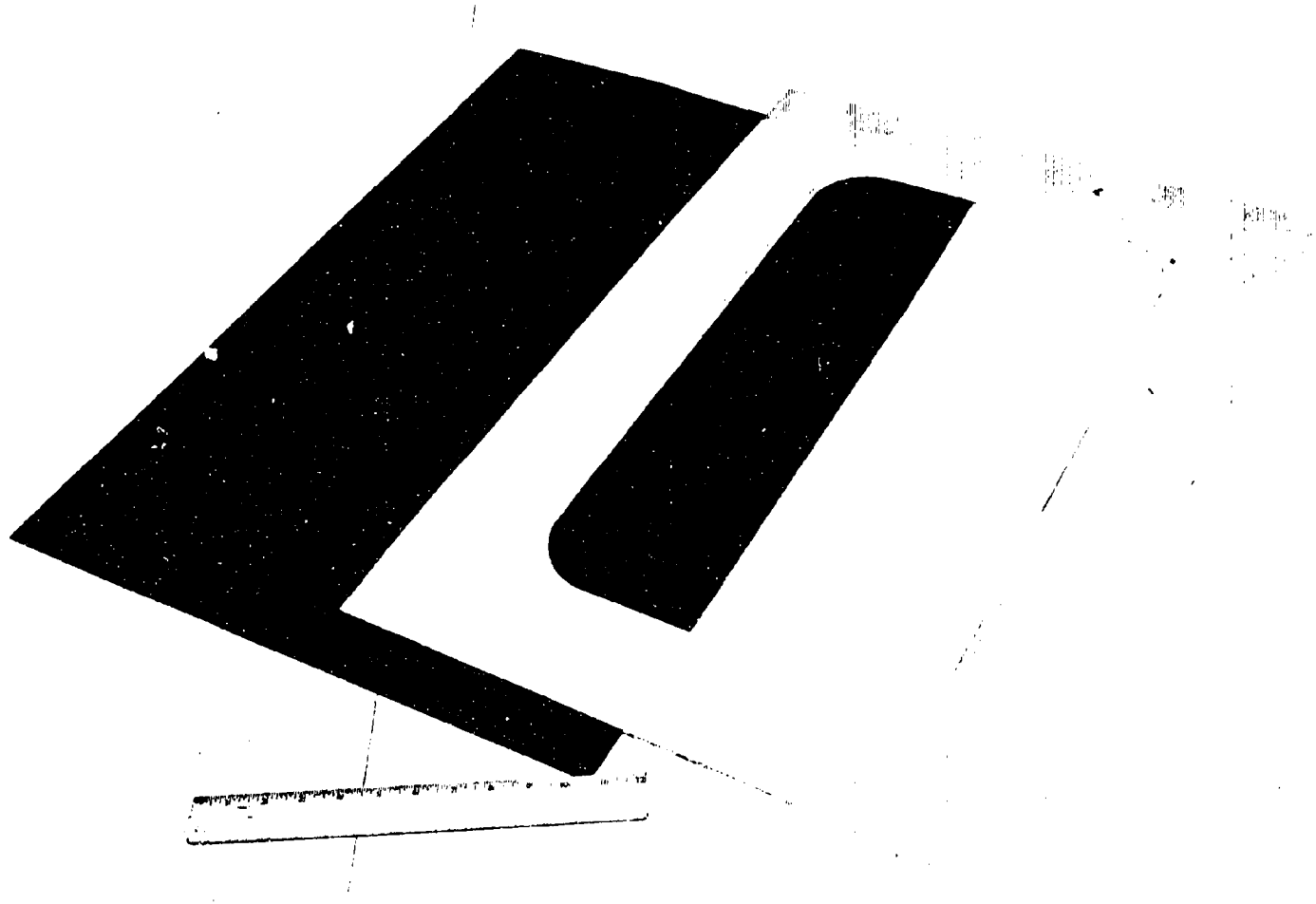

FIGURE 8. 6-PLY $[0/\pm 45]_S$, FOTHERGRILL/HARVEY COURTAULDS HT-S/4617 Number 70-02814
GRAPHITE-EPOXY SKIN AND 13-PLY NARMCO 500/1581 GLASS DOUBLER

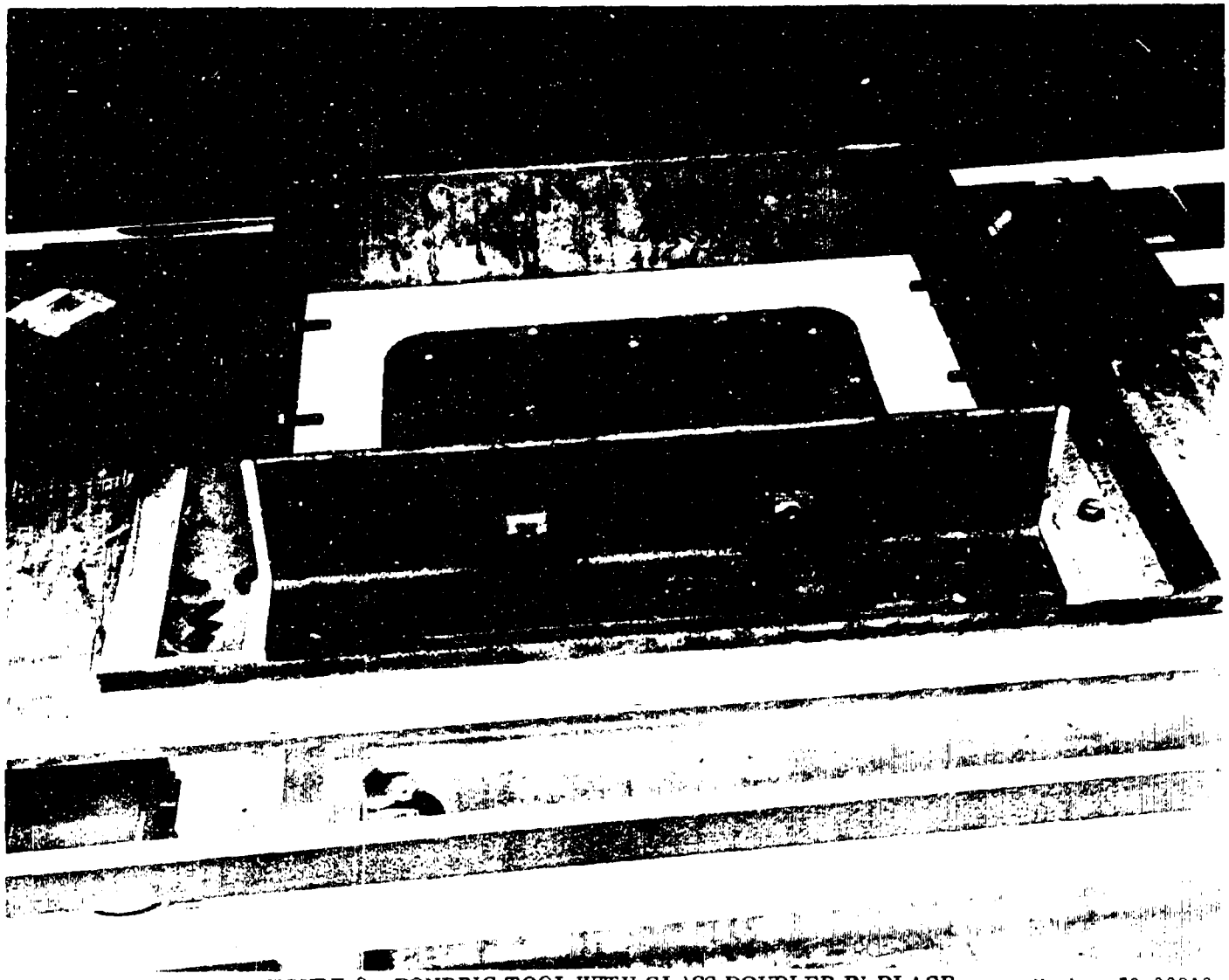

FIGURE 9. BONDING TOOL WITH GLASS DOUBLER IN PLACE Number 70-02818

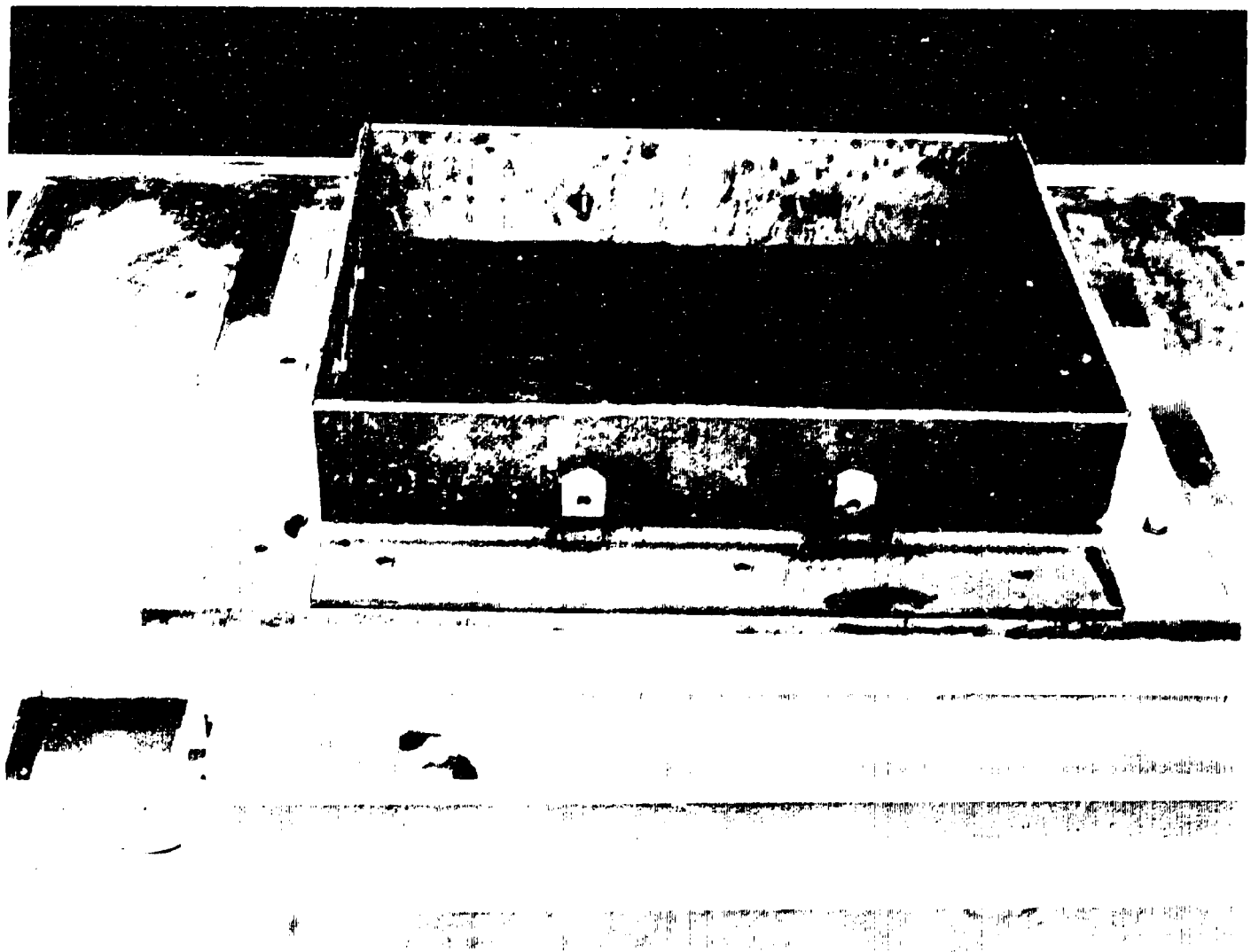

FIGURE 10, BONDING TOOL WITH GRAPHITE-EPOXY SKIN IN PLACE ON TOP OF GLASS DOUBLER

Number 70-02817

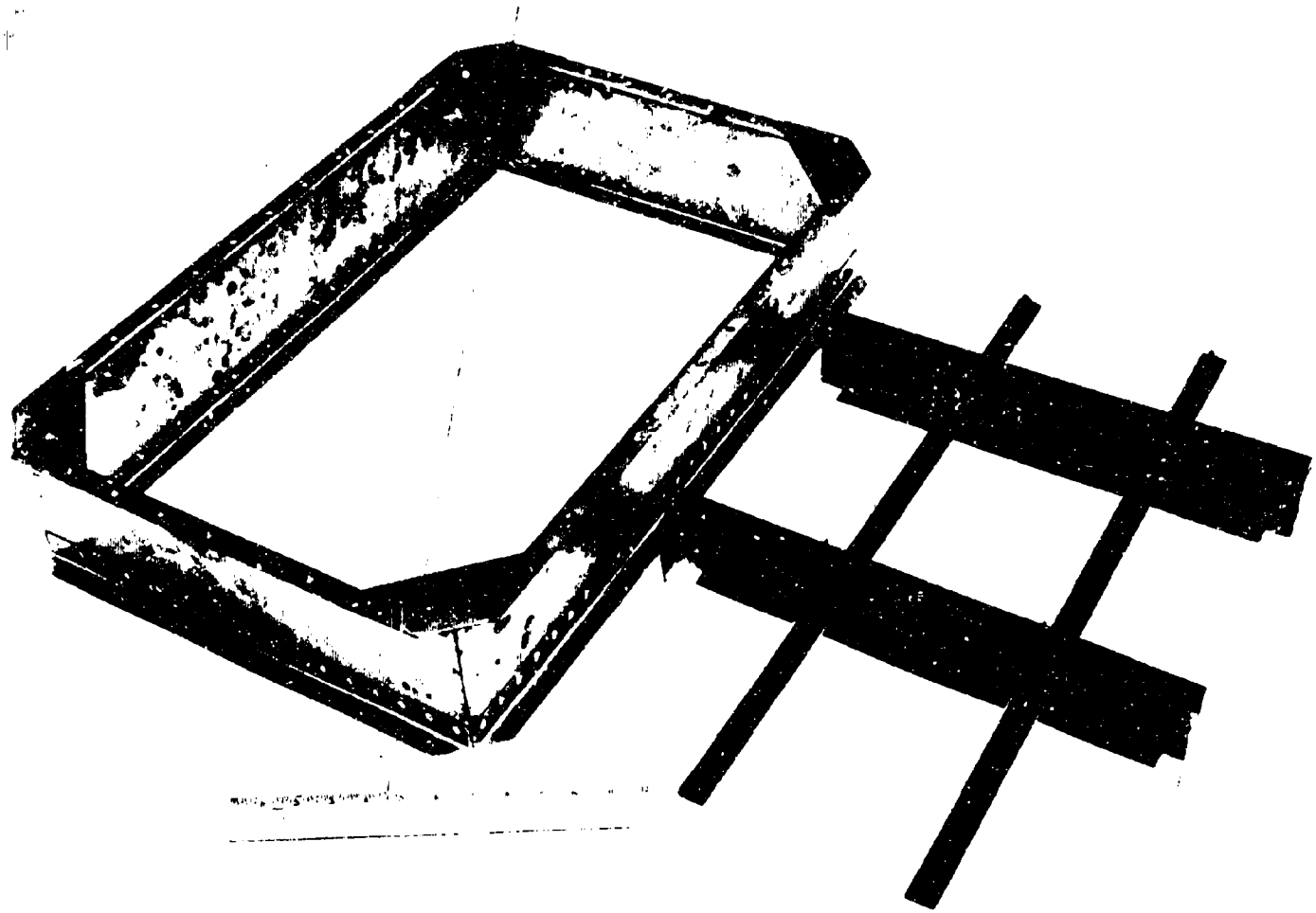

FIGURE 11. 6AL-4V TITANIUM Z AND ANGLE FRAME AND CROSS-STIFFENED GRAPHITE-EPOXY DETAIL

Number 70-02813

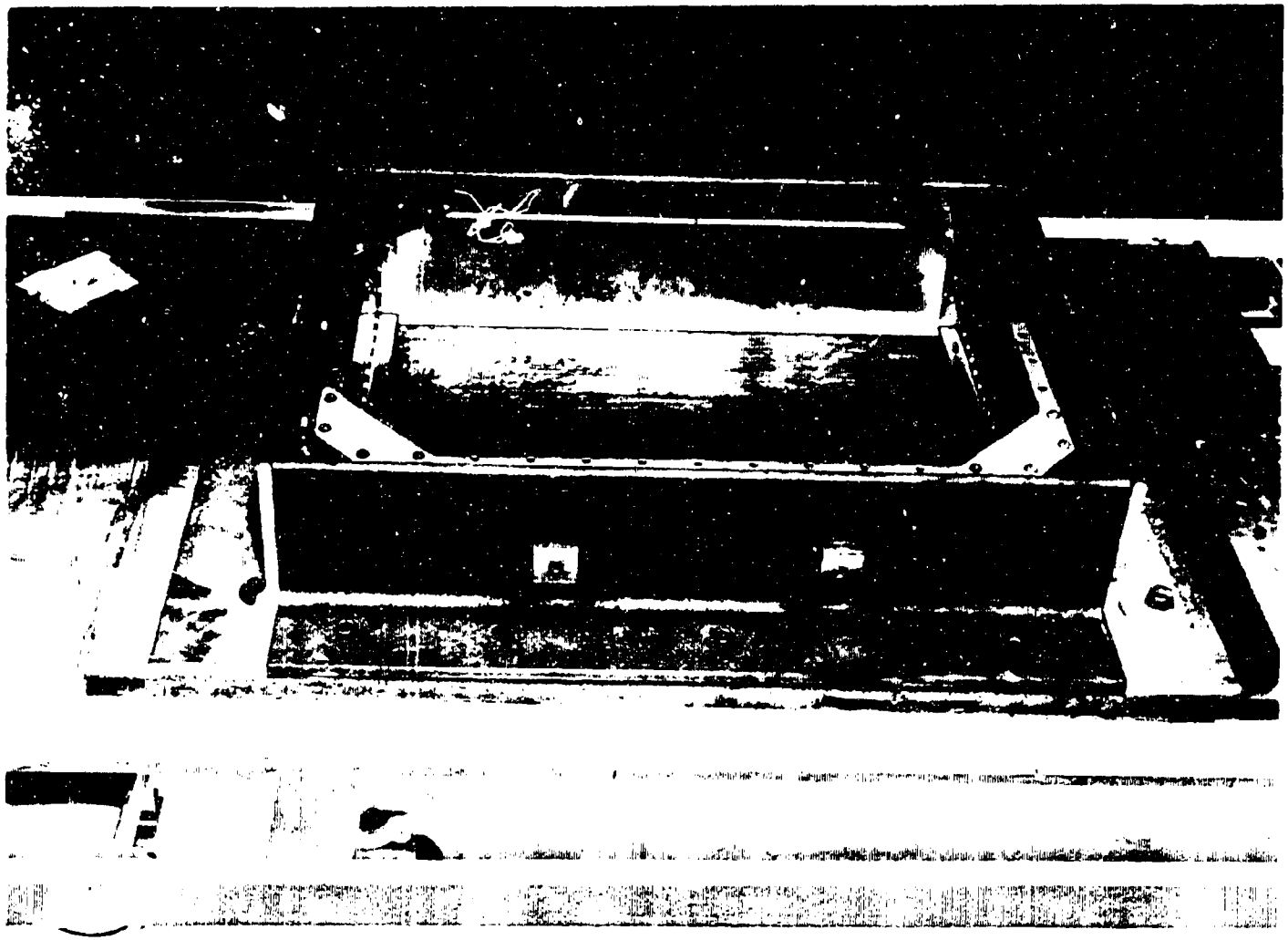

FIGURE 12. BONDING TOOL WITH TITANIUM FRAME IN PLACE ON TOP OF GRAPHITE-EPOXY SKIN AND GLASS DOUBLER Number 70-02815

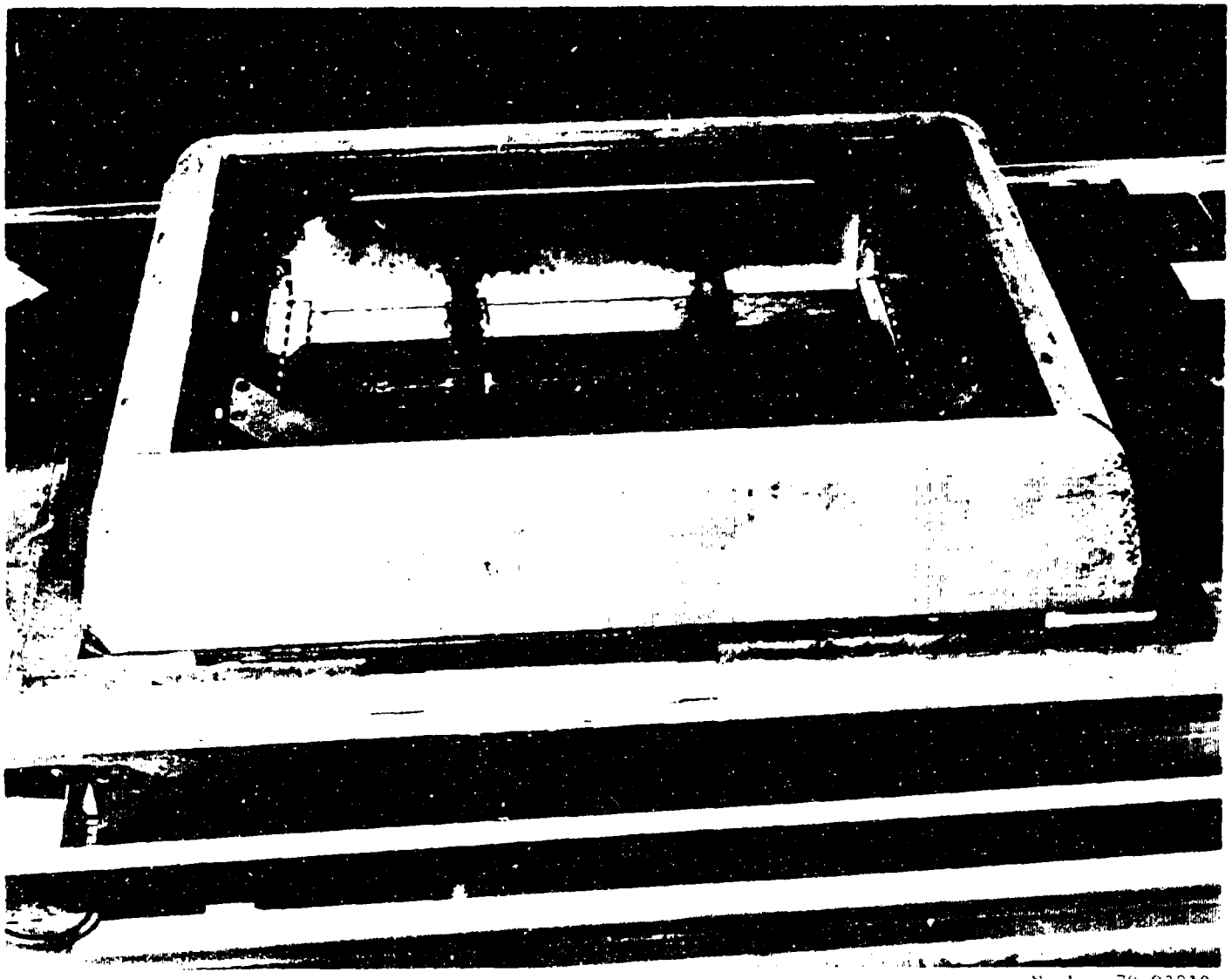

Number 70-02819

FIGURE 13. BONDING TOOL WITH CROSS-STIFFENED GRAPHITE-EPOXY DETAIL IN PLACE INSIDE OF TITANIUM FRAME ON TOP OF GRAPHITE-EPOXY SKIN AND GLASS DOUBLER

III. 1. (b) Plan for Manufacturing Panel A-GG-B-2

Based on the acoustic test results of panel A-GG-B-1 and an analytic investigation, it was apparent that changes (from panel A-GG-B-1) were needed in the configuration and manufacturing process of the fixture section (i.e., the peripheral portion) of the remaining acoustic test panels but that no changes were necessary in the acoustic test section (i.e., the central bay and adjacent parts of the outer bays). The changes described below were intended to guard against both oil canning of the panel in the manufacturing process and obtaining a fatigue failure in the fixture section during the acoustic test.

The following plan was therefore proposed for the manufacture of panel A-GG-B-2:

1. Manufacture the tee section and I-beam details with no design change from these details of panel A-GG-B-1.

2. Manufacture the 6-ply skin with no design change from the skin of panel A-GG-B-1.

3. Manufacture the clips and doublers (no design change from panel A-GG-B-1) for attaching the tee section and I-beam details to each other and to the skin.

4. Manufacture a stepped graphite-epoxy doubler (Figure 14) to replace the glass doubler (Section H-H of Figure 3). The purpose of replacing the glass doubler with the graphite-epoxy doubler was to guard against the mismatch of thermal coefficients of expansion of the skin and doubler of panel A-GG-B-1 when the bonding between these two items is conducted at 250F. The alternate approach of using the glass doubler and bonding the glass doubler to the skin with a room temperature curing adhesive was rejected, since the lower strengths of room temperature curing adhesives might lead to the initial acoustic fatigue in the fixture section. The length of the final step of the graphite-epoxy doubler was chosen to be at least as great as one-half the width of the flange of the I-beam sections in order to reduce the likelihood of a fatigue failure at the junction of the unsupported skin and the peripheral doubler. Furthermore, a 4.00-inch radius (in place of the 2.00-inch radius) was proposed for the corners of the graphite-epoxy doubler of panel A-GG-B-2 to guard against corner cracks.

5. Assemble the details in items 1-4 and bond the graphite-epoxy doubler (item 4) to the skin and bond the skin to the tee section and I-beam details with FM-123-2 adhesive at 250F. Use glass impact beads to obtain the pressure during bonding.

6. Manufacture the peripheral titanium alloy members and steel clips with no design change from these peripheral members of panel A-GG-B-1.

7. Assemble the titanium alloy edge frame and bond the titanium alloy edge frame to the already bonded assembly of the skin, tee section and I-beam details, and graphite-epoxy doubler. For this bonding operation, the EC 2216 room temperature curing adhesive was chosen. The room temperature curing EC 2216 adhesive rather than the 250F curing FM-123-2 adhesive was chosen to guard against oil canning of the acoustic test panel during the cool down from the bonding of the titanium alloy material to the graphite-epoxy material with dissimilar thermal coefficients of expansion. The acoustic test

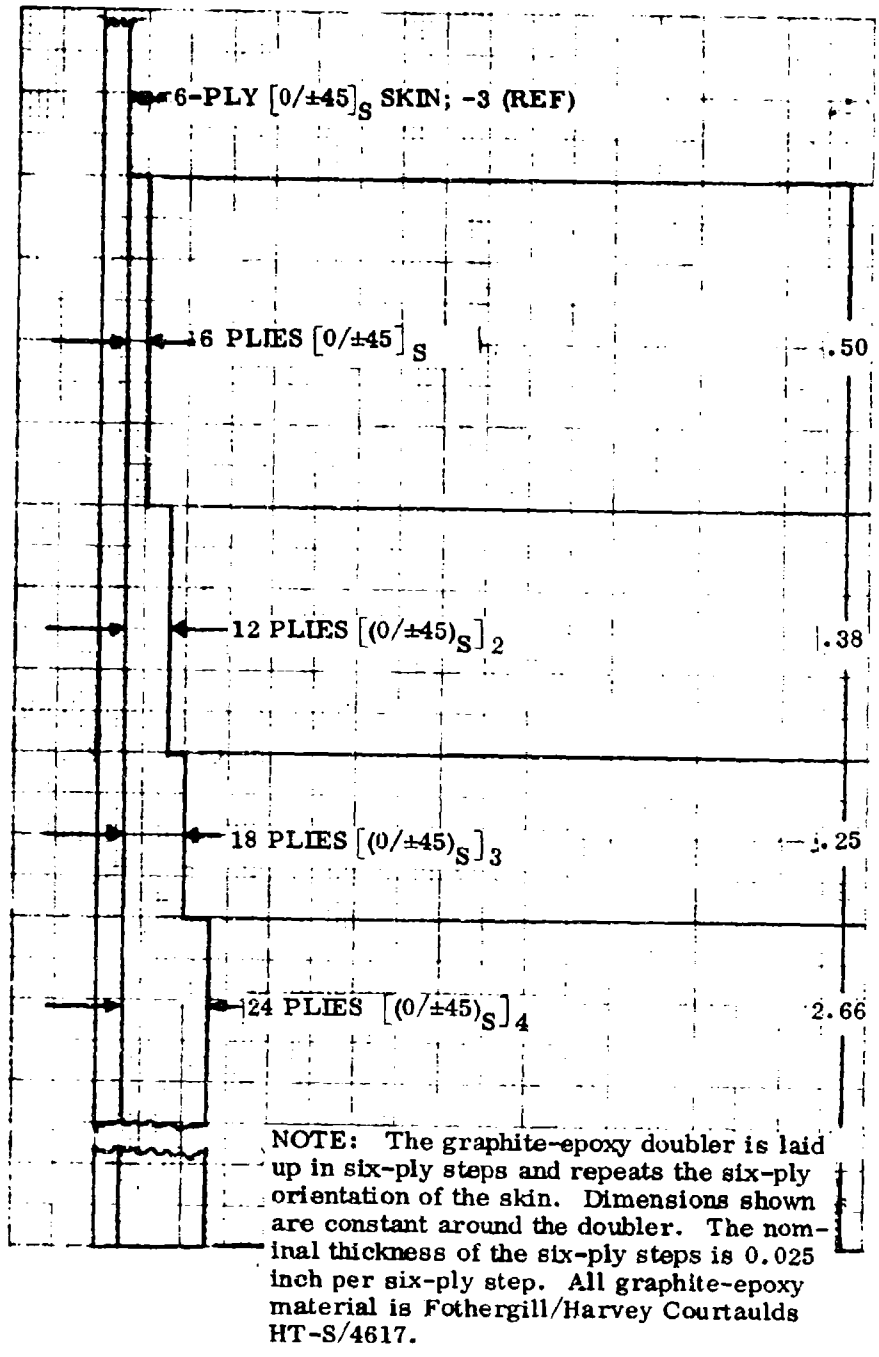

FIGURE 14. GRAPHITE-EPOXY DOUBLER CROSS SECTION TO REPLACE SECTION H-H OF FIGURE 3

results of panel A-GG-B-1 indicated that the bond between the titanium alloy frame and the graphite-epoxy skin and tee section details was less severely loaded than the bond between the glass doubler and the skin, and, therefore, the EC 2216 adhesive would perform adequately during the acoustic test.

8. Perform the final riveting and trimming operations as was done for panel A-GG-B-1.

No increase in the number of plies of the skin was recommended since more plies would reduce the likelihood of a skin failure in the acoustic fatigue test. No decrease in the number of plies of the skin was recommended since it was anticipated that six-ply skins will likely be used more often than four-ply skins in hardware applications. No acoustic fatigue failure was anticipated in the six-ply tee section and I-beam details and therefore there was no change in their design.

III. 1. (c) Manufacture of Panels A-GG-B-2 and A-GG-B-3

REJECTION OF CROSS-STIFFENED COMPONENT OF PANEL A-GG-B-2. The fabrication of the second acoustic panel proceeded according to the plan described in III. 1. (b), but was halted following the FM-123-2 bonding (in one operation) of the skin to the stepped graphite-epoxy doubler and to the I-beam and tee section stiffeners with the following observations:

1. The skin was flat following the bonding, i.e., there was no oil canning.

2. The bond of the skin to the graphite-epoxy stepped doubler (see Figure 15) was satisfactory as evidenced by a visual inspection and a Fokker-bond test.

3. The bond of the graphite-epoxy skin to the graphite-epoxy I-beam and tee section details and the -37 doublers was unsatisfactory in several areas as evidenced by a visual inspection (see Figure 16) and a Fokker-bond test. The areas between the arrows of Figure 16 represent areas of defective bonds.

Because of the unsatisfactory subsassembly in item 3, above, the fabrication of acoustic panel A-GG-B-2 was halted to determine the cause of the defective subassembly and to plan remedial action. It was deemed unwise to ignore the defect or to attempt to repair the defect and utilize the subassembly in Panel A-GG-B-2, since it was considered that not enough worthwhile data would be obtained from the acoustic test to justify the cost of the final panel assembly, the instrumentation for the acoustic test, and the acoustic test itself.

The cause of the defect in the bonded subassembly was attributed to nonuniform pressure applied in the bonding operation, which may have existed (although to a lesser degree) during the fabrication of acoustic panel A-GG-B-1. (The premature fatigue failure of the acoustic panel A-GG-B-1 was finally attributed to nonuniform pressure during the bonding as well as to residual thermal stresses induced in the fabrication of panel A-GG-B-1 and to a biaxial stress state that existed during the acoustic test of panel A-GG-B-1).

The fabrication technique with the use of beads to apply pressure that had been proposed for the fabrication of panels A-GG-B-1 and A-GG-B-2 was based on the belief that the fabrication method, which was relatively inexpensive, would produce high quality advanced-composite panels for acoustic test. The application of beads to apply

FIGURE 15. VIEW OF GRAPHITE-EPOXY SKIN AND STEPPED DOUBLER OF BONDED SUBASSEMBLY

FIGURE 16. VIEW OF CROSS STIFFENERS OF BONDED GRAPHITE-EPOXY SUBASSEMBLY

the pressure during bonding had been successfully used in small programs of bonding metallic panels when it was uneconomical to fabricate precision form blocks that were needed in transmitting vacuum or autoclave pressure to the assembly. Because of the lack of success with the use of beads to obtain a satisfactory bond, the method outlined under Remedial Action below was then formulated as the preferable approach to obtain the desired uniform pressure to produce acoustic panel A-GG-B-2.

REMEDIAL ACTION. Various procedures (without changing the acoustic panel design) were considered for the successful fabrication of acoustic panels A-GG-B-2 and A-GG-B-3. The procedure described below was chosen and resulted in the successful manufacture of panels A-GG-B-2 and A-GG-B-3.

1. Fabrication of Graphite-Epoxy Doubler and 6-Ply Graphite-Epoxy Skins

   The graphite-epoxy doubler and 6-ply graphite-epoxy skin were fabricated as previously and trimmed to allow for final machining to the titanium frame dimensions.

2. Fabrication of Doubler/Skin Bond

   (a) The skin was laid up on a flate plate and the surface area to be bonded was sanded and MEK wiped.

   (b) The layer of FM-123-2 adhesive was placed on the doubler top face to be bonded. All graphite-epoxy surfaces to be bonded were light-sanded and MEK wiped.

   (c) The doubler was laid down on the skin surface and taped to insure index position.

   (d) The entire assembly was then vacuum bagged, checked and cured for 1 hour at 250F at 30 psig. Thermocouples were placed on the doubler and on the skin to obtain thermal differentials during cure.

   (e) After cure, the doubler/skin assembly was checked for warpage, etc. The adhesive flash was trimmed prior to the next steps.

3. Fabrication of Tee Section Details on Doubler/Skin Assembly-Prefit and Bond

   (a) The entire tool surface was covered with one layer of nonporous armalon and the doubler/skin assembly was laid up on the tool. The surfaces to be bonded were indexed; however, neither sanding nor MEK wipe was performed.

   (b) A simulated adhesive was placed on the surface to be bonded and the tee sections were laid up and taped in place.

   (c) The entire assembly was then vacuum bagged and cured using the cure cycle detailed in Step 2-d. Thermocouples were placed as above.

   (d) Upon completion of cure, the degree of uniformity of simulated adhesive deformation resulting from the pressure was ascertained.

   (e) Any shimming required was performed and the entire sequence (Steps 3-a through 3-d) repeated until the desired uniformity resulted.

(f) After completion of the prefit sequence, FM-123-2 adhesive was used and the cure accomplished as in Steps 3-a through 3-d.

4. Fabrication of I-Beam Details on Doubler/Skin Assembly — Prefit and Bond

(a) All titanium alloy rivet backup plates were phosphate-fluoride etched and cleaned and adhesive placed on the surfaces to be bonded.

(b) The I-beam details were covered on their respective to-be-bonded surfaces with a simulated adhesive as in Step 3. These details were then assembled on the skin/doubler assembly and taped to insure compliance with the index markings.

(c) A simulated cure cycle as in Step 2-d was performed after vacuum bagging. Extreme care was exercised to ensure uniform vacuum pressure on the surfaces to be bonded.

(d) After cure, the degree of pressure uniformity was evaluated and the necessary shimming performed. Steps 4-b through 4-d were repeated until the desired uniformity was accomplished.

(e) FM-123-2 adhesive was then placed on the sanded/MEK-wiped graphite-epoxy surfaces to be bonded and the entire assembly vacuum bagged and cured as in Steps 4-b through 4-d. All screws used as simulated rivets to provide alignment were coated with mold release prior to assembly.

5. Fabrication of Titanium Alloy Frame Assembly onto Doubler/Skin Assembly

(a) The titanium alloy assembly (frame) was phosphate-fluoride etched on the surface to be bonded.

(b) These surfaces were coated with EC 2216 adhesive and fitted to the doubler/skin/stiffener assembly and simultaneously riveted to the stiffener assembly. The bottom flange adjacent to the graphite-epoxy skin was clamped about the periphery to ensure uniform pressure over the EC 2216 bondline. A dam arrangement was placed on the graphite-epoxy skin in the outer 8 bays of the test box to ensure against flow of the EC 2216 over onto the skin. The entire assembly was heated to 100F for a period of 6 hours.

(c) Upon completion of the bonding operation, the panel was final trimmed to the applicable drawing dimensions, 10-32 flat head steel machine screws with elastic stop nuts were installed around the outer periphery of the panel (as an added precaution against a catastrophic acoustic fatigue failure), and the panel was delivered to instrumentation and test.

Before choosing the above fabrication plan, the effect of multiple cures on the FM-123-2 adhesive and the graphite-epoxy components was investigated. Data (Figure 17) furnished by the manufacturer of FM-123-2 adhesive had indicated that multicures do not markedly affect the tensile shear (i.e., lap shear) strength of FM-123-2 adhesive with 301 stainless steel adherends. In addition, quality control tests with FM-123 adhesive and graphite-epoxy adherends conducted by Northrop under three-stage multiple cures for another program had produced no evidence of significant degradation of the adhesive or adherends. Therefore, it was believed that the multiple cure of adhesive or adherends would not result in significant structural degradation when the fabrication procedure outlined above was followed.

FM-123-2 Adhesive Multiple Cure Cycles with 301 Stainless steel
Cure Cycle: 60 min. at 250°F. with 40 psi
This data is supplied by source other than our
Laboratories and is believed to be reliable

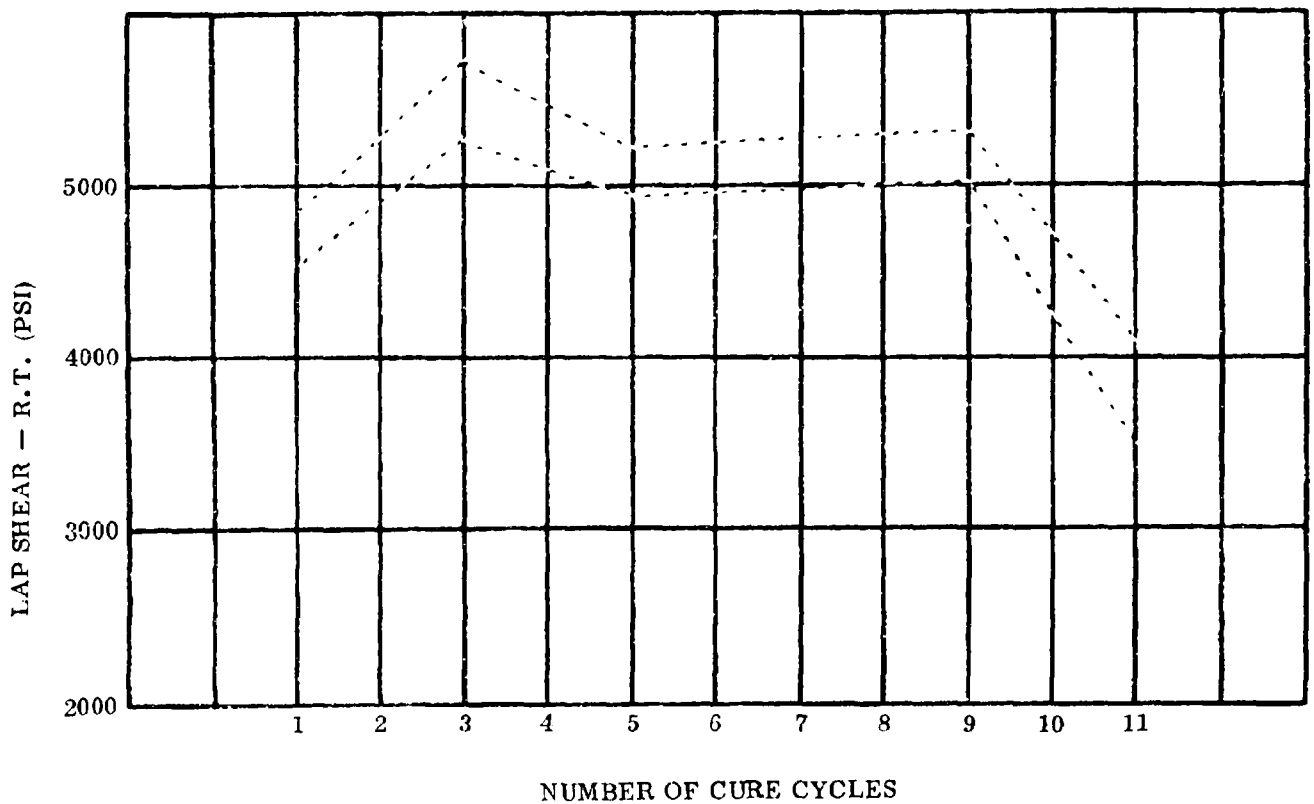

FIGURE 17. EFFECT OF MULTI-CURE CYCLES ON ADHESIVE STRENGTH

ASSEMBLY OF PANEL A-GG-B-3. The only defect in the rejected cross-stiffened component (Figure 16) for panel A-GG-B-2 was the adhesive bond between the skin and I-beam and tee section details. Therefore, it was possible to salvage the I-beam and tee section details and the graphite-epoxy doublers while destroying the graphite-epoxy skin and the FM-123-2 bond on both sides of the skin. Following the salvage operation, a new skin for panel A-GG-B-3 was manufactured and successfully bonded to the salvaged I-beam and tee section details and graphite-epoxy doubler according to the bonding procedure that resulted in the successful manufacture of the cross-stiffened detail of panel A-GG-B-2. The remainder of the manufacture of panel A-GG-B-3 prior to delivery to test followed the procedure used in manufacturing panel A-GG-B-2 except for minor items that are discussed below.

Glass doublers (Figure 18) were bonded around the periphery of the titanium alloy frame to prevent a frame failure such as had occurred near the end of the acoustic test of panel A-GG-B-2.

In riveting one clip attaching an I-beam detail with the titanium alloy frame, a misalignment between holes occurred and resulted in a small crack in the web of the I-beam near the frame. The crack was reinforced with a glass doubler (Figure 19). Because the crack was in the fixture portion of the test panel, the repair was not expected to (and apparently did not) affect appreciably the response of the central bay or even the response of the two bays adjacent to the crack.

III.2 SHAKER SPECIMENS

III.2.(a) Initial Design

An adhesive-bonded joint configuration and a riveted joint configuration were chosen for the test program. In the riveted joint configuration, a titanium alloy reinforcement was bonded to the skin prior to the riveting operation. The reinforcement was to provide skin thickness for the installation of countersunk rivets in joining the thin gage skin to the internal structure and for the satisfactory performance of the riveted joints in a fatigue application. Countersunk rivets were used in the shaker test program in order to maintain flat surfaces that are expected for service requirements under acoustic exposure. The two joint configurations for the shaker test program are representative of designs used frequently in aircraft.

For the shaker test specimens three skin to internal structure material combinations were chosen. The material combinations and the types of joints are summarized in Table I.

TABLE I. TYPES OF SHAKER TESTS

MATERIAL COMBINATIONS		TYPE OF JOINT
SKIN	INTERNAL STRUCTURE	
Graphite-Epoxy	Graphite-Epoxy	Adhesive-bonded
Graphite-Epoxy	Graphite-Epoxy	Riveted
Graphite-Epoxy	6Al-4V Titanium Alloy	Adhesive-bonded
Graphite-Epoxy	6Al-4V Titanium Alloy	Riveted
Boron-Epoxy	6Al-4V Titanium Alloy	Adhesive-bonded
Boron-Epoxy	6Al-4V Titanium Alloy	Riveted

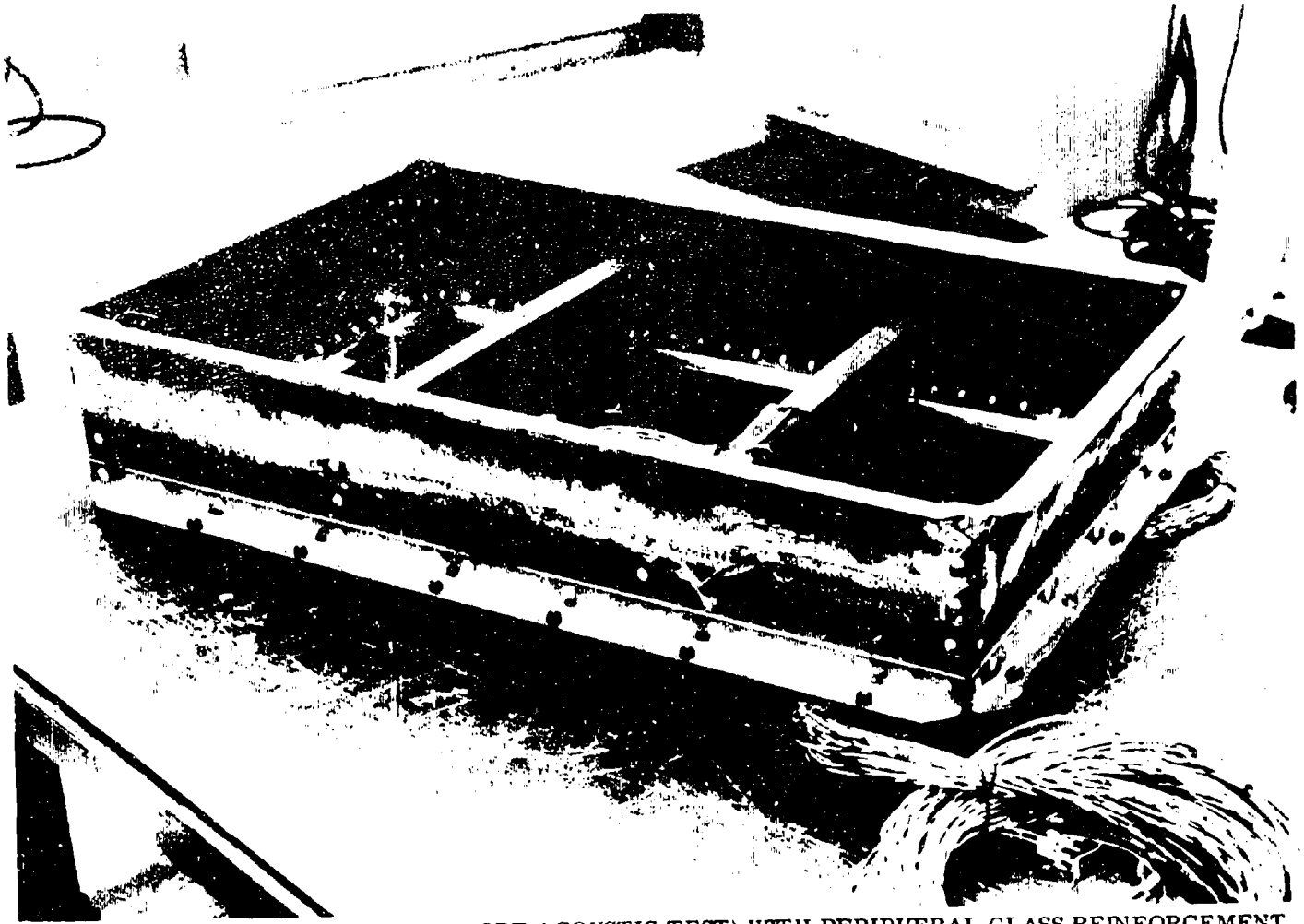

FIGURE 18. PANEL A-GG-B-3 (BEFORE ACOUSTIC TEST) WITH PERIPHERAL GLASS REINFORCEMENT

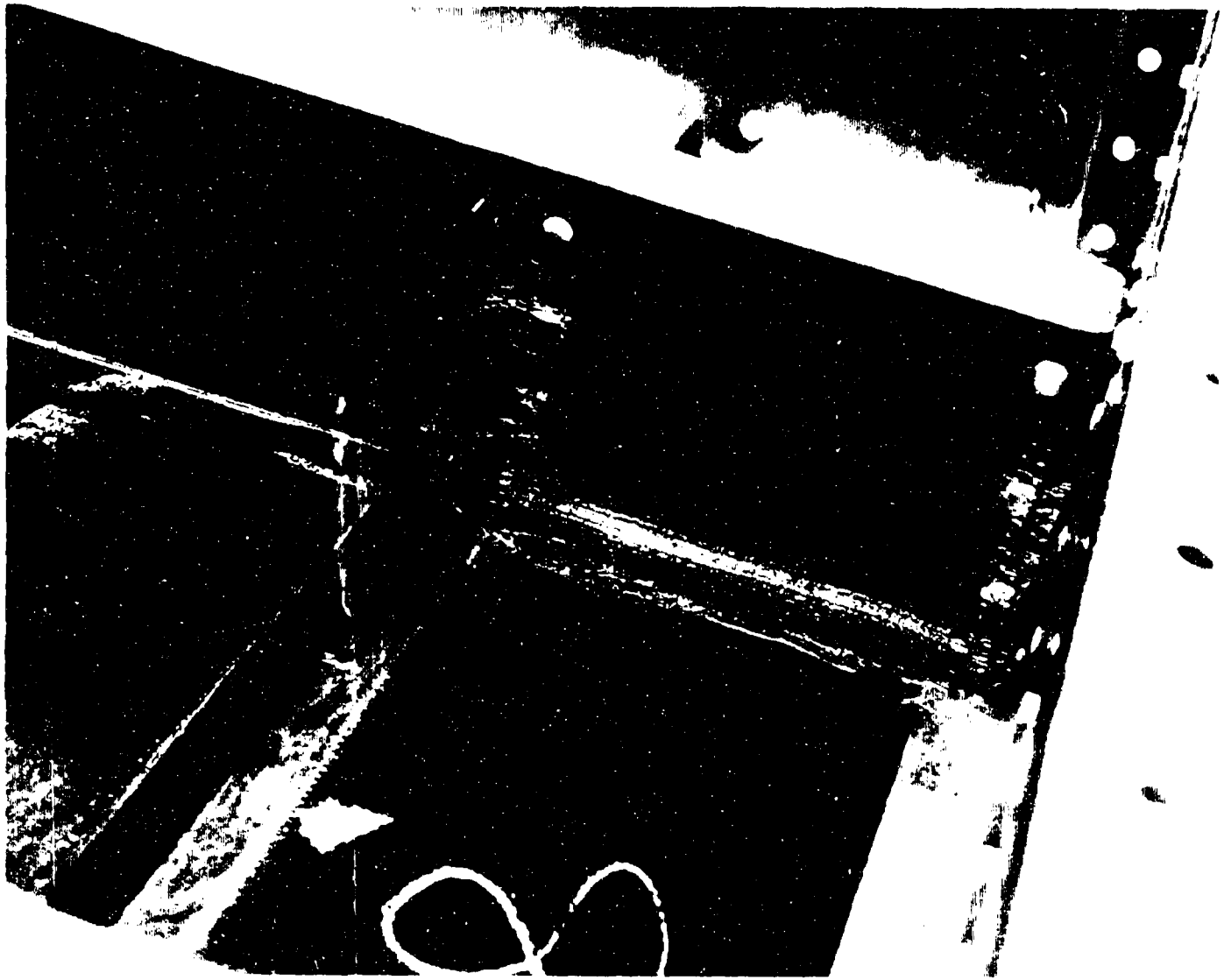

FIGURE 19. REPAIR OF A WEB OF AN I-SECTION OF PANEL A-GG-B-3

Two shaker specimen configurations designated as Candidate A-1 specimens (Figure 20) and Candidate A-2 specimens (Figure 21) were investigated before a choice was made to proceed with Candidate A-2 type specimens. The detail design of the specimens in Figures 20 and 21 is in drawings ACD-G-235, ACD-G-236, and ACD-B-216, which are Figures 22, 23, and 24, respectively.

The left side of Figure 20 presents information on shaker specimens simulating ribs bonded to skin, whereas the right side presents information on shaker specimens simulating ribs riveted to skin. The planned number of specimens and material combinations for skins and ribs is at the bottom of each side of Figure 20. The left side of Figure 21 presents information on shaker specimens simulating stringers bonded to skin, whereas the right side presents information on shaker specimens simulating stringers riveted to skin. The planned number of specimens and material combinations for skins and stringers is at the bottom of each side of Figure 21.

The discrepancy between the cross sections of ribs (stringers) in Figure 20 (Figure 21) and the ribs (stringers) in drawings ACD-G-235, ACD-G-236, and ACD-B-216 was intentional. The geometry of the ribs and stringers in Figures 20 and 21 are expected in service. Because in the experimental shaker program to be discussed subsequently, the ribs (stringers) were to be clamped to the test fixture, only the portion of the rib (stringer) between the clamp and skin was to be fabricated as shown in drawings ACD-G-235, ACD-G-236, and ACD-B-216.

For Candidates A-1 and A-2 shaker specimens, the ends of the beam specimen were to be fastened to the shaker by means of a test fixture. The lengths of the specimens were selected to obtain approximately the expected fundamental frequency at the center bay of the acoustic test panels.

Negligible motion of the ribs and stringers of the acoustic test panels had been predicted in the preliminary analysis. Therefore, for the shaker tests the rib at the center of the Candidate A-1 specimens and the stringer at the center of the Candidate A-2 specimens were to be fastened to the test fixture to prevent relative lateral motion between the rib and the two ends of the Candidate A-1 specimens and between the stringer and the two ends of the Candidate A-2 specimens. With two bay shaker specimens, it was expected that nonlinear response data could be obtained that could be used in the design of acoustic panels.

The shaker test fixture was designed to achieve the clamped-edge conditions and to provide the capability of testing three shaker specimens simultaneously.

The final choice between the Candidate A-1 and Candidate A-2 shaker specimens was postponed until after the first acoustic panel was tested in order to observe the experimental mode of failure, if any, (i.e., failure of a joint assembly at a stringer or at a rib) before selecting and fabricating the shaker test specimens. The Candidate A-1 shaker specimen was to be chosen if the initial joint failure of the remaining acoustic panels could be expected to occur at a rib whereas the Candidate A-2 shaker specimen was to be chosen if the initial joint failure of the remaining acoustic panels could be expected to occur at a stringer. Another reason for postponing the decision between the Candidate A-1 and Candidate A-2 specimens was to enable analytic predictions to be made on the relative merits of the two shaker specimen types. Following the test of the first acoustic test panel (panel A-GG-B-1), the decision was made to go ahead with the manufacture and test of the Candidate A-2 type specimens.

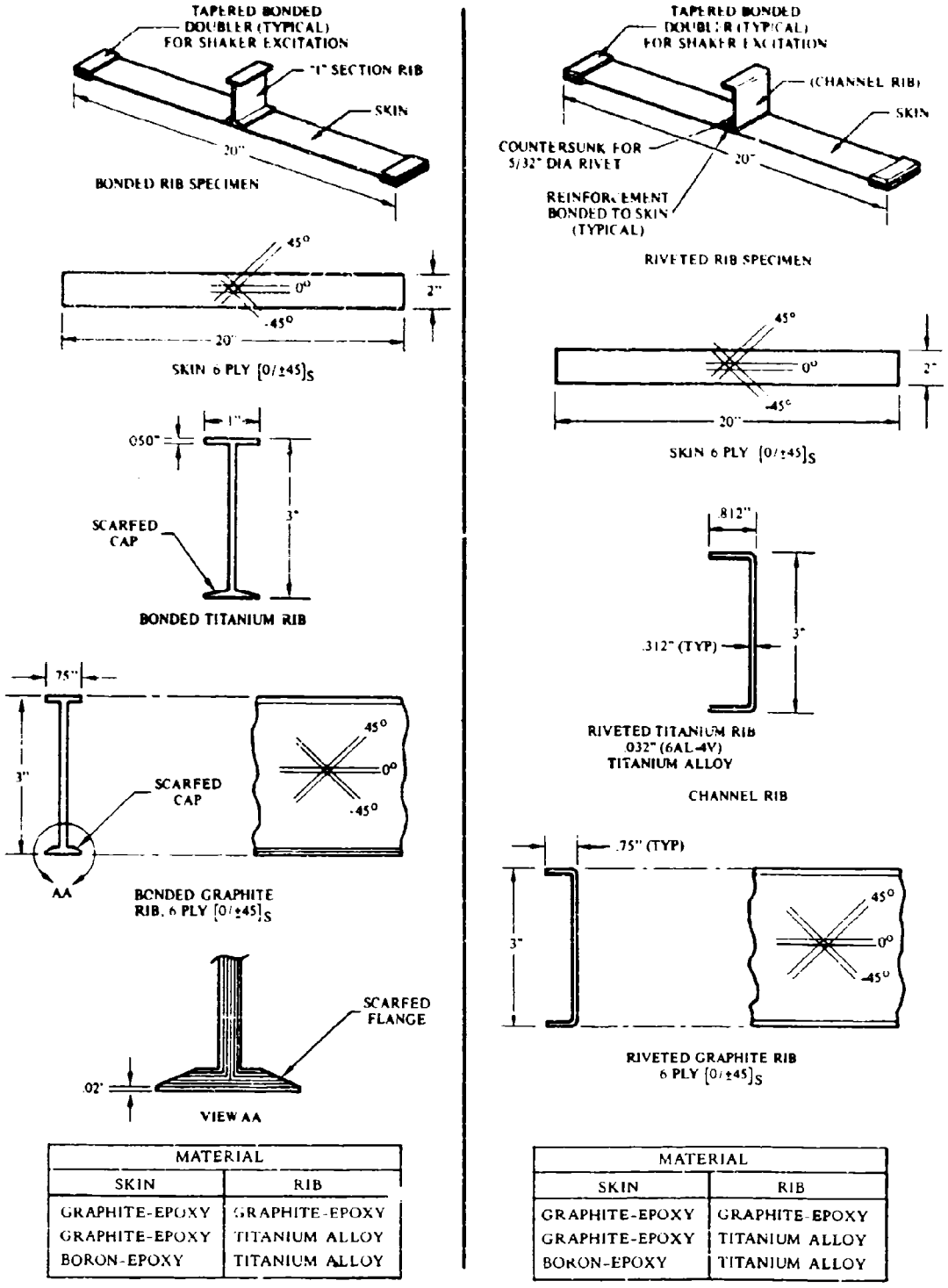

MATERIAL	
SKIN	RIB
GRAPHITE-EPOXY	GRAPHITE-EPOXY
GRAPHITE-EPOXY	TITANIUM ALLOY
BORON-EPOXY	TITANIUM ALLOY

MATERIAL	
SKIN	RIB
GRAPHITE-EPOXY	GRAPHITE-EPOXY
GRAPHITE-EPOXY	TITANIUM ALLOY
BORON-EPOXY	TITANIUM ALLOY

FIGURE 20. CANDIDATE A-1 SHAKER SPECIMENS

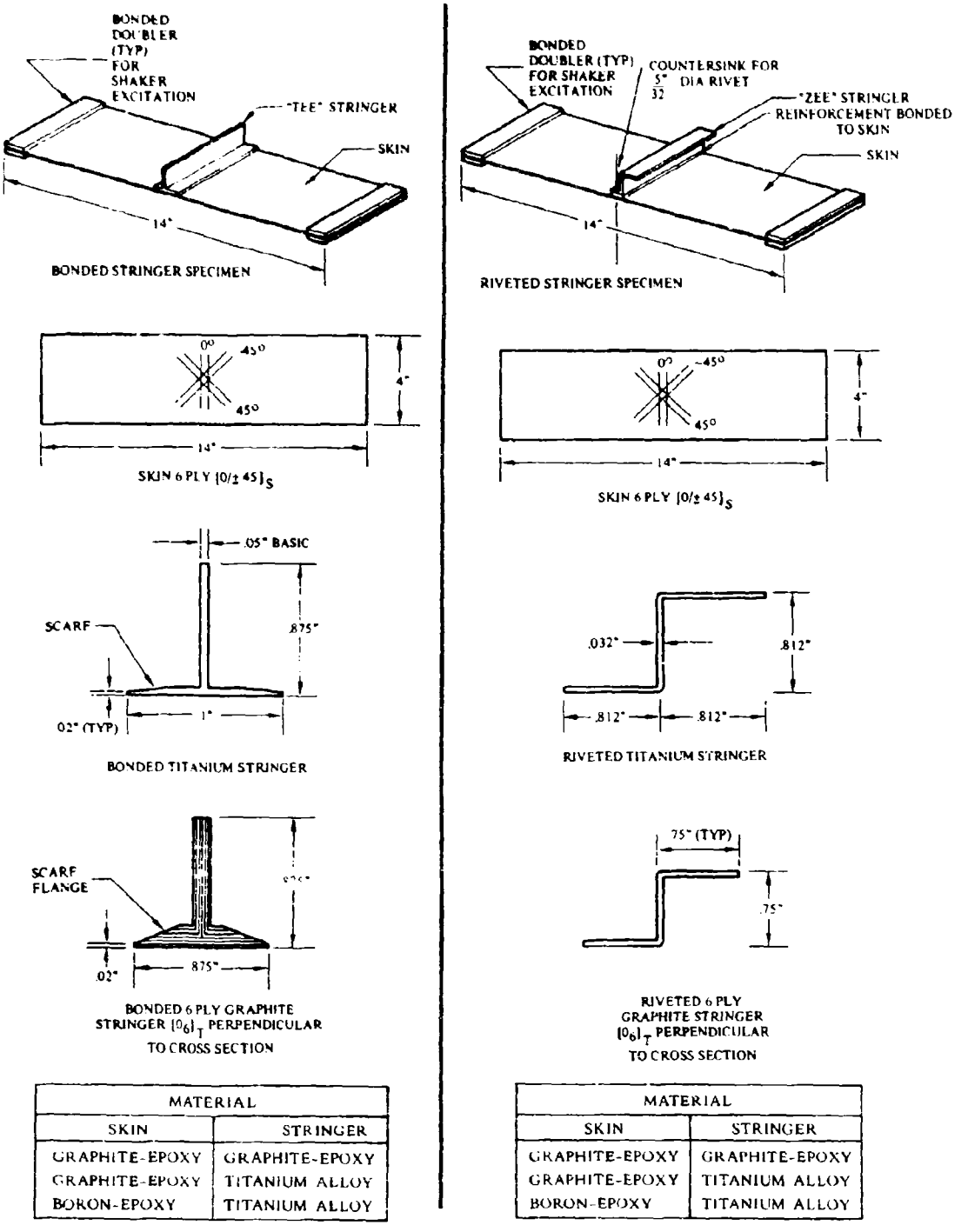

MATERIAL	
SKIN	STRINGER
GRAPHITE-EPOXY	GRAPHITE-EPOXY
GRAPHITE-EPOXY	TITANIUM ALLOY
BORON-EPOXY	TITANIUM ALLOY

MATERIAL	
SKIN	STRINGER
GRAPHITE-EPOXY	GRAPHITE-EPOXY
GRAPHITE-EPOXY	TITANIUM ALLOY
BORON-EPOXY	TITANIUM ALLOY

FIGURE 21. CANDIDATE A-2 SHAKER SPECIMENS

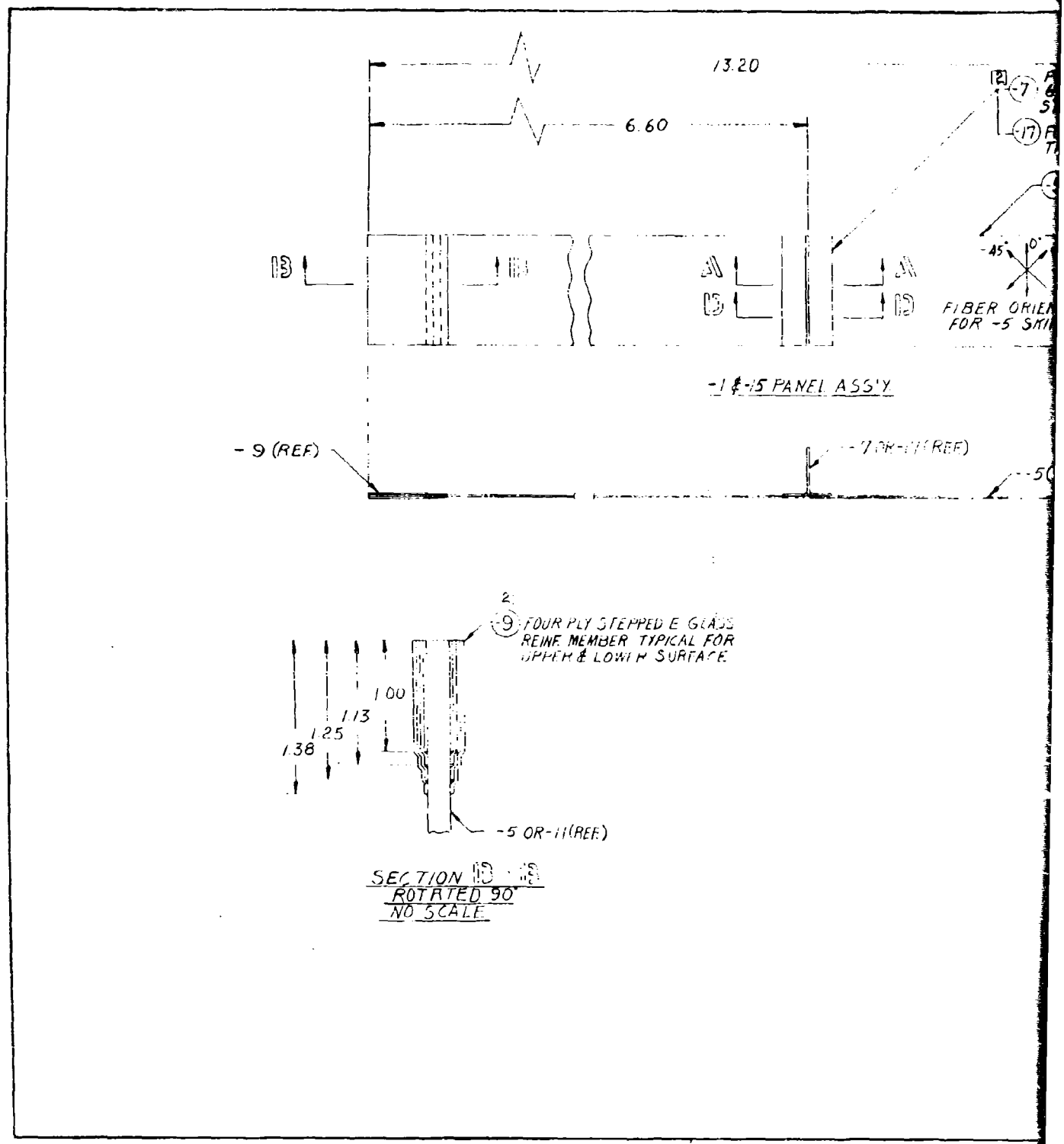

FIGURE 22. GRAPHITE-EPOXY SHAKER TEST SPECIMENS (BONDED SPECIMENS)

PRECEDING PAGE BLANK-NOT FILMED.

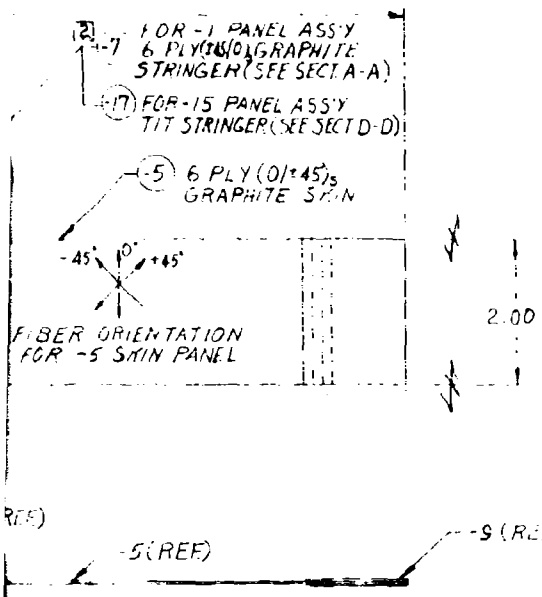

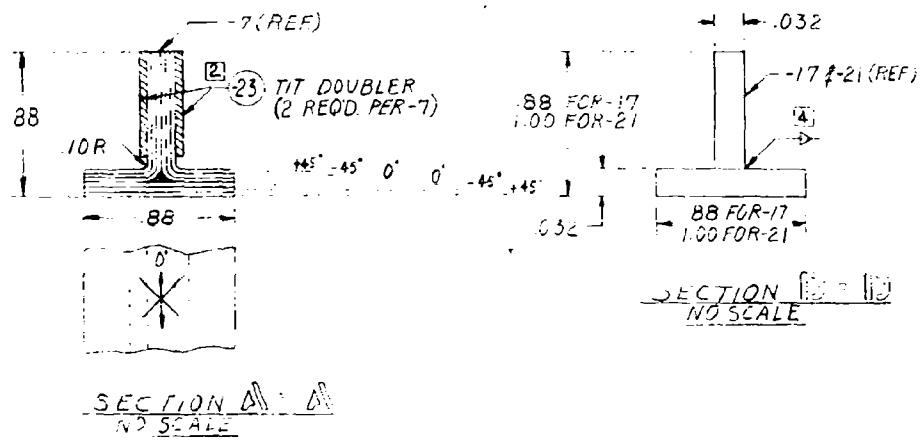

2

PRECEDING PAGE BLANK-NOT FILMED.

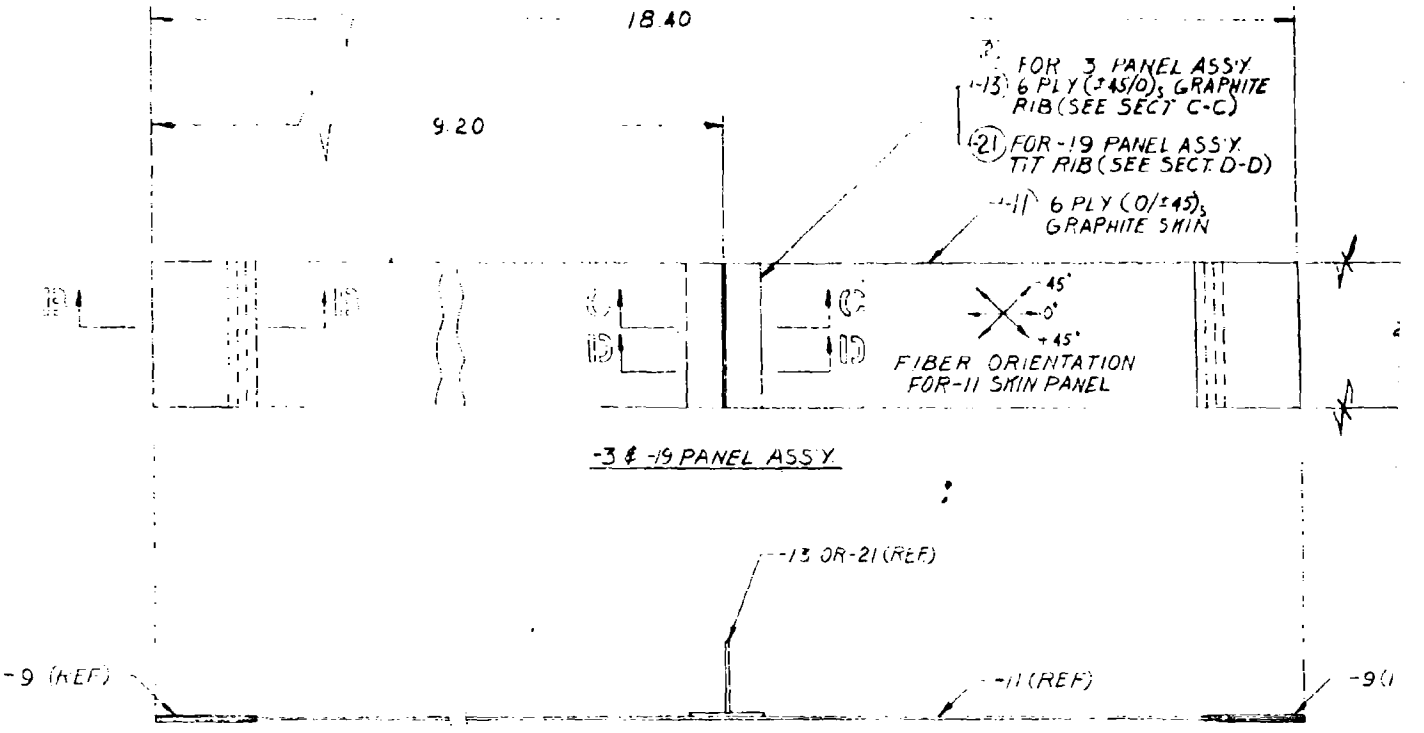

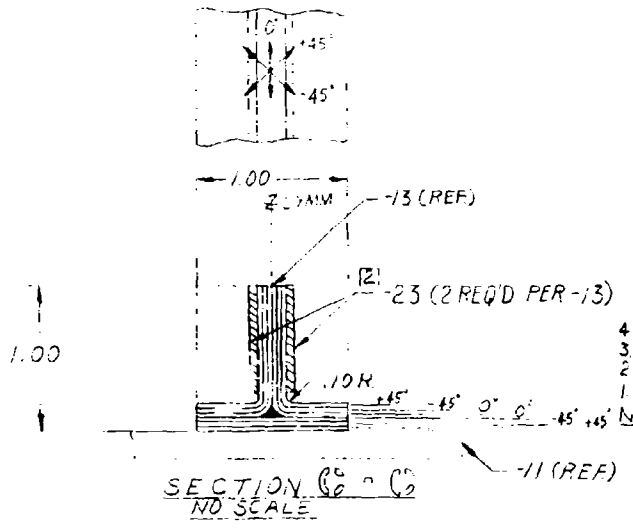

NOTES UNLESS OTHERWISE SPECIFIED:
1. MAKE FROM FOTHERGILL & HARVEY 4617/COURTAULDS HT-S
2. USE FM-123-2 ADHESIVE TO BOND -7, -9 & -17 TO -5; -9, -13 & -21 TO -11; -23 TO -7 AND
3. USE MATERIAL IN ANNEALED CONDITION. NO HEAT TREAT REQ'D
4. STRESS RELIEVE AFTER WELDING

3

PRECEDING PAGE BLANK-NOT FILMED.

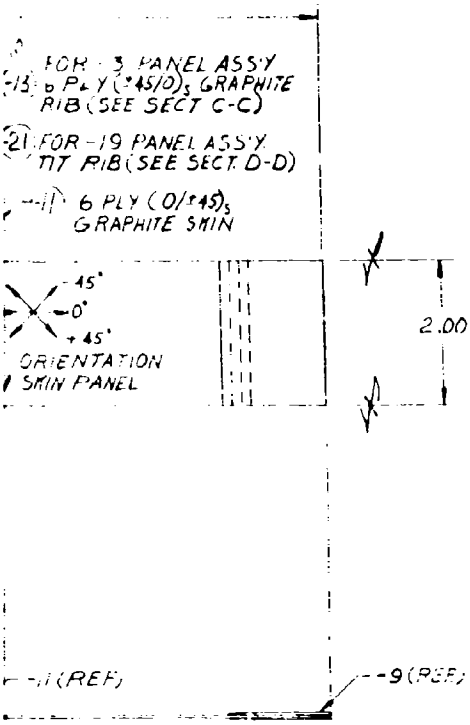

PER -19	PER -15	PER -3	PER -1								
		2	2	-23	3	DOUBLER	TIT (6AL-4V)	.020 x 3/4 x 2	MIL-T-9046		
1				-21	3, 4	RIB	TIT (6AL-4V)	1 x 1 x 2 1/2	MIL-T-9046		
				-19		PANEL ASS'Y					
	1			-17	3, 4	STRINGER	TIT (6AL-4V)	1 x 1 x 2 1/2	MIL-T-9046		
				-15		PANEL ASS'Y					
		1		-13	1	RIB	GRAPHITE COMPOSITE	6 PLIES 2 x 2 1/2			
1		1		-11	1	SKIN	GRAPHITE COMPOSITE	6 PLIES 3 x 20			
4	4	4	4	-9		EDGE MEMBER REINF.	150/181 E-GLASS	4 PLIES 2 x 2 1/2			
			1	-7	1	STRINGER	GRAPHITE COMPOSITE	6 PLIES 2 x 3			
	1		1	-5	1	SKIN	GRAPHITE COMPOSITE	6 PLIES 3 x 14 1/2			
				-3		PANEL ASS'Y					
				-1		PANEL ASS'Y					
PART OR IDENTIFYING NO.				SEE NOTES	NOMENCLATURE OR DESCRIPTION		MATERIAL OR CODE IDENT NO.	SIZE OR PROCUREMENT DATA		ZONE	ITEM

PARTS LIST

...DING
CONDITION NO HEAT TREAT REQ'D
...ND -7-9 & -17 TO -5; -9, -13 & -21 TO -11; -23 TO -7 AND -23 TO -13
...EY 4617/COURTAULDS HT-S
...ECIFIED:

UNLESS OTHERWISE NOTED
LINEAR TOLERANCES X = ±.1, XX = ±.04, XXX = ±.010
LINEAR DIM. ARE IN INCHES
ANGULAR TOL EXCEPT SHEET METAL FLG ± 0° 30'
...TANCE TOL PER ... 10V201
FINISH PER NORAIR SPEC NO'S
ODD DASH NO. SHOWN EVEN DASH NO. OPPOSITE

CONTRACT NO.
DRAWN P.J. DANA 6/1/70
DESIGN
CHECKED
PROGRAM
NORAIR APPROVAL
OTHER APPROVAL

NORTHROP NORAIR
A DIVISION OF NORTHROP CORPORATION, HAWTHORNE, CALIF.

SHAKER TEST SPECIMENS
GRAPHITE COMPOSITE
(BONDED SPECIMENS)

SIZE
CODE IDENT NO. 7682.
ACD-G-235
SCALE FULL & NOTED
SHEET OF

4

PRECEDING PAGE BLANK-NOT FILMED.

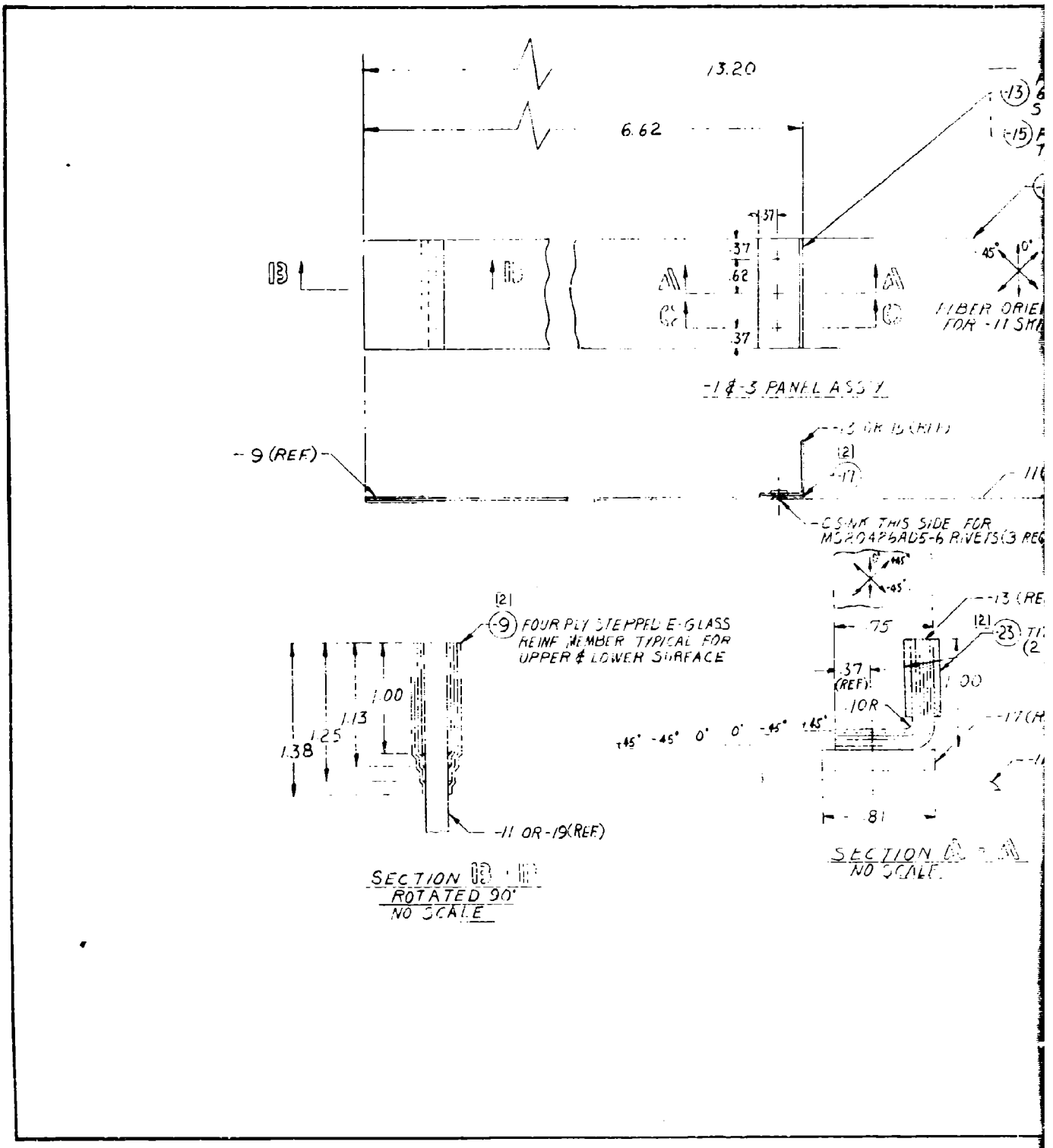

FIGURE 23. GRAPHITE-EPOXY SHAKER TEST SPECIMENS (RIVETED SPECIMENS)

PRECEDING PAGE BLANK-NOT FILMED.

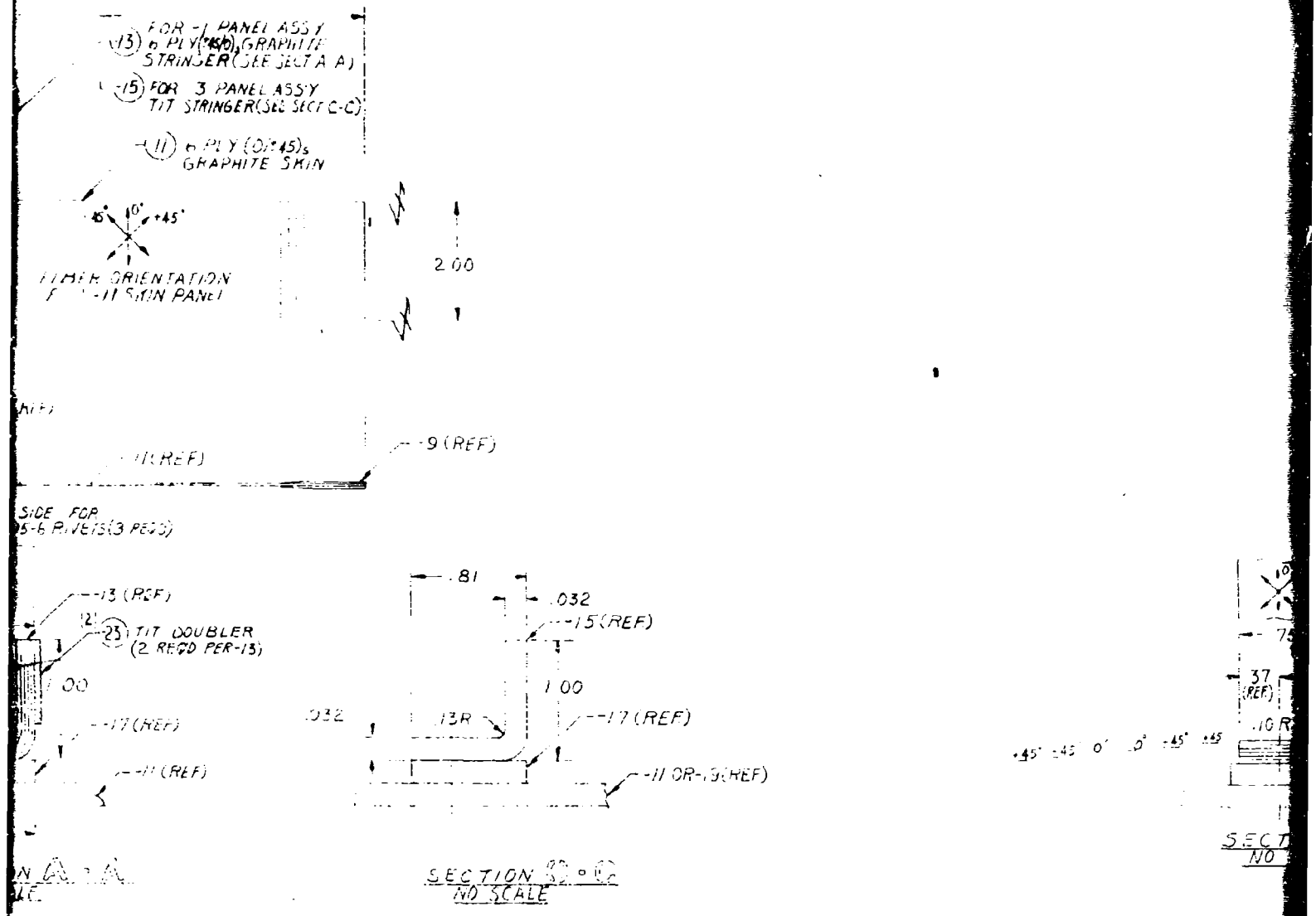

2

PRECEDING PAGE BLANK-NOT FILMED.

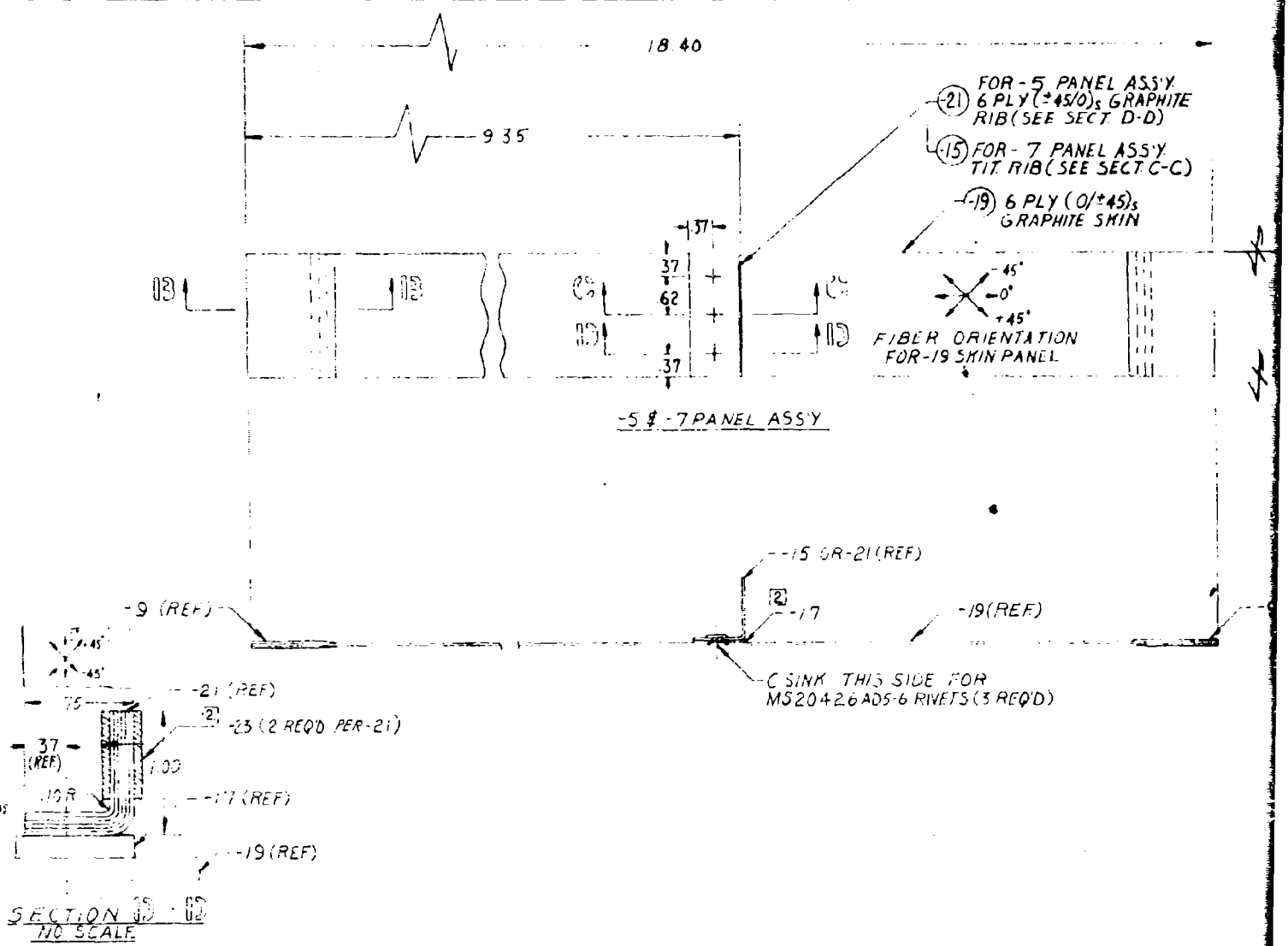

4. STRESS RELIEVE AFTER FORMING
3 USE MATERIAL IN ANNEALED CONDITION. NO HEAT TREAT REQ'D.
2 USE FM-123-2 ADHESIVE TO BOND 9 & -17 TO -11, -9 & -17 TO -19, -23 TO -1
1 MAKE FROM FOTHERGILL & HARVEY 46177 COURTAULDS
NOTES UNLESS OTHERWISE SPECIFIED:

3

PRECEDING PAGE BLANK-NOT FILMED.

FOR -5 PANEL ASS'Y
6 PLY (±45/0)$_s$ GRAPHITE
RIB (SEE SECT D-D)

FOR -7 PANEL ASS'Y
T.T. RIB (SEE SECT C-C)

(9) 6 PLY (0/±45)$_s$
GRAPHITE SKIN

-45°
-0°
+45°
ENTATION
IN PANEL

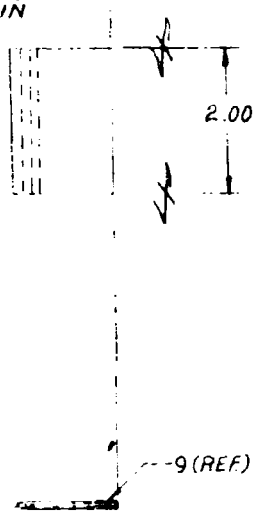

(3 REQ'D)

	2		2	-23	3	DOUBLER	TIT (6AL-4V)	.020x1½x2	MIL-T-9046		
3	3	3	3			RIVET (FLUSH HD)	MS20426AD5-6				
	1			-21	1	RIB	GRAPHITE COMPOSITE	6 PLIES 2 x 3			
1	1			-19	1	SKIN	GRAPHITE COMPOSITE	6 PLIES 3 x 20			
1	1	1	1	-17	3	DOUBLER	TIT (6AL-4V)	.040x1x2½	MIL-T-9046		
1		1		-15	3, 4	STR. OR RIB	TIT (6AL-4V)	.032x2x2½	MIL-T-9046		
			1	-13	1	STRINGER	GRAPHITE COMPOSITE	6 PLIES 2 x 2½			
		1	1	-11	1	SKIN	GRAPHITE COMPOSITE	6 PLIES 3 x 14½			
4	4	4	4	-9		EDGE MEMBER REINF.	150/181 E-GLASS	4 PLIES 2 x 2½			
				-7		PANEL ASS'Y					
				-5							
				-3							
				-1		PANEL ASS'Y					

PART OR IDENTIFYING NO.	SIZE NOTED	NOMENCLATURE OR DESCRIPTION	MATERIAL OR CODE IDENT NO.	SIZE OR PROCUREMENT SPEC.	NOT SHOWN ON DWG	ZONE	REVISIONS

PARTS LIST

TION NO HEAT TREAT REQ'D.
-9 -17 TO -11, -9 & -17 TO -19, -23 TO -13 AND -23 TO -21
BETWEEN CONTAINING 2 PLIES
TED.

UNLESS OTHERWISE NOTED
LINEAR TOLERANCES X = ±.1, XX = ±.06, XXX = ±.010
LINEAR DIM. ARE IN INCHES
ANGULAR TOL EXCEPT SHEET METAL FLB = 0° 30'
MFG ACCEPTANCE TOL PER NORAIR STD 10V201
FINISH PER NORAIR SPEC NFS
ODD DASH NO. SHOWN EVEN DASH NO. OPPOSITE

CONTRACT NO.
DRAWN P. I. DANNA 6/19/76
DESIGN
CHECKED
PROGRAM
NORAIR APPROVAL
OTHER APPROVAL

NORTHROP NORAIR
A DIVISION OF NORTHROP CORPORATION, HAWTHORNE, CALIF.

SHAKER TEST SPECIMENS
GRAPHITE COMPOSITE
(RIVETED SPECIMENS)

SIZE | CODE IDENT NO. 76823 | ACD-G-236
SCALE FULL & NOTED | SHEET OF

4

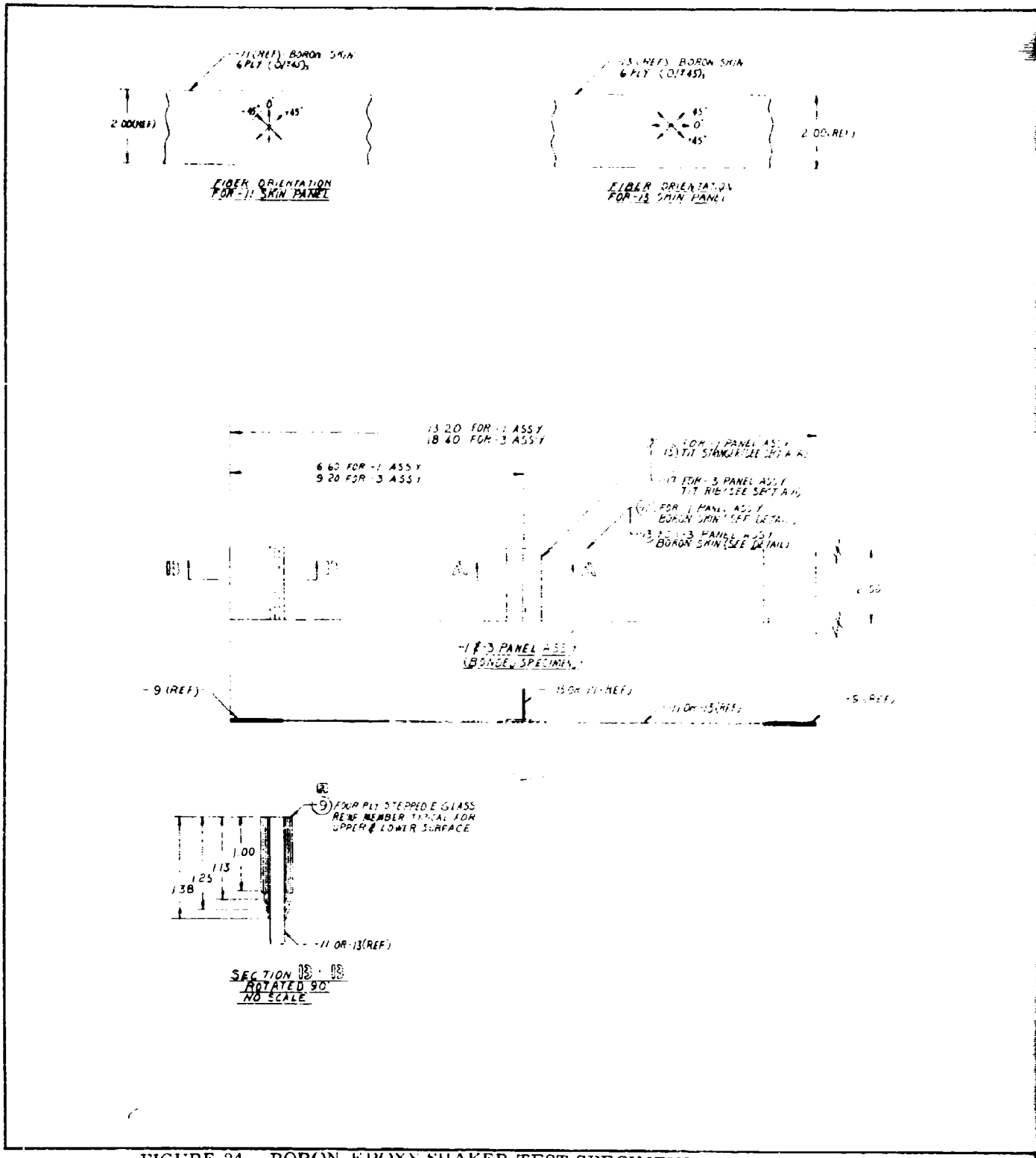

FIGURE 24. BORON-EPOXY SHAKER TEST SPECIMENS

PRECEDING PAGE BLANK-NOT FILMED.

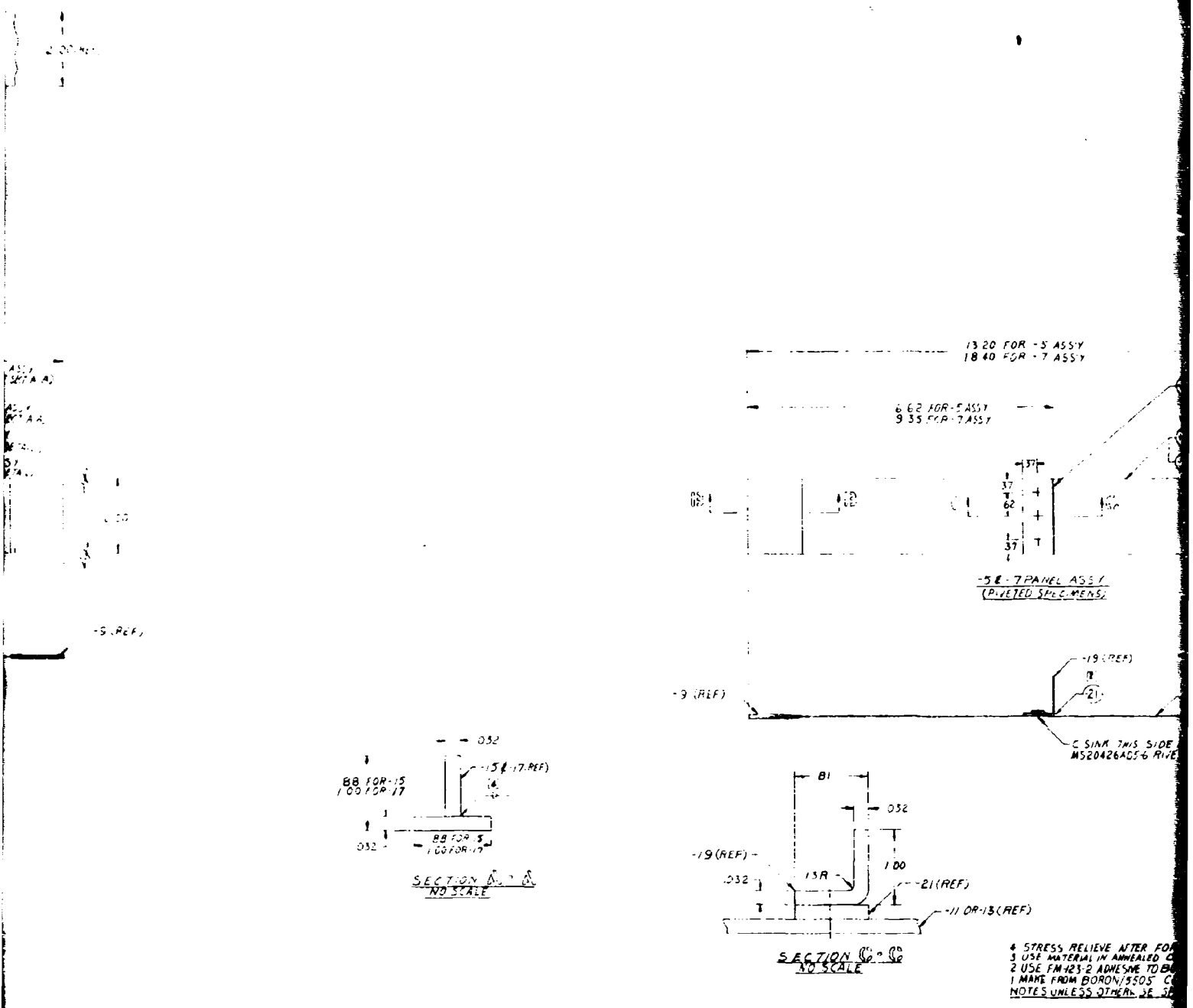

2

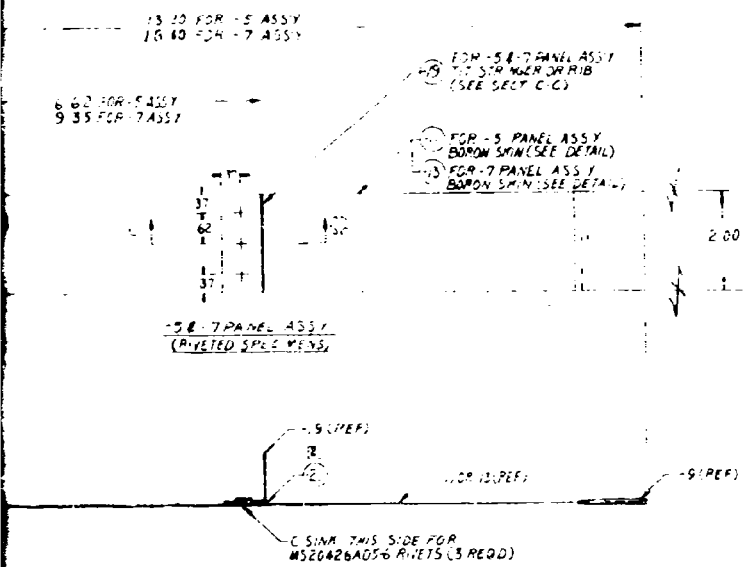

4 STRESS RELIEVE AFTER FORMING OR WELDING
3 USE MATERIAL IN ANNEALED CONDITION NO HEAT TREAT REQD
2 USE FM-123-2 ADHESIVE TO BOND -9,-15 & -21 TO -11 AND -9,-17 & -21 TO -13
1 MADE FROM BORON/5505 COMPOSITE (NARMCO)
NOTES UNLESS OTHERWISE SPECIFIED:

-7	-5	-3	-1						
3	3					RIVET (FLUSH HD)	MS20426AD5-6		
1	1			-21	3	DOUBLER	TIT (6AL-4V)	.060 x 1x2	MIL-T-9046
1	1			-19	3,4	STRINGER/RIB	TIT (6AL-4V)	.032 x 2 x 2	MIL-T-9046
		1		-17	3,4	RIB	TIT (6AL-4V)	1 x 1 x 2	MIL-T-9046
			1	-15	3,4	STRINGER	TIT (6AL-4V)	1 x 1 x 2	MIL-T-9046
1		1		-13	1	SKIN	BORON COMPOSITE	6 PLIES 3 x 20	
	1		1	-11	1	SKIN	BORON COMPOSITE	6 PLIES 3 x 10	
4	4	4	4	-9		FACE MEMBER BLANK	ISO/NBI E-GLASS	4 PLIES 2 x 12	
				-7		PANEL ASSY	(RIVETED)		
				-5		PANEL ASSY	(RIVETED)		
				-3		PANEL ASSY	(BONDED)		
				-1		PANEL ASSY	(BONDED)		

PARTS LIST

A DIVISION OF NORTHROP CORPORATION, HAWTHORNE, CALIF.

SHAKER TEST SPECIMENS
BORON/EPOXY COMPOSITE

ACD-B-216

3

III. 2. (b) Final Specimen Design

Several Candidate A-2 type specimens with graphite-epoxy skins bonded to graphite-epoxy doublers were fabricated using the design with the 13.20 inch length in Figure 22. During the shaker test of the first specimen with the two ends and the central tee section clamped, it was apparent that the design had resulted in a specimen that was too stiff to enable fatigue tests to be conducted at sufficient excitation levels to obtain S-N curves. Therefore, the decision was made to reduce the overall length of all the fabricated specimens by sawing off the glass doublers at the ends of the specimens that were already fabricated and to clamp the specimens only at the stiffener at the center of the specimen. The design change was satisfactory and resulted in the manufacture and fatigue test of shaker specimens without glass doublers at the ends. The tests of the shaker specimens resulted in the establishment of S-N data and curves that are reported in Section VI.

In the final shaker specimen design which applied to all the shaker specimens from which S-N data was obtained in the test program, the length of the graphite-epoxy skins was 9.24 inches and the length of the boron-epoxy skins was 9.62 inches. In the final shaker specimen design, the centerline of the leg of the tee section was 4.62 inches from each end of the bonded shaker specimens with graphite-epoxy skins and was 4.81 inches from each end of the bonded shaker specimens with boron-epoxy skins. The rivet centerline was 4.62 inches from each end of the riveted shaker specimens with graphite-epoxy skins and was 4.81 inches from each end of the riveted shaker specimens with boron-epoxy skins.

III. 2. (c) Manufacture of Shaker Specimens

The manufacturing procedure for the shaker specimens (exclusive of the manufacture and bonding procedure of the doublers that were bonded to the first few fabricated specimens but were subsequently sawed off before shaker testing) is described below.

Laminates, from which the skins of the shaker specimens were subsequently obtained, were layed up according to the design of the shaker specimens and were cured according to procedures established in the Northrop Process Specifications PL-35 and PL-36. The graphite-epoxy laminates were bagged and autoclave cured at 350 F for two hours at 100 psig. The boron-epoxy laminates were bagged and autoclave cured at 225 F for two hours followed by two hours at 325 F with 100 psig pressure applied throughout. The laminates were then sectioned with a diamond saw to get skins for the individual specimens.

The -23 titanium alloy doublers (of Figures 22 and 23) were bonded to the shaker specimens with EC 2216 adhesive rather than FM-123-2 adhesive in order to utilize a room temperature curing adhesive. The EC 2216 adhesive was adequate in transferring the relatively low skin stresses from the shaker test fixture to the shaker specimens. A photograph of a shaker specimen with the graphite-epoxy skin and stiffener prior to the bonding of the -23 titanium alloy doubler is shown in Figure 25. A photograph of the upper surface of a riveted shaker specimen after strain gaging is in Figure 26 and a photograph of the lower surface is in Figure 27.

The graphite-epoxy angle and tee sections were fabricated according to the procedures established for the internal structure of the acoustic test panels.

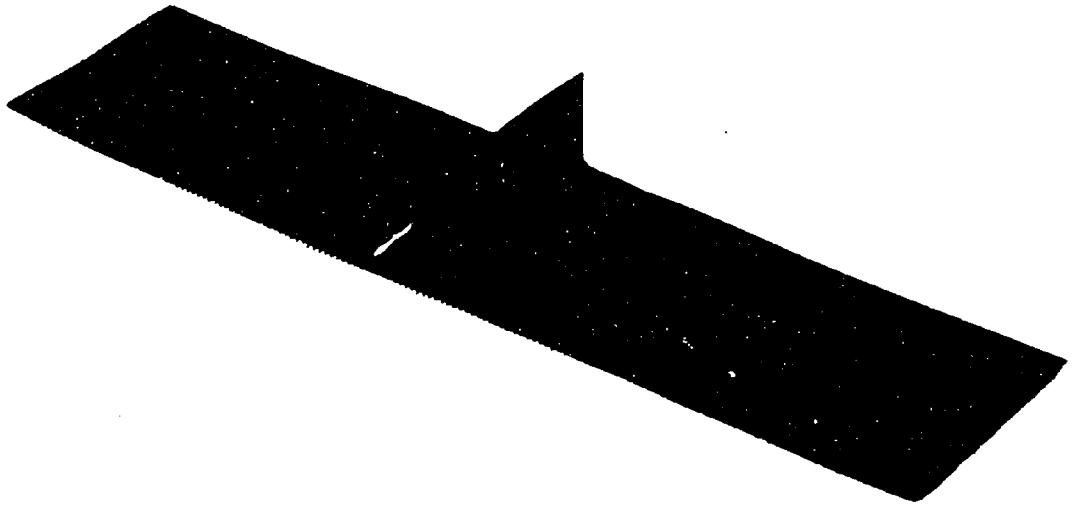

FIGURE 25. BONDED SHAKER SPECIMEN

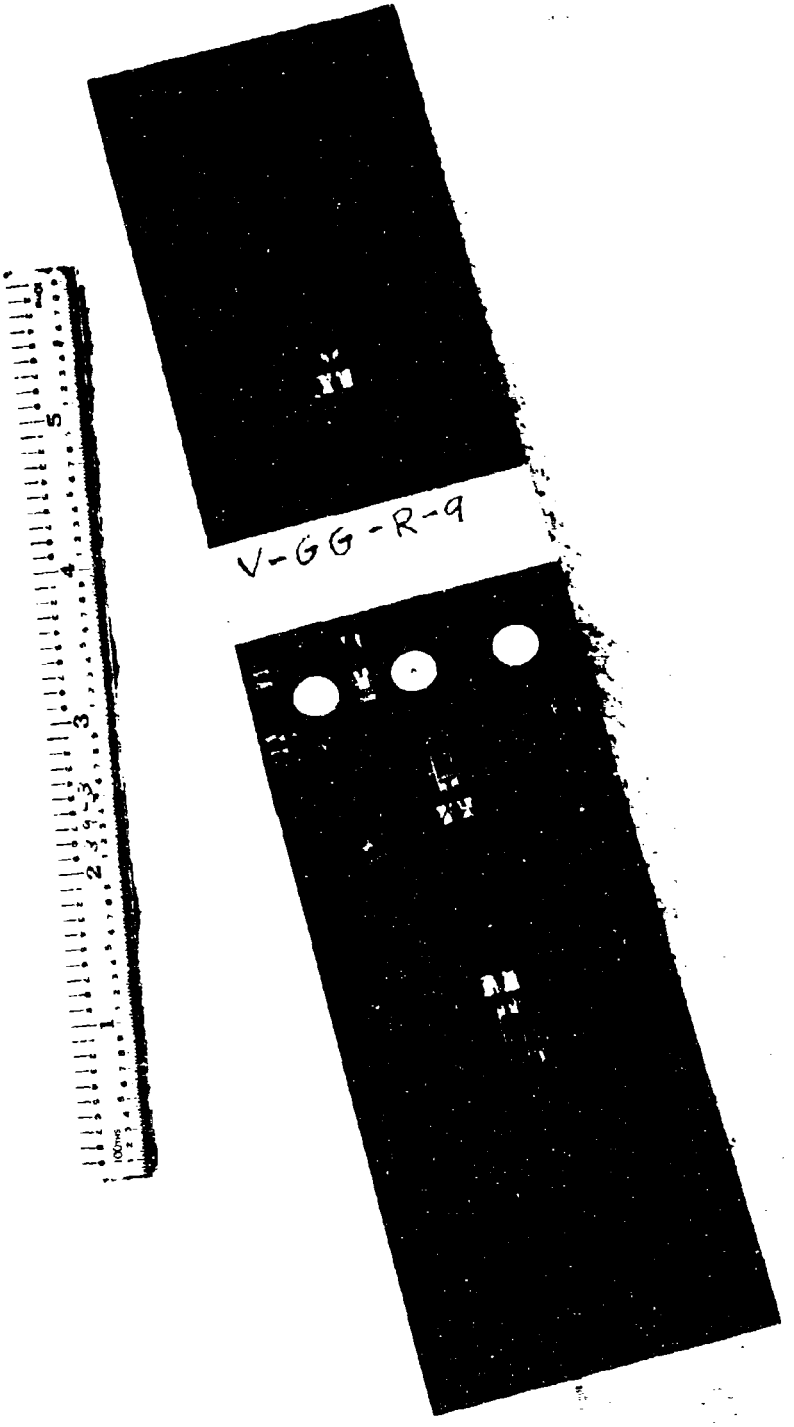

FIGURE 26. LOWER SURFACE OF A RIVETED SHAKER SPECIMEN

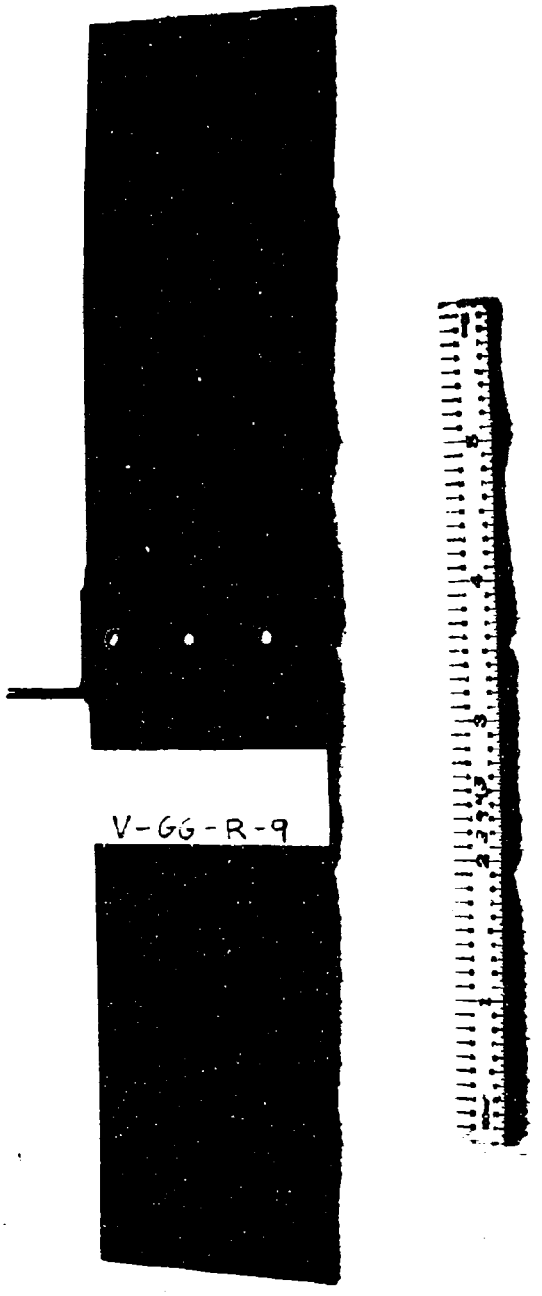

FIGURE 27. UPPER SURFACE OF A RIVETED SHAKER SPECIMEN

The fabrication of the titanium alloy tee sections was accomplished by the automatic G.T.A. (gas tungsten arc) weld process and equipment. The tee sections were constructed from two pieces of Ti-6Al-4V titanium sheet stock, the cap being .040 gage and the web being .032 gage. A weld fixture that accommodates a twenty-four inch long part was used to clamp the tee section components during the welding operation. The weldment was accomplished by burning through the cap member directly above the web, thereby fusing the cap and web together as well as creating a fillet along the backside of the welded part. The fillet size was controlled by the tool configuration. Filler wire was added to the joint to replace the metal that formed the fillet. Stress relieving was performed after welding. This was accomplished by clamping the part in a sizing tool and heating to 1250F for thirty minutes. After stress relieving and the cleaning operation, the twenty-four inch long part was sectioned into two-inch lengths for machining and trimming to final size. The weld bead and .008 excess material on the topside of the cap were machined by a conventional milling operation resulting in the desired flat surface and correct gage thickness.

Fabrication of the .032 gage x 3/4 x 3/4 x 2.0 inch titanium alloy angle sections was accomplished using conventional brake punch and die forming tools at room temperatures. Neither stress relief nor hot sizing was required.

A description of the fabrication of the bonded joint shaker specimens follows. The graphite-epoxy skin and stiffeners and the titanium alloy stiffeners were precleaned according to the appropriate of the Northrop Process Specifications PL-35 and PL-36. The stiffeners to be bonded to the skin were then layed up on an FM-123-2 adhesive prepreg sheet and then located on the shaker specimen skins. The parts were then bagged and vacuum pulled to set the adhesive. A one-hour cure cycle at 250F at 40 psig was then performed, and the adhesive flash was then trimmed using a belt sander. The titanium alloy doublers, that were subsequently clamped in the shaker test fixture during the shaker tests, were then clipped to the leg of the graphite-epoxy tee sections, and bonding was performed with EC 2216 adhesive at room temperature.

For the riveted shaker specimens, the bonding of the reinforcements to the skin of the riveted specimens followed the same procedure described above for bonding the skin to the tee or angle sections of the bonded shaker specimens. The countersunk rivets were then installed to attach the skin to the internal structure, i.e., the tee or angle sections. The titanium alloy doublers (when used), that were subsequently clamped in the shaker test fixture during the shaker tests, were then clipped to the leg of graphite-epoxy angles, and bonding was performed with EC 2216 adhesive at room temperature.

IV. APPROACH TO THE ACOUSTIC TEST PROGRAM

IV.1 OBJECTIVE

The basic objective of the acoustic tests was to obtain dynamic and acoustic fatigue characteristics of the joint assemblies of advanced-composite panels in a high intensity acoustic environment. The panel configuration for the acoustic tests was chosen to be compatible with present and expected future flight vehicle requirements.

IV.2 TEST CONDITIONS

The acoustic panels were bolted to a jig plate for acoustic testing (Figure 28) in the 48 x 48-inch test cell of the Northrop Progressive Wave Acoustic Test Chamber (Figure 29). The frames of the acoustic panels were to simulate adjacent structure in aircraft skin-rib structure, and were designed to prevent failures at the frames.

Each acoustic panel was attached to the test fixture (the jig plate in Figure 28) which, in turn, fit into the upper wall of the Northrop Progressive Wave Acoustic Test Chamber. The attachment detail design was based on preliminary analysis which satisfied the following criteria:

1. The acoustic failure would not initiate along the edge members.

2. The flexibility of the edge members as attached to the fixture would simulate the flexibility of the neighboring repetitive structures that are identical to the test specimen. In this manner, the test specimen responds to the acoustic excitation as part of a large and realistic aircraft structure assembly.

To satisfy the above two criteria, the nominal dimensions of the nine-bay acoustic panels were established at 26 x 17 inches and the panels had a rectangular, central bay that was larger than any of the other eight rectangular bays. The central bay was a nominal 10 x 7 inches, the four corner bays were a nominal 8 x 5 inches, and the remaining four exterior bays were either 10 x 5 inches or 8 x 7 inches nominally.

The approach of reducing the dimension of the edge bays of nonstiffened, acoustic test panels had been successful [6] in obtaining acoustic fatigue failures at the center bay of cross-stiffened 9-bay rectangular panels (3 bays in each direction), 25-bay rectangular panels (5 bays in each direction), and 49-bay rectangular panels (7 bays in each direction). After testing the 49-bay, the 25-bay, and the 9-bay panels, it was noted in Reference 6 that dynamic and acoustic fatigue characteristics of the central bay of both the 49-bay and 25-bay panels were obtained approximately in tests of the 9-bay panels.

Three-bay aluminum alloy panels with bays of dimensions similar to those of the proposed acoustic test panels had been tested with acoustic fatigue failures occurring

Preceding page blank

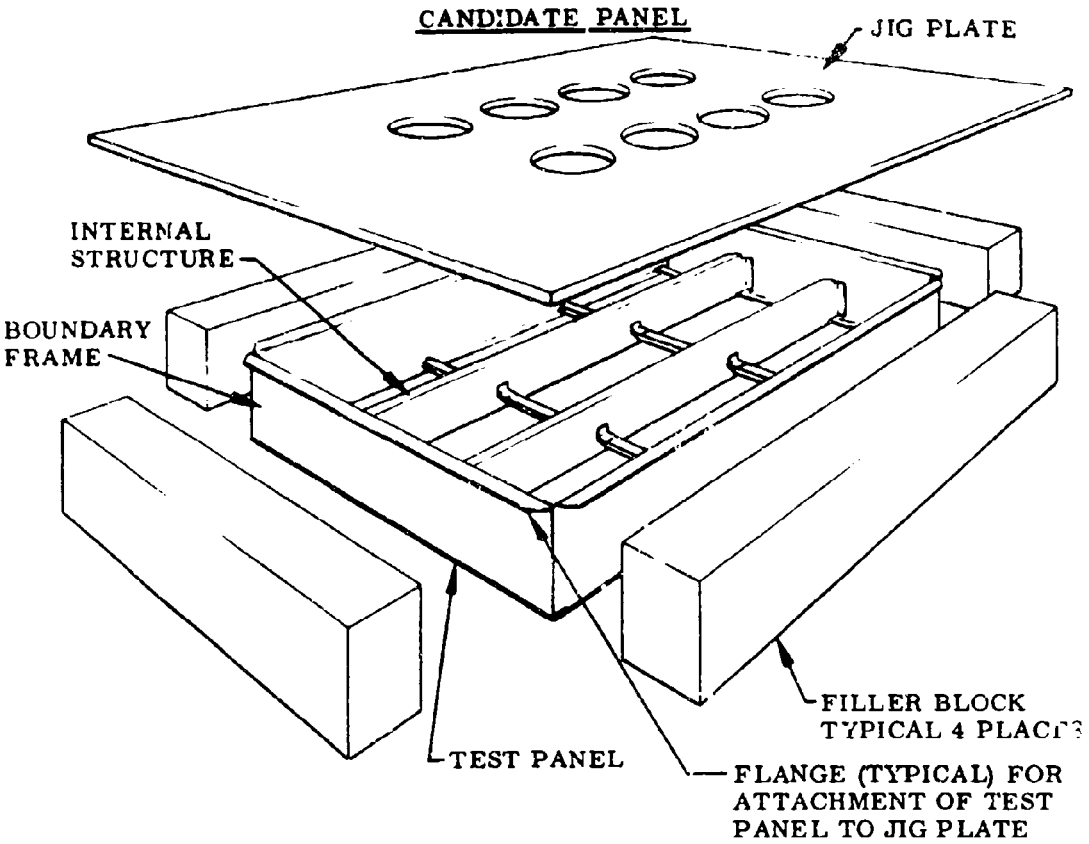

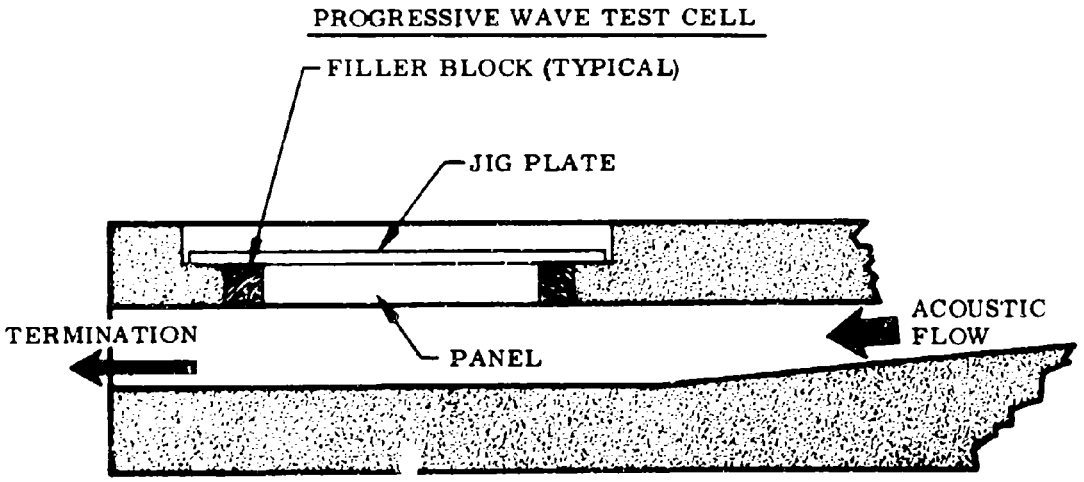

FIGURE 28. SCHEMATIC OF ACOUSTIC TEST PANEL AND ITS LOCATION IN THE PROGRESSIVE WAVE TEST CELL

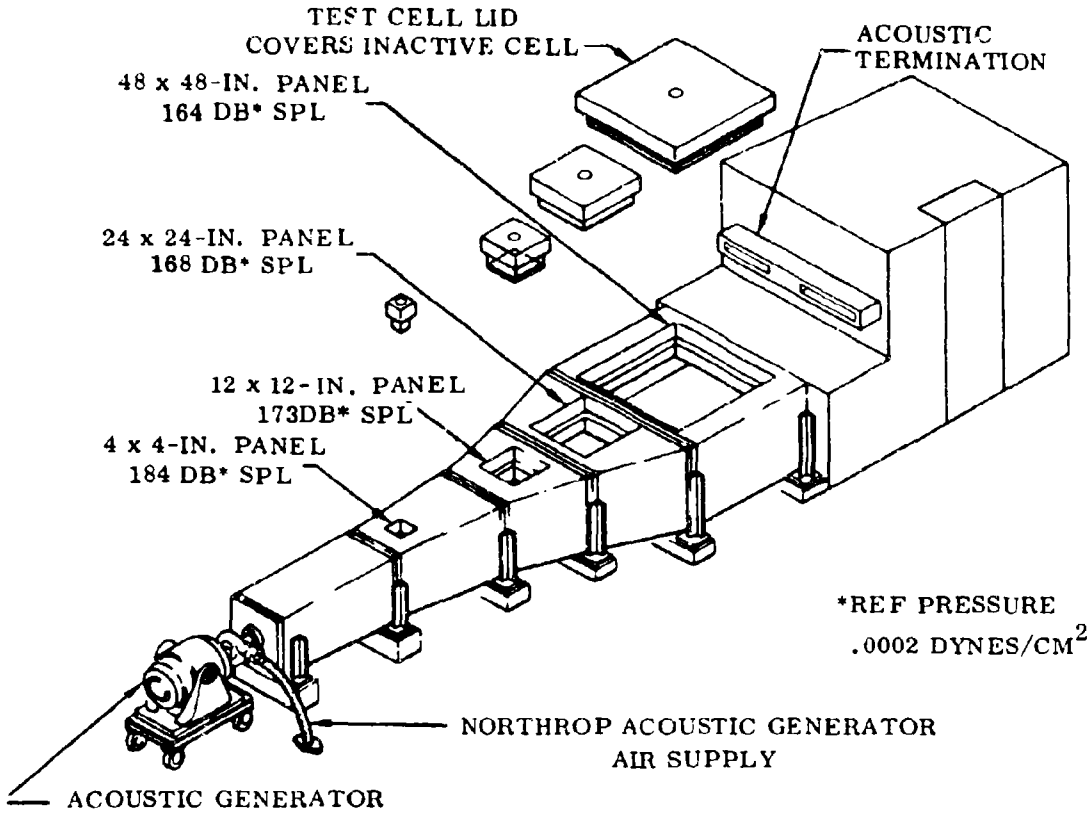

FIGURE 29. PROGRESSIVE WAVE ACOUSTIC TEST CHAMBER

in approximately three hours of exposure [7], [8]. This was one key factor in selecting the dimensions of the proposed acoustic test panels to be suitable for the acoustic test program.

The acoustic panels were subjected singly to tests in the Northrop Progressive Wave Acoustic Test Chamber under broad-band excitation. Experimental strains (versus acoustic pressure), deflections, damping factors, and noise reduction data were obtained and these items are discussed below. The panels were subjected to an acoustic fatigue test at the maximum SPL, which reached 166 db SPL.

IV.3 GENERAL TEST PROCEDURE

IV.3.(a) Modal Surveys

Modal surveys were conducted on the panels using the "salt" pattern technique and accelerometers. The "salt" pattern technique consisted of mounting a loudspeaker over the unreinforced surface of a panel that was mounted in the fixture before the fixture was placed in the test cell of the progressive wave test chamber, sprinkling noncorrosive polyvinyl chloride pellets on the flat surface, and energizing the speaker with discrete frequency excitation. With the "salt" pattern technique, the nodal lines and natural frequencies were observed. From the fixed and roving accelerometers that were mounted at various locations on the skin and the supports, relative amplitudes of vibration and phasing were obtained.

IV.3.(b) Damping Factors

Damping factors were obtained with the logarithmic decrement method utilizing the oscillograph decay record taken from the accelerometer signals during the modal survey. To obtain a resonant frequency, the loading frequency was swept to obtain a frequency (the resonant frequency) to produce a maximum voltage output from the accelerometer.

IV.3.(c) Response and Acoustic Fatigue Tests

After the modal surveys were completed and damping factors were obtained under discrete frequency excitation, the panel specimens were subjected to random acoustic loading at 136 db SPL, and strain and accelerometer data were recorded. The pressure was then increased in increments of 3 db and strain data were recorded at each SPL until the level was reached for the acoustic fatigue test. The plan was to conduct the acoustic fatigue test until the equivalent of 10^8 cycles occurred or until failure, if failure occurred first.

One purpose of this test procedure was to observe if nonlinear effects were present. The testing at levels lower than the maximum test level was conducted rapidly in order to prevent undue exposure before the intended fatigue test commenced. Once the fatigue test began, visual inspections were made at least every three hours.

IV.3.(d) Failure Detection

Visual inspections were used to detect acoustic fatigue failures, which were defined as the first observation of a fatigue crack or delamination. In addition, visual inspections were made when unexpected strain or pressure fluctuations occurred since they often give a first indication of a panel failure.

IV.3.(e) Noise Reduction

For the investigation of noise reduction, one test panel was installed in the test fixture in the progressive wave test chamber, and under a discrete frequency sweep up to approximately 350 Hz at various pressure levels the pressure was measured and recorded with microphones on both sides of the panel. The applied pressure level was set sufficiently low to prevent fatigue damage to the panel prior to the acoustic fatigue tests.

IV.4 TEST INSTRUMENTATION

Acceleration, temperature, and strain measuring equipment was used, including a system for recording the data. The essential components of the instrumentation system, employed in the test program, are shown schematically in Figure 30.

IV.4.(a) Location and Quantity of Strain Gages, Accelerometers, and Thermocouples

Strain gage locations for the acoustic test panels are in Figure 31 and included the following locations:

1. On the skin near the center of selected bays.
2. On the skin opposite or adjacent to a rib and/or stringer.
3. On a stringer(s) and/or rib(s).
4. On the skin adjacent to the peripheral doubler.

A maximum of three accelerometers (including one roving accelerometer) were used in panel modal surveys and acoustic tests to assist in the determination of mode shapes.

In the acoustic tests, heating of the panels was insignificant as had been the case for the boron-epoxy honeycomb acoustic panels tested under Contract F33615-67-C-1672. The temperature of the panel A-GG-B-1 was monitored during the acoustic test with three thermocouples per panel, located at a joint near the panel edge, at the center of a bay, and near a joint of the center bay. No temperature measurements were taken during the acoustic tests of panels A-GG-B-2 and A-GG-B-3, because there was no indication of panel heating.

IV.4.(b) Location of Microphones in the Acoustic Test Section

Prior to the start of this program, several tests to determine the acoustic pressure at various locations in the 24- by 24-inch test cell and the 48- by 48-inch test cell of the Northrop progressive wave acoustic test chamber had been conducted. During these tests, the pressure was recorded on magnetic tape and then analyzed to obtain the auto-correlation and cross-correlation functions[7] [8]. From these data, the assumption of spatial uniformity of the acoustic pressure appeared adequate for the analytic investigation conducted in this program.

For this test program the overall pressure was measured at the center of the 24- by 24-inch test cell and the 48- by 48-inch test cell with concrete plugs in both cells to get a one-to-one relation — i.e., a calibration chart between the pressure at these two locations. Then during acoustic tests with panels in the 48- by 48-inch test cell (where all acoustic tests were conducted), the pressure at the center of the 48- by 48-inch test cell was determined with the calibration chart and measurements of the pressure at the center of the upstream 24- by 24-inch test cell.

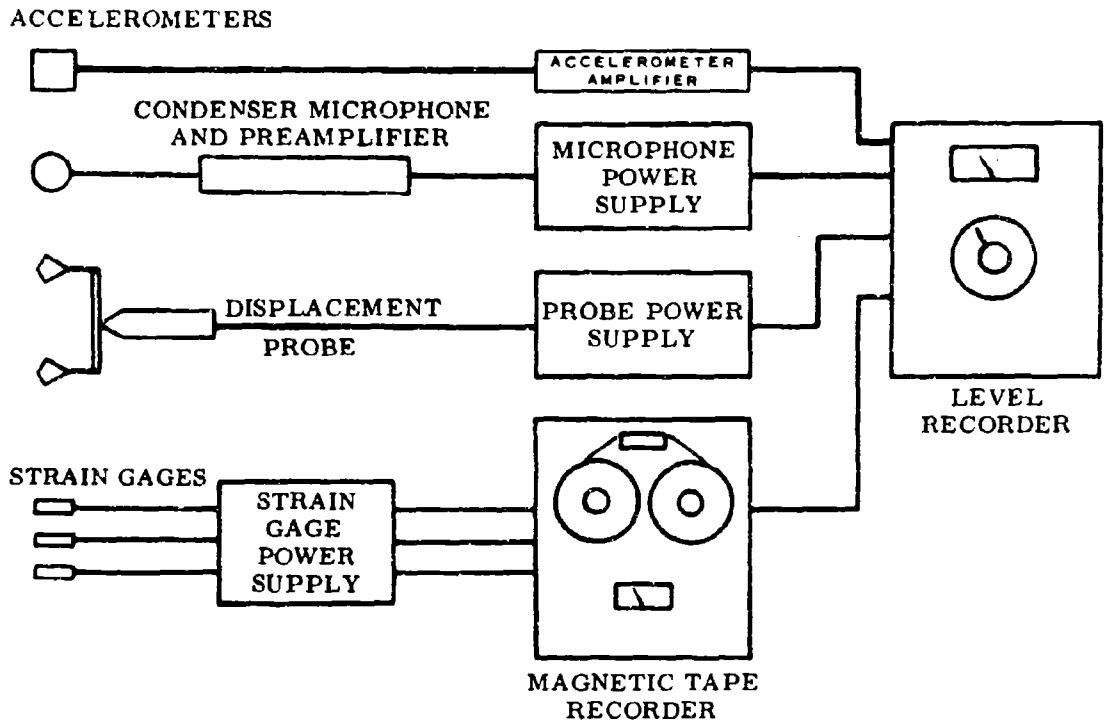

FIGURE 30. INSTRUMENTATION — SCHEMATIC DIAGRAM

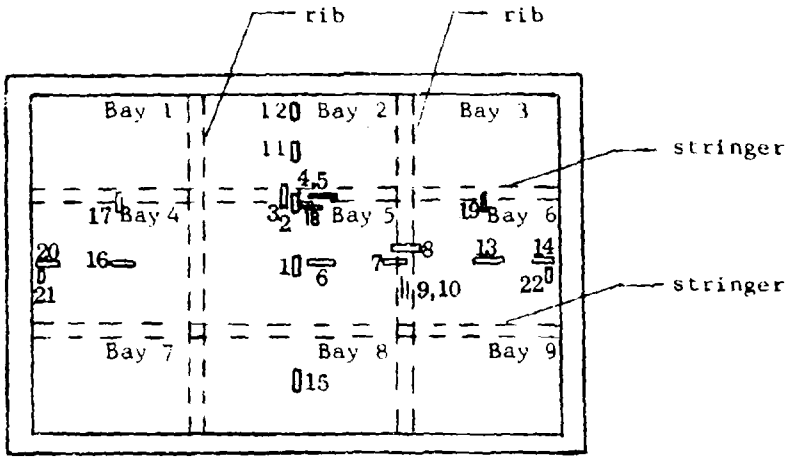

All strain gages of the acoustic panel except 5 and 10 are on the exposed surface of the skin. Gages 4 and 5 are back to back; gages 9 and 10 are back to back. Bay numbers are in the bay upper right corner. Strain gages No. 1 thru 15 were installed on panel A-GG-B-1; strain gages No. 1 thru 17 were installed on panel A-GG-B-2; and strain gages No. 1 thru 22 were installed on panel A-GG-B-3.

FIGURE 31. SCHEMATIC OF STRAIN GAGE LOCATIONS FOR THE ACOUSTIC PANELS

IV.5 TEST FACILITIES AND EQUIPMENT

A description of the progressive wave test chamber and a list of the equipment used in the acoustic test program are given below.

IV.5.(a) Progressive Wave Test Chamber

The Northrop Progressive Wave Acoustic Test Chamber in the Acoustic Test Laboratory consists of a 30-Hz exponential horn cast in reinforced concrete and diverging from a two-square-inch round cross section to a 9-inch by 48-inch cross section. The horn is terminated by a polyurethane foam-filled muffler that absorbs the sound energy. The chamber is excited by a Northrop Acoustic Generator, which is a high-pressure air modulator that is driven by an electrohydraulic shaker. The various test section lids contain microphone adapter tubes to allow sound pressure level readings to be taken at several locations in each of the test sections. By utilizing the microphone adapters in the lids plus an additional microphone location in the bottom center of the test section facing the lid, six microphones can be installed in the two-foot-square test section and ten microphones in the four-foot-square test sections.

IV.5.(b) Test Equipment

The following is a list of test equipment used to provide and monitor the acoustic environment and strain gage outputs.

1 - Northrop Acoustic Generator MK IV-H
6 - Photocon Model 524-5 Microphone
6 - Photocon Model DG605-D Dyna-Gage
2 - B & K Type 2409 Electronic Voltmeter
1 - B & K Type 2111 Audio Frequency Spectrometer
1 - B & K Type 2305C Level Recorder
3 - Northrop Strain Gage Balance Networks (four channel)
9 - Sanborn Model 8875A Differential Amplifier
1 - Sanborn Model 3914 14 Channel Tape Recorder
1 - CEC Model 5-124 Oscillograph
1 - Tektronix Model RM 565 Dual Trace Oscilloscope
1 - Allison Model 650R Random Noise Source
1 - B & K Type 123 1/3 Octave Spectrum Shaper
1 - Hewlett-Packard Model 5532A Frequency Counter
1 - Spectral Dynamics Model SD 104-5 Sweep Oscillator
1 - Spectral Dynamics Model SD 105 Amplitude Servo/Monitor
1 - Moseley Model 7035A X-Y Recorder
1 - Moseley Model 60B Log Converter
EA-13-062AA-120 Strain Gages
EA-13-062RB-120 Strain Gages

IV.6 DATA REDUCTION AND ANALYSIS

All acoustic measurements were made with condenser microphones with their associated carrier amplifiers. Acoustic signals were analyzed by a B&K Type 2111, Audio Frequency Spectrum Analyzer. Strain gage and accelerometer outputs were recorded on 1-inch magnetic tape and analysis of data was made by a constant bandwidth analyzer system for power spectral density.

Prominent items in the data reduction and analysis equipment that were used, follow.

The primary magnetic FM tape playback unit was the Minneapolis Honeywell Model 7600 Tape Playback System with a standard, extended, and double-extended variable speed capability (1-7/8, 3-3/4, 7.5, 15, 30, and 1250 ips). This unit can reproduce 1-inch tape, 14 channels. A Honeywell 7490 Tape Playback System was used for repetitive looping. A Tektronix Oscilloscope Model 561 was used to obtain instantaneous visual display of the data. The power spectral density analysis equipment consisted of Technical Products Models TP 626, TP 627, TP 633, and TP 644.

V. DETAIL DESCRIPTION OF ACOUSTIC TESTS

In this section, the modal surveys and acoustic tests of panels A-GG-B-1, A-GG-B-2, and A-GG-B-3 are reviewed in detail. In addition, there is a discussion of acoustic fatigue life prediction and the effect of the acoustic SPL on the strain response of the acoustic test panels.

V.1 TEST OF ACOUSTIC PANEL A-GG-B-1

The description of the fabrication of panel A-GG-B-1 was presented in Section III. Panel A-GG-B-1 was instrumented with strain gages No. 1 through 15 (Figure 31) and thermocouples and attached to the 4 x 4 foot acoustic test fixture. Wooden beams were also attached (Figures 32 and 33) to the acoustic test fixture to produce a relatively smooth surface for air flow across the test jig (i.e., wood fillers and the panel) during tests in the progressive wave acoustic test chamber. The panel was then subjected to (1) loudspeaker excitation to obtain modal surveys and damping factors, and (2) to acoustic excitation in the progressive wave acoustic test chamber (Figure 34) to obtain response and acoustic fatigue data. During the acoustic excitation, signals of strain, acceleration, and pressure were recorded (magnetic tape) for subsequent data analysis.

V.1.(a) Modal Surveys

Panel A-GG-B-1 was attached to the acoustic test fixture for modal surveys with a loudspeaker. Three Endevco 2222B microminiature accelerometers were used during the modal surveys to obtain natural frequencies, phasing between bays, and an estimate of nodal lines. For the modal surveys, one of the accelerometers was cemented in the center of bay 5 and another accelerometer was attached to the panel with vacuum seal putty to facilitate its use as a roving accelerometer.

Panel resonances were obtained by examining peaks of accelerometer output under loudspeaker excitation during discrete frequency sweeps up to 400 Hz. The frequencies of these acceleration peaks are reported in Table II. In obtaining the acceleration peaks, the roving accelerometer was positioned at the center of the bay being examined.

Following the determination of the frequencies of Table II, the panel mode shapes were determined from acceleration amplitude and phase readings at the center of each bay at each panel resonant frequency up to 350 Hz. The accelerometer readings shown in Figure 35 define the modal surveys. The modal surveys indicate that bay 4 contained the point of maximum panel amplitude at the 165, 184, and 233 Hz resonance; bay 5 had the point of maximum amplitude at the 343 Hz resonance; bay 6 had the point of maximum amplitude at the 219 Hz resonance; and bay 8 had the point of maximum amplitude at the 277 Hz resonance.

Preceding page blank

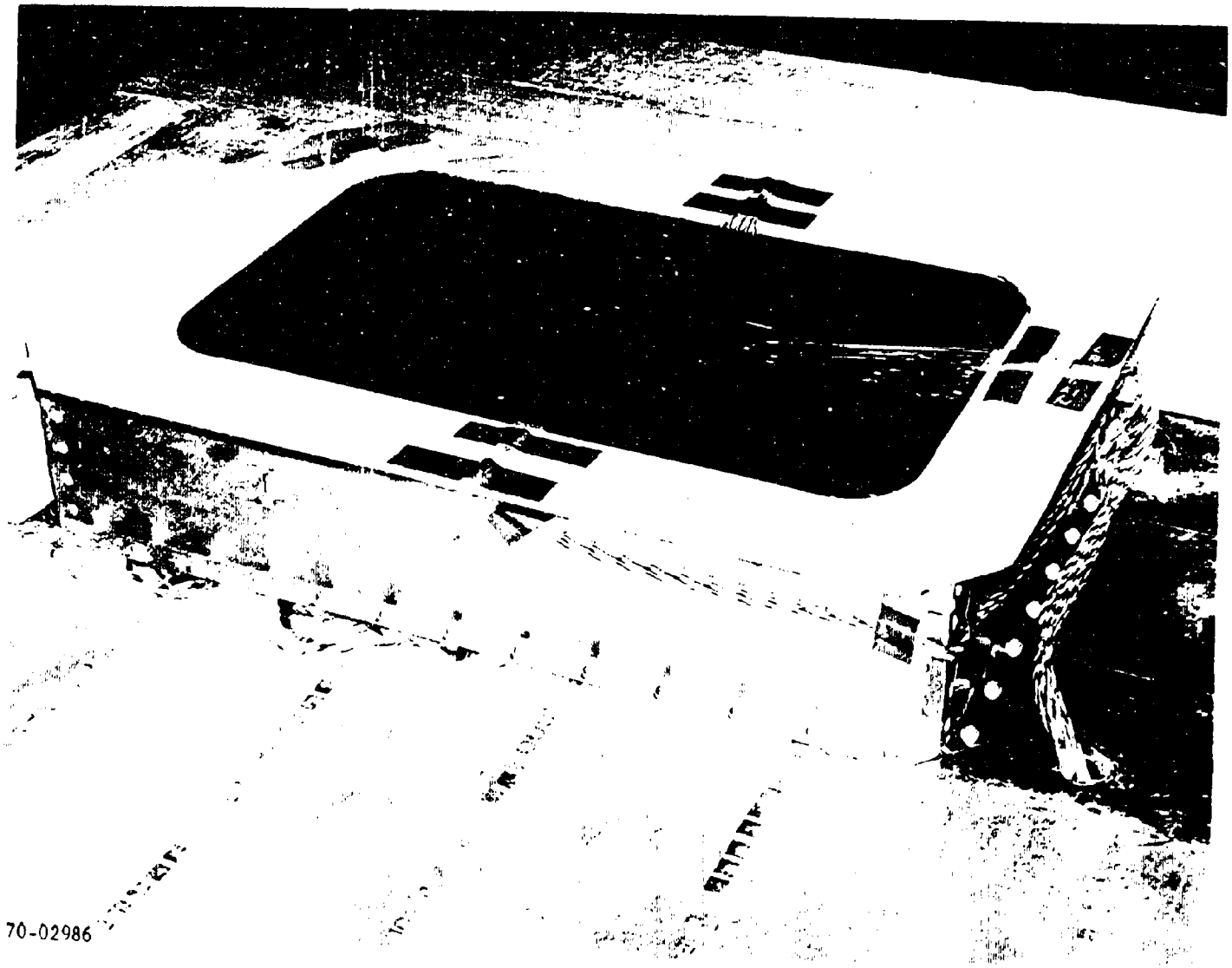

FIGURE 32. PANEL A-GG-B-1 AND PARTIAL ASSEMBLY OF WOOD FILLER BLOCKS

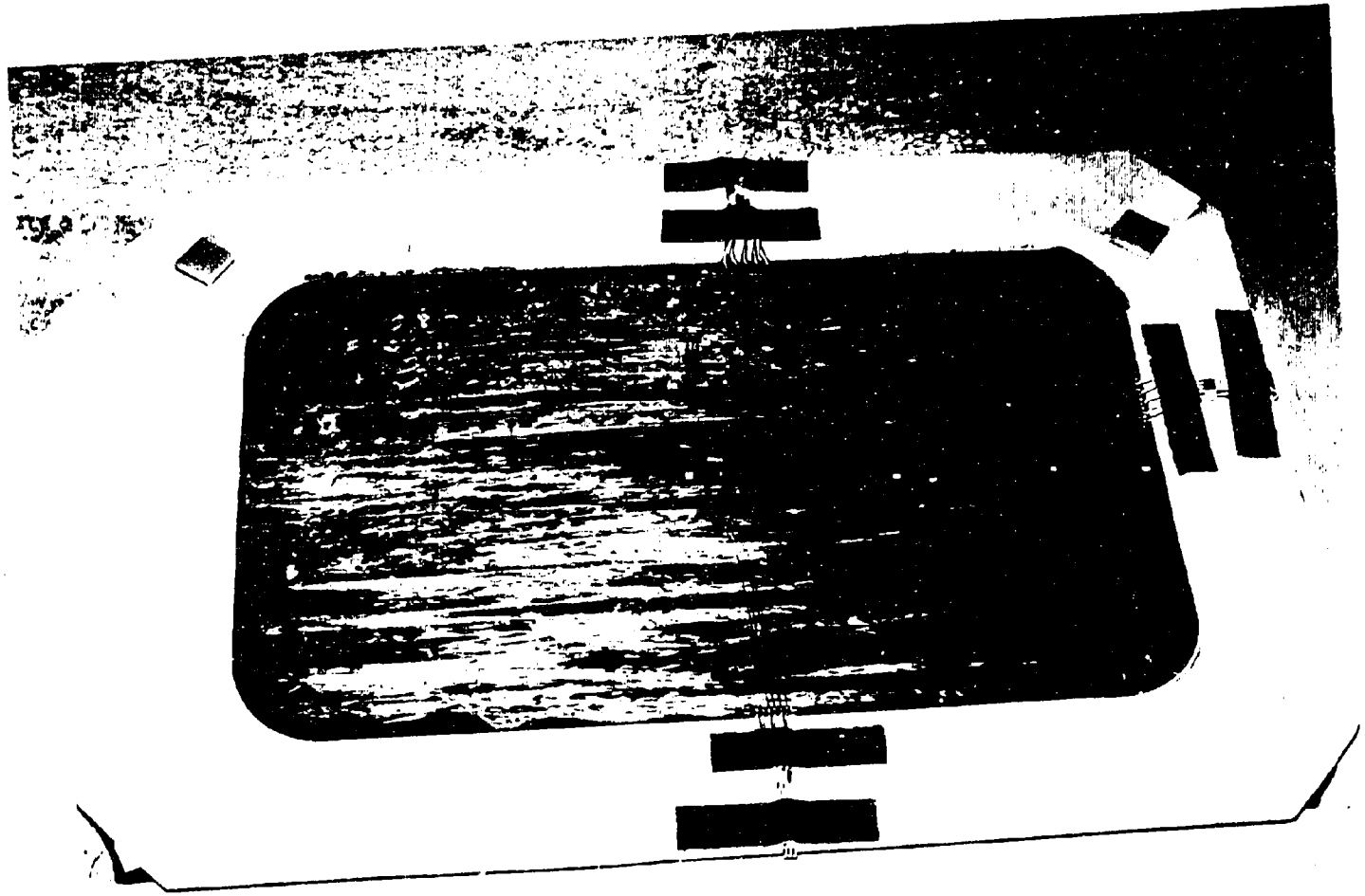

70-02987

FIGURE 33. ASSEMBLY OF PANEL A-GG-B-1 AND WOOD FILLER BLOCKS

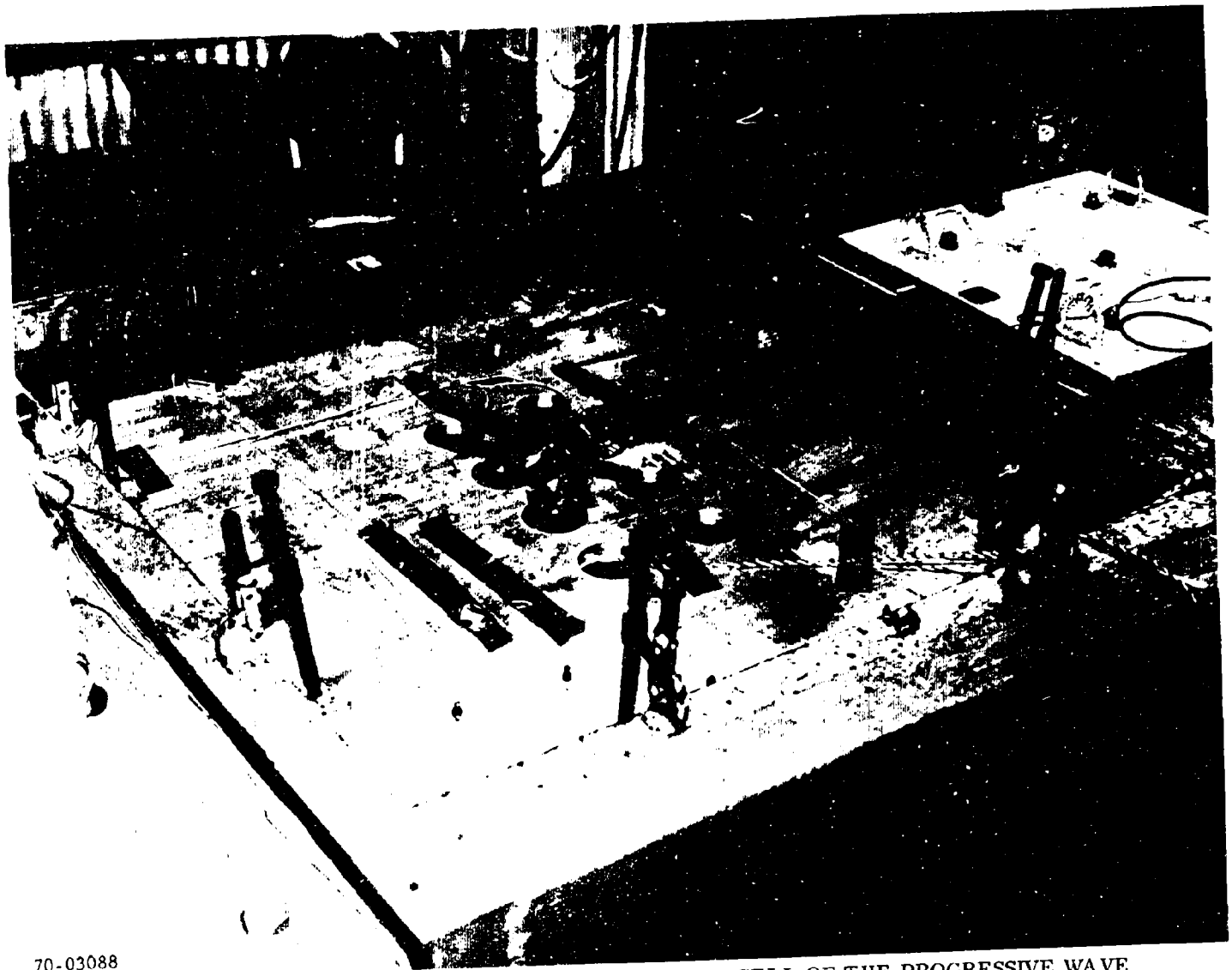

70-03088

FIGURE 34. TEST FIXTURE IN THE 4 X 4 FOOT TEST CELL OF THE PROGRESSIVE WAVE ACOUSTIC TEST CHAMBER

167 Hz

Bay 1 -115	Bay 2 +167	Bay 3 +90
Bay 4 +2240	Bay 5 +510	Bay 6 +520
Bay 7 +115	Bay 8 /80	Bay 9 +49

184 Hz

Bay 1 -170	Bay 2 -35	Bay 3 +85
Bay 4 +2500	Bay 5 +550	Bay 6 +2220
Bay 7 +50	Bay 8 -180	Bay 9 +12

219 Hz

Bay 1 /550	Bay 2 +180	Bay 3 +270
Bay 4 +280	Bay 5 +1120	Bay 6 +2540
Bay 7 -105	Bay 8 -360	Bay 9 -12

233 Hz

Bay 1 /135	Bay 2 -180	Bay 3 -190
Bay 4 +2840	Bay 5 -1450	Bay 6 +1750
Bay 7 -155	Bay 8 +670	Bay 9 -14

277 Hz

Bay 1 /224	Bay 2 -1200	Bay 3 -1000
Bay 4 +2800	Bay 5 +4700	Bay 6 +7100
Bay 7 -1500	Bay 8 -11600	Bay 9 +750

343 Hz

Bay 1 -2800	Bay 2 -3100	Bay 3 -160
Bay 4 +2350	Bay 5 +14800	Bay 6 /1100
Bay 7 -3000	Bay 8 +14400	Bay 9 /300

NOTES: The roving accelerometer readings (milli-g's) were obtained at approximately the bay center.
+ means the accelerometer reading is in phase with the reference bay.
- means the accelerometer reading is out of phase with the reference bay.
/means the accelerometer reading has approximately a +90° phase angle with the reference bay.

FIGURE 35. MODAL SURVEYS OF PANEL A-GG-B-1

TABLE II. ACCELERATION PEAK RESPONSES OF PANEL A-GG-B-1 OBTAINED UNDER DISCRETE FREQUENCY EXCITATION

Location of Accelerometer (1), (2)	Frequencies of Peak Responses (Hz)
Bay 2	165, 189, 215, 238, 278, 340, 362, 394, 415
Bay 4	187, 216, 233, 280, 300, 312, 343, 365, 393
Bay 5	165, 215, 237, 273, 350, 400
Bay 6	185, 193, 236, 273, 358, 375, 400
Bay 8	189, 215, 276, 348, 395, 413
Bay 9	185, 193, 234, 273, 295, 340, 388, 410

(1) The accelerometer is located at the center of the bay.

(2) Corner bays 1, 3, 7, and 9 had very low level response, and only the responses of bay 9 were noted.

The following items are noteworthy. Bays 4, 5, and 6 were in phase at the 167 Hz and 184 Hz resonances. Bays 5 and 6 are out of phase at the 219 Hz resonance. Bay 5 is out of phase with bays 4 and 6 at the 233 Hz resonance. Bay 8 is out of phase with bay 5 at the 277 Hz resonance and is in phase with bay 5 at the 343 Hz resonance. Because of the extensive modal survey characterization of Figure 35, it was decided not to obtain nodal lines of panel A-GG-B-1 with the "salt" pattern technique.

During the modal survey no oil canning of panel A-GG-B-1 was observed, i.e., the bays that were initially curved at the outset of the modal surveys did not pass thru their flat position.

Bay 5, the center bay, had substantially more initial curvature than any of the other bays and therefore it was not surprising that its large responses relative to other bays occurred at 277 Hz and 343 Hz rather than at the lower natural frequencies of 167, 184, 219, and 233 Hz.

V.1.(b) Damping Factors

Damping factors associated with the decay of panel resonances following the termination of loudspeaker excitation (Table III) were obtained using the logarithmic decrement method from oscillograph records of accelerometer signals. At each resonant frequency, the signals from three accelerometers were simultaneously recorded for use in the damping factor calculation. The average damping factor was 0.017 which is approximately the same damping factor reported in Reference 8 for adhesively bonded, three-bay, aluminum alloy panels with tee section stiffeners.

TABLE III. DAMPING FACTORS OF PANEL A-GG-B-1

Frequency	Viscous Damping Factors			
	Bay 4	Bay 5	Bay 6	Bay 8
(Hz)				
167	NG(1)	NG	NG	NT(2)
184	0.023	0.017	NG	NG
219	NT	NG	NG	NG
233	0.014	NG	NG	NG
277	NT	0.017	NG	0.015
343	NT	0.017	NG	NT

(1) NG means the decay record was poor and no damping factor was computed.

(2) NT means no decay record was taken for this bay at this frequency.

V.1.(c) Response to Acoustic Excitation

After the modal surveys were completed and damping factors were obtained under loudspeaker excitation, the acoustic test fixture with the panel in place was installed in the 4 x 4 foot test cell of the Northrop progressive wave acoustic test chamber for broad-band acoustic loading.

The pressure at the center of the 4 x 4 foot test cell was obtained with the use of a calibration table (relating the pressure at the center of the 2 x 2 foot test cell and the 4 x 4 foot test cell) that had been obtained with all of the concrete test cell lids of the progressive wave test chamber in place. Therefore, when panel A-GG-B-1 replaced the concrete lid of the 4 x 4 foot test cell, microphone readings at the center of the 2 x 2 foot test cell were taken for use with the calibration chart to obtain the pressure at the center of the 4 x 4 foot test cell.

Beginning with an overall sound pressure level of 136 db at the center of the 4 x 4 foot test cell, which coincided with the center of the test panel, strain and accelerometer readings were taken (Table IV) as the pressure was increased in increments of 3 db until the maximum sound pressure level of 165 db was obtained. For these acoustic tests, the accelerometer locations of Figure 36 were applicable.

Strain, accelerometer, and pressure signals were recorded on magnetic tape for spectral density analysis of the pressure and response at 139,148, and 151 db SPL.

Thermocouple readings were taken to obtain the temperature of the panel during testing. The panel remained at ambient temperature which was approximately 80F during the acoustic tests.

The tests to obtain strain data at overall sound pressure levels of 163 db and lower were conducted as rapidly as possible to prevent significant accumulation of fatigue damage in the panel prior to the acoustic fatigue test at the maximum sound pressure level of 165 db. The exposure to the acoustic excitation at the lower sound pressure levels was approximately two minutes when tape recordings were not taken and six minutes when tape recordings were taken.

TABLE IV. STRAIN GAGE RESPONSE (MICRO-INCH/INCH-RMS) AND ACCELEROMETER RESPONSE (G's-RMS) OF PANEL A-GG-B-1

	Overall Sound Pressure Level (db re 0.0002 dynes/cm^2)										
	136 db	139 db	142 db	145 db	148 db	151 db	154 db	157 db	160 db	163 db	165 db
Strain Gage											
1	76	100	112	152	220(1)	300	390	540	out(2)		
2	56	80	102	156	240	out					
3	28	36	48	62	82	112	144	180	220	250	300
4	8	10	12	16	20	26	32	100(3)	60	70	70
5	38	42	48	62	88	112	142	400(1)	out		
6	32	44	54	82	112	200(1)	260	400	320	out	
7	54	76	88	124	170	280(1)	310	360	450	520	600
8	26	32	38	52	-	220	270	158	220	230	260
9	154(3)	80(3)	18	20	22	26	30	40	60	out	
10	10	14	12	16	20	out					
11	6	10	118	174	220	310	420	520	600	64(3)	
12	120(3)	90(3)	50	80	112	166	220	260	360	80(3)	
13	76	40	140	160	210	260	260	280	360	46(3)	
14	104	128	76	100	136	200	210	240	out		
15	58	62	220	300	380	486	480	540			
Accelerometer											
1	14	25	35	58	95	150	200	320	420	580	620
2	11	18	25	40	62	95	130	180	240	310	340
3	27	55	73	125	200	225	360	530	750	1080	out

(1) Onset of oil canning.

(2) Lost gage.

(3) Questionable reading.

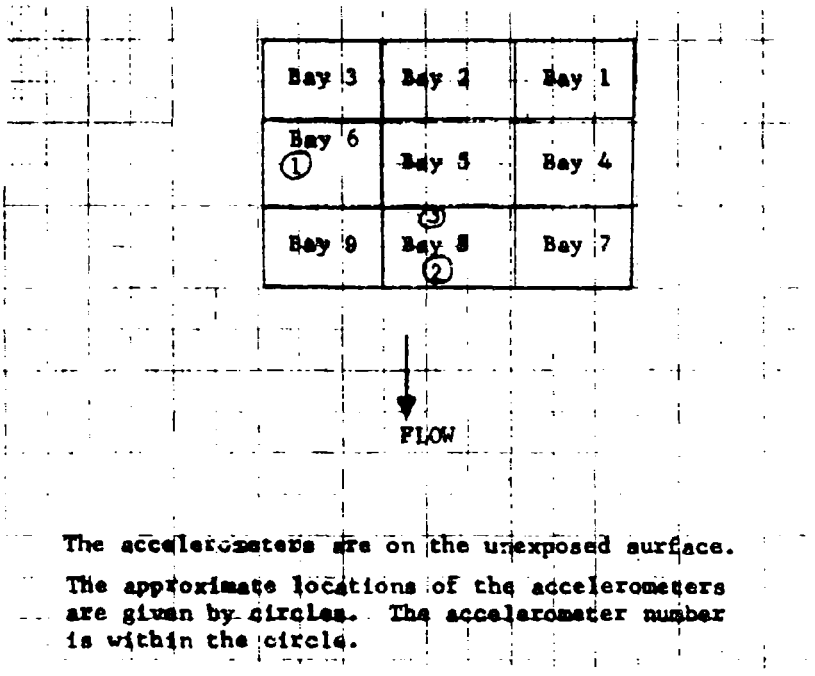

FIGURE 36. LOCATION OF ACCELEROMETERS DURING EXCITATION IN THE PROGRESSIVE WAVE CHAMBER

V.1.(d) Acoustic Fatigue Test

Prior to starting the run at 165 db SPL, a visual inspection of panel A-GG-B-1 indicated no evidence of damage. Visual inspections were subsequently made after a total of 10, 30, 45, and 60 minutes of exposure at 165 db. In addition, a continuous monitoring of strain signals was made during the first 13 minutes of exposure and of a microphone signal during the remaining 47 minutes of exposure from a microphone mounted outside of the text fixture just over a relief hole at the center of the panel.

The inspection at 10 minutes of exposure was made because of a sudden shift in the monitored strain signal. A mishap (this item is discussed in more detail at the bottom of page 72) had occurred with damage principally confined to bay 5 of the panel,

but subsequent testing indicated the mishap had little, if any, effect on the acoustic fatigue failure of the panel. At the scheduled visual inspection at 30 minutes exposure, no acoustic fatigue failure was observed. At the visual inspection at 45 minutes exposure, an adhesive failure was observed at the tee section between bays 4 and 7, (Figure 37) and resulted in the separation of the tee section and the skin. The adhesive failure was the initial acoustic fatigue failure observed in the test.

The acoustic fatigue test was then continued for 15 more minutes until 60 minutes of acoustic exposure had been obtained during the 165 db run and another visual inspection was made.

The following items were noted at the 60 minute inspection:

1. The vertical leg of the tee section that separated bays 2 and 5 had split (Figure 38).

2. An adhesive failure had initiated (Figure 39) between bays 6 and 9 that resulted in the separation of the skin and tee section.

3. Separation of the skin from the edge of the E-glass doubler had begun and progressed approximately 4 inches in bays 4 and 6. (Figure 40.)

4. Fracture of the outer ply and its separation from the inner plies had begun in a flange of an I-beam separating bays 5 and 6 (Figure 41). The white object in Figure 41 is a pencil used to lift the broken part of the flange to make it more visible in the photograph.

5. The edge of the vertical leg of the tee section segment that separates bays 5 and 8 was slightly damaged at two locations that divided the length of the tee section segment into three approximately equal segments.

6. A crack approximately 1/4 inch in the E-glass doubler was apparent at the corner of bay 9.

During the acoustic fatigue test (the 165 db run), a small aluminum block (that was part of the test fixture) vibrated loose from its supposedly fixed position after 10 minutes of testing and fell thru a relief hole in the test fixture into the test panel. The test was stopped within a few seconds because of a shift in the strain signal being monitored. Apparently during the few seconds before shutdown the block had bounced across the tee sections between the I-beams since white lines were apparent on the unexposed surfaces of bays 2, 5, and 8. The skin of the central part of bay 5 exhibited the greatest damage and was broken on the exposed surface (the block was in contact with the unexposed surface) in several places (Figure 42). However, these breaks did not grow appreciably in length during subsequent testing at 165 db SPL and apparently had little, if any, influence on the noted acoustic fatigue failures of the panel.

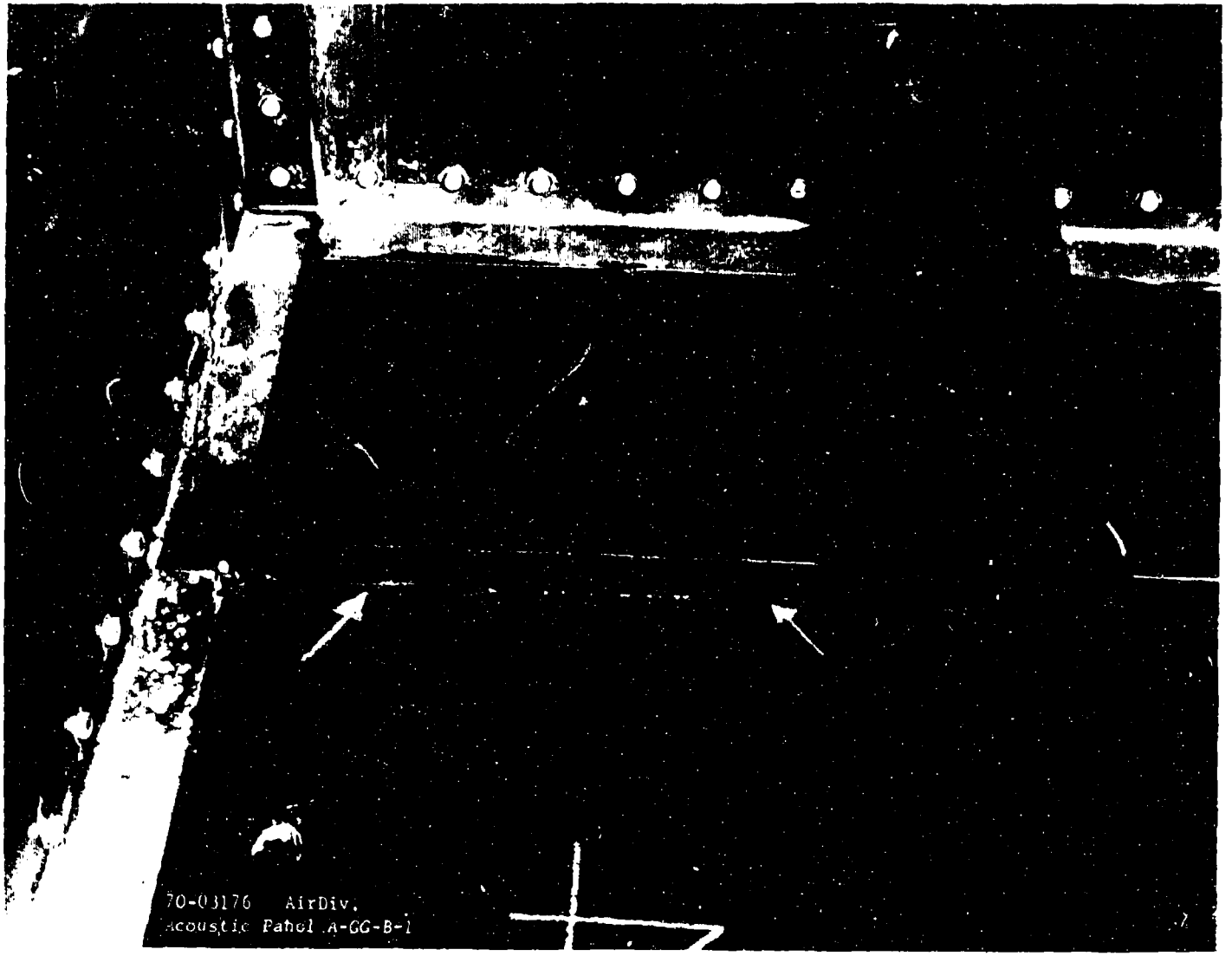

FIGURE 37. ADHESIVE FAILURE AT TEE SECTION SEPARATING BAYS 4 AND 7

FIGURE 38. TEE SECTION FAILURE BETWEEN BAYS 2 AND 5

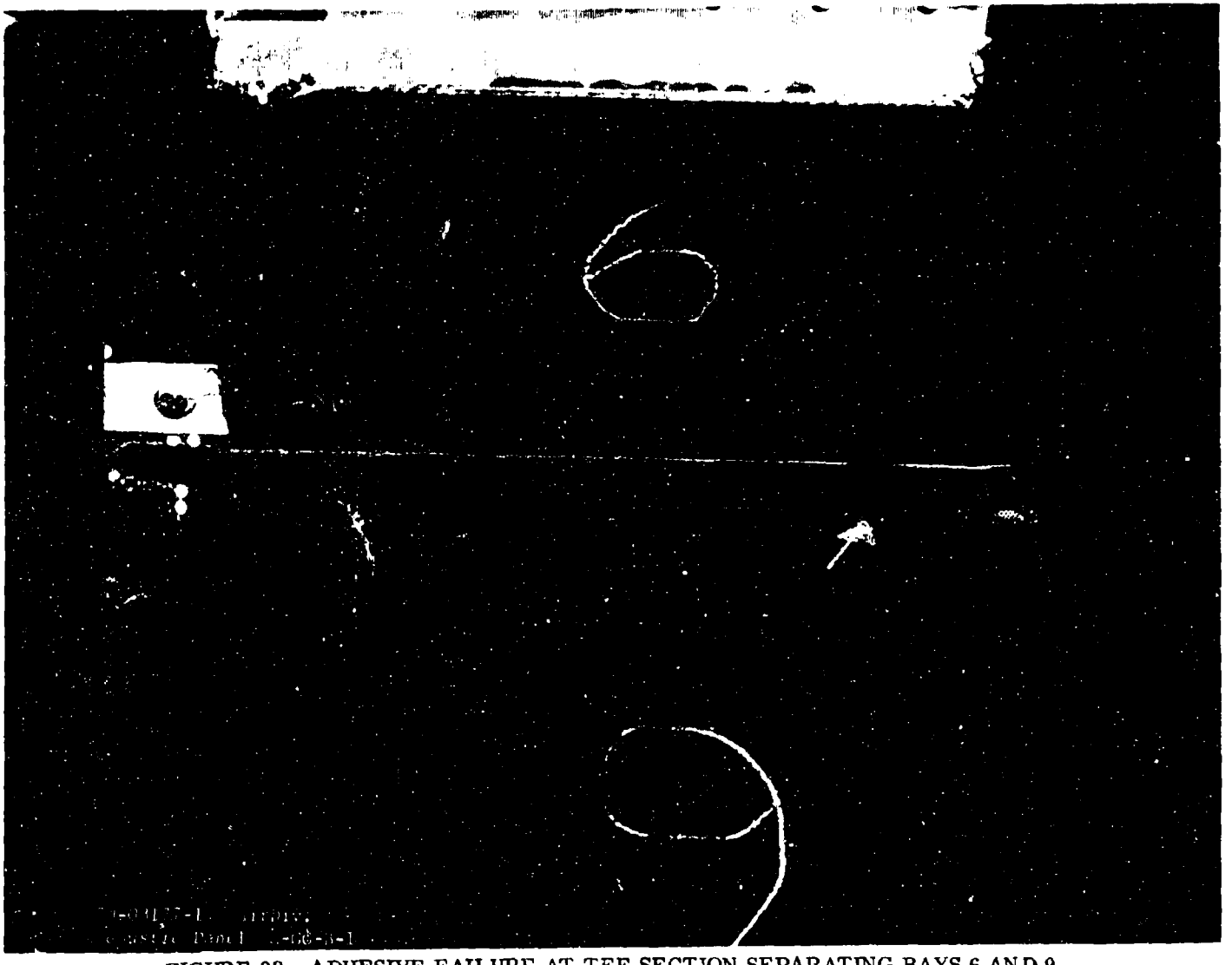

FIGURE 39. ADHESIVE FAILURE AT TEE SECTION SEPARATING BAYS 6 AND 9

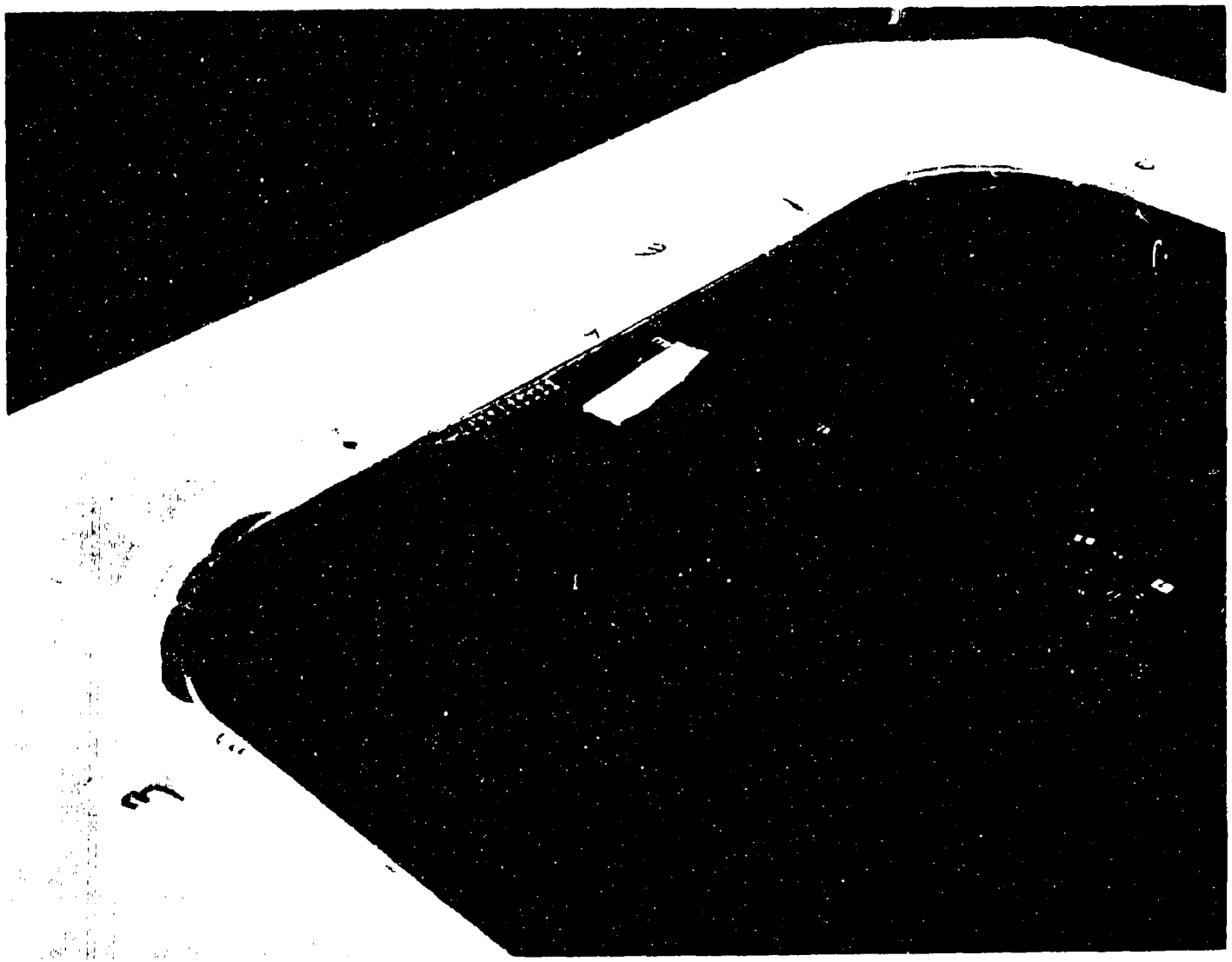

FIGURE 40. SEPARATION OF SKIN AT BAY 6 FROM GLASS DOUBLER

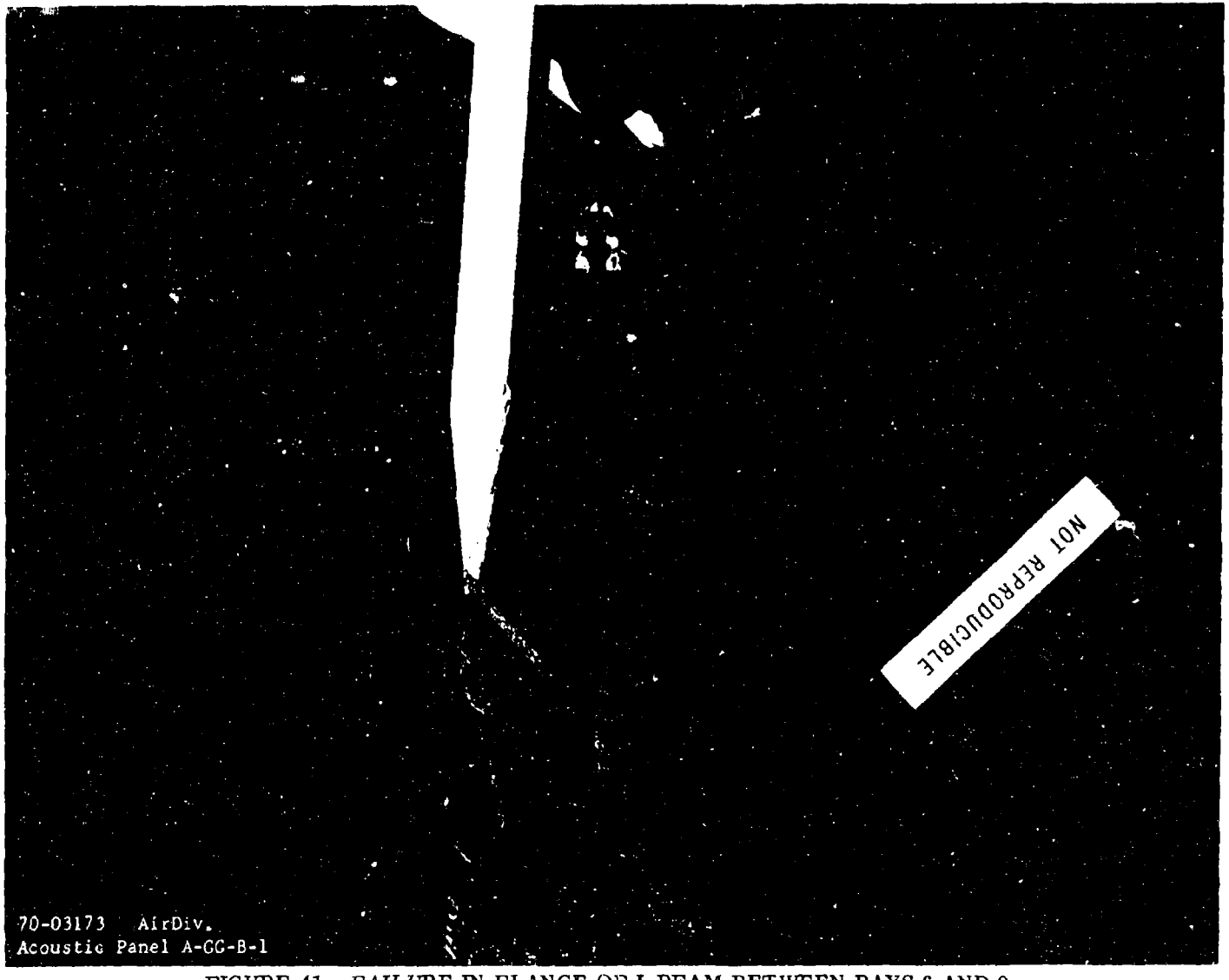

FIGURE 41. FAILURE IN FLANGE OF I-BEAM BETWEEN BAYS 6 AND 9

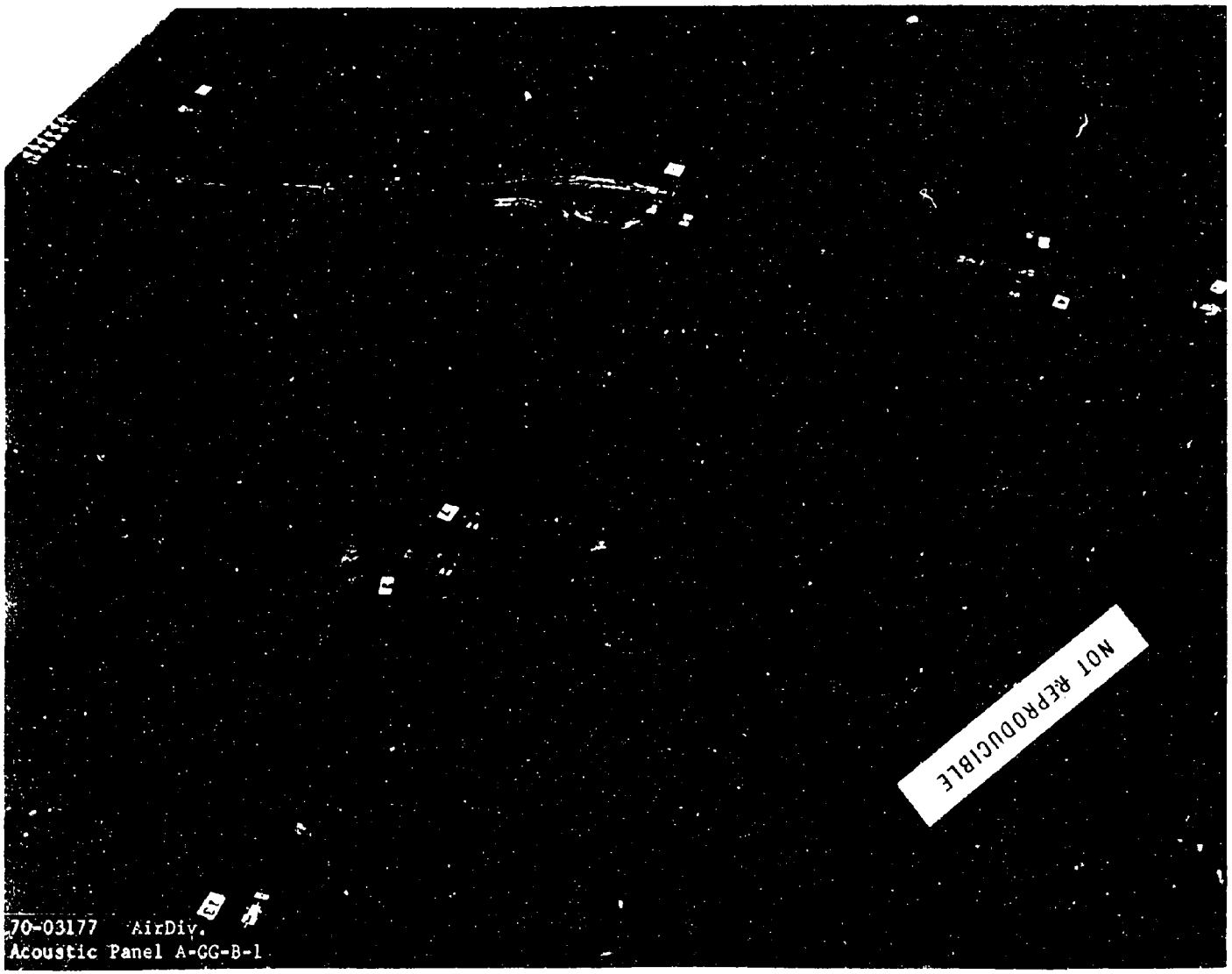

FIGURE 42. DAMAGE (ENCIRCLED AT SEVERAL LOCATIONS) ON EXPOSED SURFACE OF BAY 5

V.1.(e) Data Analysis

Narrow band spectral analysis was conducted for the strain response, accelerometer response, and pressure loading of Table IV.

There was no oil canning until 148 db SPL was reached. Beginning at the 148 db SPL, the output of gages No. 1 and 2 indicated that the bay 5 vibration was about one of the two oil canned positions for a small time period, then bay 5 snapped thru the flat position to vibrate for a smaller time period about the other oil canned position, then snapped thru the flat position to begin a repetition of the oil canning phenomenon. The spectral analysis of strain at gage No. 2 at 148 db SPL when the vibration included oil canning is in Figure 43 and when the vibration did not include oil canning is in Figure 44. When the analysis included the oil canning, the rms strain was 320 micro-inch/inch (Figure 43) as opposed to a 210 micro-inch/inch without oil canning (Figure 44). Upon comparing Figures 43 and 44, it is noted that the oil canning increases the strain spectral density to a greater extent below 100 Hz than above 100 Hz.

The strain response of gage No. 2 at different levels is in Figures 44 and 45. The spectral shape of the response changes as the level is increased to give a larger percentage of the response in the lower frequency range. (Compare Figures 44 and 45).

The pressure during the 139 db and 148 db SPL runs is shown in Figures 46 and 47, respectively.

For the data analysis presented in Figures 43 thru 47, a three second averaging time with a 0.6 Hz/sec sweep rate with a 5.3 Hz bandwidth filter for the 20 thru 250 Hz range was used. For frequencies above 250 Hz, a 1.4 second averaging time with a 3.3 Hz/sec sweep rate with a 14 Hz bandwidth filter was used. A two second loop was used in the data analysis shown in Figure 43 and a six second loop was used for the data analysis shown in Figures 44 thru 47.

V.1.(f) Discussion of Test Results

The acoustic fatigue test of panel A-GG-B-1 demonstrated that a graphite-epoxy panel with a six-ply skin of 0.025 inch thickness and with 10 x 7 inch nominal bay dimensions could be subjected up to 165 db SPL in an acoustic environment for at least a short period of time.

Oil canning during acoustic loading in the progressive wave chamber was not observed until 148 db SPL was reached. The oil canning produced an increase in the rms stress response as well as a change in the frequency content of the response. Because of the stress response increase due to the oil canning, the life of the panel was probably reduced.

The higher natural frequencies (277 Hz and 343 Hz) of the central bay relative to the other bays was probably due to the initial curvature of the central bay being substantially greater than that of the other bays. This curvature produced a higher stiffness for the central bay and tended to reduce the likelihood of the initial acoustic fatigue failure in the central bay.

It is significant that the accidental damage to the central zone of bay 5 did not propagate during the acoustic test.

Gage 2. Run 5 (148 db).
Rms strain = 320 micro-inch/inch

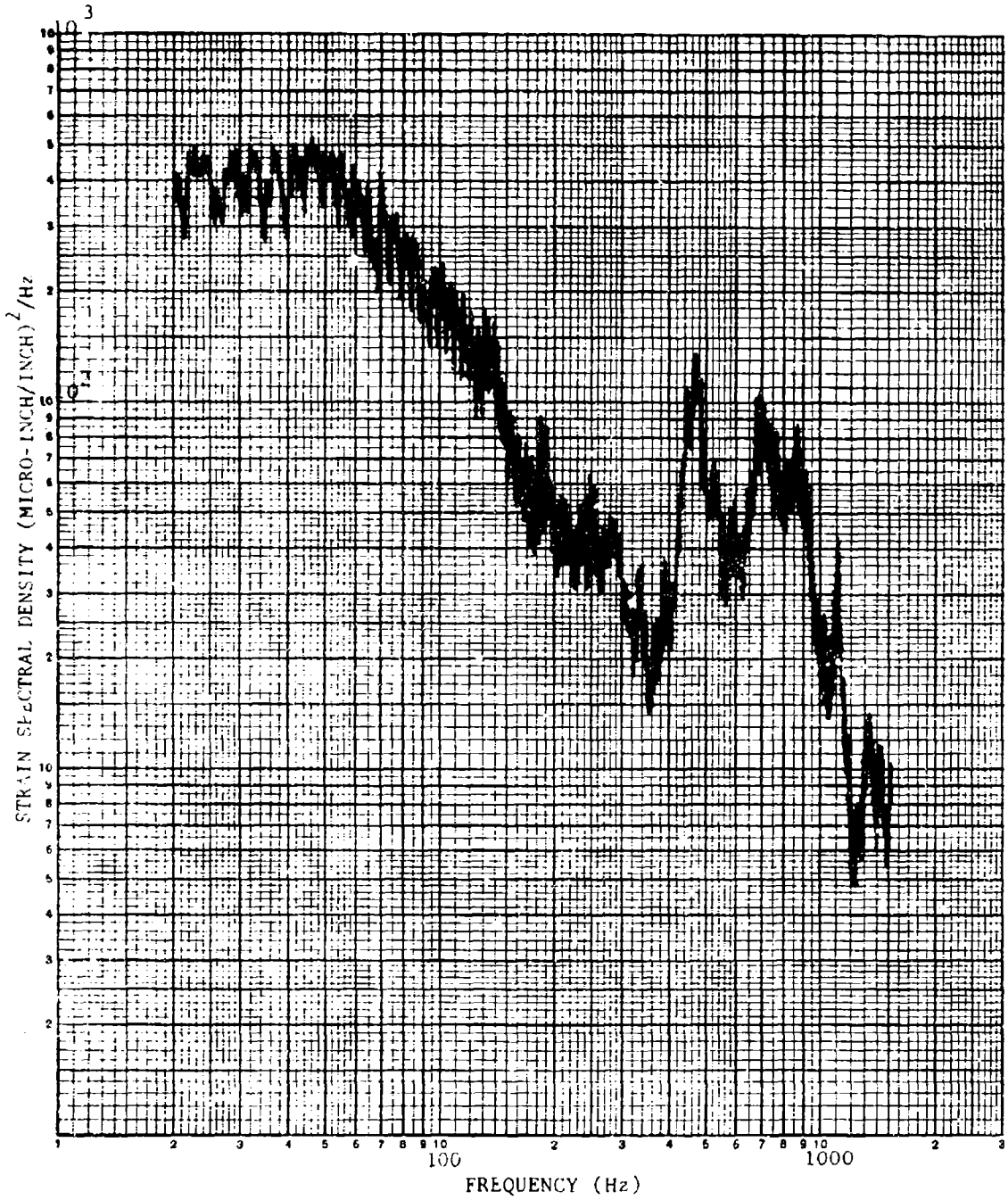

FIGURE 43. STRAIN GAGE NO. 2 RESPONSE WITH OIL CANNING AT 148 DB SPL

Gage 2, Run 5 (148 db).
Rms strain = 210 micro-inch/inch.

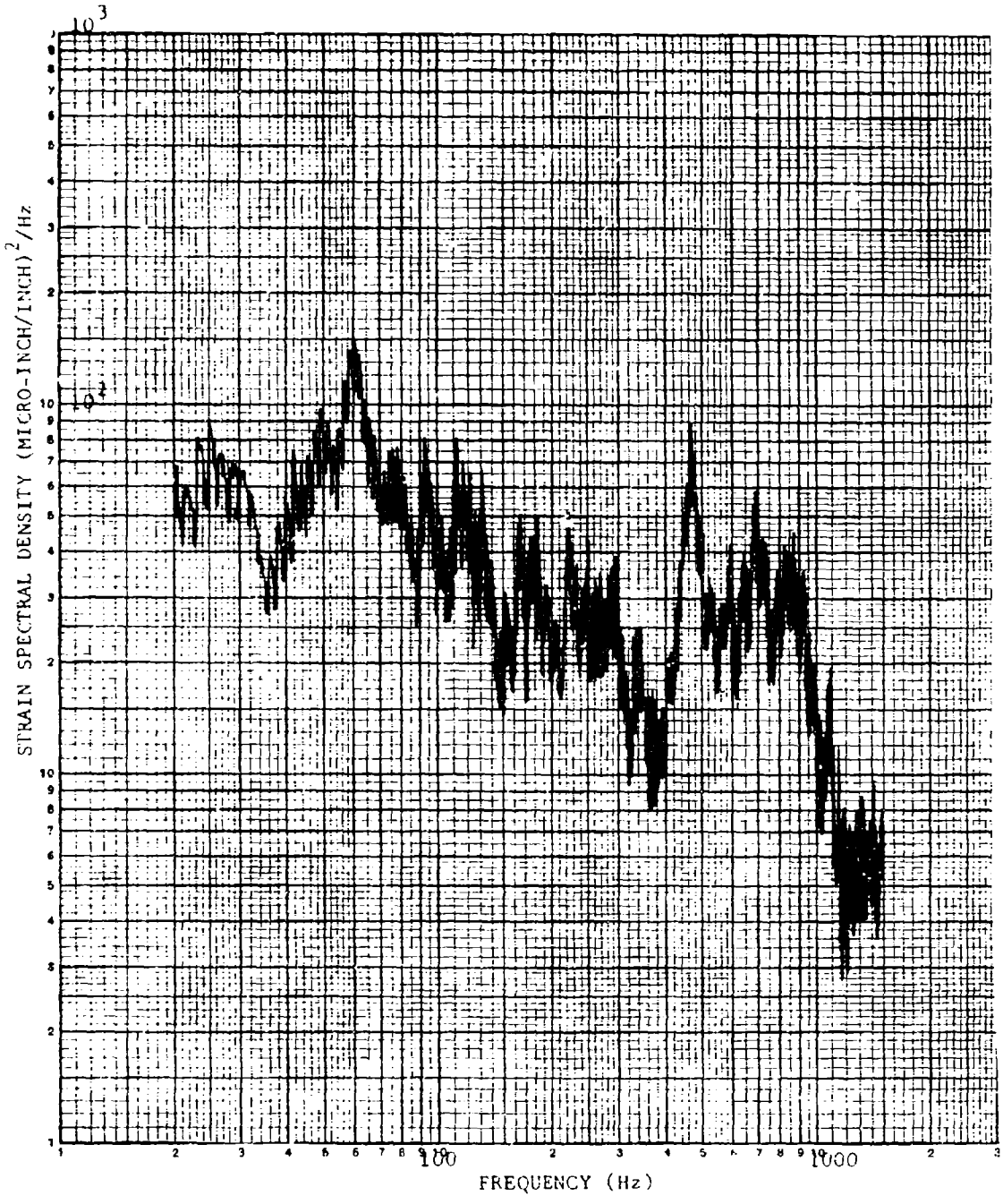

FIGURE 44. STRAIN GAGE NO. 2 RESPONSE WITHOUT OIL CANNING AT 148 DB SPL

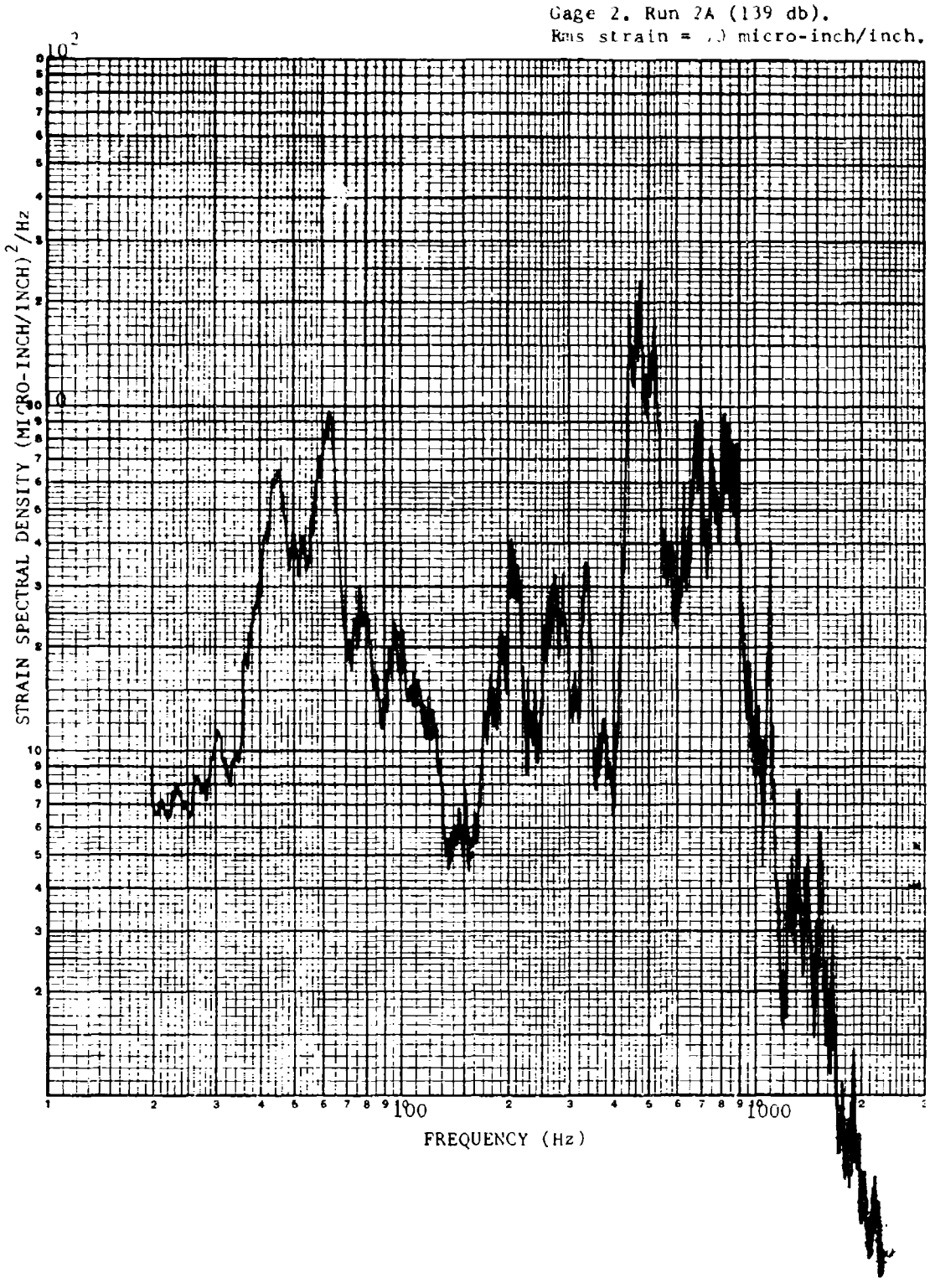

FIGURE 45. STRAIN GAGE NO. 2 RESPONSE AT 139 DB SPL

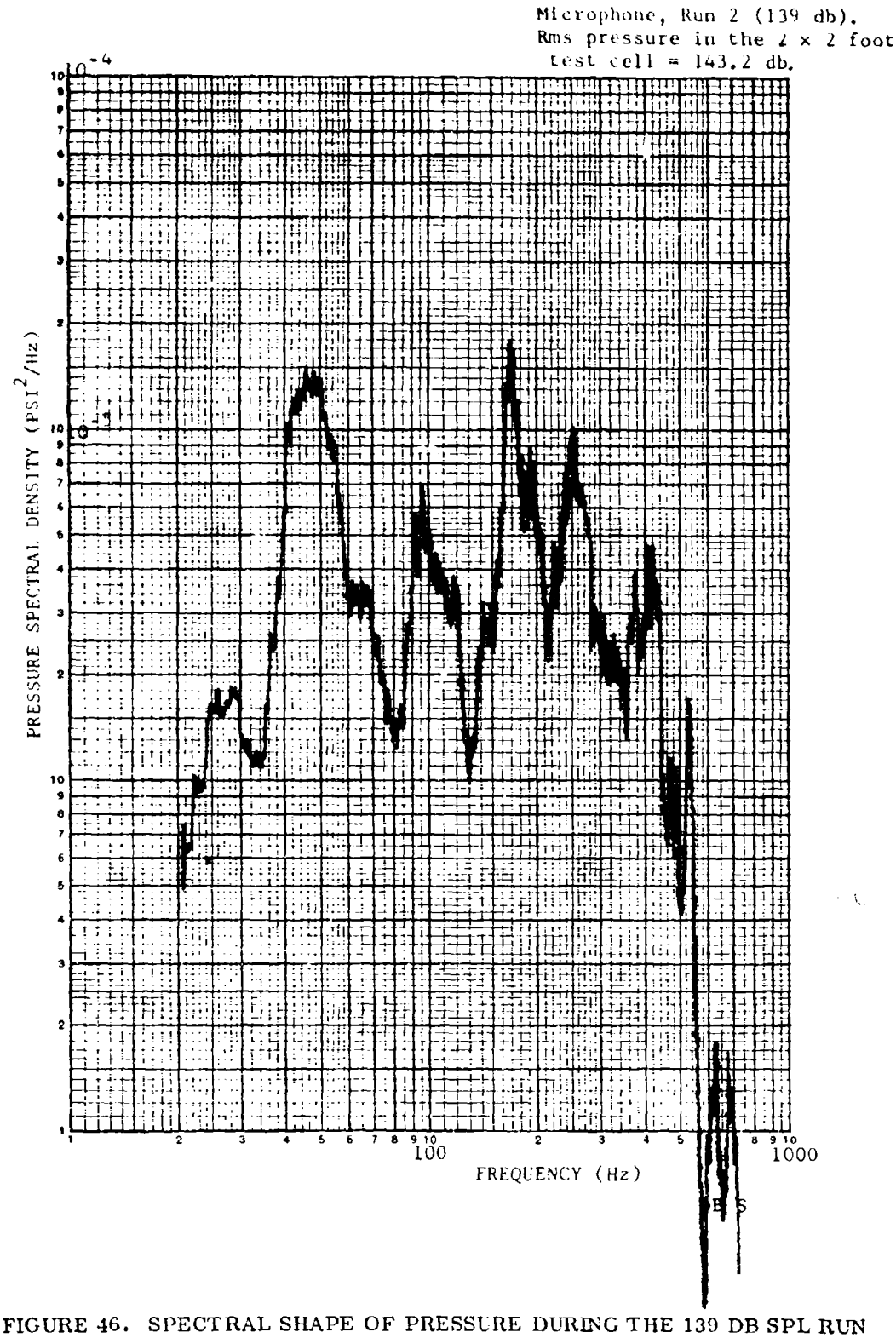

FIGURE 46. SPECTRAL SHAPE OF PRESSURE DURING THE 139 DB SPL RUN

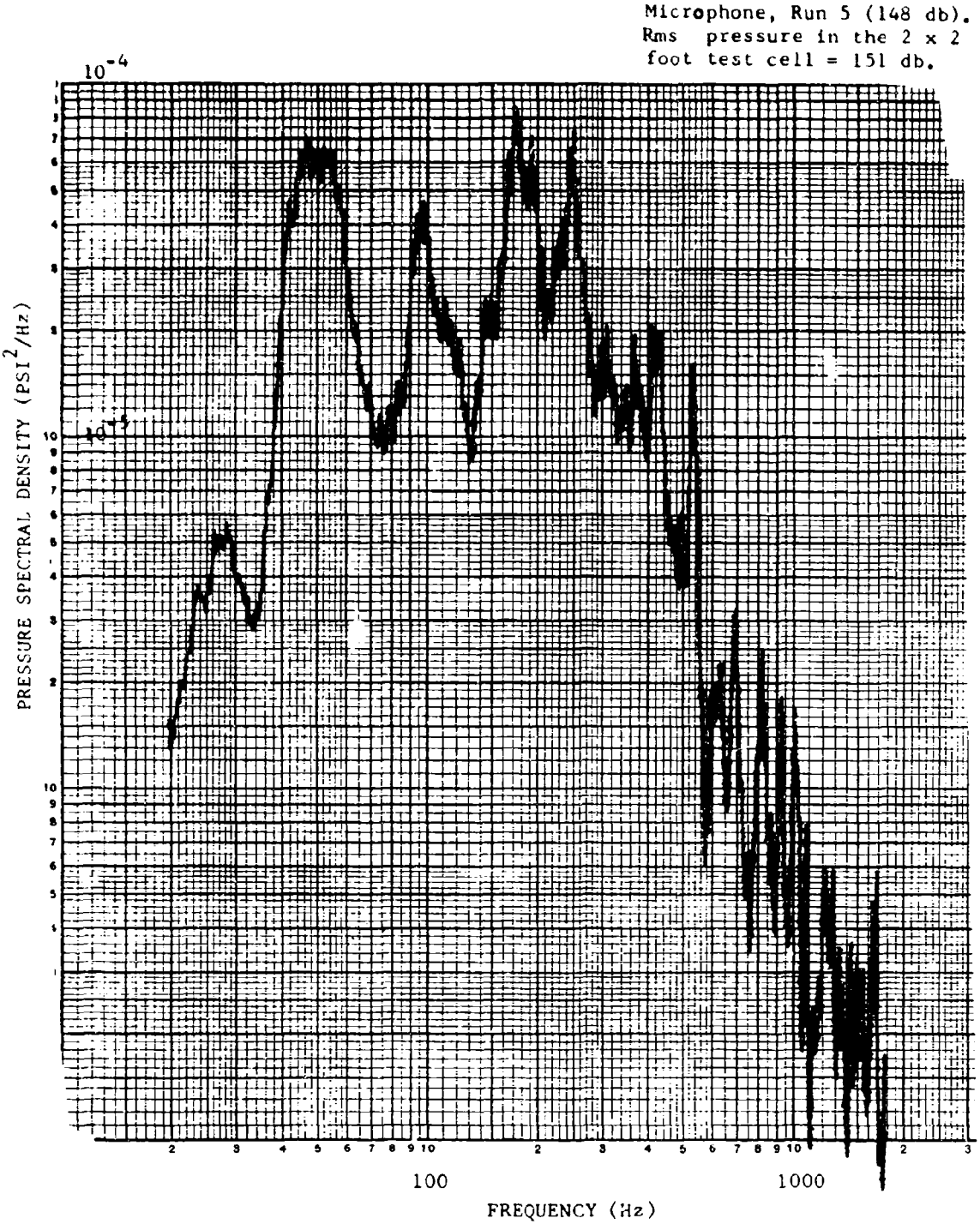

FIGURE 47. SPECTRAL SHAPE OF PRESSURE DURING THE 148 DB SPL RUN

A comparison of strains at gages No. 1 and 2 in Table IV indicate approximately equal strains. Since gage No. 1 at the center of bay 5 experiences more biaxial straining than gage No. 2 at the stiffener, it is possible that a skin failure (in the 90°-direction of the skin) at the panel center may occur prior to a skin failure at the stiffener.

A comparison of strains from gages No. 2 and 7 of Table IV indicate if a skin failure at the periphery of bay 5 would occur, then the failure would be at the gage No. 2 location, since the ultimate strain of the skin material of the central bay was less in the width direction than in the length direction (see the discussion below). This observation was utilized in the choice of the Candidate A-2 type specimen.

The average ultimate stresses reported in Figures A-1 and A-2 of the Appendix A were 182.1 ksi for the 0°-loading of a 0°-laminate and 5.82 ski for the 0°-loading of a 90°-laminate. The corresponding E's were 23,000,000 psi and 1,460,000 psi and the corresponding average ultimate strains are 7,800 micro-inch/inch and 4,000 micro-inch/inch. It should be noted that there was considerable scatter in the ultimate strength in the 0°-loading of the 90°-laminate. The maximum estimated acoustic response strains in Table V were less than 25 percent of these static ultimate strains.

If the strains at 165 db SPL at the various gages that were lost may be extrapolated based on their relation with gage No. 7 that performed thru the 165 db runs, then estimated strains may be obtained at 165 db SPL. Such strains are given in Table V.

For the strains (Table V) in the 90°-direction of the skin, the estimated maximum rms strain level was approximately 800 micro-inch/inch. The 800 micro-inch/inch estimate was at least 30 percent higher than the maximum strains measured during the acoustic tests of panels A-GG-B-2 and A-GG-B-3.

TABLE V. ESTIMATE OF RMS STRAINS OF PANEL A-GG-B-1 AT 165 DB SPL

Gage Attachment	Gage	Gage Direction(1) (degrees)	Estimated RMS Strain (Micro-inch/inch)
Skin	1	90	700-800
Skin	2	90	700-800
Skin	3	90	300(2)
Tee Section	4	0	70(2)
Tee Section	5	0	280-320
Skin	6	0	360-420
Skin	7	0	600(2)
Skin	8	0	260(2)
I-Beam	9	90	65-75
I-Beam	10	90	50-60
Skin	11	90	700-800
Skin	12	90	350-400
Skin	13	0	350-700
Skin	14	0	400-550
Skin	15	90	840-960

(1) The 0°-direction is parallel to the length of the tee sections.
(2) Measured.

V.2 TEST OF ACOUSTIC PANEL A-GG-B-2

Acoustic panel A-GG-B-2 was fabricated according to the procedure discussed in Section III. The fabrication procedure applied to panel A-GG-B-2 resulted in the manufacture of a flat panel with good, visible bond lines. Immediately before testing, 10-32 flat head steel machine screws (Figure 48) with elastic stop nuts were installed around the outer periphery of the titanium alloy frame, EC 2216 adhesive, graphite-epoxy skin, FM-123-2 adhesive, and graphite-epoxy doubler assembly as an added precaution to prevent a catastrophic failure in the fixture section of the panel during the acoustic fatigue testing.

V.2.(a) Instrumentation and the Assembly of the Panel to the Test Fixture

Panel A-GG-B-2 was instrumented with 17 strain gages (Figures 31 and 49). The first 15 were located as they had been located on panel A-GG-B-1. No thermocouples were installed on panel A-GG-B-2 since no panel heating was observed during the acoustic test of panel A-GG-B-1.

Panel A-GG-B-2 and the wooden beams (to produce a relatively smooth surface for air flow across the test jig in the progressive wave test chamber) were attached to the test fixture in the same manner that panel A-GG-B-1 and the wooden beams were attached to the test fixture.

V.2.(b) Modal Surveys

After panel A-GG-B-2 was attached to the test fixture, the panel was excited with loudspeaker excitation for modal surveys. Two Endevco 2222B microminiature accelerometers were used during the modal surveys to obtain natural frequencies, phasing between bays, and an estimate of nodal lines. For the modal surveys, one of the accelerometers was cemented in the center of bay 5, the central bay. The other accelerometer was attached to the panel with vacuum seal putty to facilitate its use as a roving accelerometer.

Panel resonances were obtained by examining peaks of accelerometer output in frequency sweeps (during a sweep, the roving accelerometer was not moved) under loudspeaker excitation up to 1,000 Hz. In obtaining the panel resonances and acceleration data, the roving accelerometer was positioned at the center of the bay being examined.

Following the determination of natural frequencies, the panel mode shapes were obtained from acceleration amplitude and phase readings at the center of each bay at resonant frequencies up to 500 Hz. The accelerometer readings in Figure 50 define the quantitative modal surveys under the loudspeaker excitation. In some cases, the bay with the maximum acceleration response was not the bay in which the roving accelerometer was located when the resonance was discovered experimentally, but this did not affect the tuning accuracy of the mode in obtaining data for Figure 50.

Nodal lines were then obtained by sprinkling non-corrosive polyvinyl chloride pellets on the surface of the skin and exciting panel resonances with the loudspeaker excitation up to 800 Hz (Figure 51).

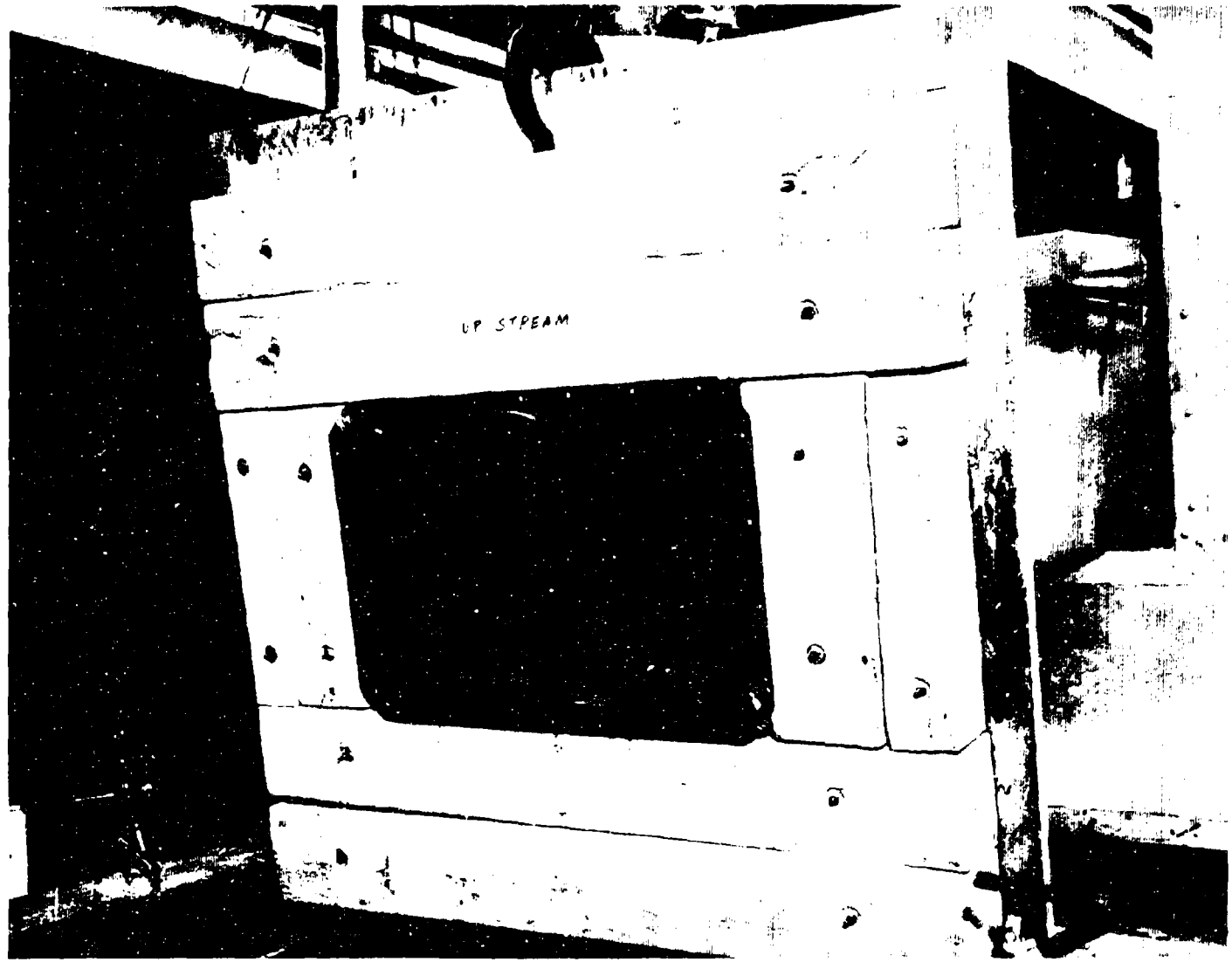

FIGURE 48. PANEL A-GG-B-2 AND WOOD BLOCKS ATTACHED TO TEST FIXTURE IN VERTICAL POSITION

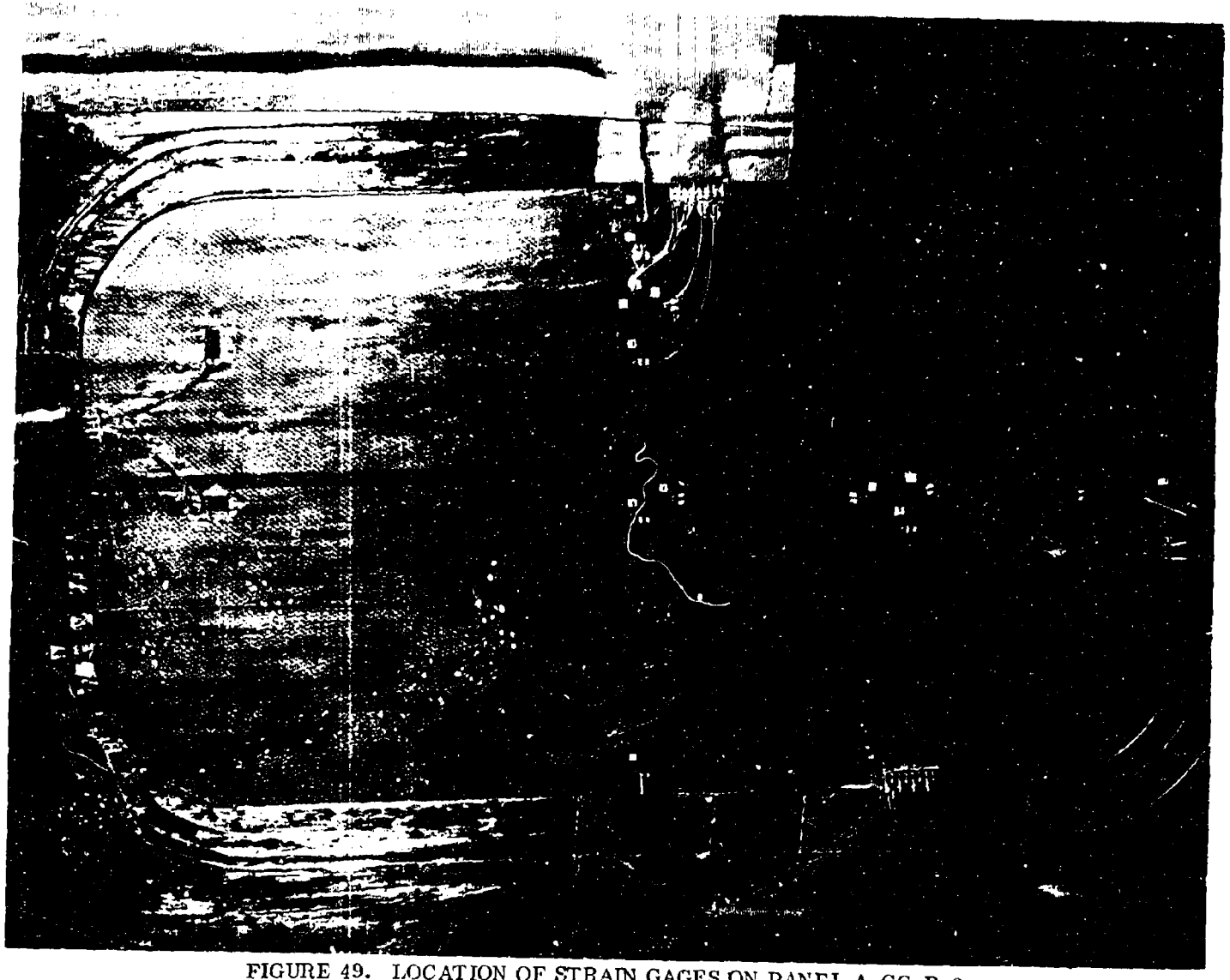

FIGURE 49. LOCATION OF STRAIN GAGES ON PANEL A-GC-B-2

126 Hz

1 <10	2 -14	3 <10
4 +37	5 +430	6 +14
7 <10	8 <10	9 <10

Peaked on Bay 5

187 Hz

1 <10	2 -94	3 <10
4 -320	5 +2360	6 -100
7 <10	8 -90	9 <10

Peaked on Bay 5

238 Hz

1 <10	2 -105	3 <10
4 -2840	5 +1760	6 -142
7 -12	8 -112	9 <10

Peaked on Bay 4

268 Hz

1 +18	2 -28	3 <10
4 +4700	5 +430	6 -73
7 -20	8 -11	9 <10

Peaked on Bay 4

325 Hz

1 -14	2 -220	3 -13
4 +1230	5 +1980	6 +620
7 +24	8 -130	9 <10

Peaked on Bay 4

356 Hz

1 <10	2 -15	3 -17
4 +160	5 +212	6 -1120
7 <10	8 -29	9 -21

Peaked on Bay 6

376 Hz

1 -15	2 -32	3 -26
4 +160	5 +12	6 -2500
7 -30	8 -13	9 -17

Peaked on Bay 6

401 Hz

1 -752	2 +650	3 +56
4 -760	5 +450	6 +3660
7 +49	8 -680	9 -15

Peaked on Bay 2

487 Hz

1 -40	2 +340	3 -27
4 +310	5 +270	6 -320
7 -60	8 +200	9 -23

Peaked on Bay 5

In this Figure, "Peaked on Bay X" means that the accelerometer was in Bay X during the frequency sweep to determine the resonances.
/ means the accelerometer reading has an approximately +90° phase angle with the reference bay.

FIGURE 50. QUANTITATIVE MODAL SURVEYS (ACCELEROMETER READINGS) OF PANEL A-GG-B-2

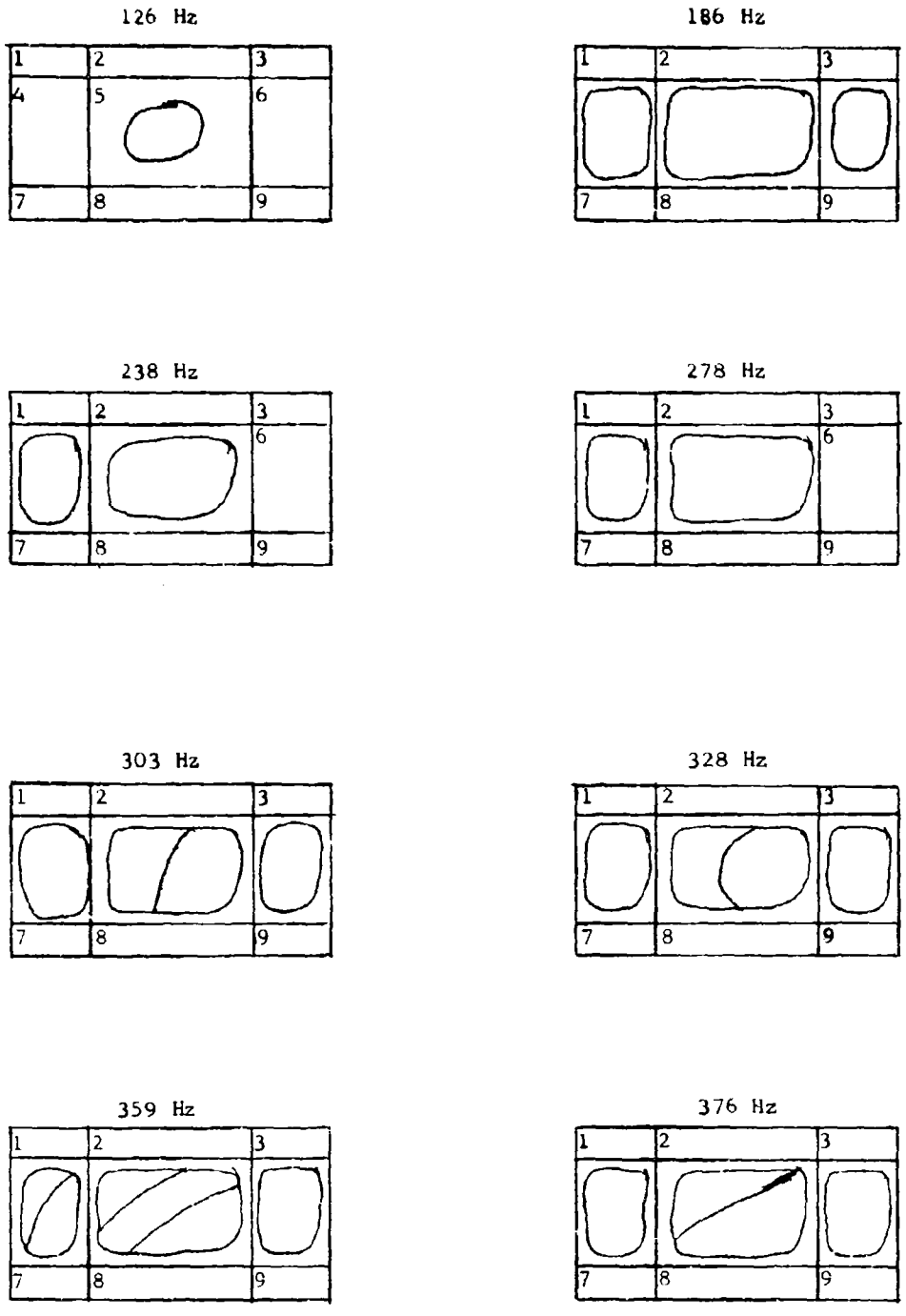

FIGURE 51. NODAL LINES UNDER LOUDSPEAKER EXCITATION OF PANEL A-GG-B-2

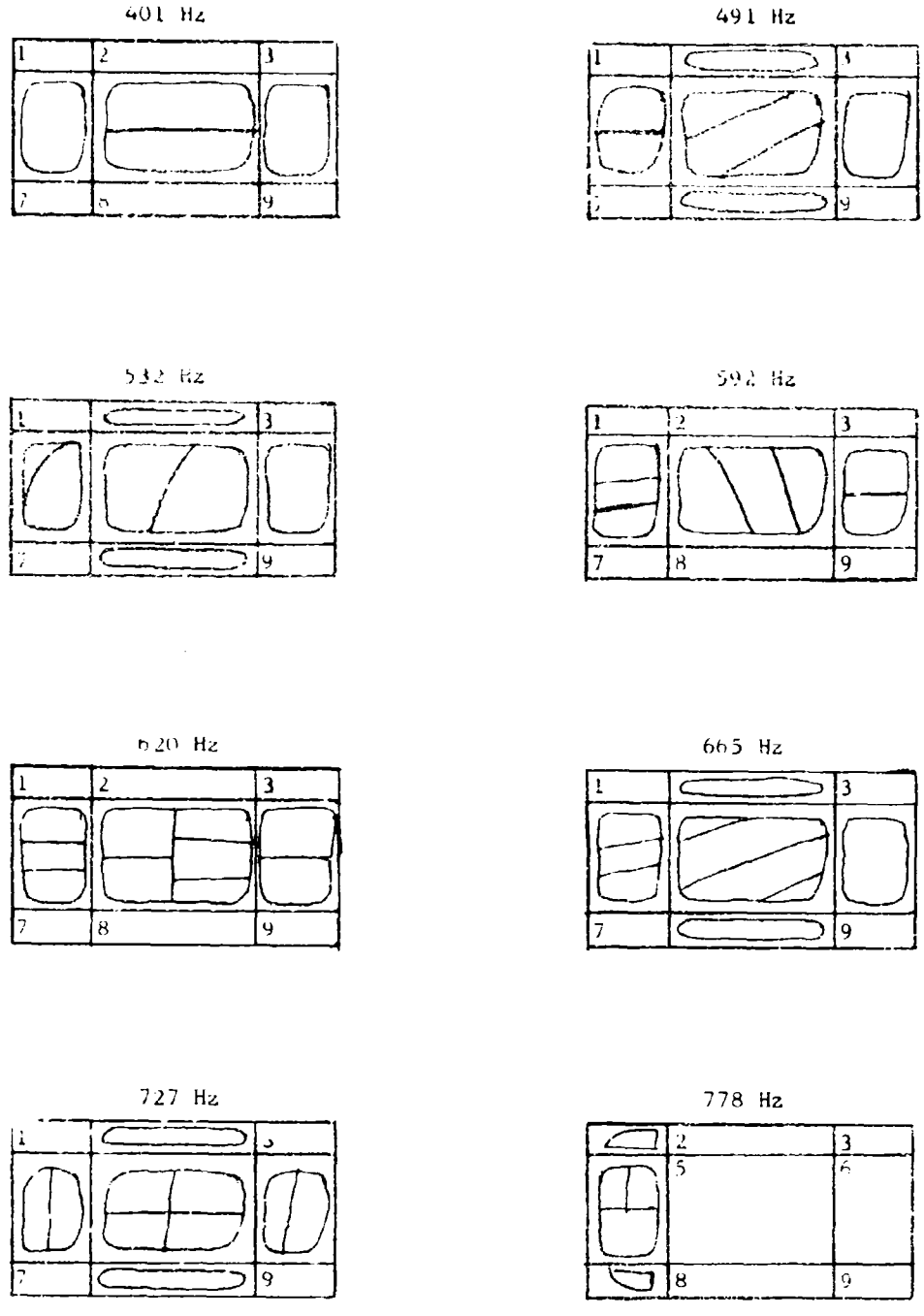

FIGURE 51. NODAL LINES UNDER LOUDSPEAKER EXCITATION OF PANEL A-GG-B-2
(Continued)

V.2.(c) Damping Factors

Damping factors (Table VI) associated with the decay of panel resonances following the termination of loudspeaker excitation were obtained using the logarithmic decrement method from oscillograph records of accelerometer signals.

At the principal resonance (187 Hz) of the center bay, a damping factor of 0.017 was obtained. The high damping in bay 4 at 236 Hz may be due to the influence of the graphite-epoxy doubler at one edge of the bay. The low damping factor of .007 at 312 Hz is probably due to the strain signal from the center of bay 5 emanating close to a nodal line.

TABLE VI. DAMPING FACTORS OF PANEL A-GG-B-2

FREQUENCY	VISCOUS DAMPING FACTORS	
	Bay 4	Bay 5
(Hz)		
127	bad	bad
187	.016	.017
238	.032	bad
260	bad	bad
312	bad	.007(1)
348	bad	bad

(1) See discussion under paragraph V.2.(c)

V.2.(d) Response to Acoustic Excitation

After the modal surveys were completed and damping factors were obtained under loudspeaker excitation, the acoustic test fixture with the panel in place was installed in the 4 x 4 foot test cell of the Northrop progressive wave acoustic test chamber for broadband acoustic loading.

The pressure at the center of the 4 x 4 foot test cell was obtained with the use of a calibration table (relating the pressure at the center of the 2 x 2 foot test cell and the 4 x 4 foot test cell) that had been obtained with all of the concrete test cell lids of the progressive wave test chamber in place. Therefore, when panel A-GG-B-2 replaced the concrete lid of the 4 x 4 foot test cell, microphone readings at the center of the 2 x 2 foot test cell were taken for use with the calibration chart to obtain the pressure at the center of the 4 x 4 foot test cell.

Beginning with an overall sound pressure level of 136 db at the center of the 4 x 4 foot test cell, which coincided with the center of the test panel, strain readings were taken (Table VII) as the pressure was increased in increments of 3 db until the maximum sound pressure level of 166 db was obtained.

TABLE VII. STRAIN GAGE RESPONSE
(MICRO-INCH/INCH-RMS) OF PANEL A-GG-B-2

	Overall Sound Pressure Level (db re 0.0002 dynes/cm^2)										
Strain Gage	136 db	139 db	142 db	145 db	148 db	151 db	154 db	157 db	160 db	163 db	166 db
1	88	112	128	152	176	200	225	260	275	300	330
2	114	160	210	260	310	345	400	450	500	545	600
3	12	20	27	38	48	62	80	108	130	170	210
4	4	5	6	9	---	---	---	---	---	---	52
5	14	23	30	42	---	---	---	---	---	200(1)	145(1)
6	68	80	90	104	114	120	140	150	160	190	210
7	72	96	110	138	164	200	240	280	320	345	390
8	14	20	24	32	40	52	70	95	115	150	180
9	4	6	8	11	---	---	---	---	---	---	70
10	8	9	10	12	---	---	---	---	---	---	78
11	26	34	44	66	80	100	140	170	230	290	350
12	17	26	32	42	---	---	---	---	---	---	260
13	21	28	34	48	---	---	---	---	---	---	220
14	25	32	40	58	80	100	140	170	210	260	out
15	24	34	40	56	---	---	---	---	---	---	320
16	88	110	128	150	170	200	225	250	out	---	---
17	78	102	120	156	190	230	300	345	430	460	530

(1) Questionable reading

Strain and pressure signals were recorded on magnetic tape for spectral density analysis of the pressure and response at 139, 148, 157, and 166 db overall SPL.

At the 139 db SPL, a noise reduction investigation was conducted under discrete frequency excitation (see Paragraph V.2.(e)).

The panel remained at room temperature during the acoustic tests. The tests to obtain strain data at overall sound pressure levels of 163 db and lower were conducted as rapidly as possible to prevent significant accumulation of fatigue damage in the panel prior to the acoustic fatigue test at the maximum sound pressure level of 166 db. The exposure to the acoustic excitation at the lower sound pressure levels was approximately two minutes when tape recordings were not taken and 6 minutes when tape recordings were taken.

V. 2. (e) Noise Reduction

An investigation of noise reduction through panel A-GG-B-2 was conducted according to the acoustic test plan of paragraph IV. 3. (e). The noise reduction was obtained with a signal from a microphone located within panel A-GG-B-2 during a discrete frequency sweep with the exposed surface of the panel subjected to 136 db SPL. At the fundamental panel resonance of 225 Hz (Figure 52), the noise reduction was 9.5 db (i.e., from 136 db SPL to 126.5 db SPL).

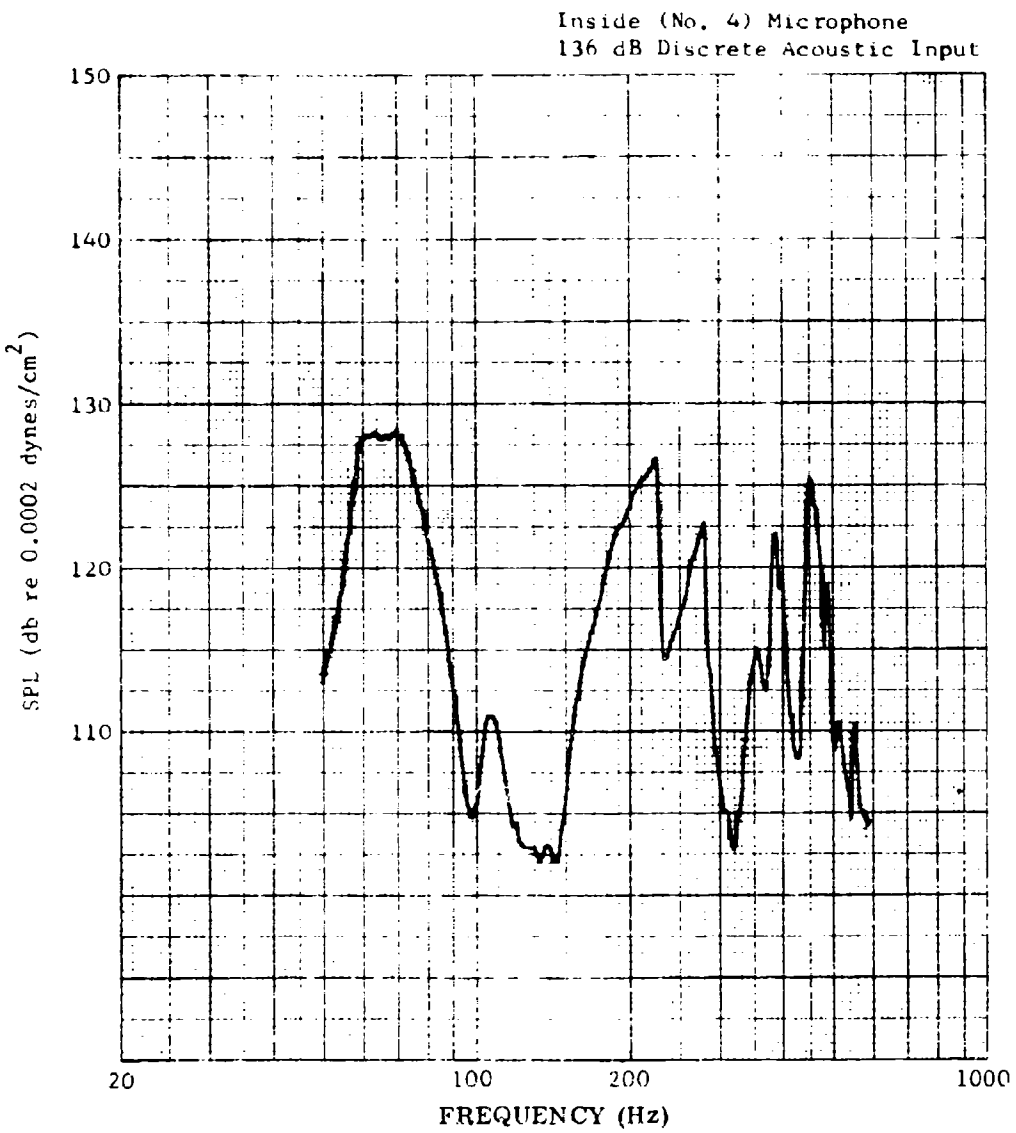

FIGURE 52. NOISE REDUCTION THROUGH PANEL A-GG-B-2

V.2.(f) Acoustic Fatigue Test

Prior to starting the acoustic fatigue test at 166 db SPL, a visual inspection of panel A-GG-B-2 indicated no evidence of damage. Visual inspections of the panel were made after every hour of acoustic exposure during the first 23 hours of the acoustic fatigue test and every three hours thereafter. In addition, a continuous monitoring of strain gage and microphone signals was made during the acoustic fatigue test.

Until 5 hours of test at 166 db SPL, all bays remained taut. Then, until 15 hours of test, the central bay 5 was substantially softer than the large rectangular bays 4 and 6. By the end of 17 hours of exposure, bay 4 had become as flexible as bay 5 and visible signs of dusting were observed near the intersection of bay 4 and the graphite-epoxy edge doubler (on the exposed surface). At the end of 23 hours of exposure, it was observed that the FM-123-2 bond between the graphite-epoxy edge doubler and bay 4 of the skin had deteriorated causing a gap (delamination) to exist between the skin and doubler (between the arrows in Figure 53). Panel A-GG-B-2 was then removed from the test fixture for a closer inspection, that revealed no failures in the test section of the panel.

The repair of panel A-GG-B-2 at the end of 23 hours of test exposure is described below. The delaminated zone in bay 4 was approximately semicircular with a 2.5 inch radius. The purpose of the repair was to allow the acoustic fatigue test of panel A-GG-B-2 to be resumed at the 166 db SPL without disturbing significantly the state of stress (during test) in the center bay 5 from the state existing during the first 23 hours of test exposure. The repair was successful and its objectives were reached.

The repair consisted of injecting (and subsequently curing) EC 2216 adhesive into the delaminated area and of bonding fiberglass/epoxy doublers in bays 4 and 6 (Figure 54). The installation of a doubler in bay 6 was both a safety precaution to prevent a failure in bay 6 such as had occurred in bay 4 and a means of maintaining weight symmetry about the center lines of the panel.

For the repair, EC 2216 adhesive was injected into the delaminated area by pushing the adhesive into the zone with a 0.005 inch aluminum shim stock. The intent was that the subsequent capillary action of the adhesive would provide a uniform film over the interior surfaces of the delaminated zone so that a viable adhesive bond would be obtained.

Four-ply disc shaped Narmco 500 E-glass (181 cloth impregnated with epoxy) were laid up, cured, and sanded to provide a taper on the doubler section extending towards the center of bay 4 and bay 6. These doublers were then assembled with EC 2216 adhesive to the skin/stiffener side of bay 4 and bay 6 (Figure 54).

In the bonding operation with the EC 2216 adhesive, the cure was at ambient temperature for approximately 120 hours. The recommended cure temperature for this adhesive system is 72 hours at 77F for full cure. The adhesive mix was prepared per the manufacturers instructions using a 100/100 weight ratio.

Following the repair described immediately above, the strain gages and lead wires of panel A-GG-B-2 were checked to determine what repairs and/or installation of new gages could be made to enable strain data to be taken when the acoustic fatigue test was resumed. Repair and the installation of new gages were performed. In particular, a new gage No. 2 was installed adjacent to the existing (fatigues) gage No. 2

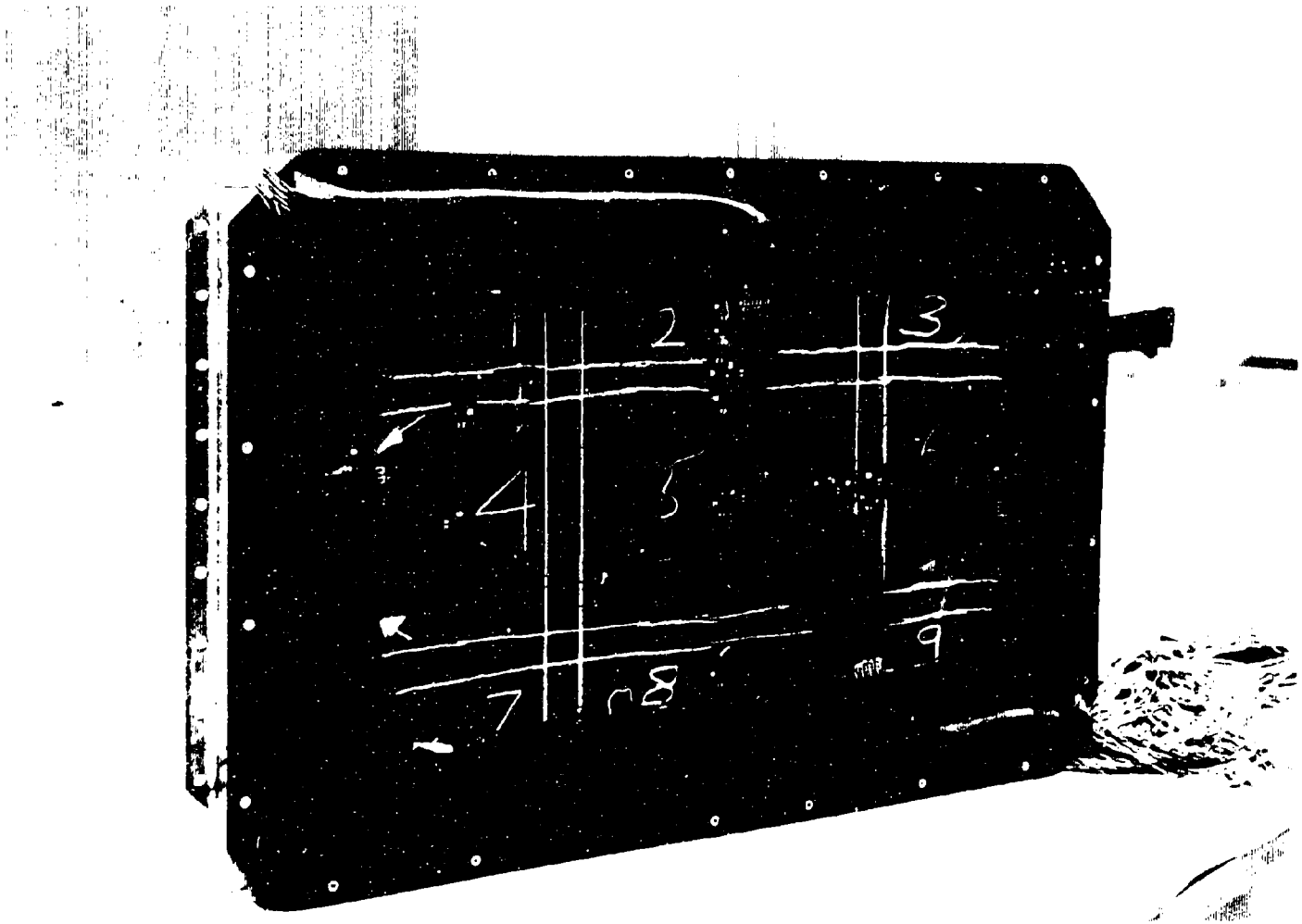

FIGURE 53. ADHESIVE FAILURE (BETWEEN ARROWS) IN BAY 4 OF PANEL A-GG-B-2

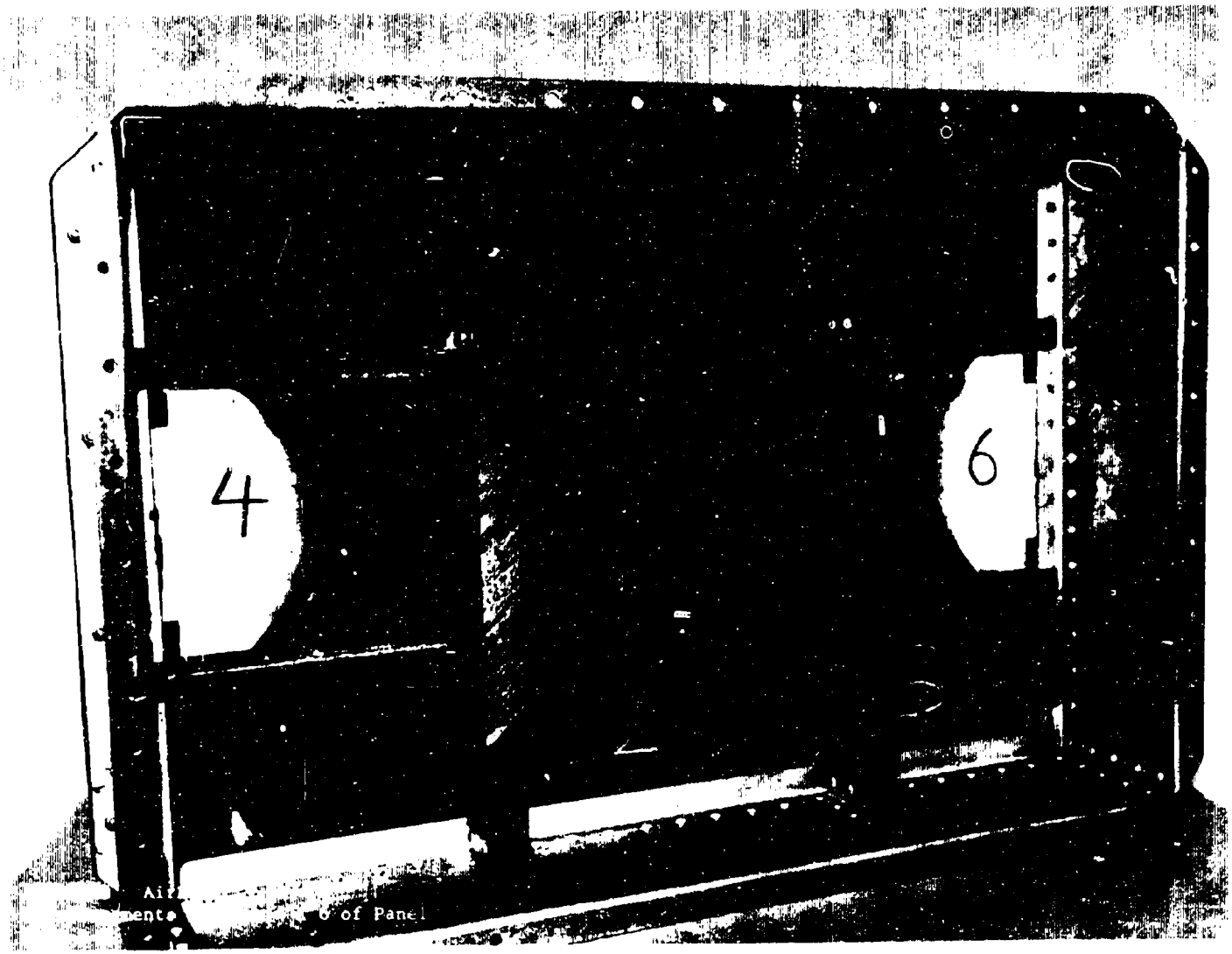

FIGURE 54. DOUBLERS IN BAYS 4 AND 6 ADDED TO PANEL A-GG-B-2

and gage No. 18 was added perpendicular and adjacent to the gage No. 2. The purpose of gage No. 19 was to obtain strain data in perpendicular directions in the skin in the vicinity of gage No. 2. The nearest edge of gage No. 18 to the tee stiffener was 0.06 in.

The rms strain readings that were taken when the acoustic fatigue test was resumed at 166 db overall SPL are in Table VIII. Also, in Table VIII are the strain readings that were recorded in the last column of Table VII, namely the strains when the acoustic fatigue test began. Except for gage No. 8, the average of the strain readings for a gage in Table VIII is within 10 percent of its extreme readings. Consequently, the conclusion was made that the addition of the adhesive and glass doublers in bays 4 and 6 did not appreciably change the acoustic response of the central bay 5.

TABLE VIII. STRAIN READINGS OF PANEL A-GG-B-2 AT 166 DB SPL

STRAIN GAGE	STRAIN A(1) (Micro-Inch/Inch-rms)	STRAIN B(2) (Micro-Inch/Inch-rms)
1	330	out
2	600	600-500(4)
3	210	220-220(4)
4	52	50
6	210	210-210(4)
7	390	400-380(4)
8	180	170-146(4)
9	70	64
11	350	320-330(4)
14	out	144
15	320	340
17	530	out
18(3)	none	56-56(4)

(1) Strain A was the strain at the beginning of the acoustic fatigue test and was recorded in the last column of Table VII.

(2) Strain B was the strain when the acoustic fatigue test was resumed after the damage (that had occurred at the 23 hour inspection) was repaired.

(3) Gage No. 18 was added following the repair.

(4) When two integers are separated by a dash, the first of the two strain readings was taken when the acoustic test was resumed and the second of the two readings was taken after approximately four more minutes of exposure. No explanation is available for the differences in excess of five percent; the differences less than five percent are within the tolerances expected for these measurements.

Following the recording of strains reported in Table VIII, the acoustic fatigue test was resumed with regular visual inspections of panel A-GG-B-2 at three hour intervals. Strain gage response was monitored with the gage No. 7 reading being 405 ± 25 micro-inches/inch rms until the test was terminated.

The addition of the glass doublers in bays 4 and 6 caused these bays to become as taut as they had been at the beginning of the acoustic fatigue test. The addition of the glass doublers in bays 4 and 6 did not affect the softness that had been noted in the center bay 5 before the test suspension at 23 hours of exposure.

The acoustic fatigue test was halted at 116.2 hours of exposure at 166 db SPL. A hole had developed in the titanium alloy frame of panel A-GG-B-2 (Figure 55) at 113.2 hours of exposure, and did not change much during the next three hours of exposure. The 116.2 hours is equivalent to 1.23×10^8 cycles when the principal response frequency (295 Hz) at gage No. 2 in bay 5 is taken as the average frequency. The 295 Hz was taken from the spectral density analysis in Figure 61. An average response of 295 Hz at gage No. 2 was assumed since the on-line third octave spectral plots of gage No. 7 in bay 5 did not appreciably change during the duration of the test at 166 db SPL.

Damage was observed on the free flanges of panel A-GG-B-2 at the 23 hour inspection. The damage was not repaired since it was felt that damage would not reach proportions to cause the acoustic test to be halted prior to reaching the test objectives. The decision not to repair the damage was a correct decision, since the objective of demonstrating that the test section of panel A-GG-B-2 could sustain 10^8 cycles of exposure was reached.

The principal quantitative items obtained in the acoustic fatigue test were the average strain readings of 550 micro-inch/inch-rms at gage No. 2 and 52 micro-inch/inch-rms at gage No. 18 and these strains in bay 5 did not produce a failure in 1.23×10^8 cycles of exposure.

V. 2. (g) Data Analysis

Narrow band spectral analysis was conducted for the strain response and pressure loading of Table VII at SPLs of 139 db, 148 db, 157 db, and 166 db. The recordings at 148 db and 157 db were taken principally to have recorded signals if the strain gages did not survive to 166 db; however, with only two exceptions all gages survived to 166 db.

The pressure during the 139 db run and the 166 db run is shown in Figures 56 and 57. The strain spectral densities at gage No. 2 (in the central bay 5 at the intersection with a tee stringer) at 139, 148, 157, and 166 db SPL are in Figures 58 through 61. The strain spectral densities of gages No. 13 (in the center of bay 6), 17 (in bay 4 at the intersection with the tee stringer), and [illegible] on the skin between bays 2 and 5 and opposite the stringer) at 139 db and 166 db [illegible] are in Figures 62 through 67. From observations of Figures 58 through 67, one may note how natural frequencies shift upward as the overall SPL increases.

For the data analysis presented in Figures 56 through 67, a 2.5 second averaging time with a 0.6 Hz/second sweep rate with a 6.3 Hz bandwidth filter for the 20 through 250 Hz range was used. For frequencies above 250 Hz, a 1.0 second averaging time with a 3.3 Hz/second sweep rate with a 14 Hz bandwidth was used. A six second loop was used in obtaining all of these data.

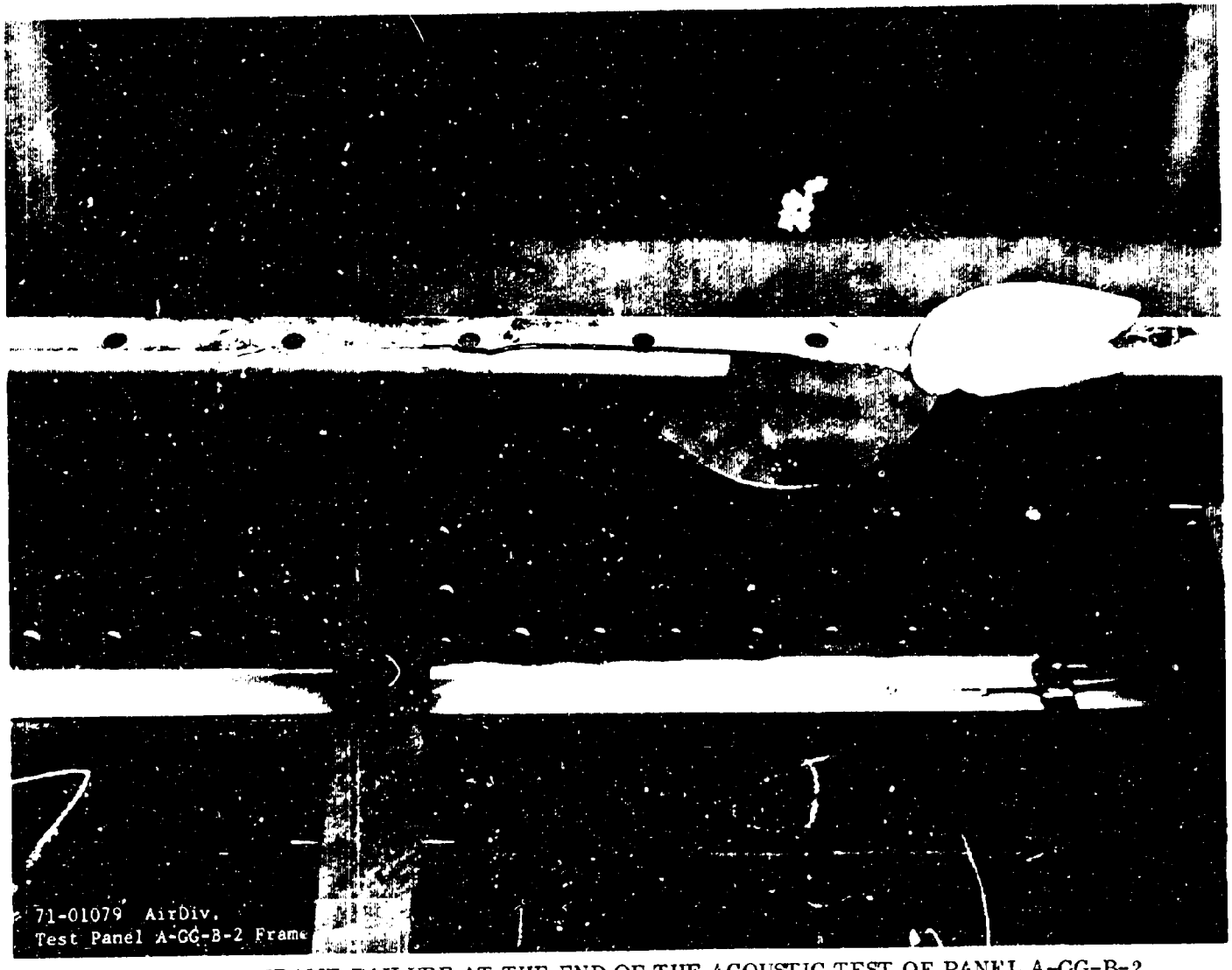

FIGURE 55. FRAME FAILURE AT THE END OF THE ACOUSTIC TEST OF PANEL A-GG-B-2

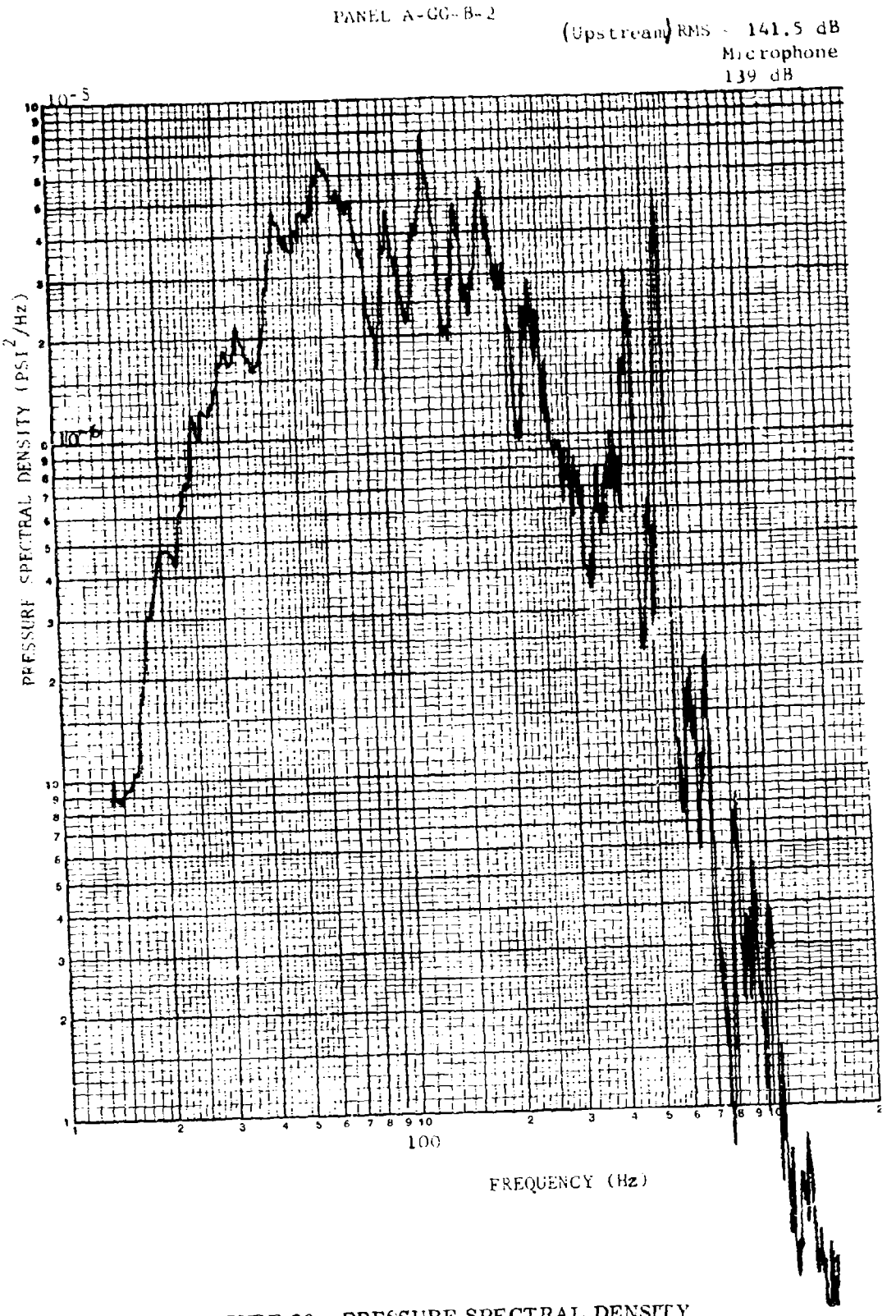

FIGURE 56. PRESSURE SPECTRAL DENSITY

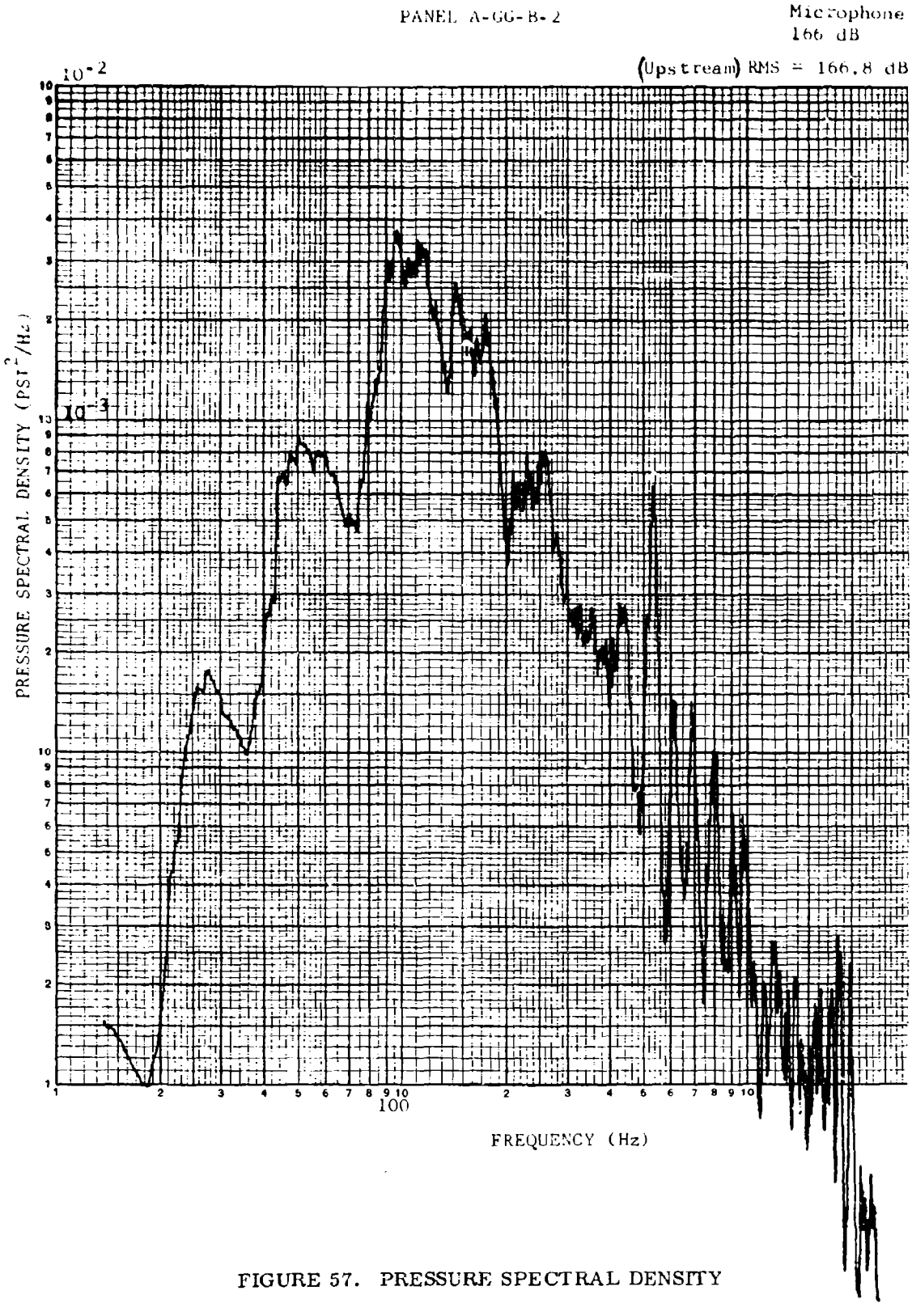

FIGURE 57. PRESSURE SPECTRAL DENSITY

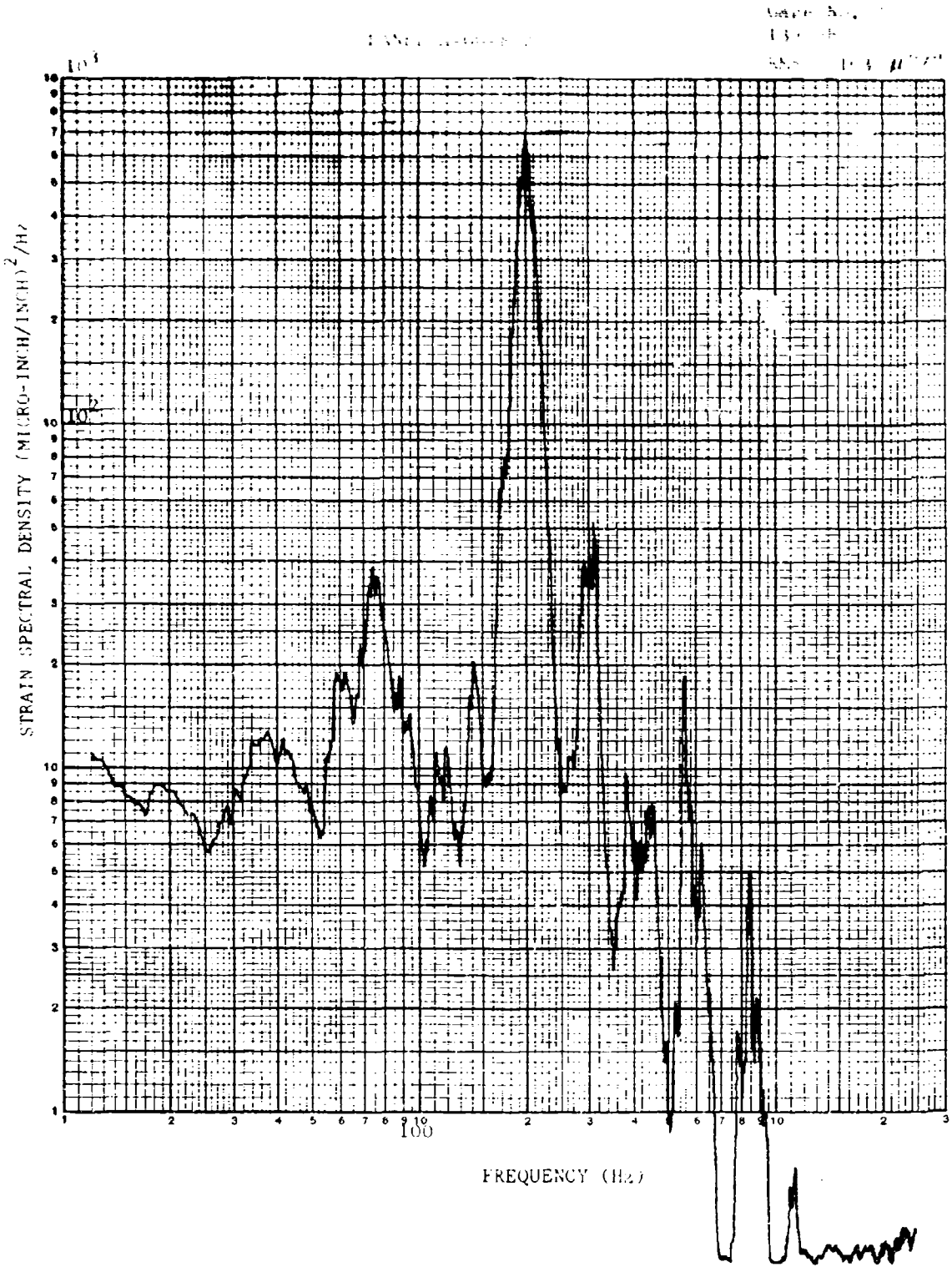

FIGURE 58. STRAIN SPECTRAL DENSITY

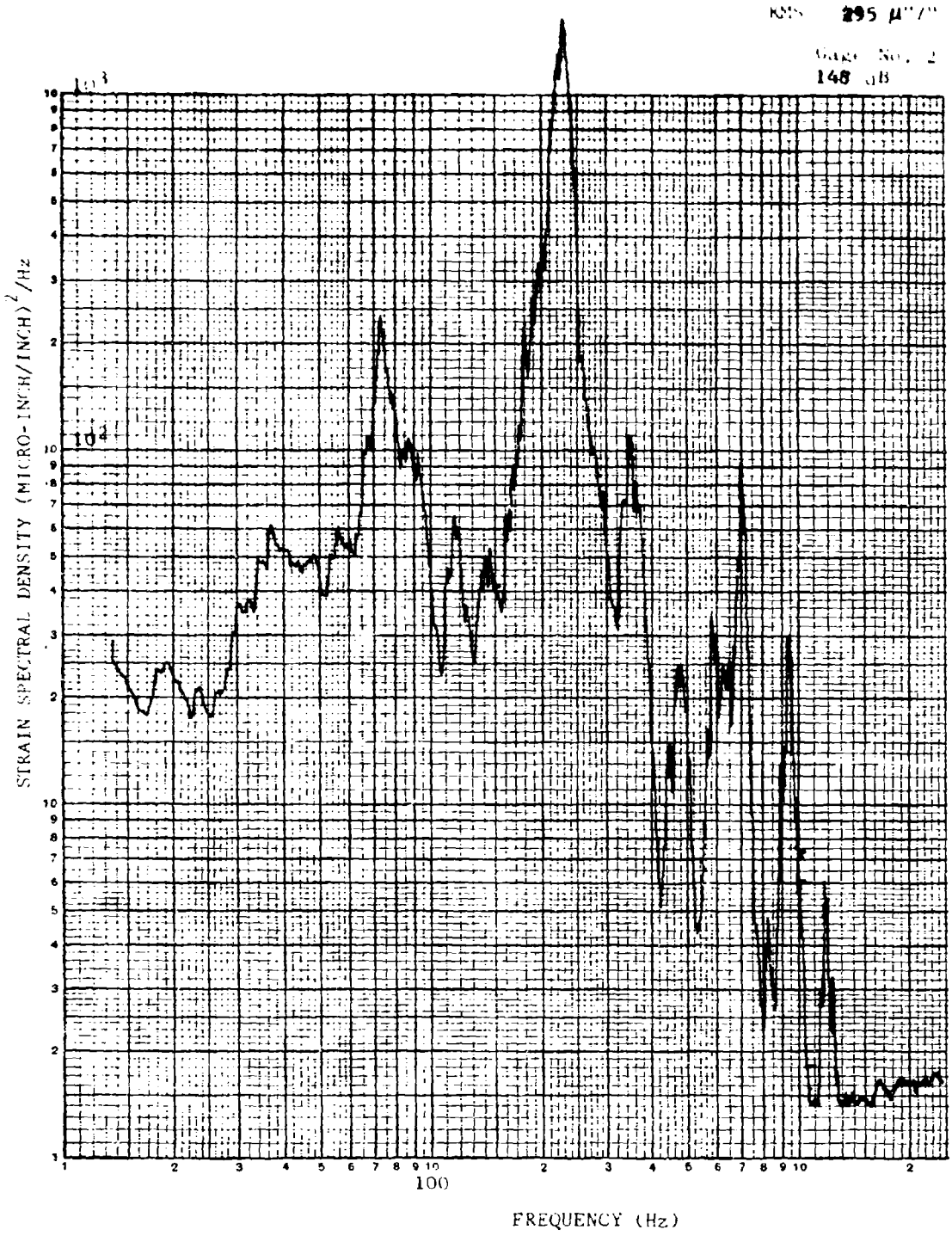

FIGURE-59. STRAIN SPECTRAL DENSITY

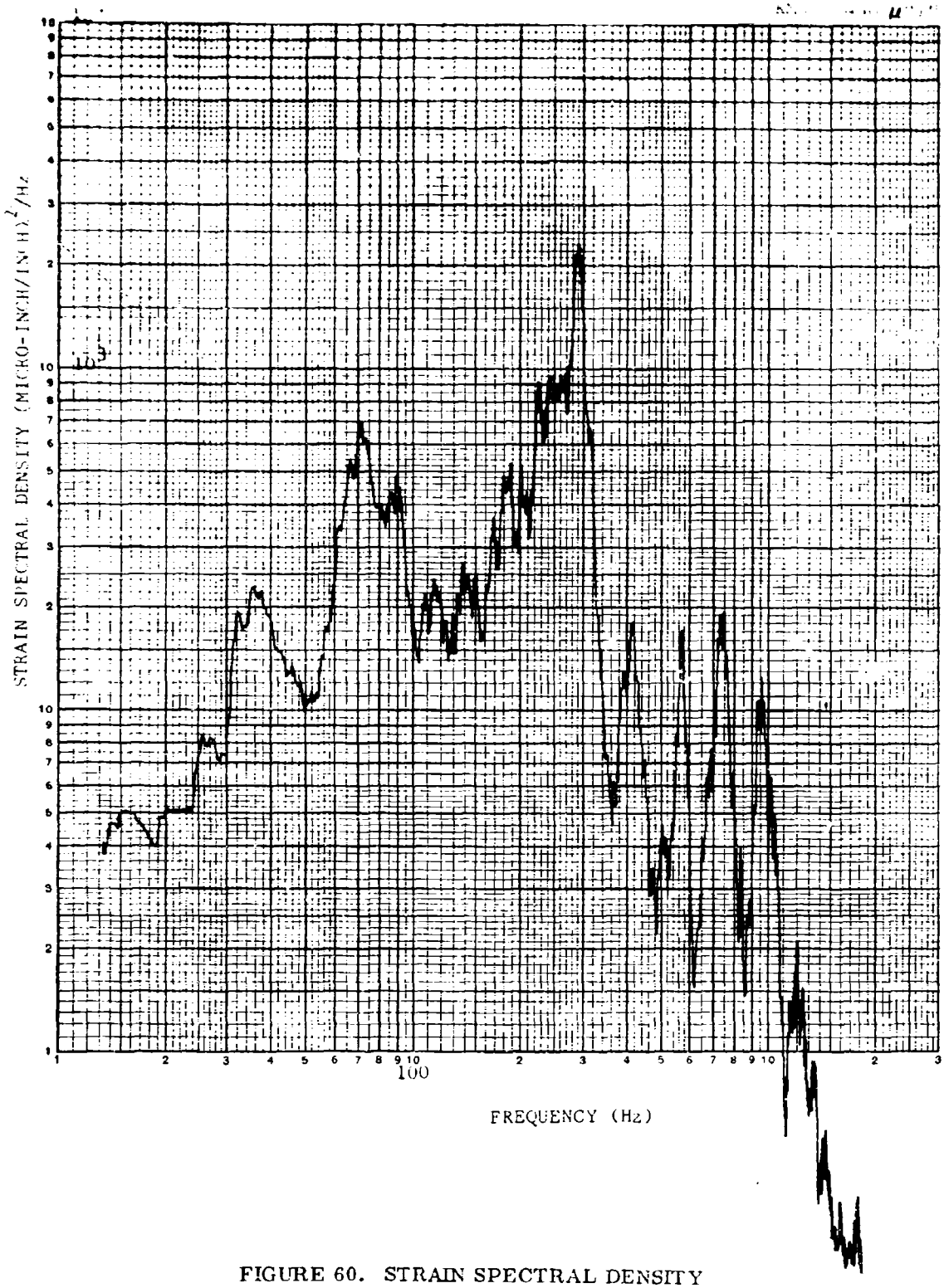

FIGURE 60. STRAIN SPECTRAL DENSITY

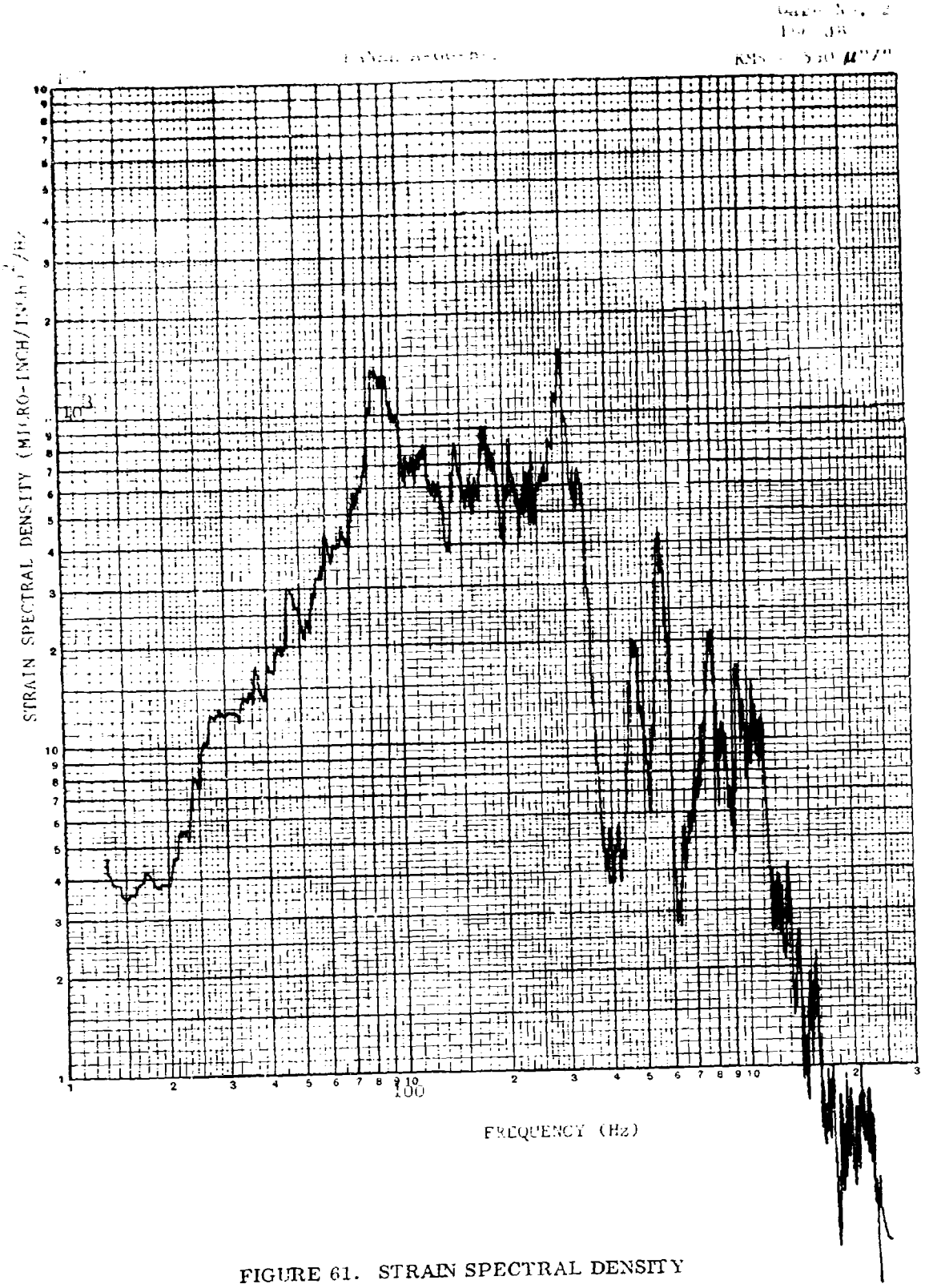

FIGURE 61. STRAIN SPECTRAL DENSITY

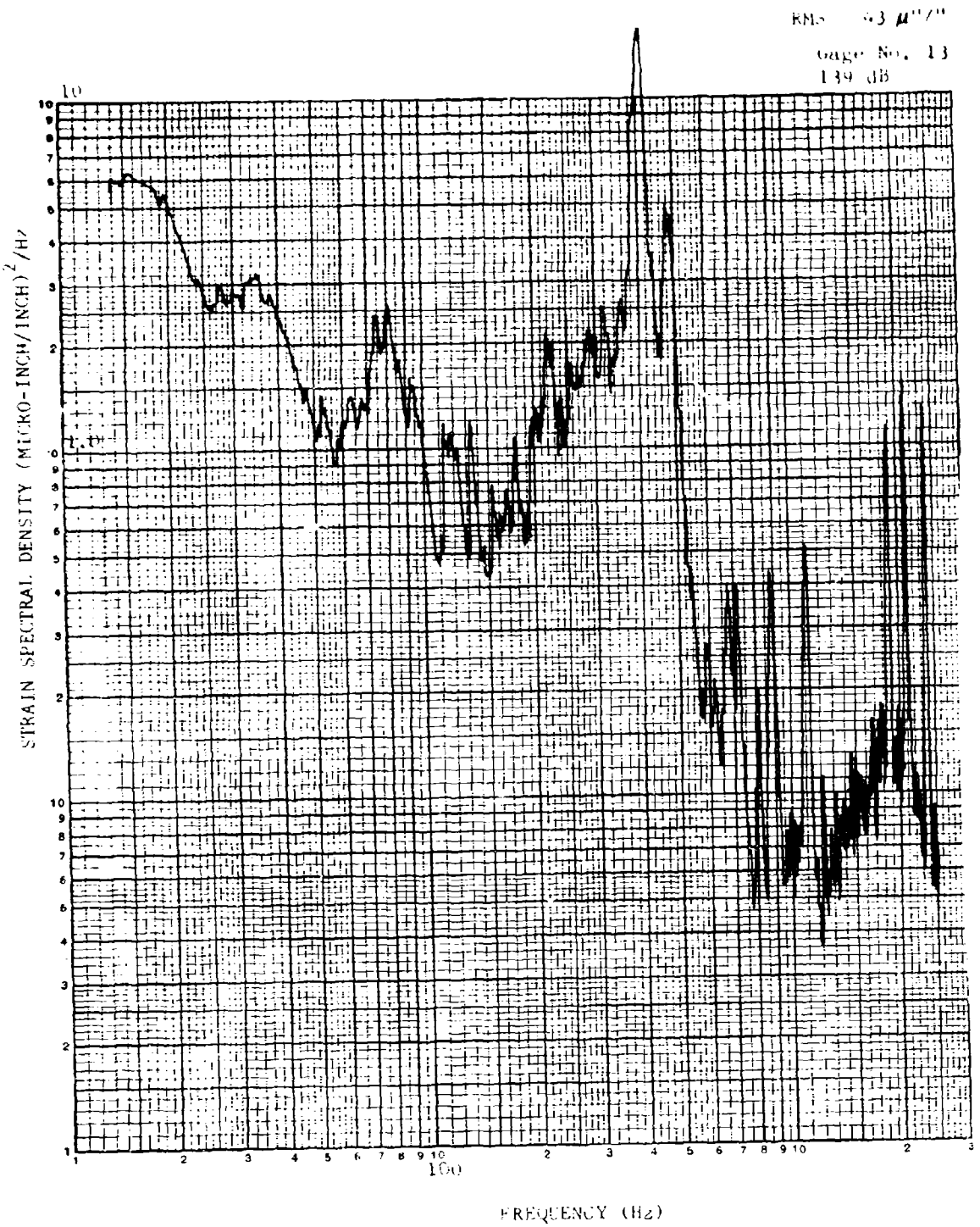

FIGURE 62. STRAIN SPECTRAL DENSITY

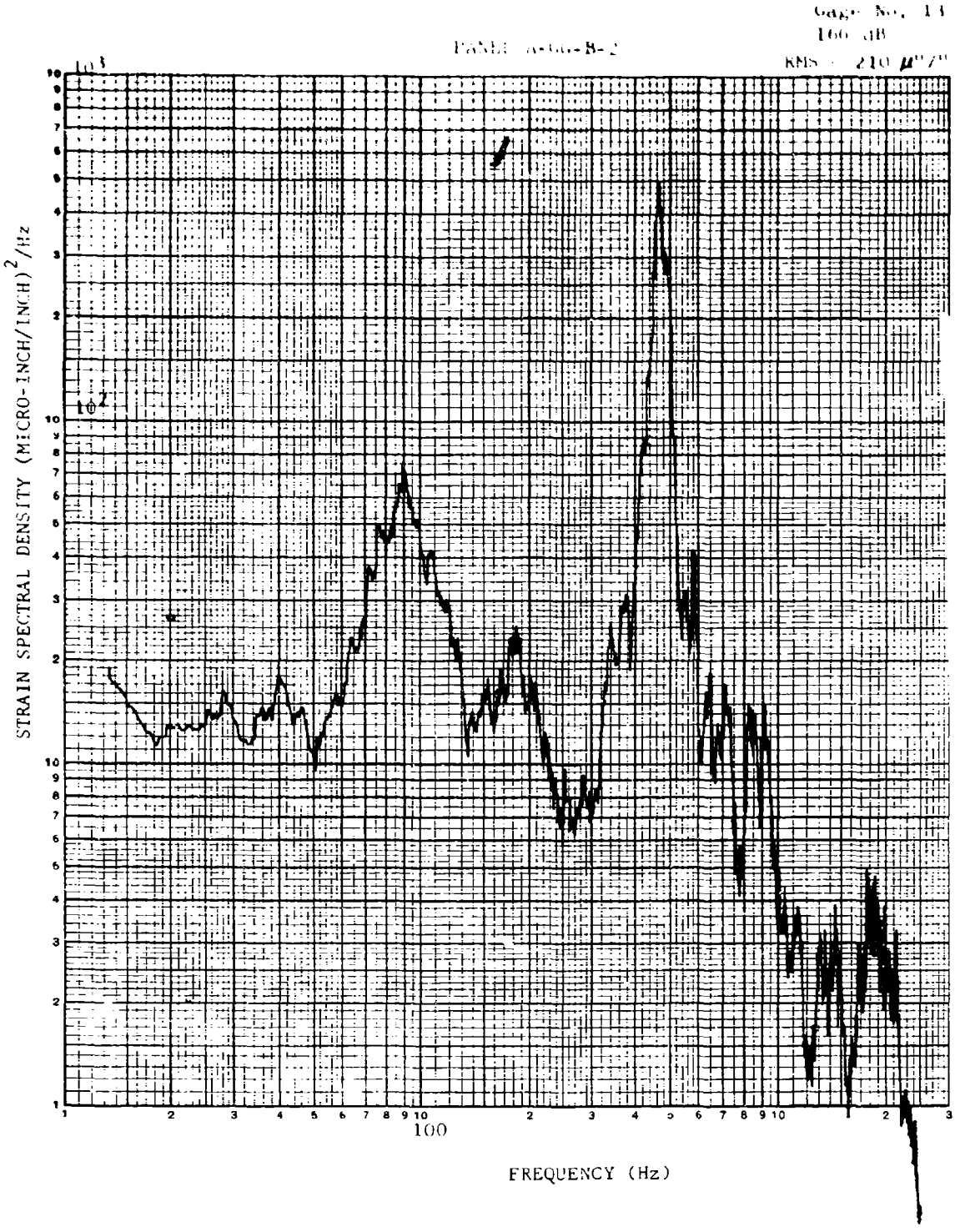

FIGURE 63. STRAIN SPECTRAL DENSITY

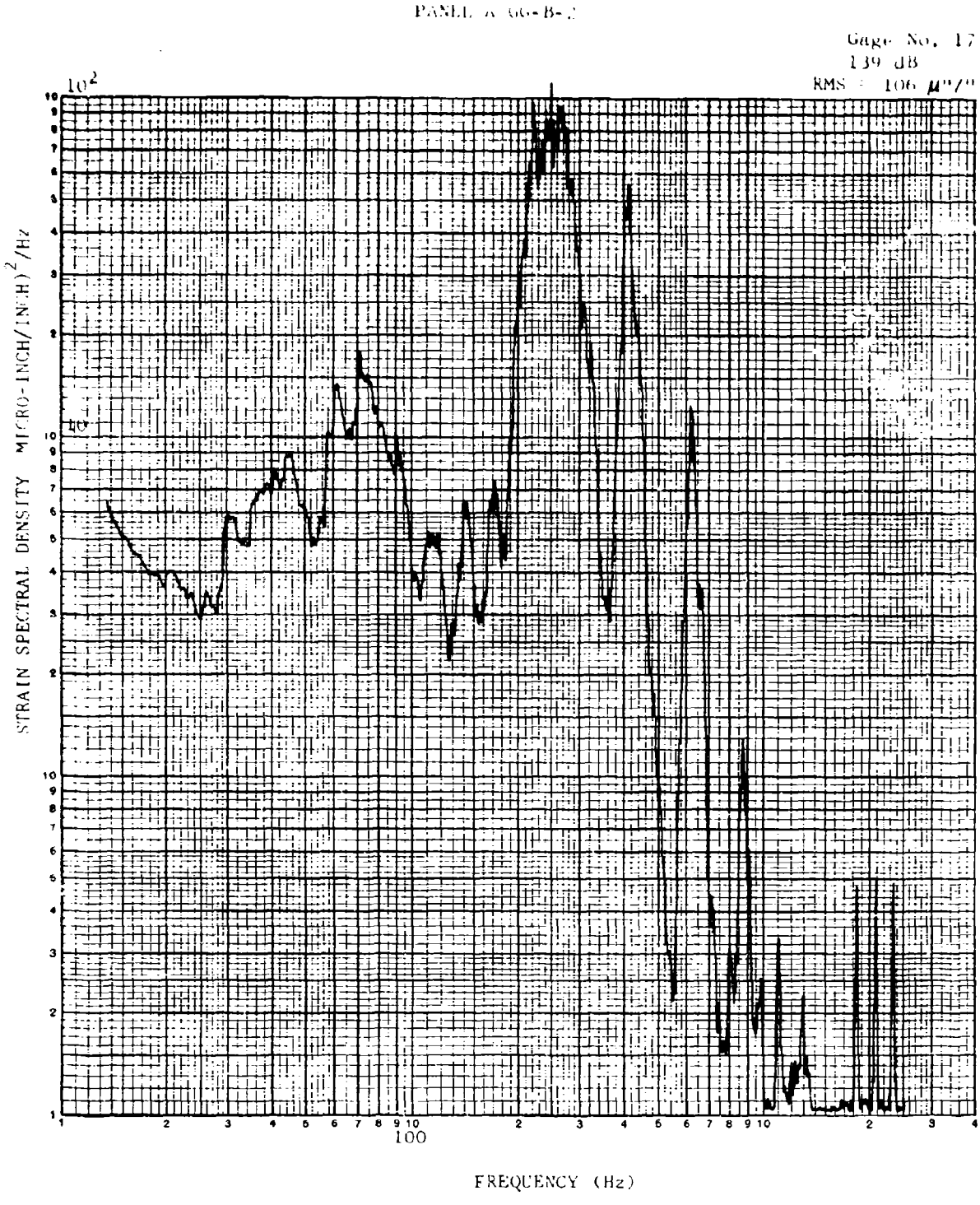

FIGURE 64. STRAIN SPECTRAL DENSITY

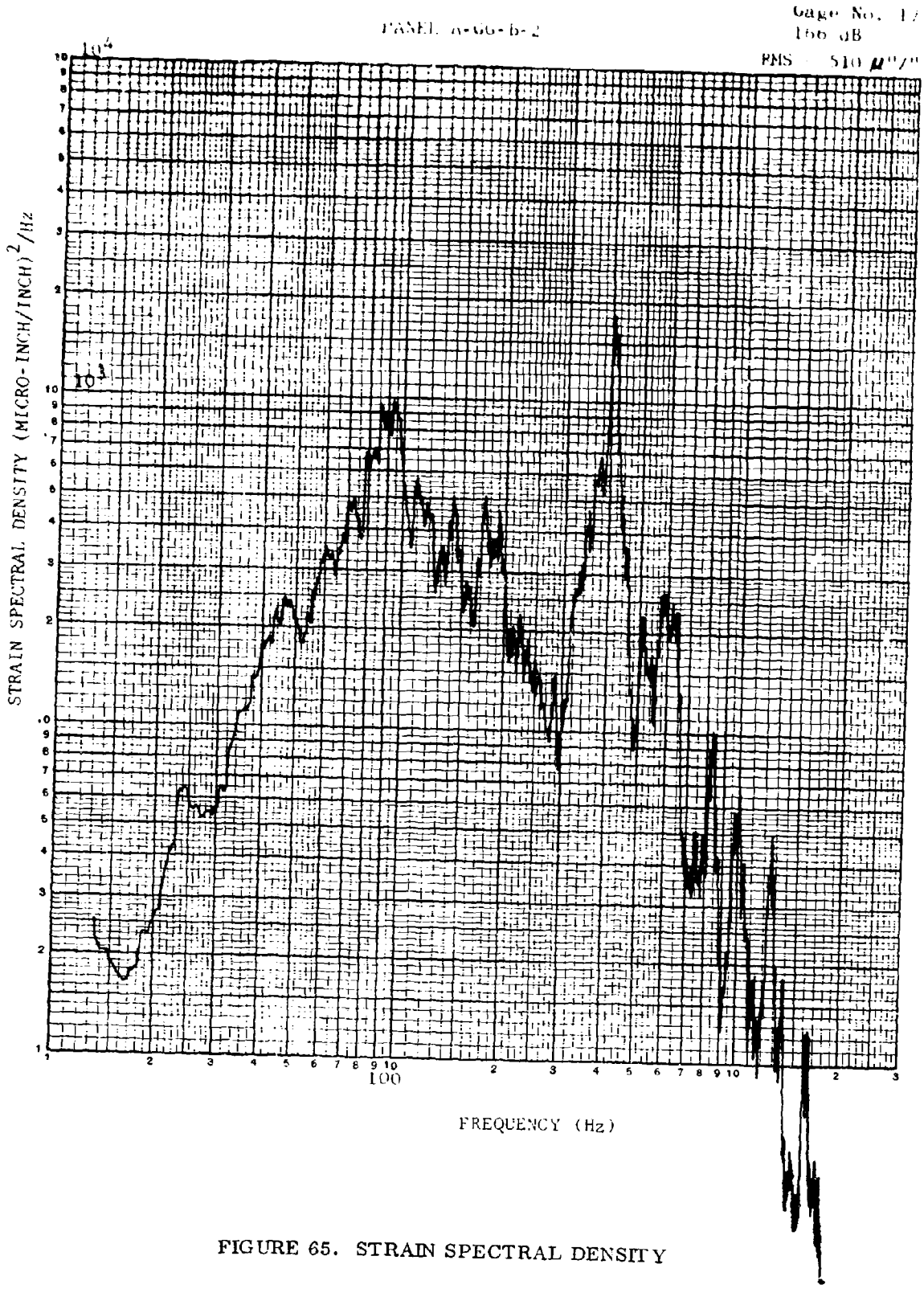

FIGURE 65. STRAIN SPECTRAL DENSITY

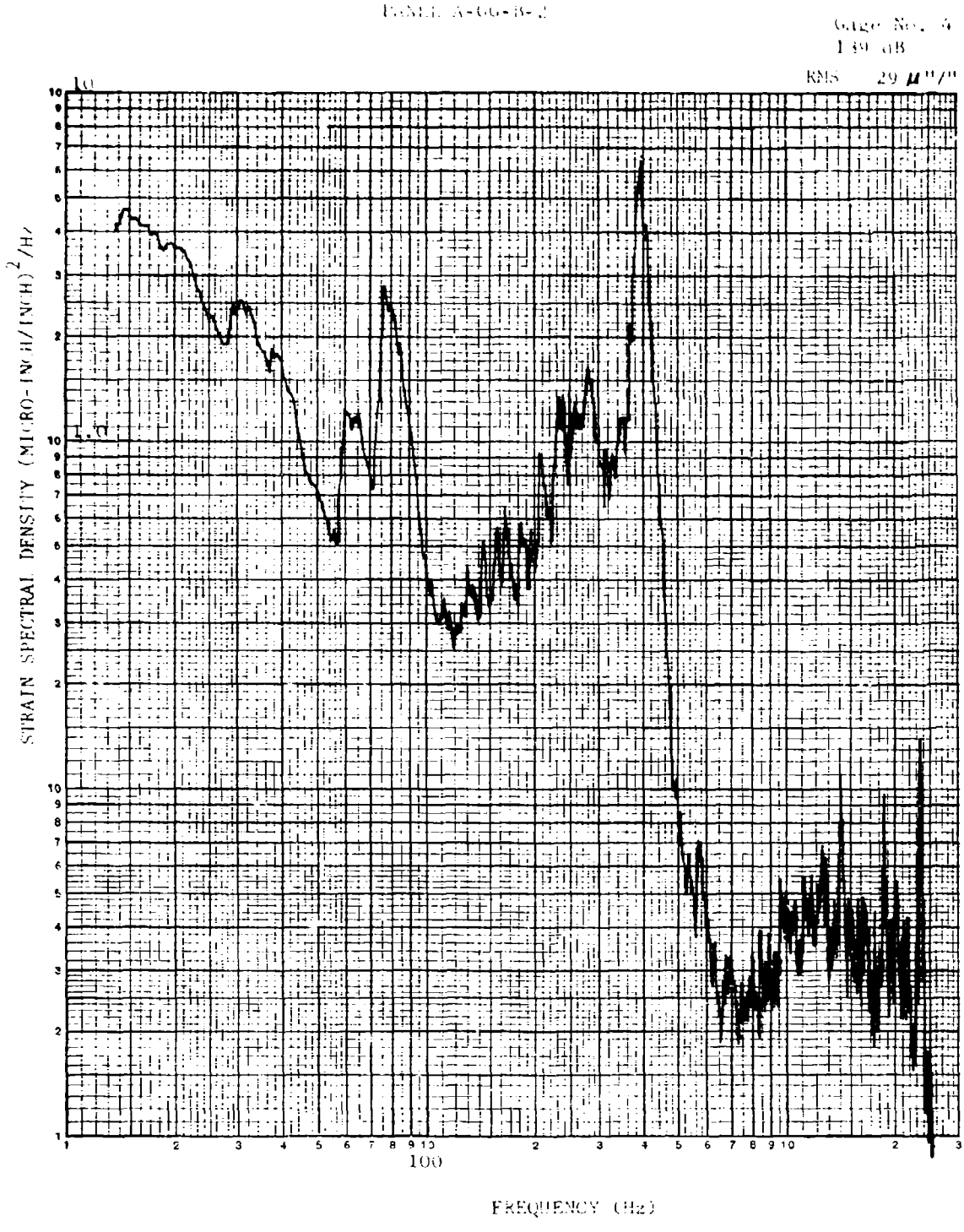

FIGURE 66. STRAIN SPECTRAL DENSITY

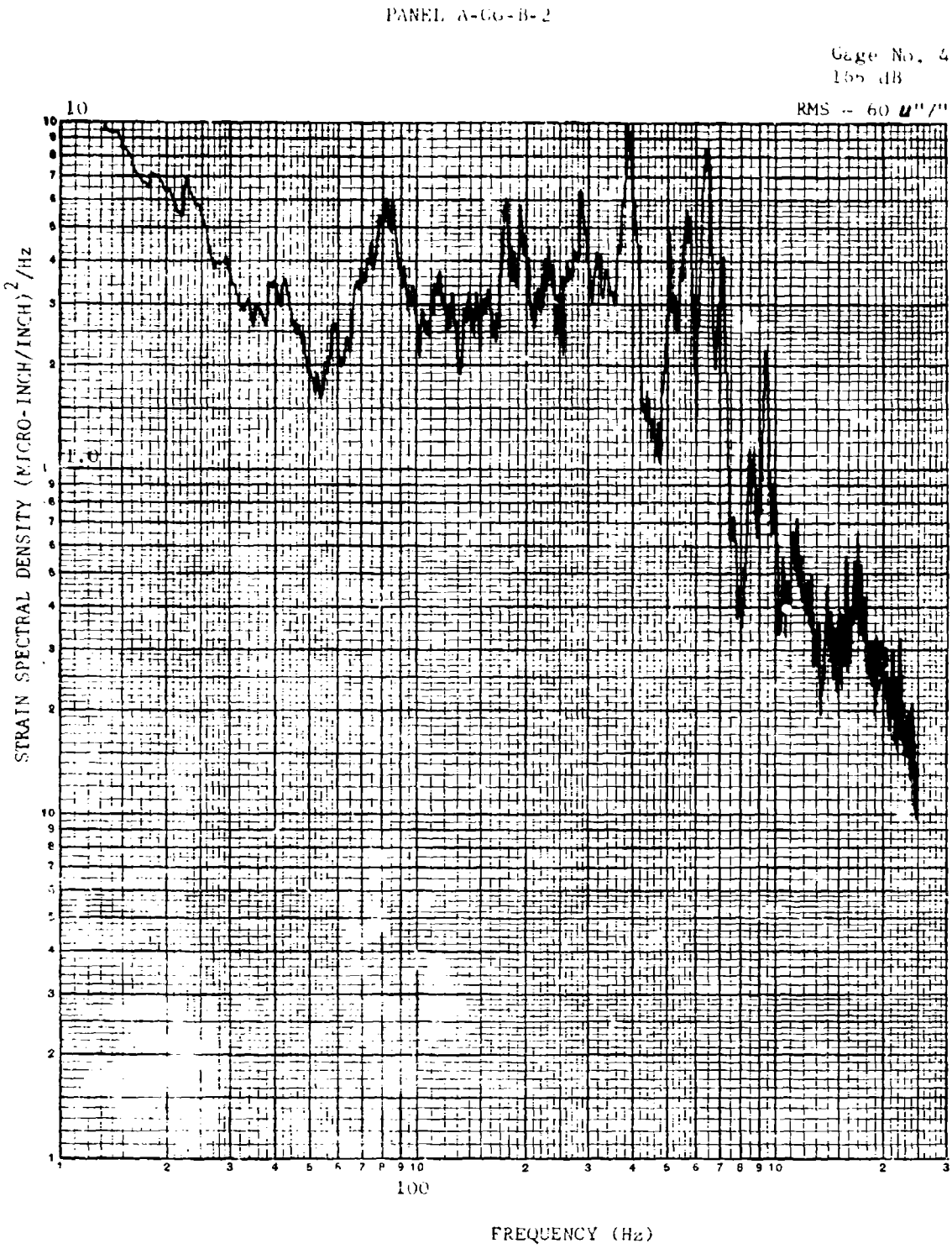

FIGURE 67. STRAIN SPECTRAL DENSITY

V.3 TEST OF ACOUSTIC PANEL A-GG-B-3

Acoustic panel A-GG-B-3 was fabricated according to the procedure discussed in Section III. The fabrication procedure as applied to panel A-GG-B-3 resulted in the manufacture of a flat panel with good visible bond lines. Glass doublers were bonded around the periphery of the titanium alloy frame (Figure 18) to prevent nuisance failures such as had occurred in the acoustic test of panel A-GG-B-2.

V.3.(a) Initial Modal Survey

In contrast to the procedure followed for panel A-GG-B-2, an initial modal survey of panel A-GG-B-3 was conducted prior to the installation of strain gages, primarily because the strain gages and the associated wiring of panel A-GG-B-2 were a hindrance in obtaining the nodal lines with polyvinyl chloride pellets.

In Figure 68 are the natural frequencies, nodal lines, and the bay of peak response in the initial modal survey of panel A-GG-B-3.

V.3.(b) Instrumentation, Damping Factors, and Repetition of Modal Survey

Strain gages were installed on panel A-GG-B-3 and the locations are shown in Figure 31. Gages No. 19 through 22 were not used on panels A-GG-B-1 and A-GG-B-2, but were installed on panel A-GG-B-3 to obtain data at acoustic fatigue sensitive locations.

After the strain gages were installed, the damping factors (Table IX) associated with the bay of the panel resonances following the termination of loudspeaker excitation were obtained using the logarithmic decrement method from oscillograph records of accelerometer signals.

TABLE IX. DAMPING FACTORS OF PANEL A-GG-B-3

Frequency	Viscous Damping Factors		
(Hz)	Bay 4	Bay 5	Bay 6
170	—	.013	—
177	.013	—	.012
288	—	—	Bad
348	—	—	.015
517	—	—	.011
563	—	—	.016
609	—	—	Bad
721	—	—	Bad
817	Bad	—	—

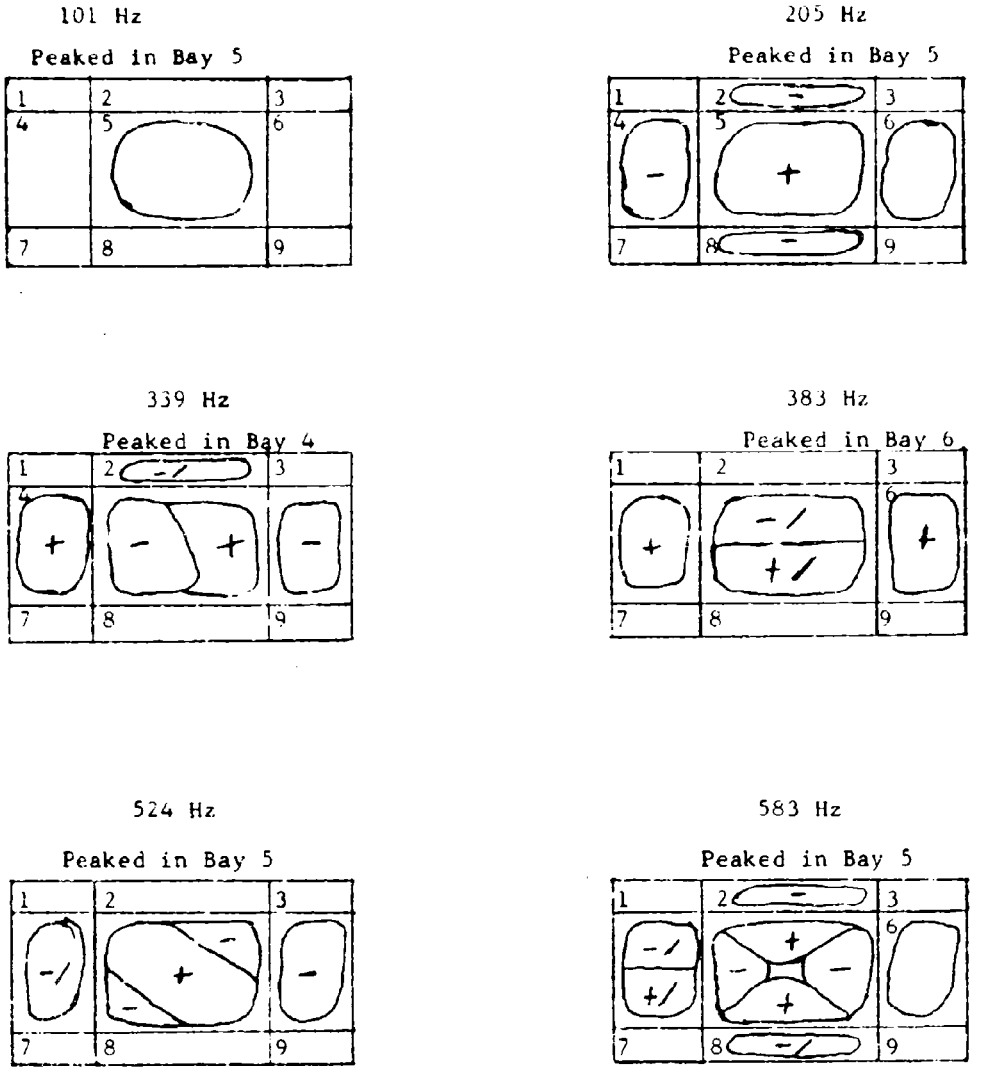

Phasing Notation: + means 0 degrees
- means 180 degrees
/ means 90 degrees

FIGURE 68. NODAL LINES UNDER LOUDSPEAKER EXCITATION OF PANEL A-GG-B-3

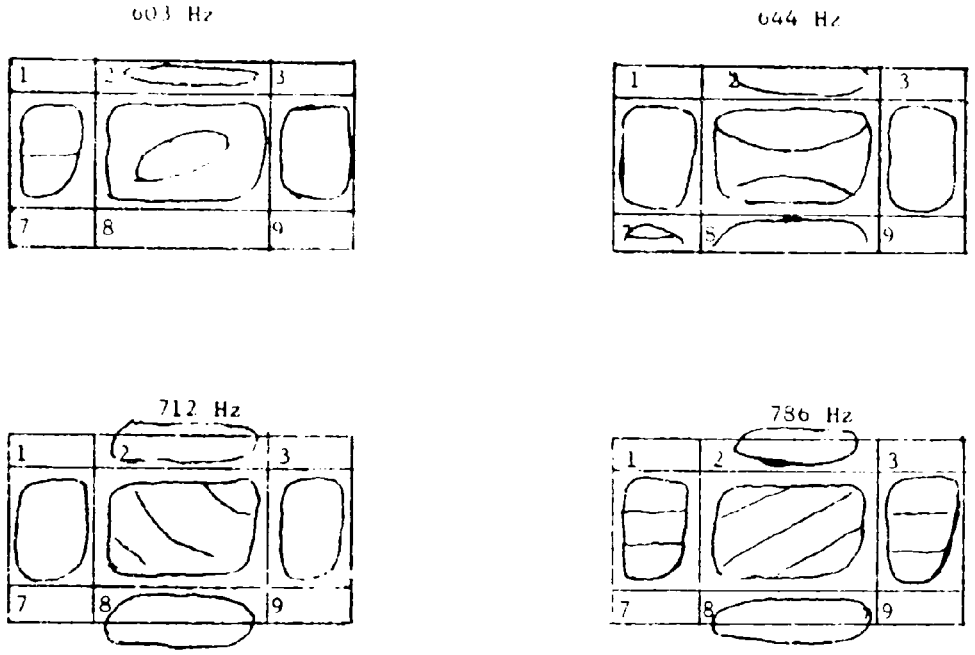

(At the 712 and 786 Hz natural frequencies, the nodal lines for bays 2 and 8 include areas of the graphite-epoxy edge doubler of the panel)

FIGURE 68. NODAL LINES UNDER LOUDSPEAKER EXCITATION OF PANEL A-GG-B-3 (Continued)

Because the natural frequencies reported in Table IX did not duplicate the natural frequencies of the modal survey reported in Figure 68, the modal survey was repeated (Figure 69). The frequencies reported in Figure 69 were in general lower (see the following paragraph) than the ones reported for a given mode shape in Figure 68. The lowest natural frequency dropped from 205 Hz to 179 Hz. The reason for the drop was not substantiated but can be at least partially attributed to the following hypotheses: (1) the addition of strain gages and associated wiring increased the mass and lowered the natural frequencies, or (2) the stiffness of the panel had decreased because the remounting in the test fixture resulted in different boundary conditions.

The lowest resonant response of panel A-GG-B-3 reported in Figure 68 was 101 Hz. The lowest resonant response of panel A-GG-B-3 reported in Figure 69 is 90 Hz. But these 101 and 90 Hz frequencies are not natural frequencies. These responses are due to the excitation not being truly sinusoidal in time and therefore there is an appreciable excitation level at twice the excitation frequency, which is the lowest natural frequency of the panel. Therefore, the lowest natural frequency in Figure 68 is 205 Hz and in Figure 69 is 179 Hz.

In Figure 69 only the lower mode shapes are shown and these were estimated with the use of the roving accelerometer to determine phase changes.

179 Hz

Peaked in Bay 5

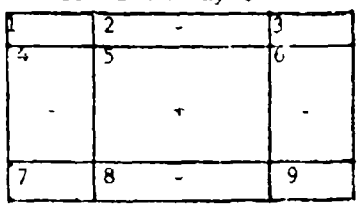

292 Hz

Peaked in Bays 4 and 6

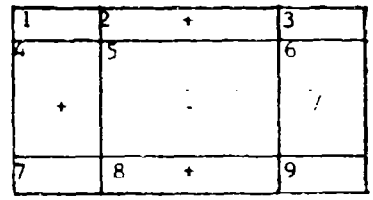

342 Hz

Peaked in Bay 6

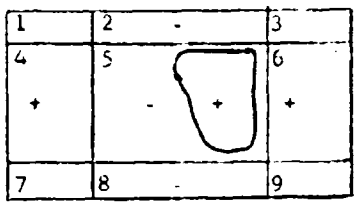

517 Hz

Peaked in Bays 5 and 6

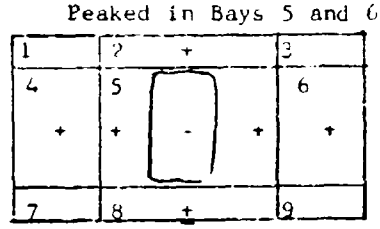

562 Hz

Peaked in Bay 5

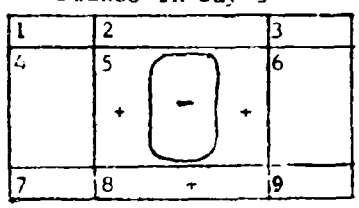

609 Hz

Peaked in Bay 5

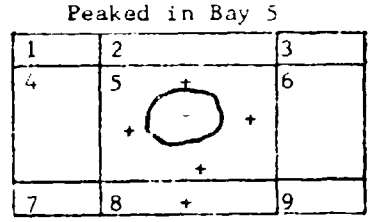

Phasing Notation: + in a bay means 0 degrees for the bay

- in a bay means 180 degrees for the bay

/ in a bay means 90 degrees for the bay

FIGURE 69. MODAL SURVEY OF PANEL A-GG-B-3 WITH NODAL LINES ESTIMATED WITH ACCELEROMETER SIGNALS

721 Hz

Peaked in Bay 5

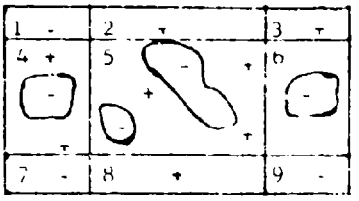

816 Hz

Peaked in Bay 6

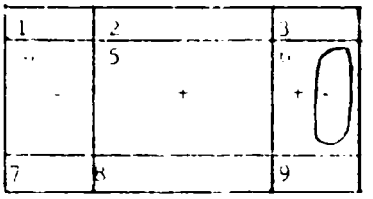

Phasing Notation: + in a bay means 0 degrees for the bay

- in a bay means 180 degrees for the bay

/ in a bay means 90 degrees for the bay

FIGURE 69. MODAL SURVEY OF PANEL A-GG-B-3 WITH NODAL LINES ESTIMATED WITH ACCELEROMETER SIGNALS (Continued)

V.3.(c) Response to Acoustic Excitation

The procedure used in obtaining the response to the acoustic excitation of panel A-GG-B-2 was repeated for panel A-GG-B-3.

The strain readings taken as the SPL was increased in 3 db increments are given in Table X. All of the gages were read at sound pressure levels through 145 db. In order to conserve test time, signals from only ten strain gages were recorded at pressure levels above 145 db. It is noteworthy that some strains remained rather steady in going from 145 to 148 db and no discussion is offered, other than the strains occurred in bay 6.

V.3.(d) Acoustic Fatigue Test

A visual inspection of panel A-GG-B-3 was made when 30 minutes exposure had elapsed at 166 db SPL. No damage to the panel was observed. Visual inspections were then made when 60 minutes and when 100 minutes of exposure had elapsed with no signs of damage to the joints and the skin of the panel. Subsequently, inspections were made every 100 minutes until a total of 100 hours exposure at 166 db SPL had occurred.

TABLE X

STRAIN GAGE RESPONSE (MICRO-INCH/INCH-RMS) OF PANEL A-GG-B-3

	Overall Sound Pressure Level (db re 0.0002 dynes/cm^2)										
STRAIN GAGE NO.	136 db	139 db	142 db	145 db	148 db	151 db	154 db	157 db	160 db	163 db	166 db
1	68	100	116	152	200	234	244	268	290	310	out
2	104	164	190	260	310	374	400	430	480	500	560
3	26	44	44	68							
4	6	8	12	14							
5	14	20	26	36							
6	34	56	78	108	124	138	144	150	180	200	220
7	36	74	100	120	136	164	186	216	250	270	320
8	--	8	8	12	14	20	22	28	36	40	56
9	22	34	44	52							
10	6	6	8	12							
11	32	46	60	86							
12	14	20	30	54							
13	16	56	84	110	108	130	154	180	220	230	290
14	58	84	112	140	141	170	214	250	280	310	370
15	20	28	38	54							
16	36	50	70	104							
17	48	74	100	146	164	240	300	370	420	470	610
18	12	16	18	22							
19	60	86	120	150	154	210	260	326	384	430	550
20	40	58	80	108	108	144	186	220	250	260	310
21	4	6	6	10							
22	4	8	10	10							

In addition to the visual inspections at 100 minute intervals, a continuous monitoring of strain from gage No. 8 and microphone signals was made to detect a possible acoustic fatigue failure. No sign of panel failure was obtained from the strain and microphone signals.

At the 1000 minute inspection, it was noted that there was severe damage in two of the adjacent ±45 degree plies of the vertical leg of the tee stiffener between bays 5 and 8 (see Figure 70). The damage included splitting of those plies and delamination. It was hypothesized that the failure was of a local nature and probably due to bleeding off too much resin in the cure of the tee sections. Therefore, the damage was not repaired and the acoustic fatigue test was continued. The damage to the tee section did not propagate appreciably during the remainder of the acoustic fatigue test, which was terminated after a total of 100 hours at 166 db SPL was reached.

V.3.(e) Data Analysis

As in the case of panel A-GG-B-2, narrow band spectral analyses for panel A-GG-B-3 were conducted for the strain response and pressure loading of Table X at SPLs of 139 db, 148 db, 157 db, and 166 db. The narrow band analyses in the panel A-GG-B-3 acoustic test are similar to the analyses of panel A-GG-B-2 given in Figures 56 through 67.

The power spectral density of the pressure during the 139 db run and the 166 db run of panel A-GG-B-3 is shown in Figures 71 and 72. The strain spectral densities at gage No. 2 (in the central bay at the intersection with a tee stringer) at 139, 148, 157, and 166 db SPL are in Figures 73 through 76. The strain spectral densities of gages No. 16 (in the center of bay 4) and 19 (in bay 6 at the intersection with the tee section at 139 db and 166 db SPL are in Figures 77 through 80. From observations of Figures 73 through 80, one may note how natural frequencies shift upward as the overall SPL increases.

Other PSD plots of interest are strain gage No. 17 at 166 db SPL (Figure 81) and strain gage No. 11 at 139 db SPL (Figure 82).

An examination of Figures 71 through 76 that is discussed in the following paragraphs yields information that reflects differences in dynamic response characteristics during runs at different excitation levels.

From an examination of Figures 71 and 73 during the 139 db SPL run, there are peaks, similar to the resonant response of single degree of freedom spring-mass-dashpot systems, of the strain spectral density at strain gage No. 2, at several natural frequencies (with the lowest natural frequency at 200 Hz). The rms strain response in Figure 73 in the neighborhood of 200 Hz is significantly higher than the rms response in the neighborhood of 100 Hz although the PSD of the excitation pressure in Figure 71 is somewhat higher in the neighborhood of 100 Hz than in the neighborhood of 200 Hz.

From an examination of Figures 72 and 76 during the 166 db SPL run, the strain spectral density at strain gage No. 2 at 91 Hz is approximately equal to the strain spectral density at 290 Hz which is the lowest natural frequency. The spectral shape of the strain response in the neighborhood of 91 Hz is characterized by its similarity to the shape of the spectral density of the acoustic pressure (Figure 72) whereas the spectral shape of the strain response at 290 Hz is characterized by its similarity to the resonant response of the single degree of freedom spring-mass-dashpot system.

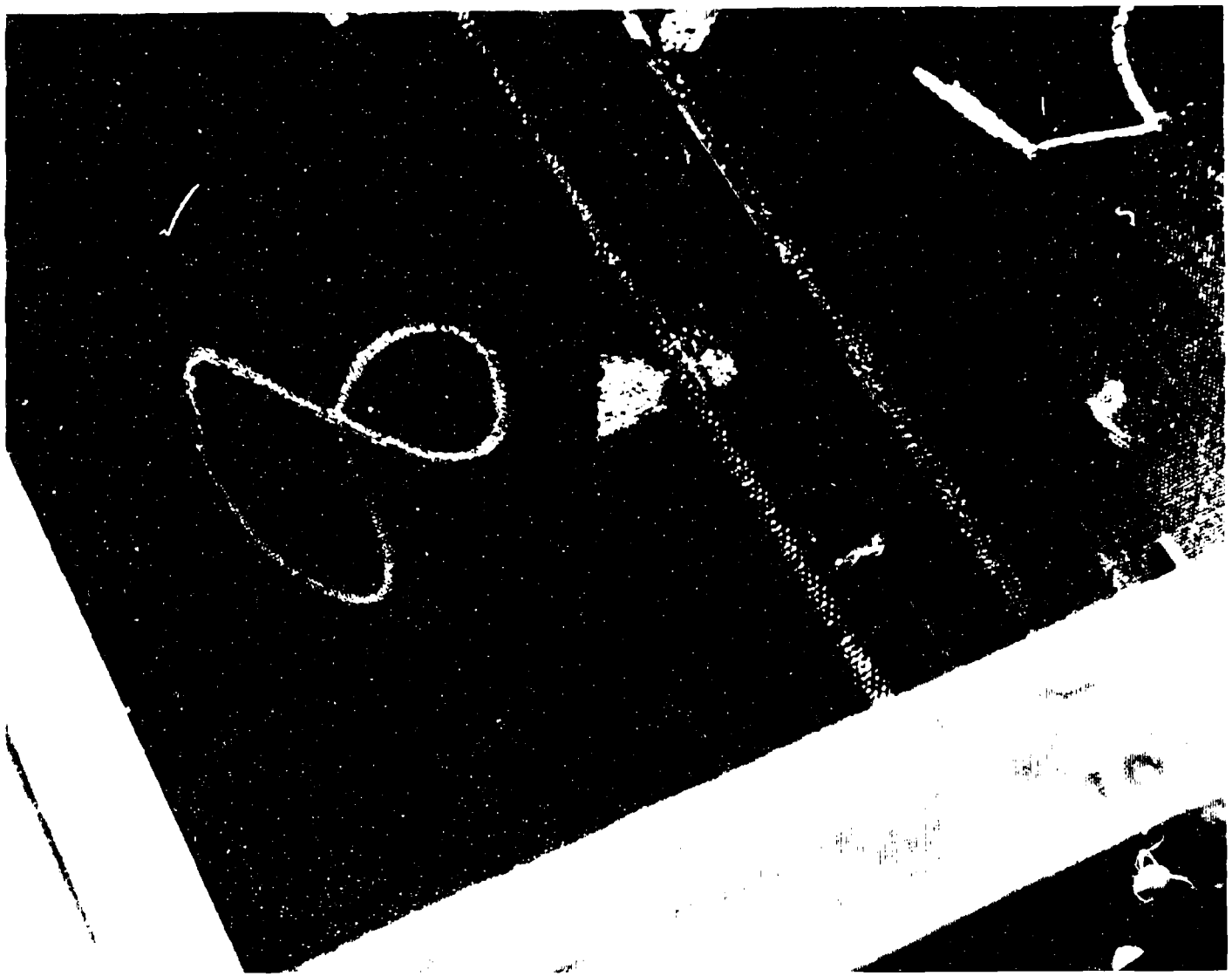

FIGURE 70. TEE SECTION DAMAGE DURING ACOUSTIC FATIGUE TEST OF PANEL A-GG-B-3

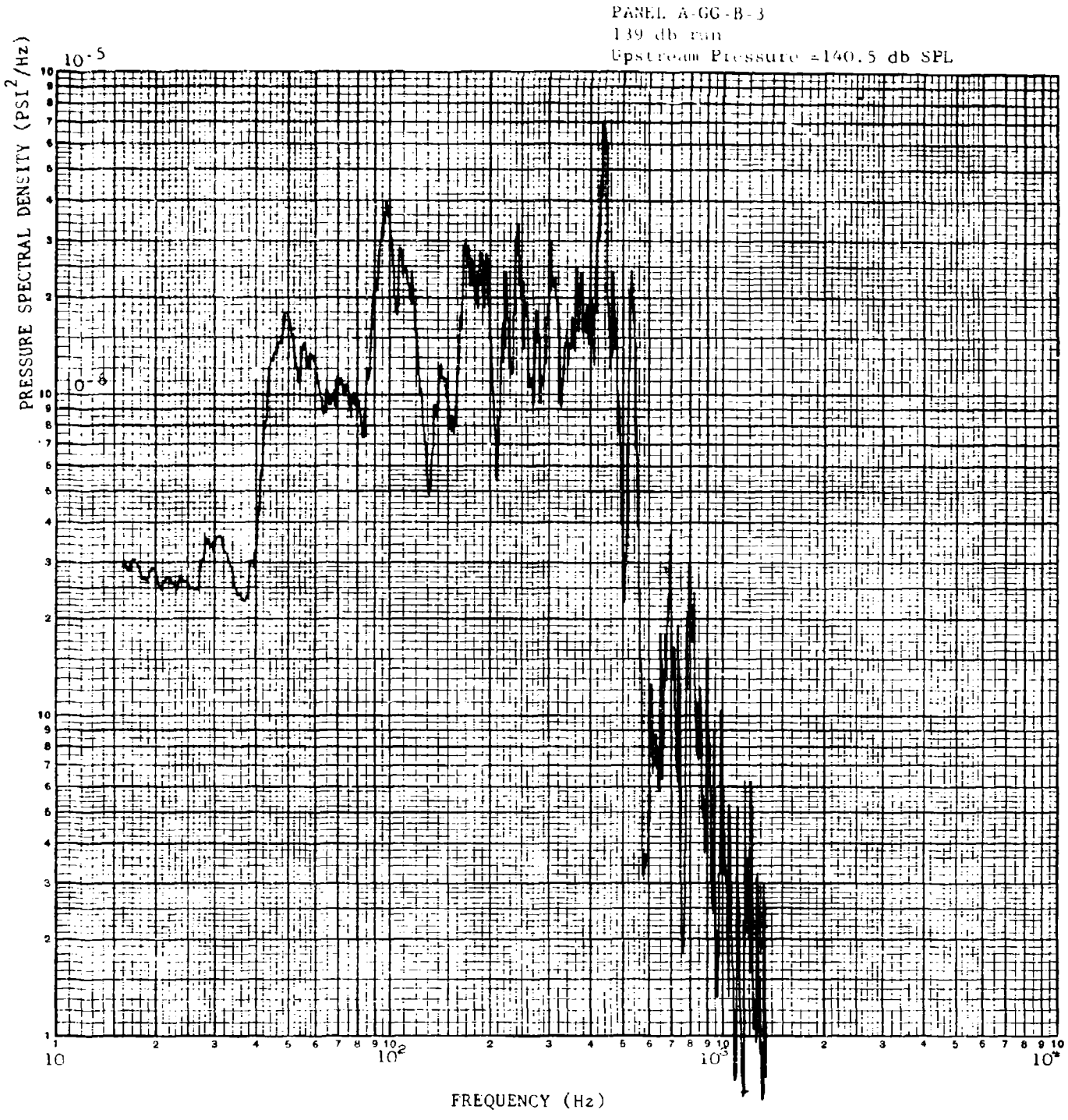

FIGURE 71. PRESSURE SPECTRAL DENSITY

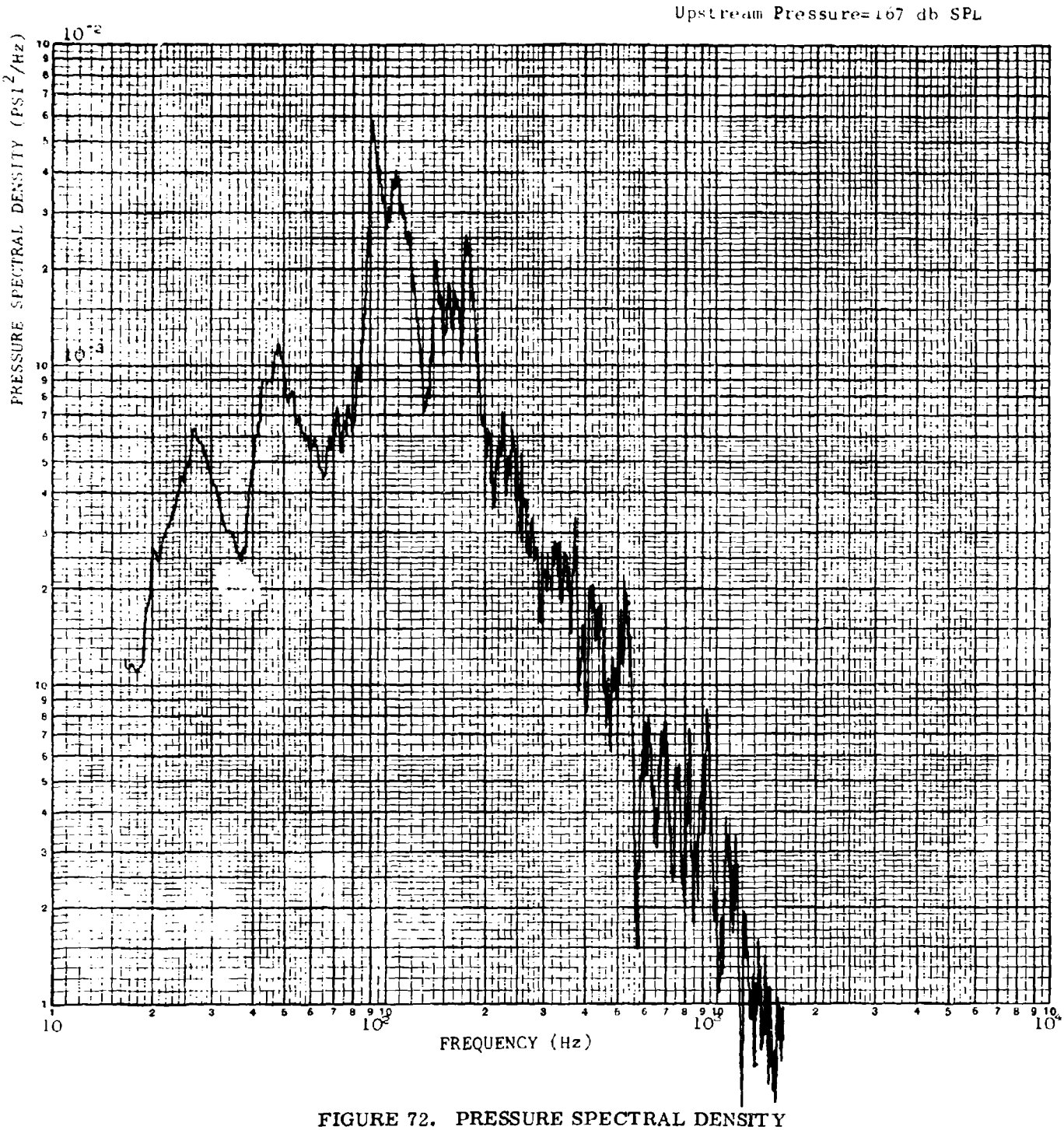

FIGURE 72. PRESSURE SPECTRAL DENSITY

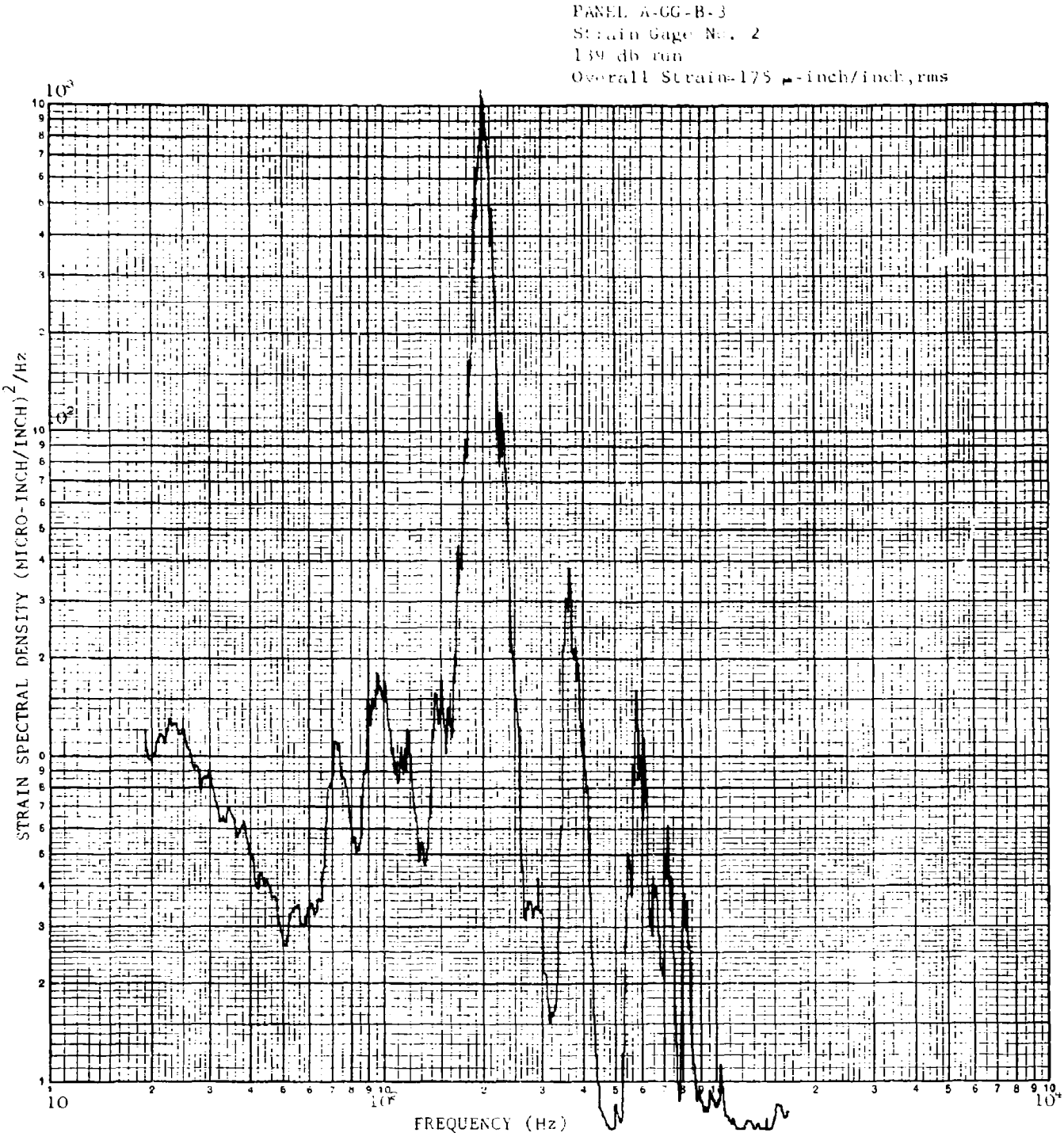

FIGURE 73. STRAIN SPECTRAL DENSITY

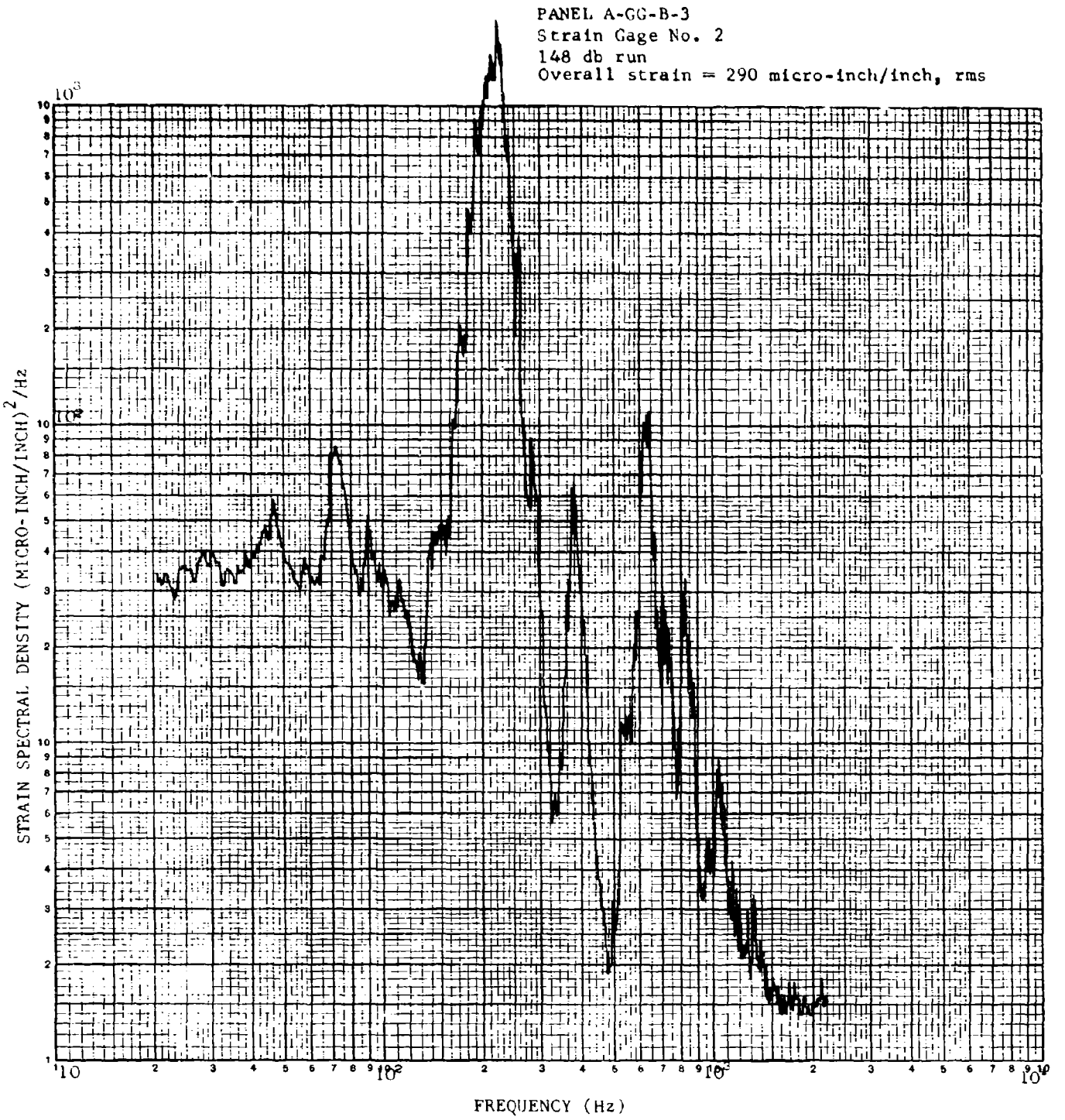

FIGURE 74. STRAIN SPECTRAL DENSITY

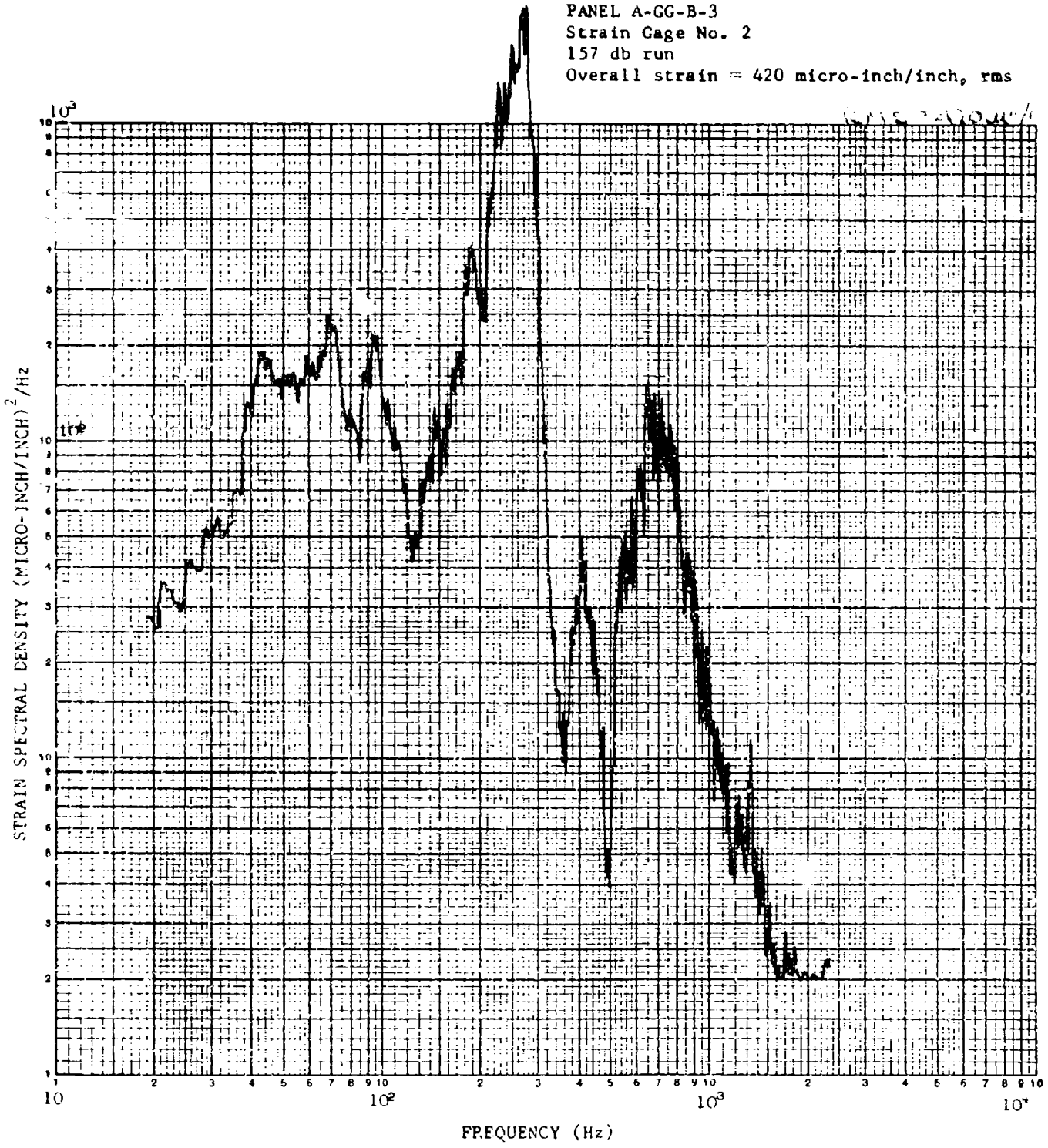

FIGURE 75. STRAIN SPECTRAL DENSITY

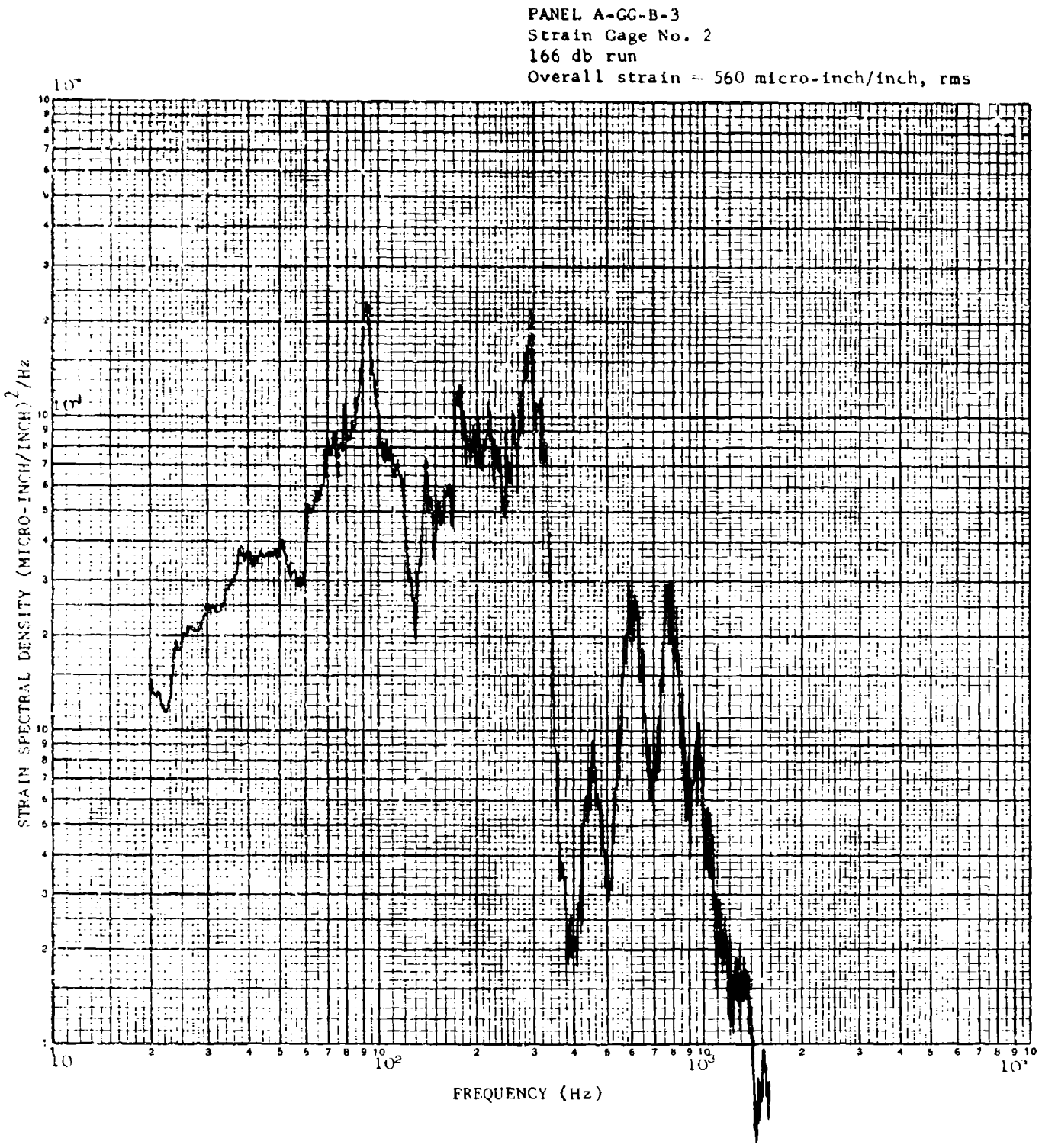

FIGURE 76. STRAIN SPECTRAL DENSITY

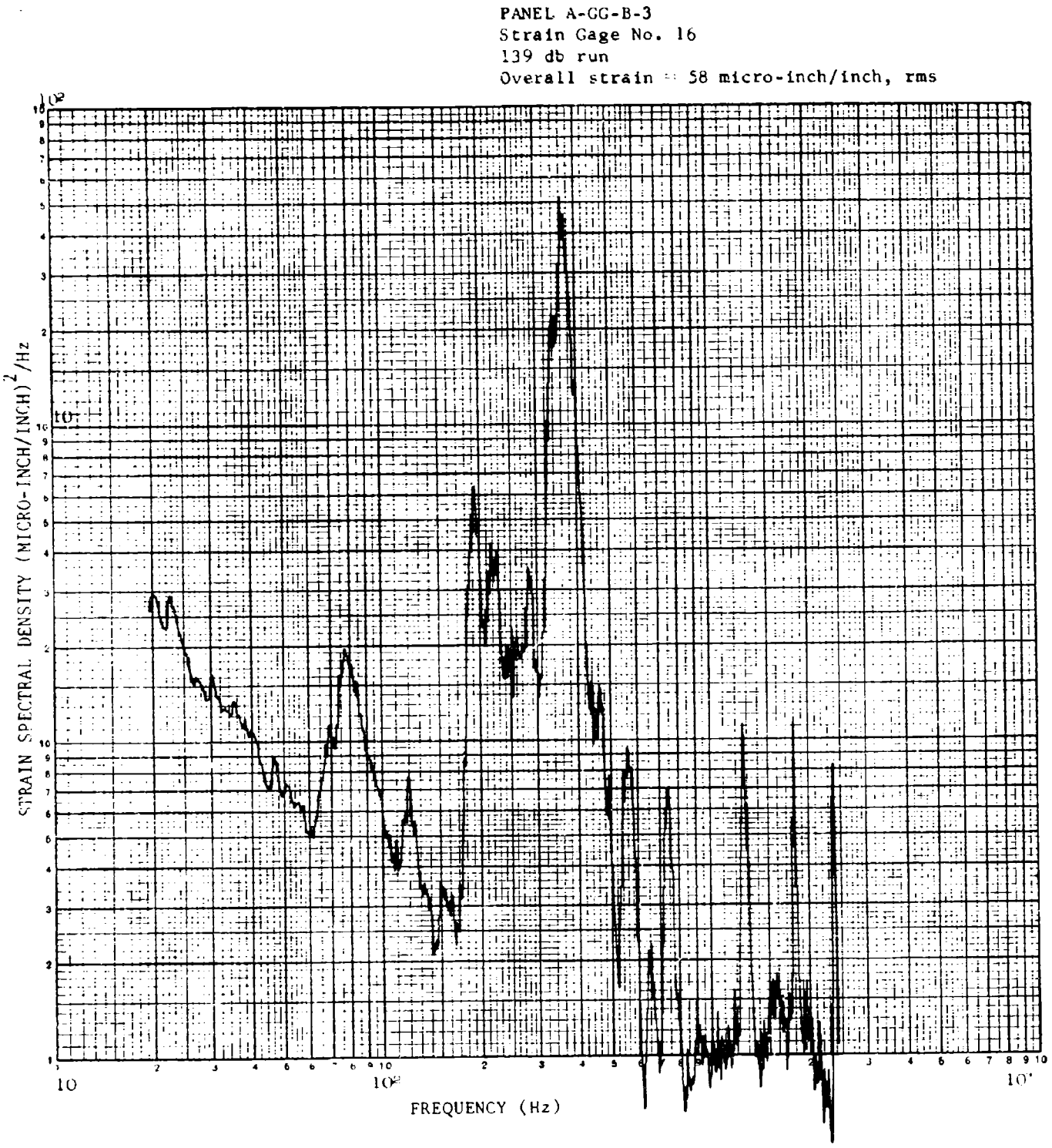

FIGURE 77. STRAIN SPECTRAL DENSITY

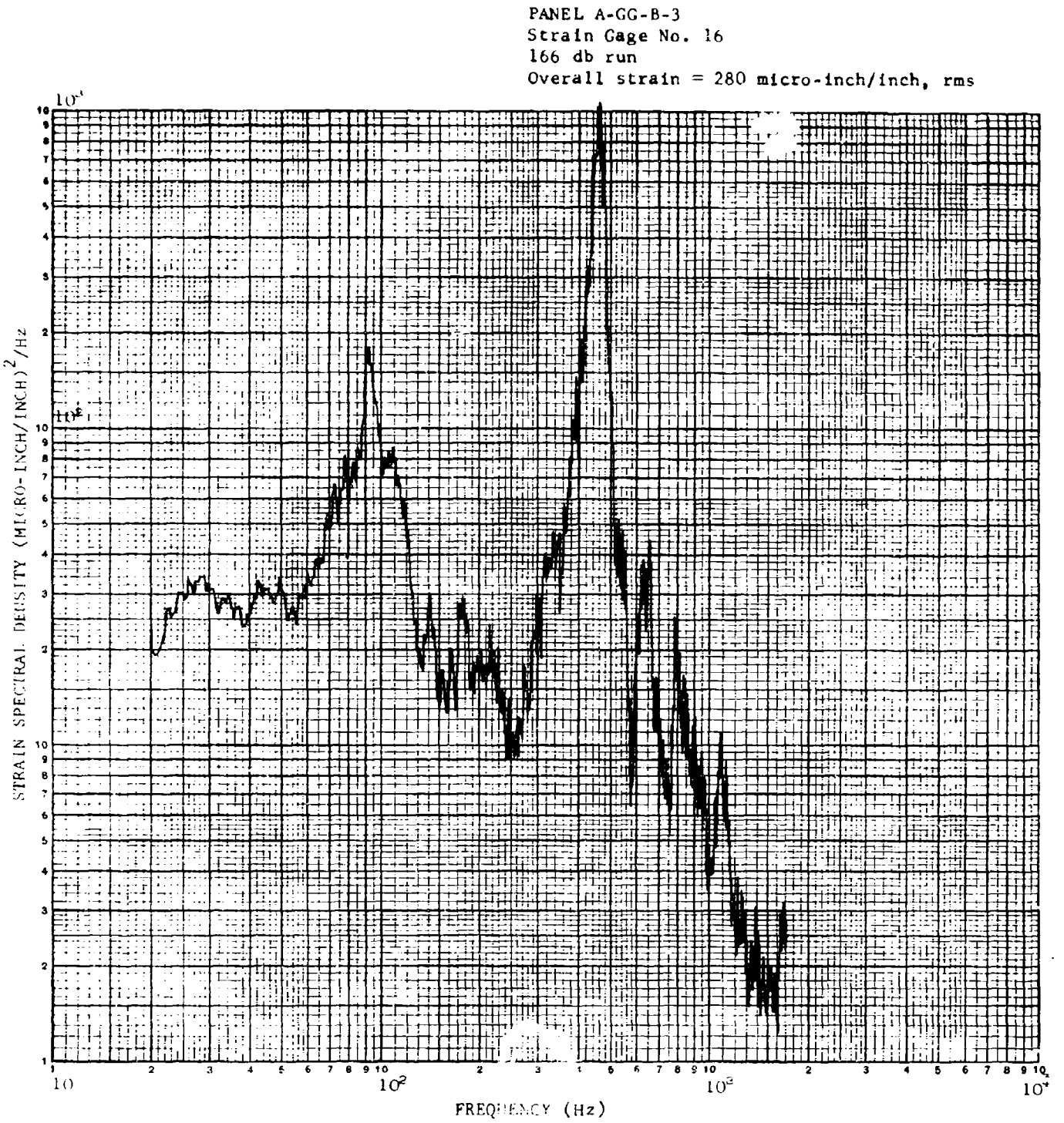

FIGURE 78. STRAIN SPECTRAL DENSITY

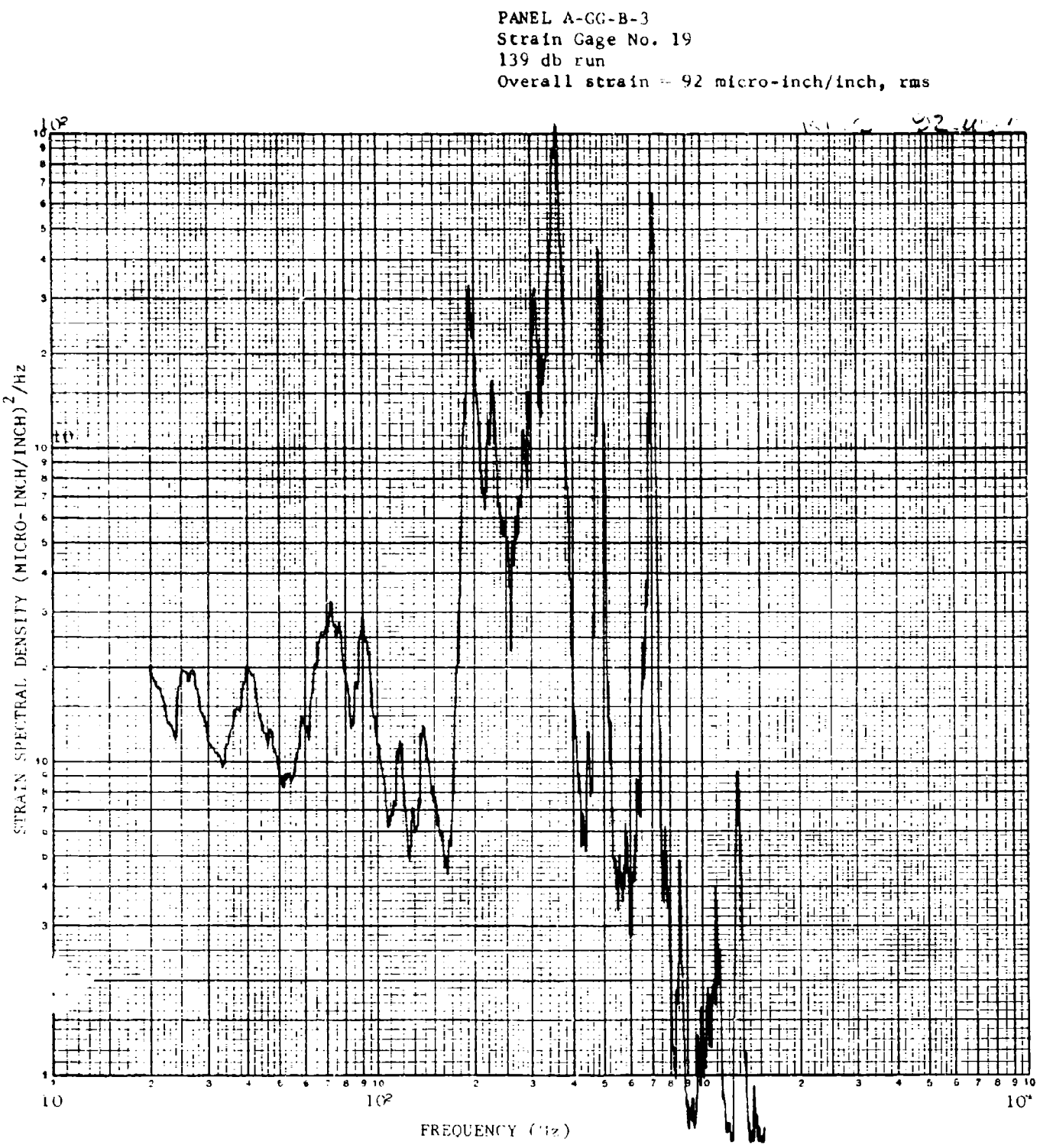

FIGURE 79. STRAIN SPECTRAL DENSITY

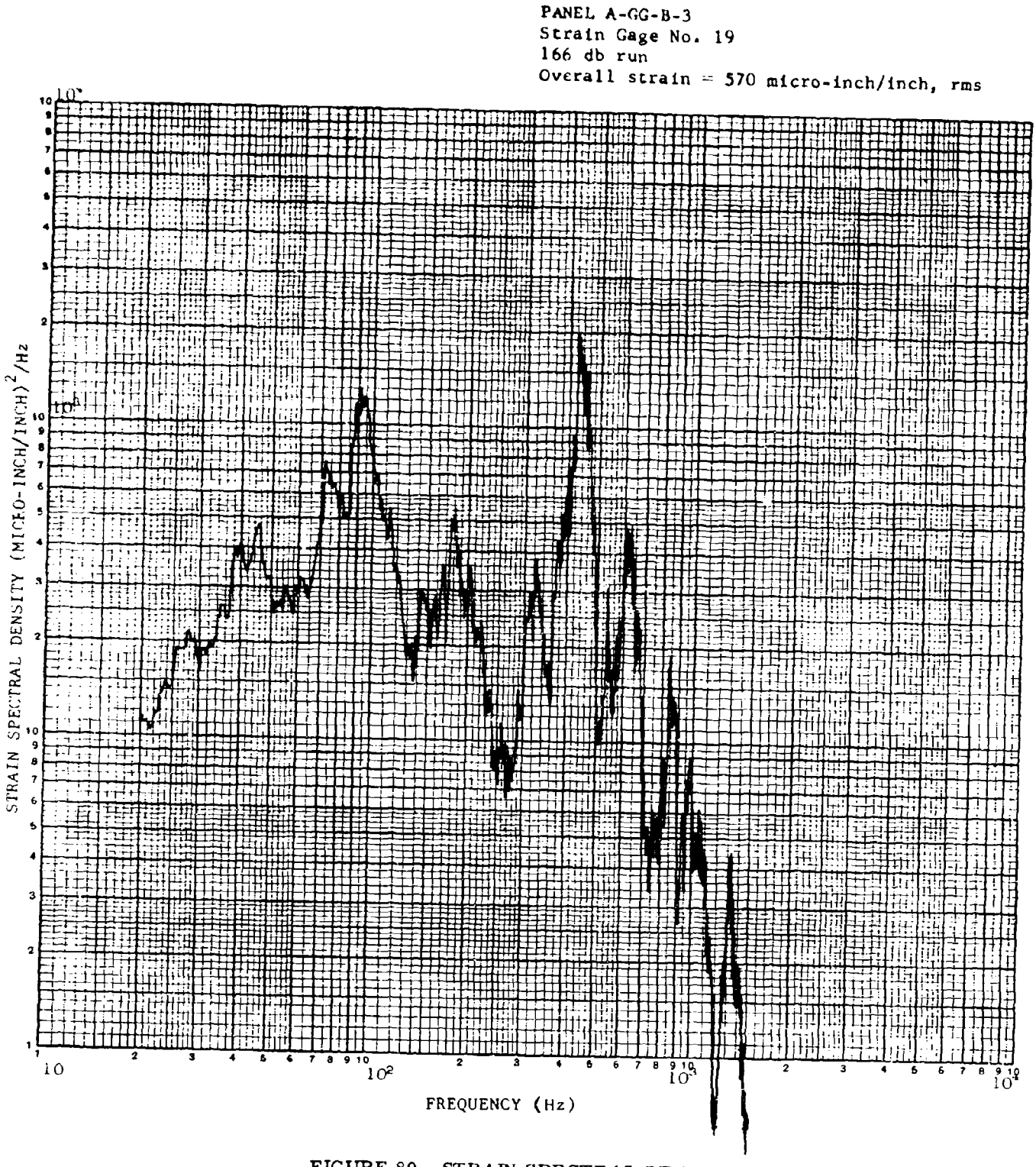

FIGURE 80. STRAIN SPECTRAL DENSITY

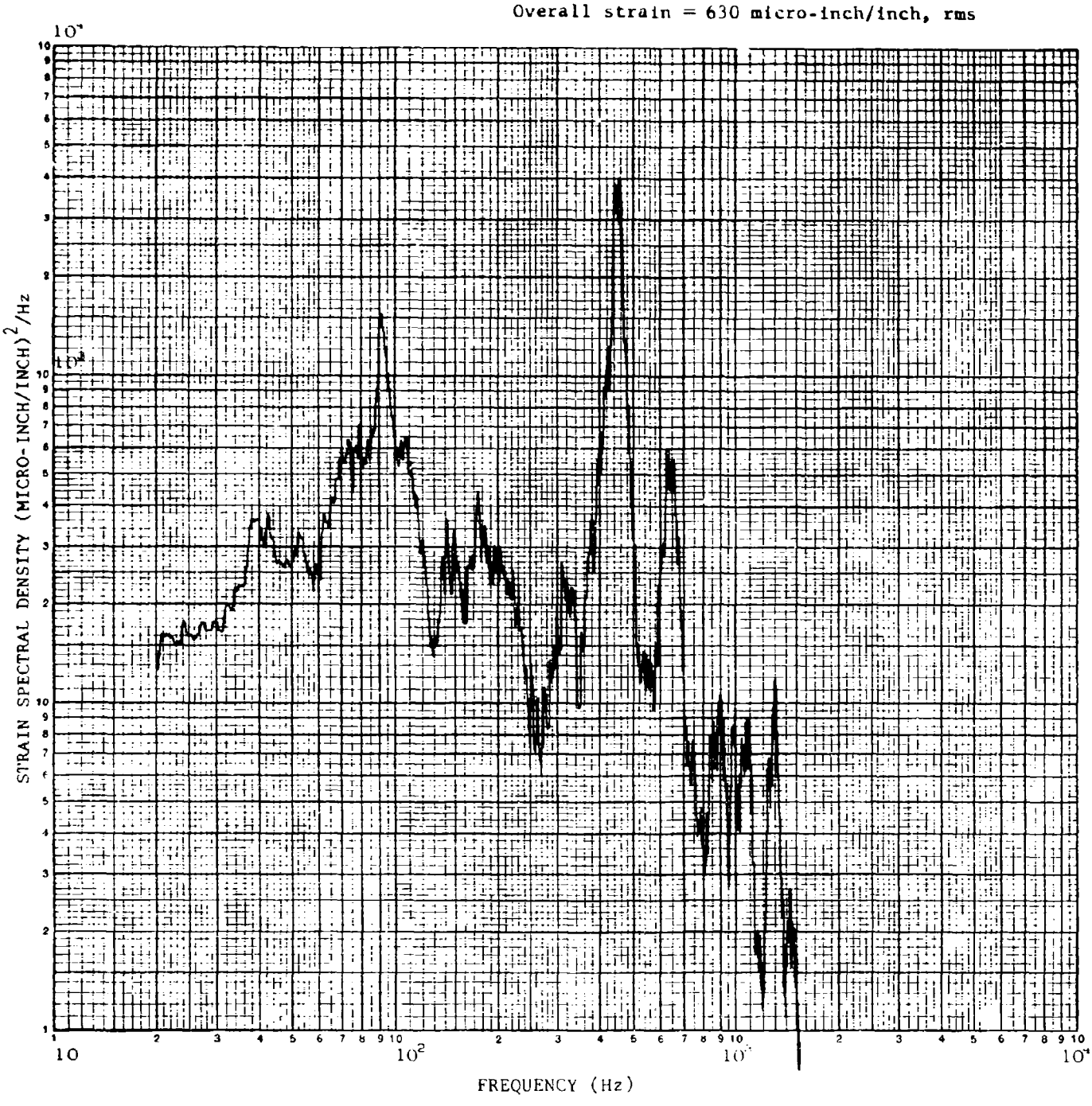

FIGURE 81. STRAIN SPECTRAL DENSITY

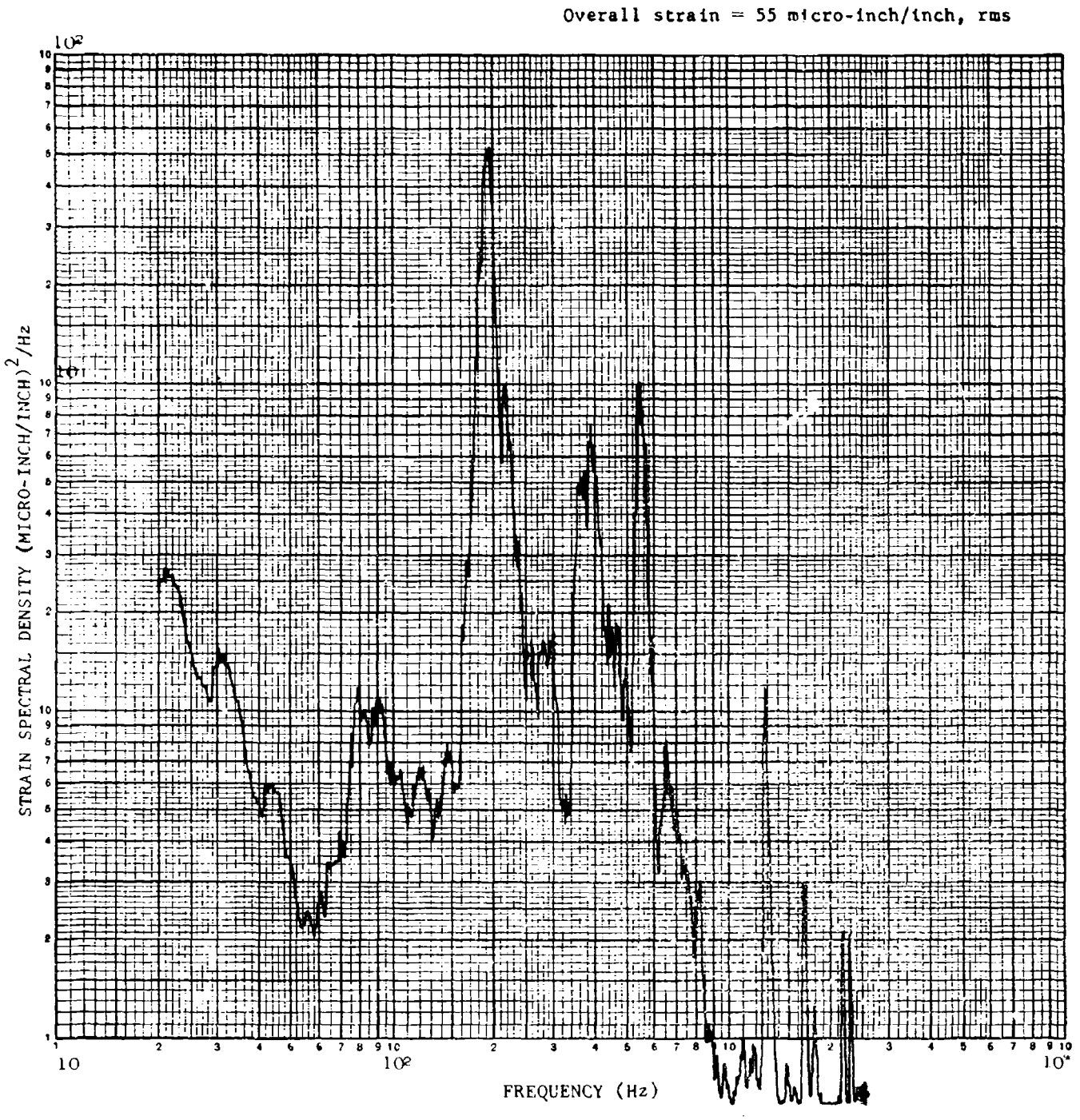

FIGURE 82. STRAIN SPECTRAL DENSITY

An examination of Figures 73 through 76 shows that the lowest natural frequency increases as the pressure applied to the panel is increased. Under loud-speaker excitation, the lowest natural frequency in Table IX was at 174 ±5 Hz. Under the acoustic pressure in the progressive wave test chamber, the lowest natural frequency in Figures 73 through 76 increased from 200 Hz to 290 Hz as the SPL was increased from 139 db to 166 db. The increase in natural frequency with increasing pressure is attributed to large deflections that result in membrane stresses that become increasingly significant relative to the bending stresses. The similarity of the pressure PSD and the strain PSD in the neighborhood of 91 Hz during the 166 db SPL run is also attributed to the increasingly significant membrane stresses relative to bending stresses as the acoustic pressure is increased.

For the data analysis presented in Figures 71 through 82, a 2.5 second averaging time with a 0.6 Hz/second sweep rate with a 6.3 Hz bandwidth filter for the 20 through 250 Hz range was used. For frequencies above 250 Hz, a 1.0 second averaging time with a 3.3 Hz/second sweep rate with a 14 Hz bandwidth was used. A six second loop was used in obtaining all of these data.

V.4 ACOUSTIC FATIGUE LIFE

Since the prediction of the acoustic fatigue life of metallic structures is a technical area in which improved prediction methods are still being sought, it is not surprising that a prediction method for the acoustic fatigue of advanced-composite structures, that include the cross-stiffened panels of the acoustic test program, is still in an early stage of its development.

In this program, a two-step method which appears promising, was used for the prediction of the presence (or absence) of an acoustic fatigue failure in the cross-stiffened, graphite-epoxy panels. In the first step, experimental strains were obtained at acoustic fatigue critical locations (the occurrence of an acoustic fatigue failure in of the test panels if it would occur at all, was expected at strain gage No. 2, 17, or 19). In the second step, the absence of an acoustic fatigue failure (in 100 hours of exposure at 166 db SPL) was predicted on the basis of an experimental S-N curve obtained in the shaker test program. The criterion used for predicting an acoustic fatigue failure was that failure (at some specified number of cycles of panel response to the random, acoustic pressure) would occur if the overall rms strain (parallel to the I-beam details) response in the skin of the acoustic test panels equalled the overall rms strain response that was obtained in the shaker test program with V-GG-B shaker specimens (the appropriate S-N curve from the shaker test program is in Figure 98). The method of obtaining an average frequency of response to relate time to failure and random cycles is given in Section V.5.

An improvement to the two-step method described above would consist of predicting the acoustic fatigue strain level by analytic or empirical methods in order to avoid rather expensive acoustic fatigue panel tests to obtain experimental strains. Methods for the analytic prediction of strain at relatively low excitation levels when linear, strain-pressure relations are applicable are developed in Sections VII and VIII. When nonlinear strain-pressure relations exist because of large deformations at high excitation levels, at the present state-of-the-art it is necessary to resort to empirical methods of predicting the strain. Neither an empirical nor a nonlinear analytic study was conducted in the present investigation.

A second item in improving the two-step prediction method would be to include the effect of biaxial strains at the acoustic fatigue critical locations. Since it appears that the acoustic fatigue critical locations (the joint assemblies) of thin-skinned, cross-stiffened panels such as those tested in this program, appear to be essentially under uniaxial strain, the effect of the smaller of the biaxial strains may be of a secondary nature. However, the effect of biaxial strains on the acoustic fatigue life (Reference 1) was not inconcsequential in the acoustic fatigue failures in the center of the fiber-reinforced facings of several honeycomb panels.

V.5 ACOUSTIC FATIGUE PREDICTION FOR PANEL A-GG-B-3

An application and discussion of the two-step acoustic fatigue prediction method that was presented in Section V.4 follows. The panel under consideration is acoustic test panel A-GG-B-3.

The PSD curves of strain of gages no. 17, 2, and 19 that are at the center of long edges of bays 4, 5, and 6, respectively, (see Figures 81, 76, and 80) indicate that there is significant strain response at different frequencies under 1000 Hz. In using the S-N data resulting from the test of panel A-GG-B-3, the overall rms strain, e, given in Figures 81, 76, and 80 was assumed to exist at an average frequency,

$$f_{av} = \frac{\sum_i f_i \, e_i^2}{e^2} \tag{1}$$

where the curves in Figures 81, 76, and 80 are broken into i intervals and

f_i is the average frequency of the ith interval

e_i^2 is the mean square strain of the ith interval

and

e is the rms strain

Calculations were made according to equation (1) and resulted in:

f_{av} = 256 Hz for gage 2 (from Figure 76) (2)

f_{av} = 408 Hz for gage 17 (from Figure 81) (3)

and

f_{av} = 359 Hz for gage 19 (from Figure 80) (4)

The conversion to cycles of strain from the 100 hours of acoustic exposure of panel A-GG-B-3 at 166 db SPL at the average frequencies of equations (2) through (4) is given in Table XI. Also in Table XI are the predominant resonant frequencies from Figures 81, 76, and 80 and the cycles corresponding to those frequencies during 100 hours of acoustic exposure.

TABLE XI. CYCLES OF RESPONSE OF PANEL A-GG-B-3 DURING 100 HOURS OF ACOUSTIC EXPOSURE

Strain Gage No.	Average Frequency, f_{av}	Random Cycles at f_{av}	Predominant Resonance	Random Cycles at Predominant Resonance
	Hz		Hz	
2	256	0.9×10^8	292	1.0×10^8
17	408	1.5×10^8	450	1.6×10^8
19	359	1.3×10^8	420	1.5×10^8

The overall strains of strain gages No. 2, 17, and 19 of panel A-GG-B-3 during the 166 db SPL acoustic fatigue test that was halted (without acoustic fatigue failures in the joint assemblies) at approximately 1×10^8 random cycles of response were 560, 630, and 590 micro-inch/inch-rms, respectively. From the V-GG-B S-N curves (Figure 98 of Section VI), the fatigue strength at 10^8 random cycles is in the vicinity of 1100 micro-inch/inch-rms. Since the overall strain (Table X) in the gage No. 2 direction was approximately ten times the overall-rms strain in the gage No. 18 direction (the two gages being perpendicular to each other), the effect of the biaxial strain was neglected in predicting the acoustic fatigue life. Therefore, based on the comparison of strains from acoustic tests and from shaker tests (see the preceding sentence) and the neglect of the effect of the smaller of the biaxial strains, the prediction was made that acoustic panel A-GG-B-3 (and also acoustic panel A-GG-B-2) would not experience acoustic fatigue failures in the joint assemblies. The accuracy of the prediction of no acoustic fatigue failures in the joint assemblies of the flat, acoustic test panels was verified in the acoustic tests.

In order to determine the influence of the SPL on the rms-strain response in the fundamental resonance mode of the panels relative to the overall rms-strain response, the rms strains that respond at the predominant resonances of Table XI were calculated and are compared with the overall rms strains in Table XII. The partial rms strains in Table XII are those rms strains in the frequency range between the lower and upper frequencies of Table XII. The partial rms strains in Table XII were obtained by hand calculations of the area under curves of Figures 76, 80, 81, and 73 after the curves were redrawn on linear graph paper. In Table XII the partial rms strains represent between 50 and 68 percent of the overall rms strains for gages No. 2, 17, and 19 during the 166 db SPL run and 95 percent of the overall rms strain for gage No. 2 during the 139 db SPL run. The conclusion is that at low excitation levels when the strain-pressure relation is approximately linear, the strain response is essentially in the fundamental mode; whereas at the highest excitation level, a significant nonlinear strain-pressure relation existed, the multi-modal effects were quite apparent in the strain response.

TABLE XII. CALCULATED RMS STRAINS OF PANEL A-GG-B-3

SPL	Strain Gage No.	Lower Frequency	Upper Frequency	Peak PSD	Partial Rms Strain	Overall Rms Strain
db		(Hz)	(Hz)	((micro-inch/inch)^2/Hz)	(micro-inch/inch)	(micro-inch/inch)
166	2	260	340	2000	283	560
166	17	400	490	4000	425	630
166	19	390	610	2000	347	590
139	2	170	250	1100	166	175

V.6 CONCLUSIONS FROM THE ACOUSTIC TEST PROGRAM

The tests of panels A-GG-B-2 and A-GG-B-3 demonstrated that high quality, graphite-epoxy panels with thin 6-ply skins can be fabricated and exposed to a high intensity broad-band acoustic environment for at least 10^8 cycles without experiencing acoustic fatigue failures in the skin and/or in the joints. The strain and life data obtained in the acoustic tests of the two panels showed rather close agreement.

The nominal bay dimensions chosen for the acoustic tests of the cross-stiffened panels were typical of dimensions in thin-skinned metallic, aircraft structures. The strains developed in the acoustic tests were too low to produce acoustic fatigue failures and therefore it is not possible to compare directly the lives of the vibration specimens in the program with the acoustic panels. However, by fabricating acoustic panels with larger bays it should be possible in acoustic tests to obtain cross-stiffened panel failures under multimodal strain response (at some average frequency, f_{av}) that can be compared directly with vibration specimen failures under unimodal strain responso. Such tests would indicate the usefulness of the fatigue life theory based on the average response frequency and the overall rms response. Also, the effect of biaxial strains on fatigue life could be observed under such acoustic tests.

The acoustic response tests have resulted in modal and strain response data that can be compared with theoretical predictions based on orthotropic theory. The comparison of predicted versus experimental panel natural frequencies and bending strains is discussed in Section VIII.

VI. SHAKER TEST PROGRAM

VI.1 OBJECTIVE

There were two principal objectives of the shaker tests. One objective was to obtain experimental S-N data for different joint configurations and material systems to determine the relative advantages of the various types of specimens. The other objective was to demonstrate that experimental S-N data can be obtained and applied in the design of joints of advanced-composite panels in acoustic environments without having to resort to acoustic tests with their inherently higher costs to obtain the experimental S-N data for the joints.

VI.2 GENERAL INFORMATION ON SHAKER TESTING

The shaker specimens were fatigue tested either individually (Figure 83) or three at a time (Figure 84). The noncontacting displacement probe and the strain gages are shown in Figures 83 and 84. When the specimens were tested individually, three specimens were tested at the same strain level at a referenced location (namely, strain gage No. 2 in Figure 85). When three specimens were tested simultaneously, it was not possible to begin a test with all three specimens at the same strain level at the referenced location (namely, strain gage No. 2), although the strain of any of the three specimens varied, in general, less than ten percent from the median strain of the three specimens.

A brief general discussion on the shaker excitation and the methods of determining the response of the specimens follows.

VI.2.(a) Vibration Input Spectrum

For the various specimens the response frequencies of the two sides could be adjusted to be less than ten Hz. The adjustment was made by grinding material from the end of the side with the lower response frequency. The response band width of each side was less than five Hz. Thus, to emcompass the band widths of the two sides, a 20 Hz bandwidth signal was selected as the standard input. A tracking filter was used to provide the input signal, which allowed the operator to manually tune the input to follow the specimen resonant frequency throughout the test. The input to the tracking filter was obtained from a random noise source with a Gaussian amplitude distribution.

VI.2.(b) Response Measurement Methods

Three types of transducers were used to monitor the specimen response. These were accelerometers, strain gages, and a capacitive displacement probe.

The primary measurement was the strain response of the specimen. Input vibration levels were set and controlled to produce predetermined strain levels. The other transducers were used to maintain this strain response after the failure of the strain gages.

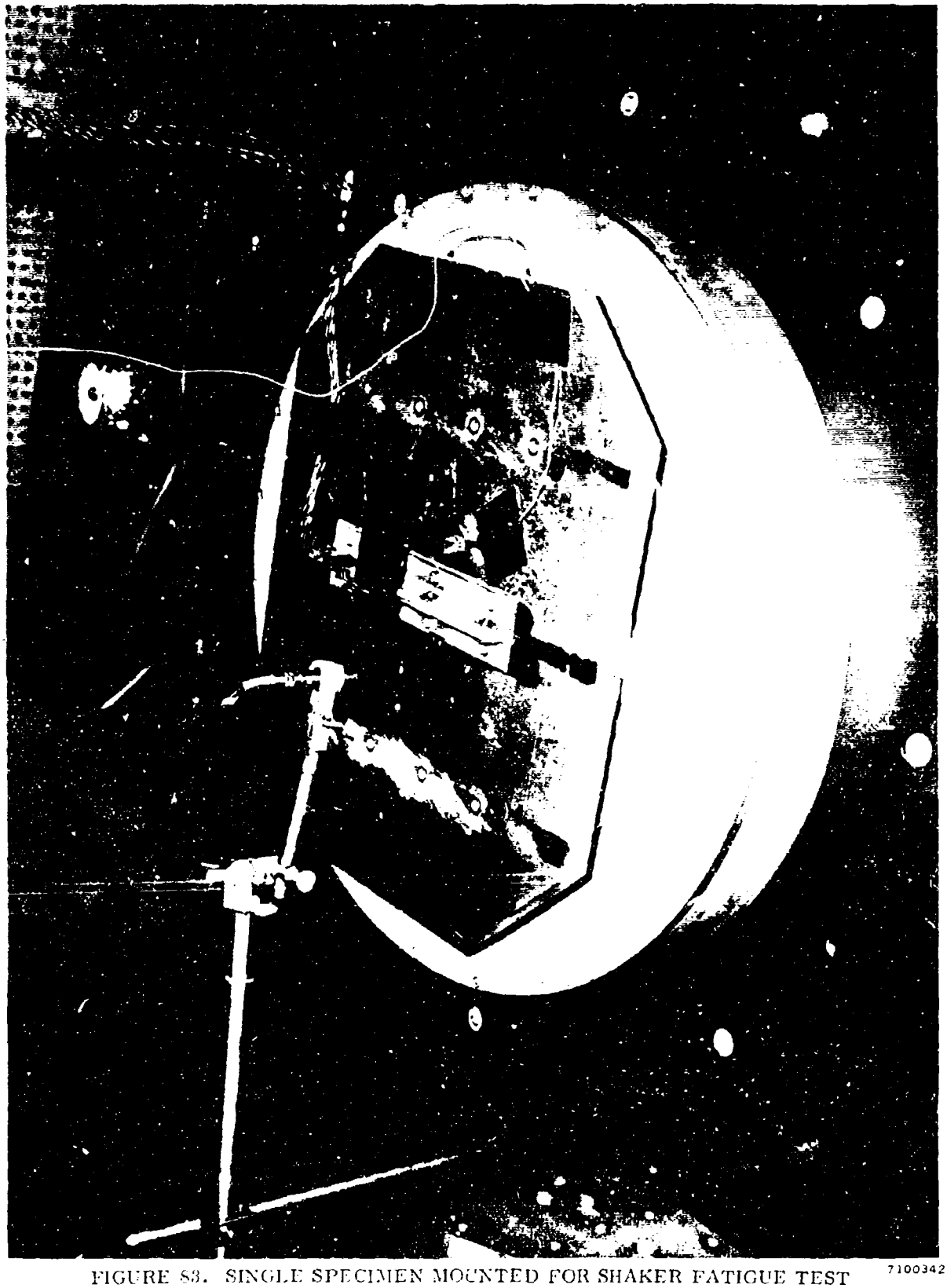

FIGURE 83. SINGLE SPECIMEN MOUNTED FOR SHAKER FATIGUE TEST 7100342

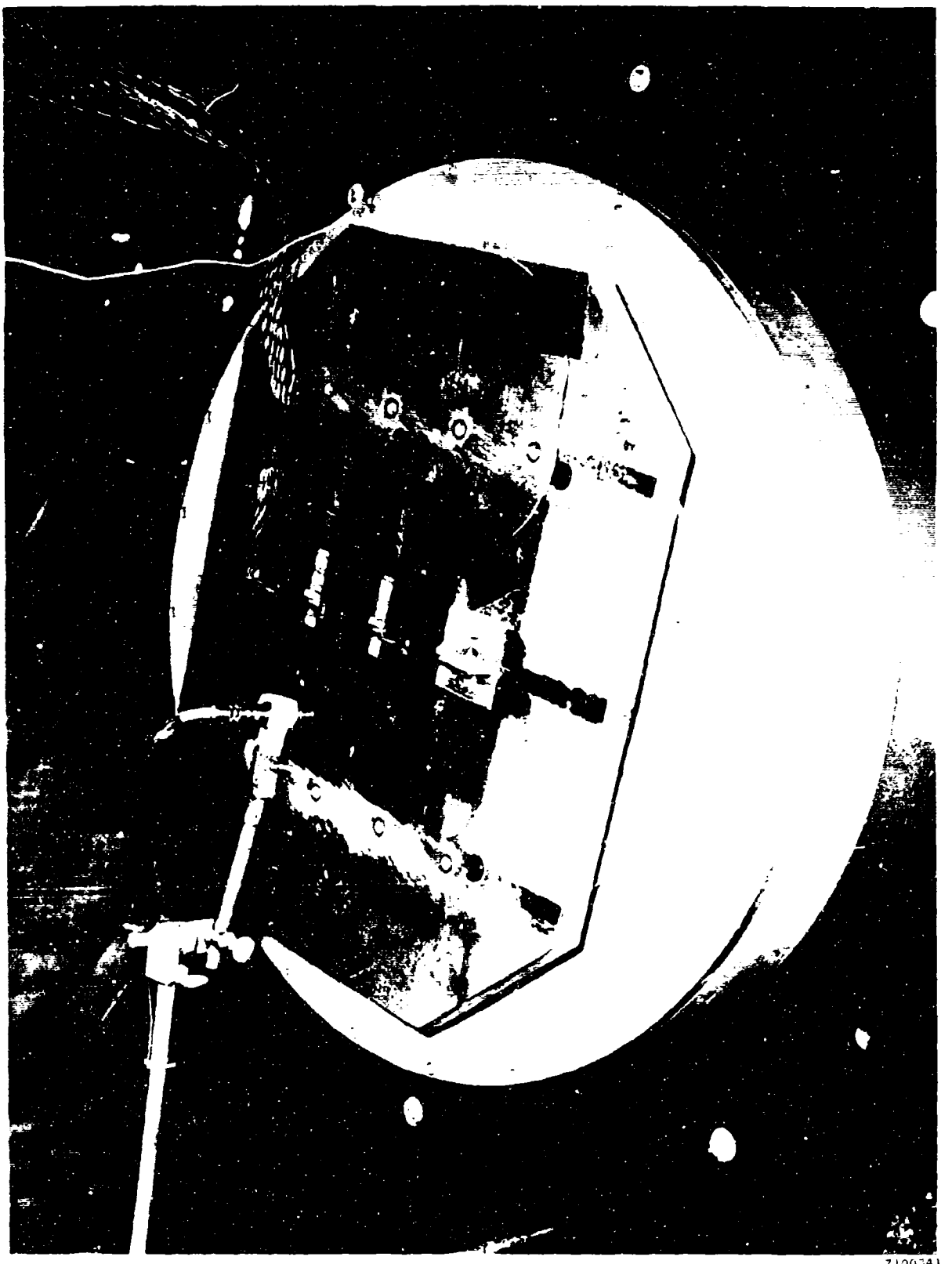

7100341

FIGURE 84. THREE SPECIMENS MOUNTED FOR SHAKER FATIGUE TESTS

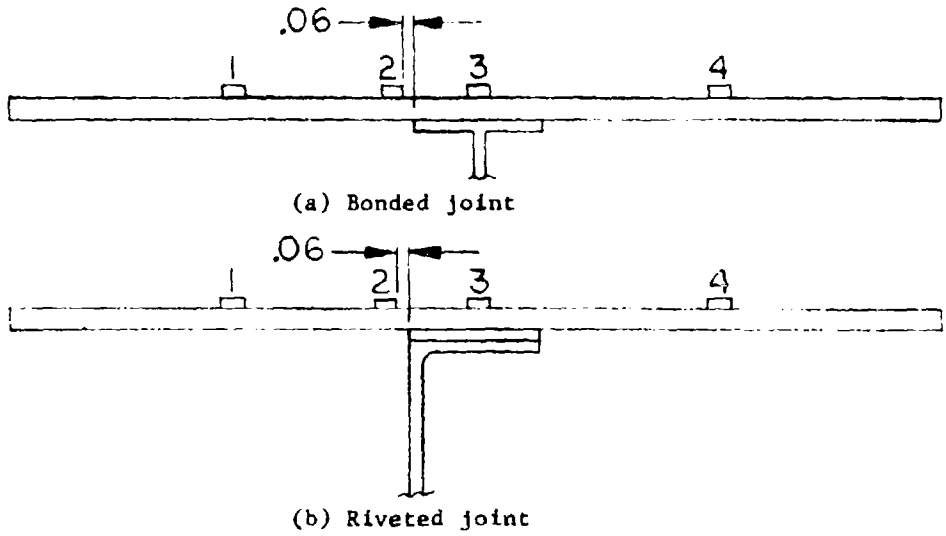

FIGURE 85. STRAIN GAGE LOCATIONS ON SHAKER SPECIMENS

VI.2.(c) Strain Gage System

Several types of strain gages were evaluated for use with these specimens. The gage selected as offering the longest life at high strain levels was the Micro-Measurements Type EA 13-250-BG-120 with the W option. This option provided separate solder tabs with strain relief connections to the element. The tabs, lead wires, and gage element were all encapsulated in a plastic envelope. Gage failures were usually due to breaks of the foil element over small surface cracks in the specimen. Gage installation and operational procedures included the following:

1. Site preparation was by airbrasive treatment and cleaning with acetone.

2. Gages were bonded in place with W.T. Bean type BR-104 epoxy cement, clamped with a rubber faced pressure pad, and heat cured at 170F for 2 hours.

3. Lacquer insulated, 34 AWG copper wire was used as transition leads from the gage to solder tabs at the center of the specimen. The transition leads were secured to the specimen with Duco Cement.

4. Short lead wires joined the single active gage to the three passive elements of the bridge. No temperature compensation was required for the dynamic measurements made during this program.

5. The bridge voltage and balance was controlled by a Northrop built system. Shunt resistor calibrations were also provided. To minimize heat buildup in the gage, one volt, dc, was used on the bridge.

6. A dc amplifier with variable gain, up to X1000, was used to drive the strain gage signal. Calibrations were set at 2000 micro-inch/inch equals one volt.

7. Shifts in dc output were used to detect gross change in the strain gage or shaker specimen response, and an attempt was made to determine the cause of the shift. (This procedure was also used for acoustic test panels.) The shift was then balanced out (no measurement was made of the shift) and the test was continued.

8. At least four strain gages were installed on each shaker specimen and the location of the strain gages is shown in Figure 85. Strain gages No. 1 and No. 4 were useful in determining the response frequencies of the two sides of the shaker specimens. Strain gage No. 3 was used to monitor the strain after the other three gages had failed. Strain gage No. 2 was the reference gage for S-N data and was not directly above the supporting stiffener; the closest edge of the grid of strain gage No. 2 was 0.06 inch from the plane of the edge of the stiffener.

VI.2.(d) Accelerometer System

Microminiature accelerometers were used to backup the strain gage to maintain specimen response levels after strain gage failure. Endevco Model 2222B accelerometers were used. Tridox F88 cement was used to install the accelerometer to the specimen.

VI.2.(e) Displacement Probe

An uncalibrated capacitive displacement probe, using a one-inch diameter disk on a Photocon Model PT-3 coil, was used to maintain surveillance over the specimen natural frequency after the loss of all other transducers. A change in specimen natural frequency was apparent if the rms output of the capacitance gage dropped since the input spectrum to the shaker was stationary.

VI.3 FINAL ESTABLISHMENT OF THE SPECIMEN LENGTH AND END CONDITIONS

The A-2 type shaker specimen (Figure 22), 13.20 inches long with a graphite-epoxy skin bonded to a graphite-epoxy tee section stringer, was the first shaker specimen that was tested. The specimen edges and web of the tee section were clamped by the test fixture. A maximum sustained strain level of 660 micro-inch/inch-rms at strain gage No. 2 was obtained under narrow band random input encompassing the lowest natural frequency of 282 Hz. This strain was considered too low to produce the desired failure times for the planned S-N curves, so alternate configurations described below were investigated.

By freeing the two ends of the specimen described in the previous paragraph, but still clamping the web of the tee section, the natural frequency of the second symmetrical bending mode of the specimen was 74 Hz. Under narrow band random loading encompassing 74 Hz, a maximum sustained strain level of 1300 micro-inch/inch-rms at strain gage No. 2 was obtained.

Then the glass doublers and skin at the two ends of the test specimen were sawed off, thereby reducing the length to 9.24 inches. The specimen was remounted in the test fixture and was clamped only at the web of the tee section. For this design and test condition, the natural frequency of the second symmetrical bending mode was 174 Hz and the strain response at strain gage No. 2 was 2000 micro-inch/inch-rms under narrow band random loading. A multiple flash exposure with a shaker specimen responding in its second symmetrical bending mode is shown in Figure 86. The general configuration and clamping conditions were judged satisfactory and used for the remaining shaker tests.

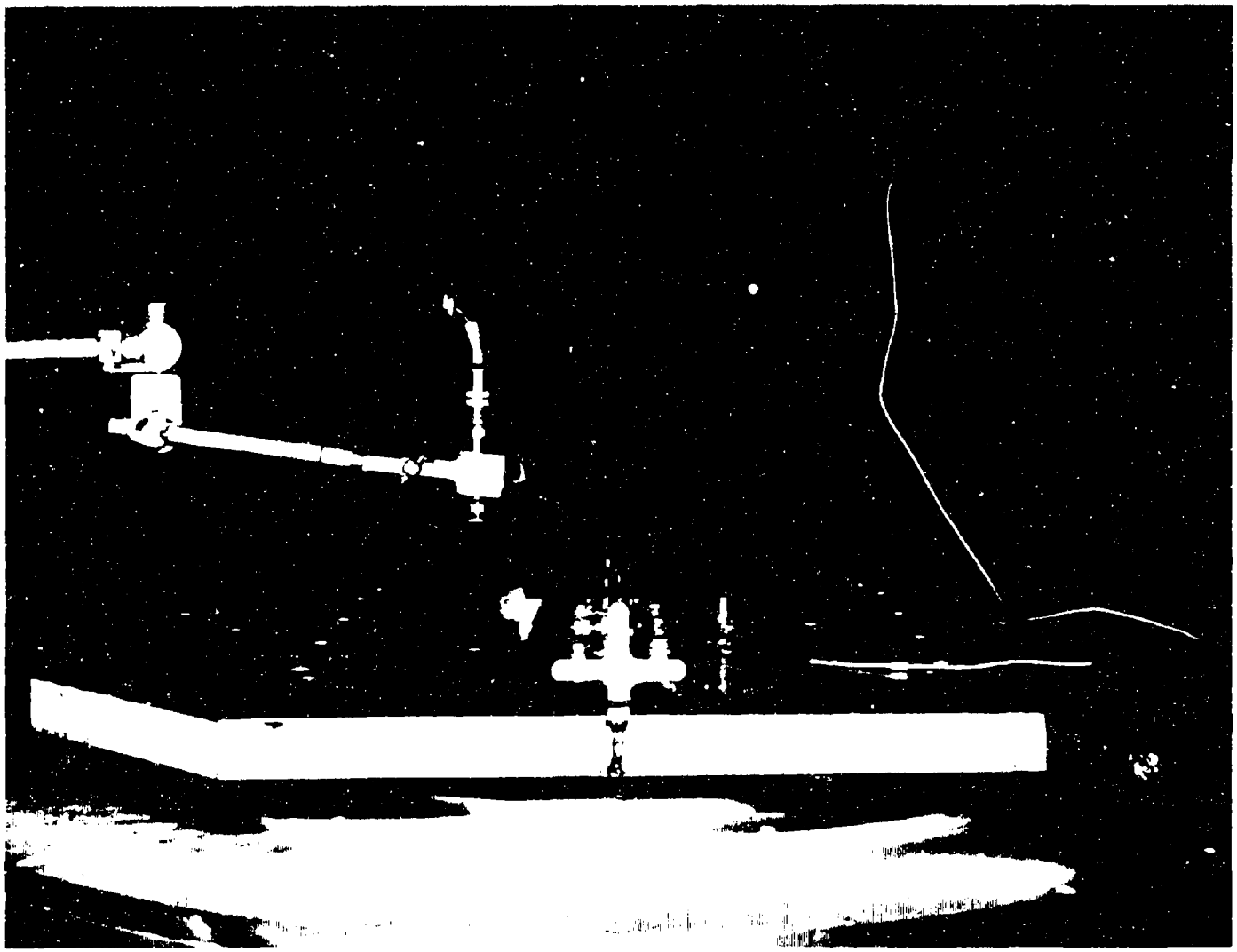

FIGURE 86. MULTIPLE FLASH EXPOSURE DURING A SHAKER SPECIMEN FATIGUE TEST

VI.4 SPECIMEN CODING

The following coding was used to identify the shaker specimens:

1. V-GG-B to designate Vibration specimen, Graphite-epoxy skin to Graphite-epoxy tee section, Bonded joint.

2. V-GG-R to designate Vibration specimen, Graphite-epoxy skin to Graphite-epoxy angle section, Riveted joint.

3. V-GT-B to designate Vibration specimen, Graphite-epoxy skin to Titanium alloy tee section, Bonded joint.

4. V-GT-R to designate Vibration specimen, Graphite-epoxy skin to Titanium alloy angle section, Riveted joint.

5. V-BT-B to designate Vibration Specimen, Boron-epoxy skin to Titanium alloy tee section, Bonded joint.

6. V-BT-R to designate Vibration specimen, Boron-epoxy skin to Titanium alloy angle section, Riveted joint.

To identify a single specimen out of a group, a dash and number were added as in the following example:

V-GG-B-9 designates the ninth of the V-GG-B specimens.

The coding of the three acoustic panels (A-GG-B-1, A-GG-B-2, and A-GG-B-3) was based on a similar coding method whereby A-GG-B designated Acoustic panel, Graphite-epoxy skin to Graphite-epoxy I-beams and tee sections, Bonded joints. For example, panel A-GG-B-2 was the second of the acoustic test panels.

VI-5 FATIGUE FAILURES

The fatigue failures of all the shaker specimens initiated in the skin. For the bonded specimens, the failure location was at the ends of the bonded joint connecting the skin to the tee sections (Figure 87). For the riveted specimens, the failure location was at the end of the bonded attachment connecting the skin to the backup detail (Figure 88) that had been bonded to the skin prior to the riveting.

Prior to the start of tests, it was decided that a test would be terminated at 10^8 cycles if no failure occurred, at a drop of 20 percent in the response frequency from its value at the beginning of the fatigue test (only specimen V-GT-B-3 had a 20 percent frequency drop and a fatigue failure was observed at the final inspection), or if a failure was observed. An observed failure was defined as a visible crack (without the use of a microscope) of approximately 0.01 inch. During the tests, when a crack was approximately 0.01 inch long, it would often propagate rapidly with a simultaneous sharp drop in the response frequency.

Specimens V-GT-R-2 and V-BT-R-2 were sectioned and photomicrographs were taken (Figures 89 and 90). The photos give detail indicative of the types of failures experienced in the shaker tests. Typical magnification in the photomicrography was 50X and standard encapsulation/mounting techniques were employed.

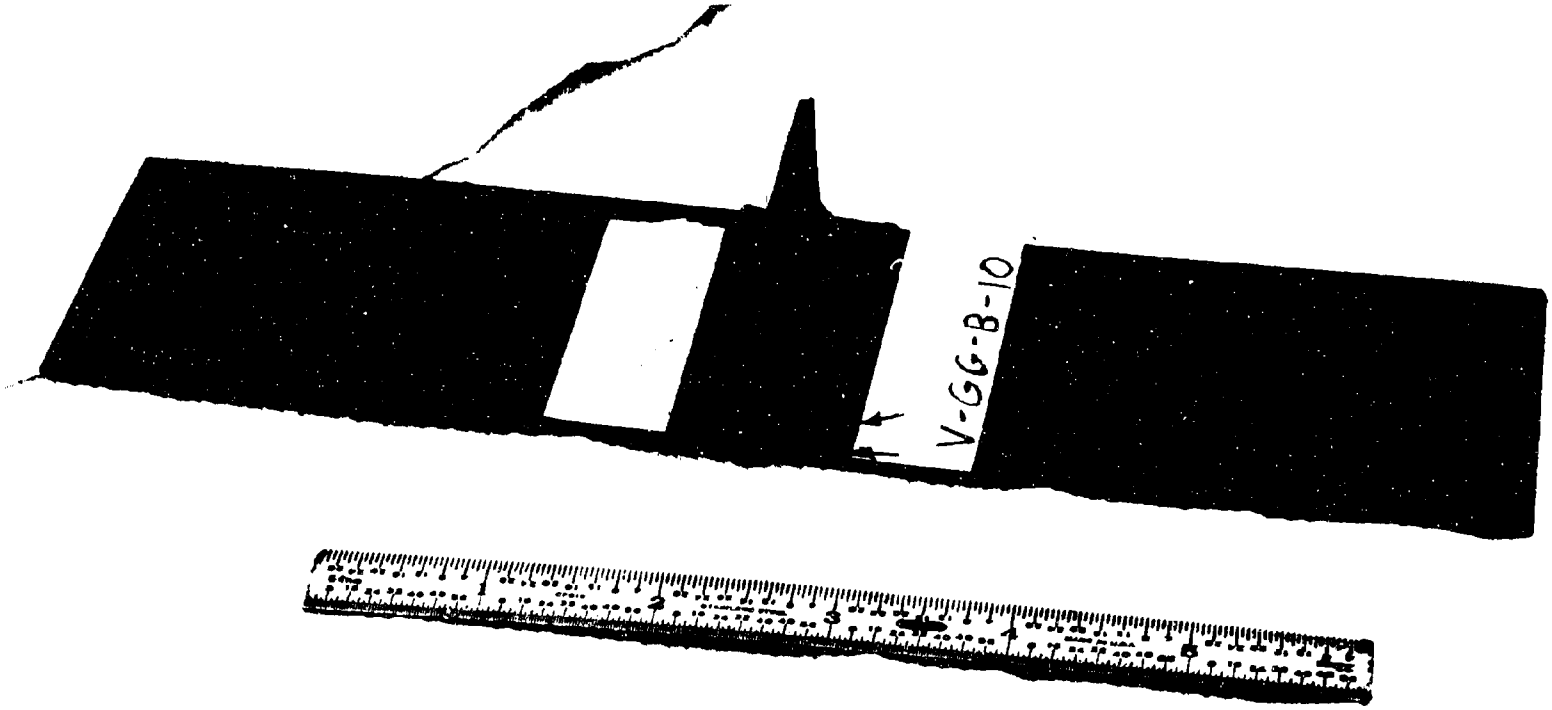

FIGURE 87. SKIN FATIGUE FAILURE (BETWEEN ARROWS) OF A SHAKER SPECIMEN WITH A BONDED JOINT

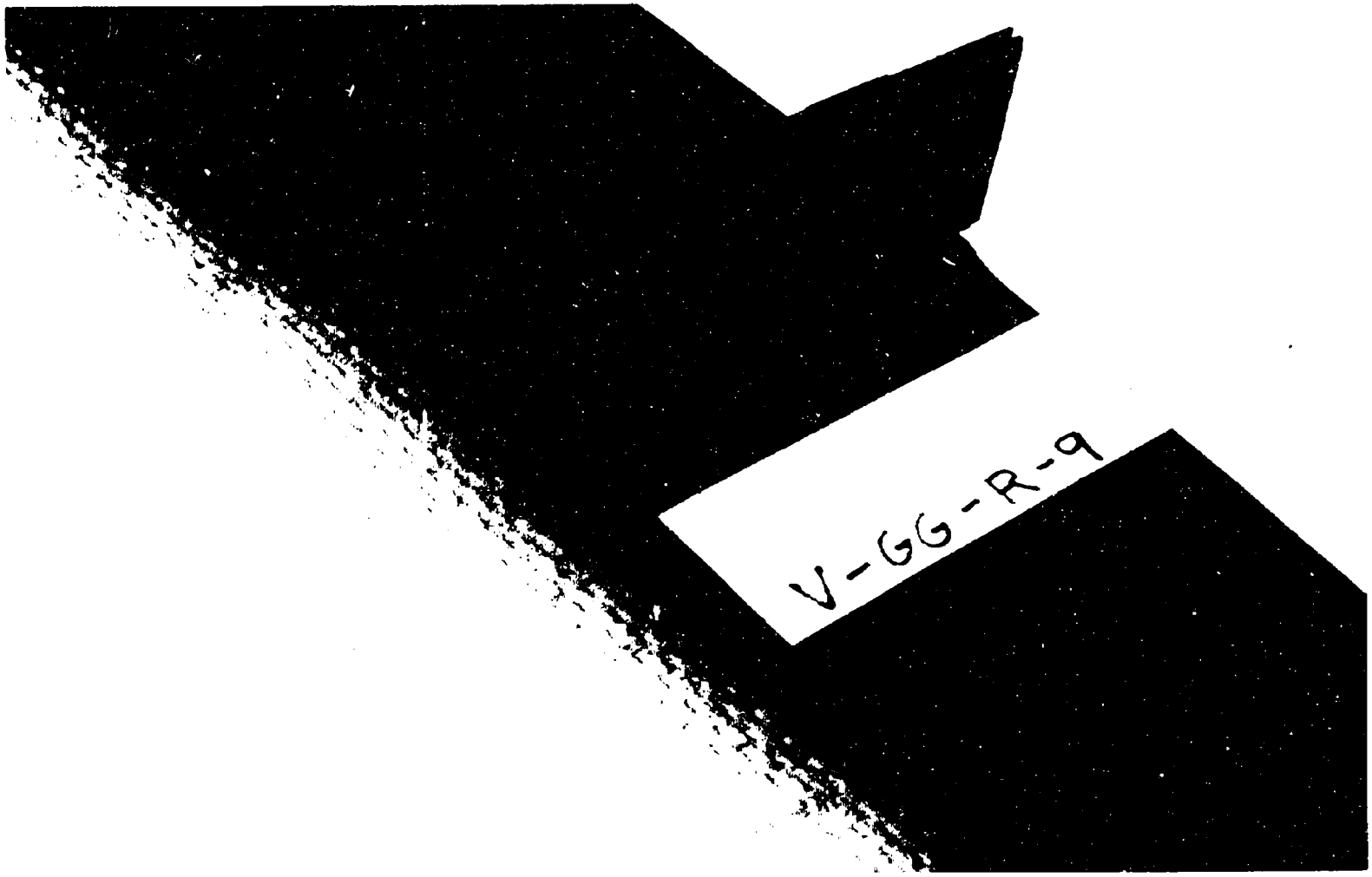

FIGURE 88. SKIN FATIGUE FAILURE ACROSS THE WIDTH OF A SHAKER SPECIMEN WITH A RIVETED JOINT

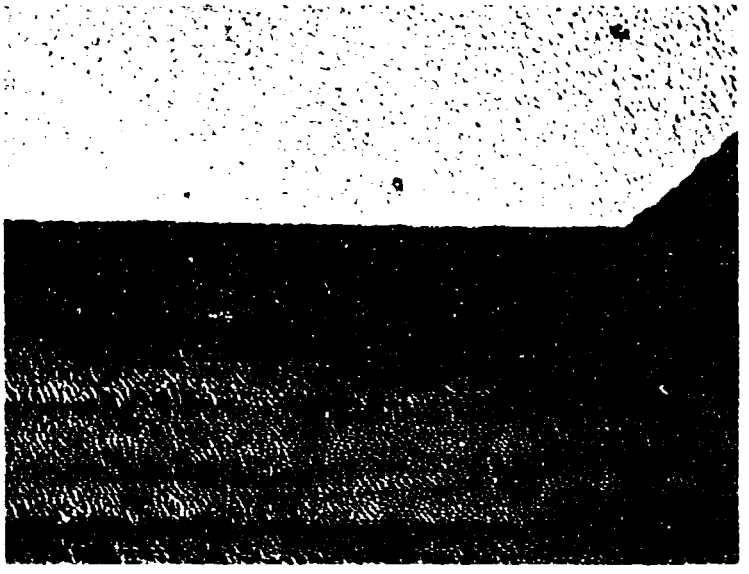

FIGURE 89. PHOTOMICROGRAPH OF FATIGUE FAILURE OF VIBRATION SPECIMEN V-GT-R-2

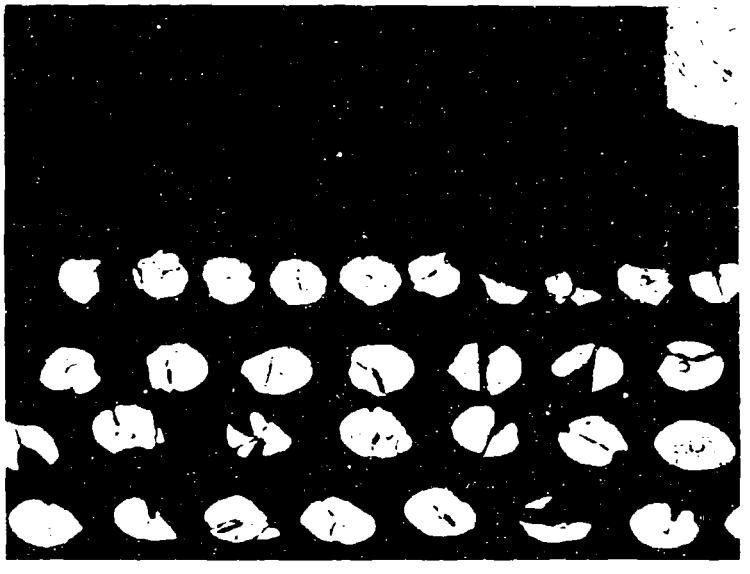

FIGURE 90. PHOTOMICROGRAPH OF FATIGUE FAILURE OF VIBRATION SPECIMEN V-BT-R-2

Figure 89 shows five plies of the 6-ply $[90 \pm 45]_S$ graphite-epoxy skin (the lower half of the photo), the FM-123-2 adhesive, and the encapsulating compound. The Ti-6Al-4V backup plate and the angle section are not shown, but are to the right and above the adhesive that is shown. Figure 89 also shows a tensile failure in the surface ply of the graphite-epoxy skin and the interlaminar degradation between the surface ply and the adjacent 45-degree lamina. The interlaminar degradation extends beyond the right of the picture.

Figure 90 shows four plies (the lower half of the figure) of the 6-ply $[90 \pm 45]_S$ boron-epoxy skin, the FM-123-2 adhesive, the encapsulating compound and the titanium alloy backup plate (upper right corner). The Ti-6Al-4V stiffener is not shown. A fatigue failure in the surface ply is evident in the left edge of the figure and an interlaminar failure is shown through the length of the figure.

The failures shown in Figures 89 and 90 are typical of the failures observed macroscopically in all of the tested shaker specimens that experienced fatigue failures.

VI.6 COMPUTATION OF CYCLES TO FAILURE

The test cycles at failure were computed by summing the products of the specimen natural frequency (second bending mode) and the noted duration that the response remained at that frequency. Changes in the response natural frequency, occurring as the bond deteriorated, were noted by manually retuning the shaker input to maximize the response amplitude. This retuning was performed whenever a change was noted in the response amplitude or on a periodic basis (usually one hour) even if no changes were noted. An example of calculating the cycles to failure follows for specimen V-GG-B-8 tested at 1800 micro-inch/inch-rms strain.

TABLE XIII. SAMPLE COMPUTATION OF CYCLES TO FAILURE

Accumulated Test Time (min)	Incremental Test Time (min)	Response Frequency* (Hz)	Incremental Life (cycles)	Cumulative Life (cycles)
2	2	175	21,000	21,000
7	5	175	52,500	73,500
22	15	171	153,900	227,400
37	15	167	150,300	377,700
39	2	153	18,360	396,060
		FAILURE**		

*The response frequencies noted are the center frequencies of the 20 Hz band width input signal to the shaker which maximized the specimen response at the beginning of the time increment.

**$N = 3.96 \times 10^5$ cycles at failure.

VI.7 TEST PROCEDURE IN INDIVIDUAL SPECIMEN TESTING

Data that were obtained during the test of specimen V-GG-B-5 are presented in Figures 91 through 97. The curves of these figures are typical of curves obtained on tests of other vibration specimens and their presentation is used to demonstrate the test procedure. The data analysis equipment and procedures used were the same as for the acoustic panels A-GG-B-2 and A-GG-B-3.

Figure 91 is a sine sweep to determine natural frequencies at a base acceleration, excitation level of 1.7 g's rms. The fundamental bending frequency is at 28 Hz, the second bending mode frequencies of the two sides of the specimen are at 165 ±5 Hz, and the first torsional frequency is at 200 Hz.

The spectral shapes of the rms strain response at strain gage No. 2 are in Figures 92, 93, and 94. The base accelerations of 5, 10, and 20 g's rms are given in Figures 95, 96, and 97. Note (from Figures 92, 93, and 94) that the peak resonant response frequency increases from 160 Hz to 175 Hz as the base acceleration input increases from 5 g's to 20 g's rms. The increase of the second bending resonance is attributed to nonlinearities resulting from large deflections at higher excitation levels.

The strain gages, in general, did not have a life of more than a few minutes at rms strains in excess of 600 micro-inch/inch. In recognition of that fact, the calibration of the reference strain gage (i.e., rms strain response versus rms shaker base acceleration excitation) was conducted as rapidly as possible before a gage gave faulty readings. In the conduct of an S-N test, when there was a discrepancy between the indicated strain reading and the calibration strain, the accuracy of the calibration strain was relied upon.

VI.8 MULTIPLE SPECIMEN TESTS

To achieve an anticipated shaker specimen fatigue life of 10^8 cycles at an average frequency of 180 Hz requires 153 hours of vibration, which would require two to three weeks calendar time with two shift operations per day. Therefore, in order to conserve calendar time, the simultaneous test of three matched specimens mounted side by side on the shaker (Figure 84) was performed.

The response frequencies of the three beams for simultaneous testing, at their second symmetrical bending mode, were matched by trimming the lengths of one or both sides of the shaker specimens. Then each shaker specimen was calibrated for its strain response as a function of input vibration level. A plot of the rms strain level versus rms vibration level was made as the vibration input, a 20 Hz bandwidth of random noise tuned to maximize the second bending response, was increased.

Using the aforementioned procedure, the attempt to match the strains at gage No. 2 of three V-GG-B beams with equal second bending frequencies was unsuccessful. However, satisfactory success in matching strains at gage No. 2 in three V-GT-B beams at the second symmetrical mode was achieved. For specimens V-GT-B-10, V-GT-B-11, and V-GT-B-12, the second symmetrical bending frequencies were adjusted to 191 ±2 Hz. At 17 g's rms vibration and tuned to 191 Hz with a 20 Hz bandwidth, the strains at gage No. 2 of the shaker specimens were 1150 ±50 micro-inch/inch-rms. The strain deviation was extremely satisfactory for proceeding with the fatigue test, which is described in some detail on page 156.

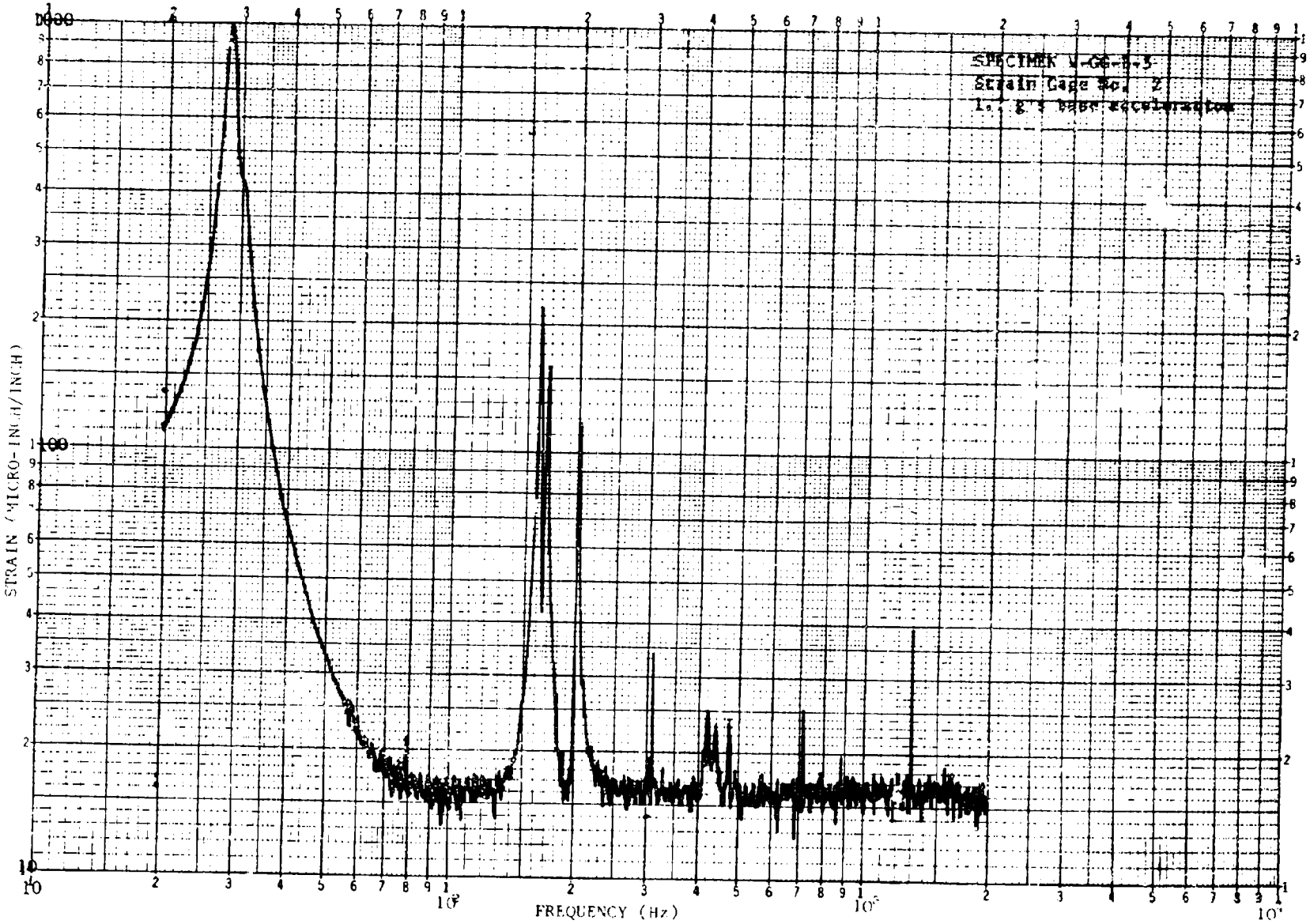

FIGURE 91. SINE SWEEP TO DETERMINE NATURAL FREQUENCIES

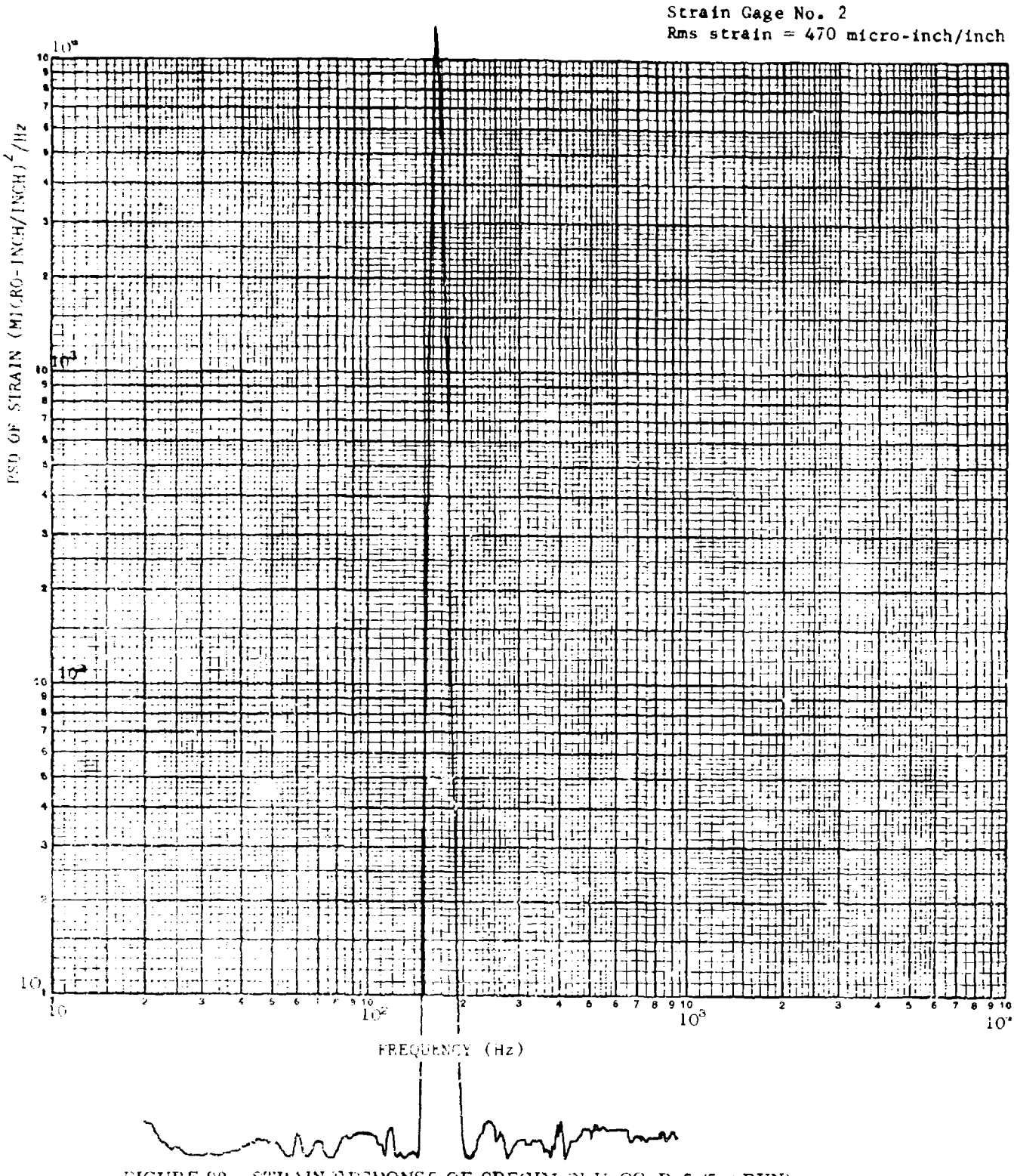

FIGURE 92. STRAIN RESPONSE OF SPECIMEN V-GG-B-5 (5 g RUN)

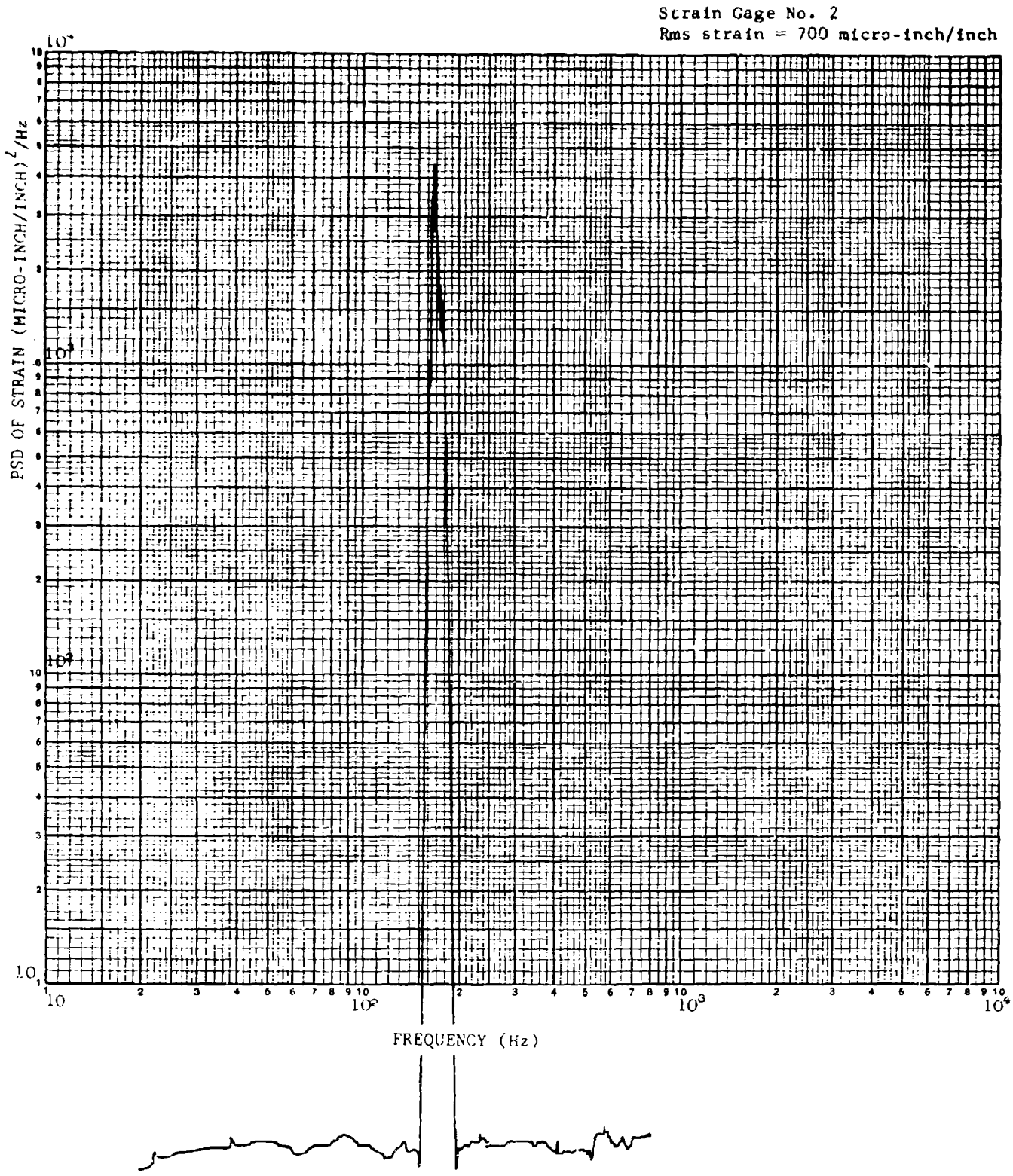

FIGURE 93. STRAIN RESPONSE OF SPECIMEN V-GG-B-5 (10 g RUN)

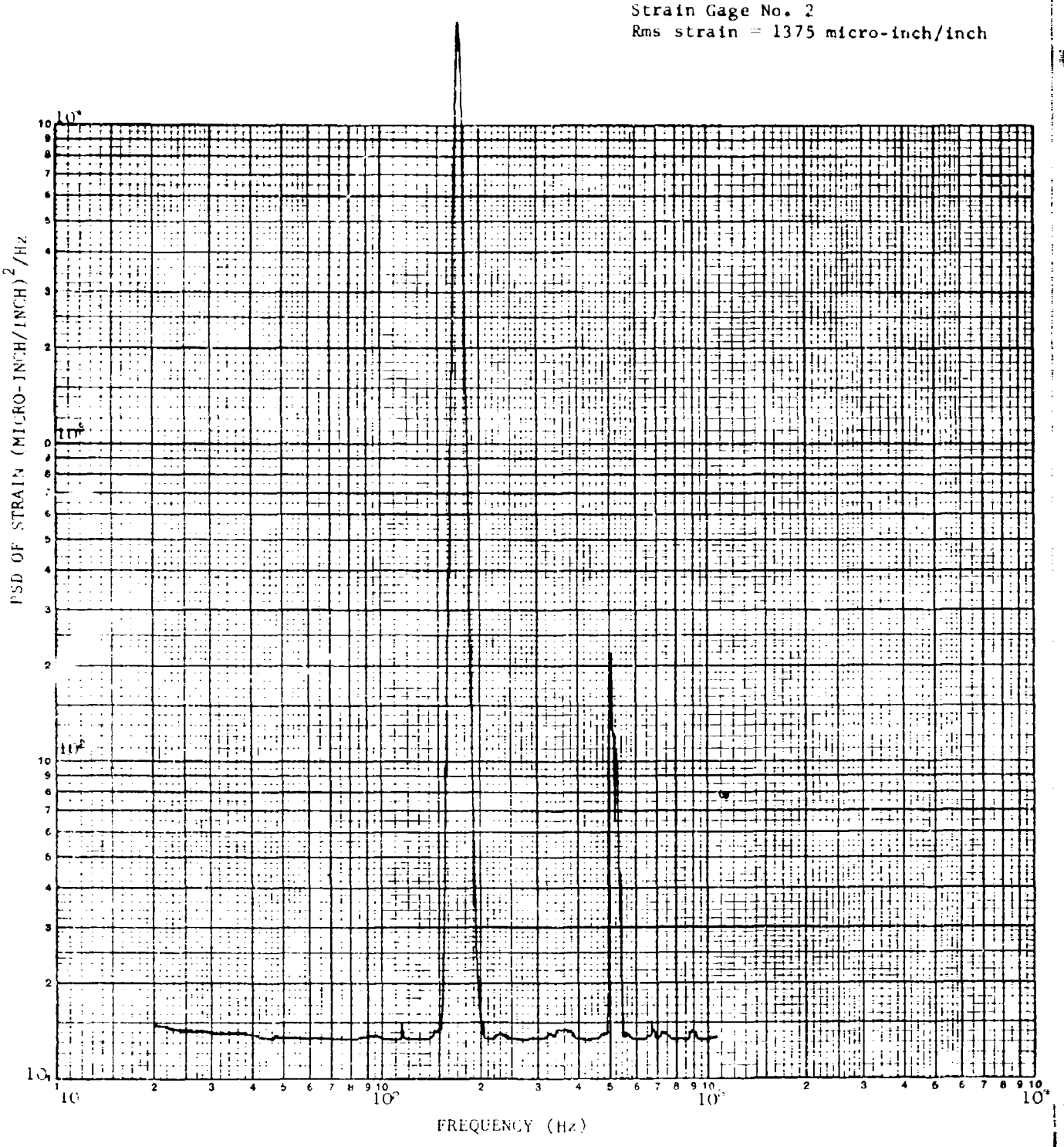

FIGURE 94. STRAIN RESPONSE OF SPECIMEN V-GG-B-5 (20 g RUN)

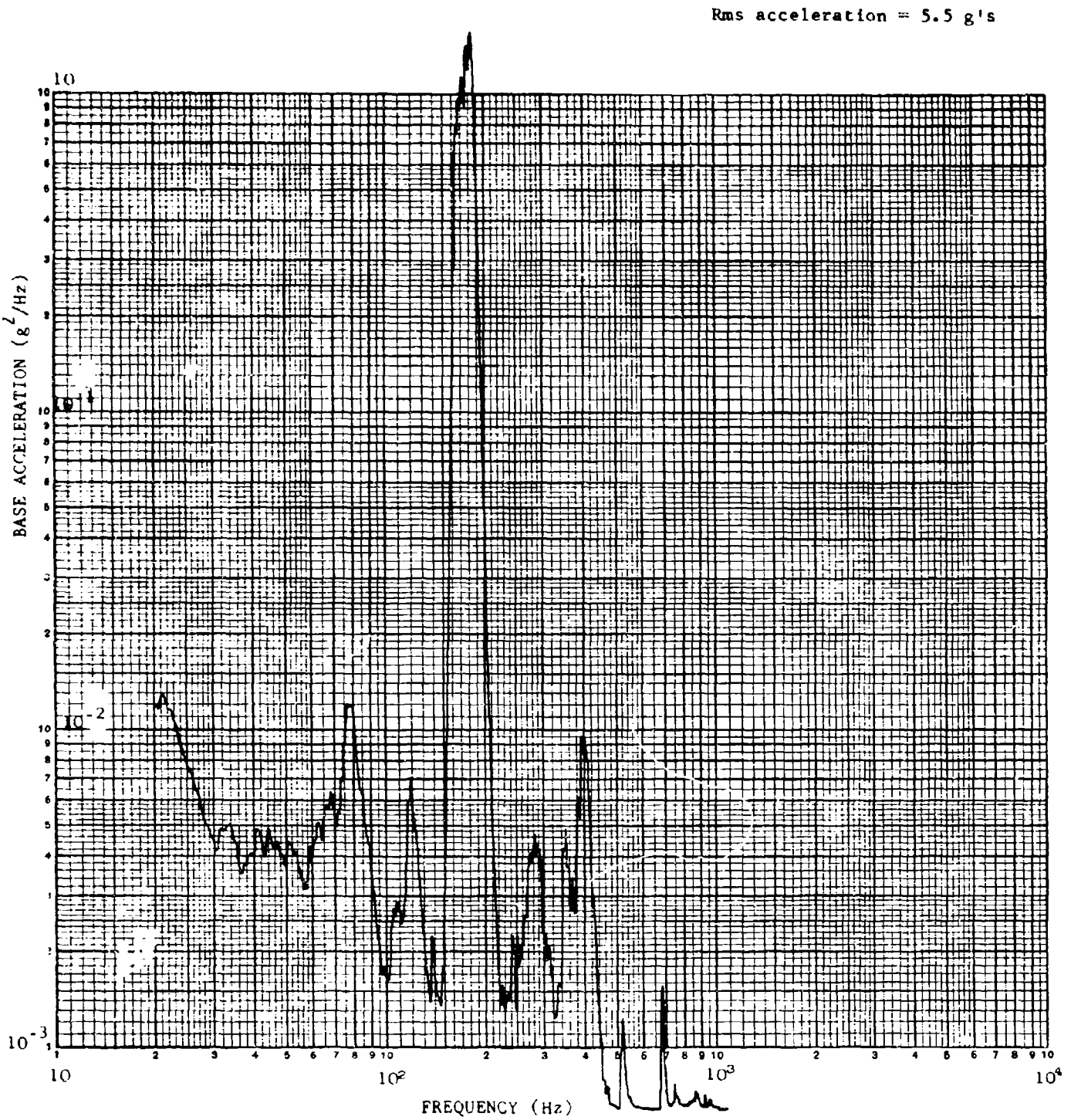

FIGURE 95. BASE ACCELERATION OF SPECIMEN V-GG-B-5 (5 g RUN)

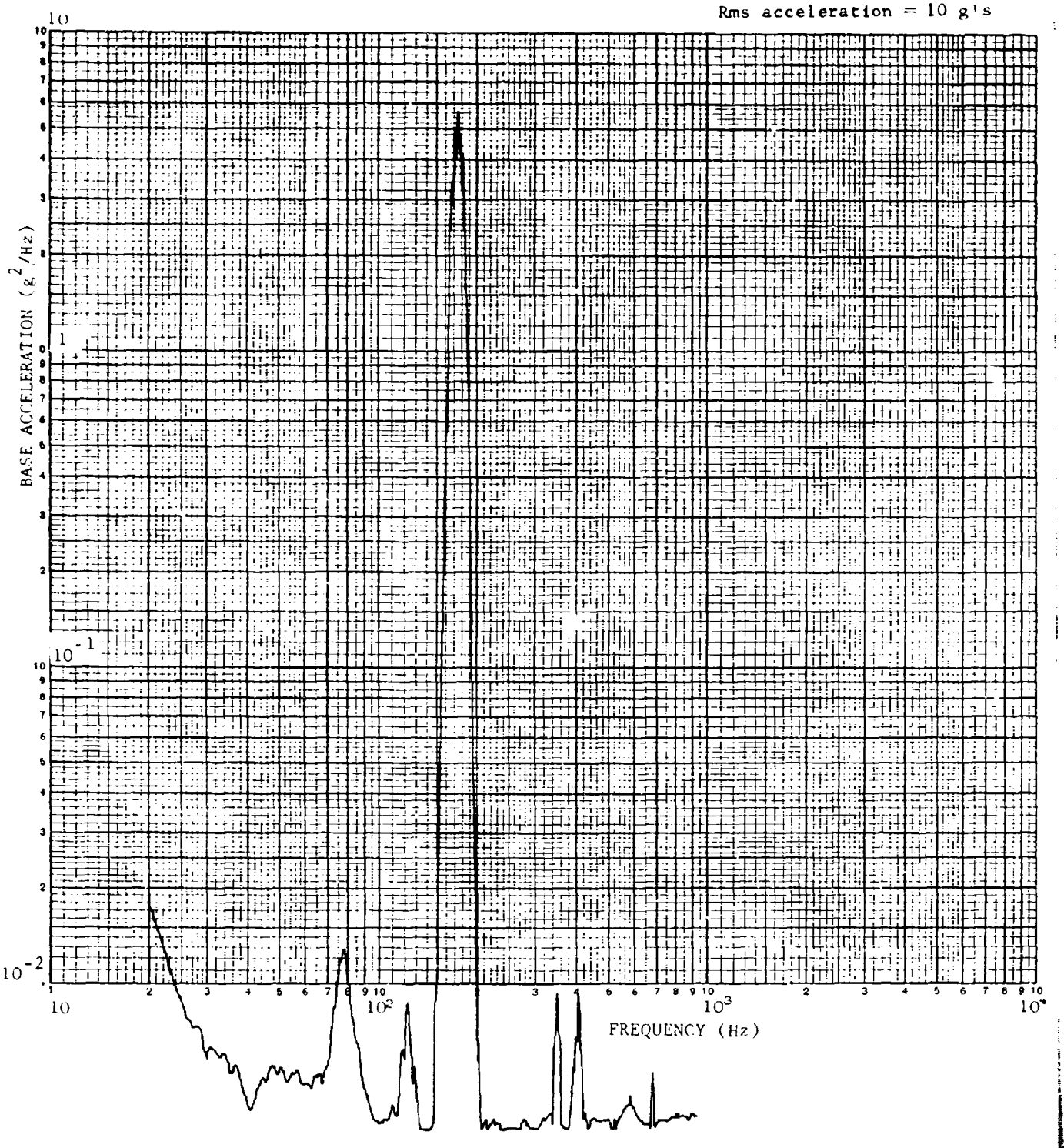

FIGURE 96. BASE ACCELERATION OF SPECIMEN V-GG-B-5 (10 g RUN)

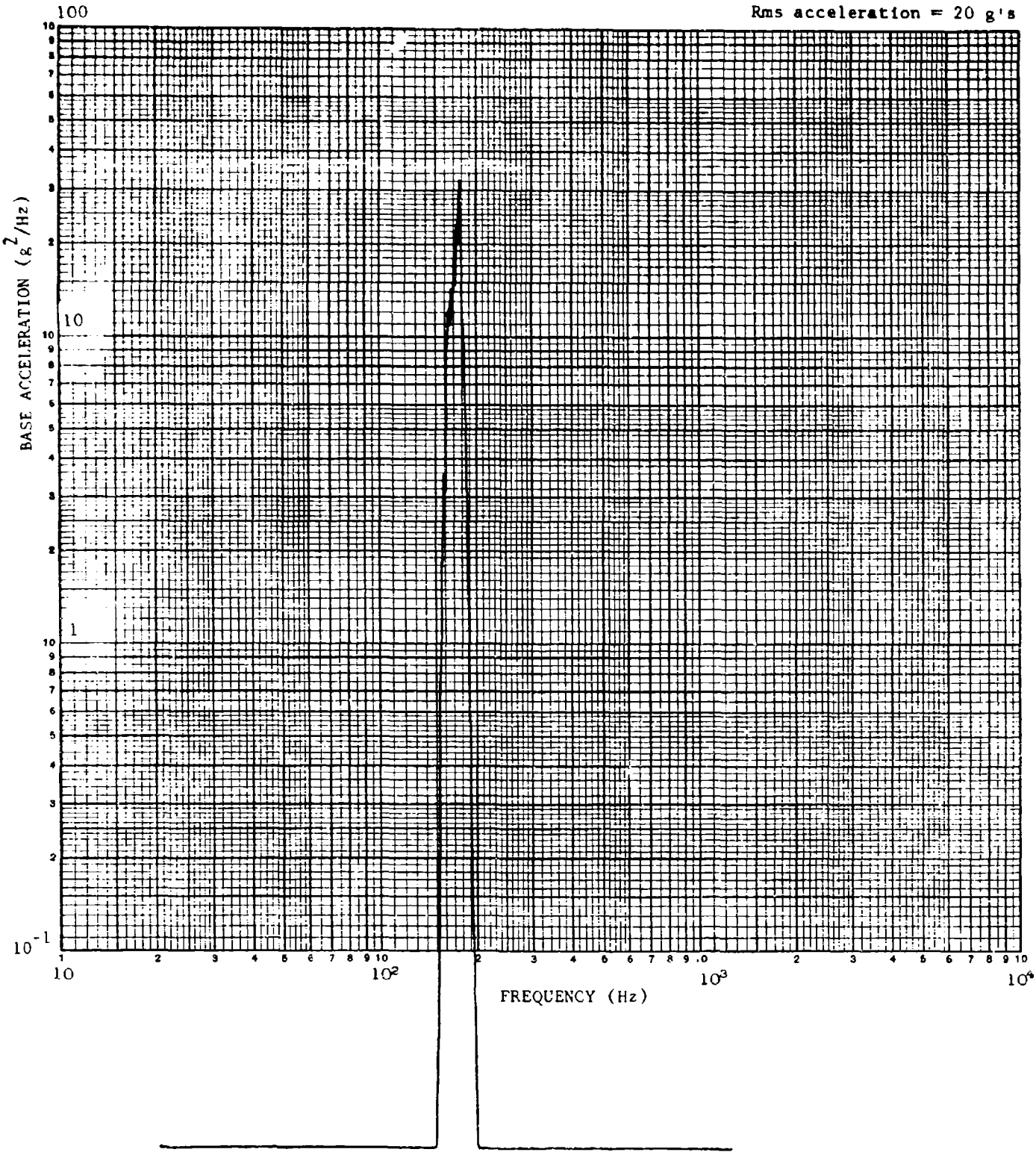

FIGURE 97. BASE ACCELERATION OF SPECIMEN V-GG-B-5 (20 g RUN)

During the multiple beam fatigue test, that began with a nominal 1150 micro-inch/inch-rms strain at gage No. 2, the frequencies of beams V-GT-B-10, V-GT-B-11, and V-GT-B-12, shifted approximately uniformly. The first frequency shift occurred at 7.5 hours of vibration of beam V-GT-B-12, which failed at 63 hours of test (4.3×10^7 cycles). Beam V-GT-B-11 failed at 82.7 hours (5.5×10^7 cycles). Beam V-GT-B-10 failed at 131 hours (8.7×10^7 cycles).

The specimens tested in multiple beam tests are noted in Table XIV which contains a summary of the single specimen and multiple specimen fatigue test results. The final test frequency in Table XIV being less than the initial test frequency is attributed to a decrease in stiffness at the joint assembly.

Both short duration and long duration S-N data may be required by the designer. Based on the experience developed in this program, simultaneous testing of vibration specimens seemed desirable when long duration data were sought, whereas individual testing seemed desirable when short duration testing was required. The crossover point between a long and a short duration test was arbitrarily set at approximately 15 hours (10^7 cycles at 200 Hz).

The benefits of simultaneous testing in long duration tests are that much calendar time and labor costs can be saved. The problems of simultaneous testing include the following:

The response frequency of each of the specimens in the set must be within some prescribed frequency range throughout the test. The prescribed frequency range used in this test program was 6 Hz.

Since the frequencies of all of the specimens do not drop uniformly, it is usually necessary to remove and reinstall specimens before the entire simultaneous test is completed.

Since, in general, the strain gage at the fatigue sensitive location has already experienced an internal fatigue failure when a specimen is removed, it is not possible to be positive that the same strain exists when the test of a specimen is resumed as existed when the specimen was removed from the test fixture. While recognizing that there was a possible change in strain, the change in strain from specimen removal and remounting was considered to be of secondary importance and was neglected in the shaker test program.

It is extremely difficult to obtain test specimens with the same strain at the reference location at the beginning of the simultaneous fatigue test, even though each of the specimens has an acceptable initial frequency. Therefore, some acceptable tolerance on the prescribed strain level at the beginning of simultaneous testing should be defined. It may well be that any deviation from the average strain of the specimens at the beginning of test is acceptable for a particular test program to generate experimental S-N data.

TABLE XIV. SUMMARY OF SHAKER S-N DATA

Specimen Number	Base Acceleration (g's, rms)	Initial Strain at Gage No. 2 (micro-inch per inch-rms)	Cycles to Failure	Initial Frequency (Hz)	Final Frequency (Hz)
V-GG-B-9	55	2500	2.0×10^5	170	144
V-GG-B-4	55	2500	1.0×10^5	173	142
V-GG-B-11	55	2500	2.5×10^4	190	159
V-GG-B-5	50	2300	1.8×10^5	161	149
V-GG-B-14	45	2000	8.8×10^5	196	186
V-GG-B-2	40	2000	2.9×10^5	172	145
V-GG-B-15	48	2000	2.1×10^5	185	178
V-GG-B-1	40	1800	1.1×10^6	173	140
V-GG-B-8	42	1800	4.0×10^5	175	153
V-GG-B-6	44	1800	3.0×10^5	180	154
V-GG-B-3	35	1400	4.6×10^6	158	130
V-GG-B-10	36	1400	2.4×10^6	198	169
V-GG-B-7	35	1400	1.8×10^6	172	142
V-GG-B-17	18	1100	1.0×10^8*	197	189
V-GT-B-8	42	2500	7.8×10^5	188	166
V-GT-B-5	52	2500	6.3×10^5	181	163
V-GT-B-3	55	2500	5.9×10^5	188	149
V-GT-B-7	35	1800	1.6×10^6	183	169
V-GT-B-2	38	1800	8.3×10^5	179	159
V-GT-B-4	37	1800	7.4×10^5	196	162
V-GT-B-1	28	1400	9.7×10^6	187	160
V-GT-B-6	28	1400	6.3×10^6	195	167
V-GT-B-9	28	1400	3.3×10^6	185	151
V-GT-B-10	17	1100**	8.7×10^7	190	174
V-GT-B-11	17	1200**	5.5×10^7	190	176
V-GT-B-12	17	1100**	4.3×10^7	189	173

*No fatigue failure when the test was terminated
**A multiple shaker specimen test

TABLE XIV. SUMMARY OF SHAKER S-N DATA (Continued)

Specimen Number	Base Acceleration (g's, rms)	Initial Strain at Gage No. 2 (micro-inch per inch, rms)	Cycles to Failure	Initial Frequency (Hz)	Final Frequency (Hz)
V-BT-B-1	40	1800	1.2×10^3	215	186
V-BT-B-3	33	1300	1.1×10^3	225	202
V-BT-B-2	40	1100	4.9×10^4	207	197
V-BT-B-8	30	900	5.8×10^5	214	178
V-BT-B-10	30	900	1.6×10^5	217	172
V-BT-B-4	30	900	7.0×10^4	213	166
V-BT-B-13	20	750	7.9×10^5	221	183
V-BT-B-11	23	750	6.3×10^5	225	186
V-BT-B-12	23	750	3.0×10^5	227	192
V-BT-B-6	21	600	4.4×10^6	212	173
V-BT-B-7	17	600	4.2×10^6	214	187
V-BT-B-9	24	600	2.4×10^6	213	184
V-BT-B-5	20	600	1.6×10^6	215	173
V-BT-B-15	14	420**	1.4×10^8*	220	204
V-BT-B-16	14	460**	1.3×10^8*	220	200
V-BT-B-14	14	430**	9.9×10^7*	220	198
V-GG-R-10	35	2500	7.6×10^5	182	163
V-GG-R-9	38	2500	3.9×10^5	185	165
V-GG-R-8	41	2500	3.1×10^5	180	157
V-GG-R-3	29	1800	5.3×10^6	198	160
V-GG-R-2	29	1800	2.4×10^6	192	167
V-GG-R-4	29	1800	1.7×10^6	185	168
V-GG-R-6	28	1400	6.3×10^6	195	171
V-GG-R-5	24	1400	6.2×10^6	189	170
V-GG-R-7	22	1400	3.4×10^6	180	166
V-GG-R-11	17	1400**	5.9×10^7	204	181
V-GG-R-13	17	1240**	1.0×10^8*	200	184
V-GG-R-12	17	1220**	1.0×10^8*	199	185

*No fatigue failure when the test was terminated
**A multiple shaker specimen test

TABLE XIV. SUMMARY OF SHAKER S-N DATA (Continued)

Specimen Number	Base Acceleration (g's, rms)	Initial Strain at Gage No. 2 (micro-inch per inch, rms)	Cycles to Failure	Initial Frequency (Hz)	Final Frequency (Hz)
V-GT-R-6	32	2600	1.5×10^6	191	170
V-GT-R-5	27	2600	1.5×10^6	186	167
V-GT-R-3	55	2600	7.8×10^5	203	162
V-GT-R-9	28	2300	3.9×10^6	184	160
V-GT-R-7	23	2300	2.0×10^6	190	167
V-GT-R-8	28	2300	1.4×10^6	188	168
V-GT-R-1	40	2000	6.1×10^6	213	185
V-GT-R-2	22	2000	5.8×10^6	180	154
V-GT-R-4	29	2000	9.4×10^5	182	168
V-GT-R-10	19	1600**	1.4×10^7***	186	181
V-GT-R-11	19	1470**	1.4×10^7***	185	181
V-GT-R-12	19	1350**	1.4×10^7***	189	183
V-BT-R-8	22	1100	1.8×10^6	215	170
V-BT-R-9	19	1100	1.1×10^6	206	168
V-BT-R-7	20	1100	7.2×10^5	201	165
V-BT-R-3	18	900	1.2×10^6	211	168
V-BT-R-1	21	900	9.2×10^5	213	171
V-BT-R-2	23	900	2.3×10^5	210	180
V-BT-R-5	13	600	1.5×10^7	205	171
V-BT-R-4	13	600	1.1×10^7	206	166
V-BT-R-6	13	600	1.1×10^7	205	170
V-BT-R-10	17	620**	4.6×10^7	205	177
V-BT-R-12	17	560**	9.4×10^7	205	175
V-BT-R-11	17	490**	1.1×10^8*	204	182

*No fatigue failure when the test was terminated

**A multiple shaker specimen test

***No visual inspection was made of these three specimens during the final two hours of test, but the retuning that was performed one hour before the end of the test indicated no weakening of the skin of any of the three specimens. The total test time of each of these specimens was 21 hours.

VI-9. SHAKER S-N DATA AND STATIC ULTIMATE TENSILE STRAINS

A summary of the shaker S-N data is in Table XIV and Figure 98. The strains in Table XIV (and also in the acoustic test program) were estimates of rms strains obtained visually from true rms voltmeters, with 1 second averaging times and the accuracy of the strains is estimated to be within ten percent.

The static ultimate tensile strains from Table A-2 of Appendix A are 9300 micro-inch/inch for the six-ply $[90 \ \pm 45]_S$ graphite-epoxy specimens and are 4100 micro-inch/inch for the six-ply $[90 \ \pm 45]_S$ boron-epoxy specimens. From Figure 98, it appears that the rms fatigue strain at 10^8 cycles under the narrow band random loading that was exciting the second symmetric bending mode is at least ten percent of the static ultimate tensile strain of the six-ply laminates.

VI.10 TEST EQUIPMENT

The vibrator system (which was capable of performing sine, narrow-band random or broad-band random testing) and its controlling instrumentation are listed below:

1 - Ling Electronics Model 335A Shaker (rated at 17,500 force pounds)
1 - Ling Electronics Model PP-70/120 VC Power Supply
1 - Ling Electronics Model SRC-401 RS Control Console containing the following major items:

  1 - Ling SCO-100 Sine Control Center
  1 - Ling AAL-101 Acceleration Limiter
  1 - Ling NSD-100 No-Signal Detector
  6 - Unholtz-Dickie D11 MVS Charge Amplifier
  1 - Unholtz-Dickie ACS-6 Accelerometer Selector
  1 - Spectral Dynamics SD 101A Tracking Filter
  1 - Hewlett Packard 7561A Log Converter
  1 - Hewlett Packard 135 AR X-Y Recorder
  1 - B & K 2416 VTVM
  1 - Ling LA-102 Mixer Amplifier
  1 - Ling ASDE 40 Random Equalizer-Analyzer

6 - Endevco 2213C Accelerometer
3 - Endevco 2222B Accelerometer (Microminiature - 0.5 gm)
2 - Photocon PT-5 Displacement Probe
2 - SKL 302 Variable Filter

VI.11 DISCUSSION OF SHAKER S-N DATA

It is significant that the backup plates (that are desirable in fatigue applications of countersunk rivets in the thin skins) that were bonded to the skins prior to riveting the skin to the stiffeners, in general, resulted in riveted, advanced-composite specimens that had longer lives than non-riveted specimens. The longer life of the riveted specimens has been attributed to less stress concentration at the edges (of the bonded area) where the fatigue failures initiated in the skins of the shaker specimens. Less stress concentration at the edges of the bonded areas is expected when the load transfer is from

the stiffeners through the three rivets into the backup plates (bonded to the skins) and into the graphite-epoxy skins.

In the test data in Figure 98, in general, the vibration specimens with graphite-epoxy skins have longer life when the stiffeners are titanium alloy rather than graphite-epoxy. The difference in life at a given strain has been attributed to the graphite-epoxy stiffener being more flexible than the titanium alloy stiffener. Hence, the strain across the specimen width (in the vicinity of a fatigue failure) is less uniform and consequently results in a higher stress concentration (and shorter life) at the edge of the width of the bonded areas (where all fatigue failures initiated) of the specimens with graphite-epoxy stiffeners.

The two preceding paragraphs imply that the specimen life is dependent on the stress concentration at the edges of the width of the bonded areas (where fatigue failures have initiated) of the vibration specimens. The use of the titanium alloy stiffeners and the use of rivets with titanium alloy back-up plates bonded to the skin apparently reduced the stress concentration and led to longer lives. Another promising method of reducing the stress concentration is to use narrower vibration specimens, although the narrower specimens may not be feasible in the case of the riveted specimens, which in this program contained only three rivets. The spacing and size of the rivets in the experimental program were based on design procedures that had been established by Northrop for riveted metallic structures. A recent investigation that includes the behavior of riveted joints in fatigue applications is reported in Reference 9. Narrower vibration specimens were not chosen for this program since one intent was to maintain the same width for non-riveted and riveted specimens.

One objective of the shaker test program was to obtain S-N curves with sets of six-ply specimens (one of the sets simulates a portion of the bonded joints of the acoustic test program). The S-N curves of Figure 98 are useful because they indicate life that can be expected from a larger population of different types of test specimens. However, because of the few specimens in each set, the confidence levels associated with life predictions based on the S-N shaker specimen test results are significantly lower than the confidence levels associated with material allowables for the design of metallic aircraft structural elements. However, it does appear that the rms fatigue strain at 10^8 cycles under the narrow band random loading of the six-ply $[90, \pm 45]_S$ graphite-epoxy and boron-epoxy laminates is at least ten percent of the static, ultimate tensile strain of the six-ply laminates.

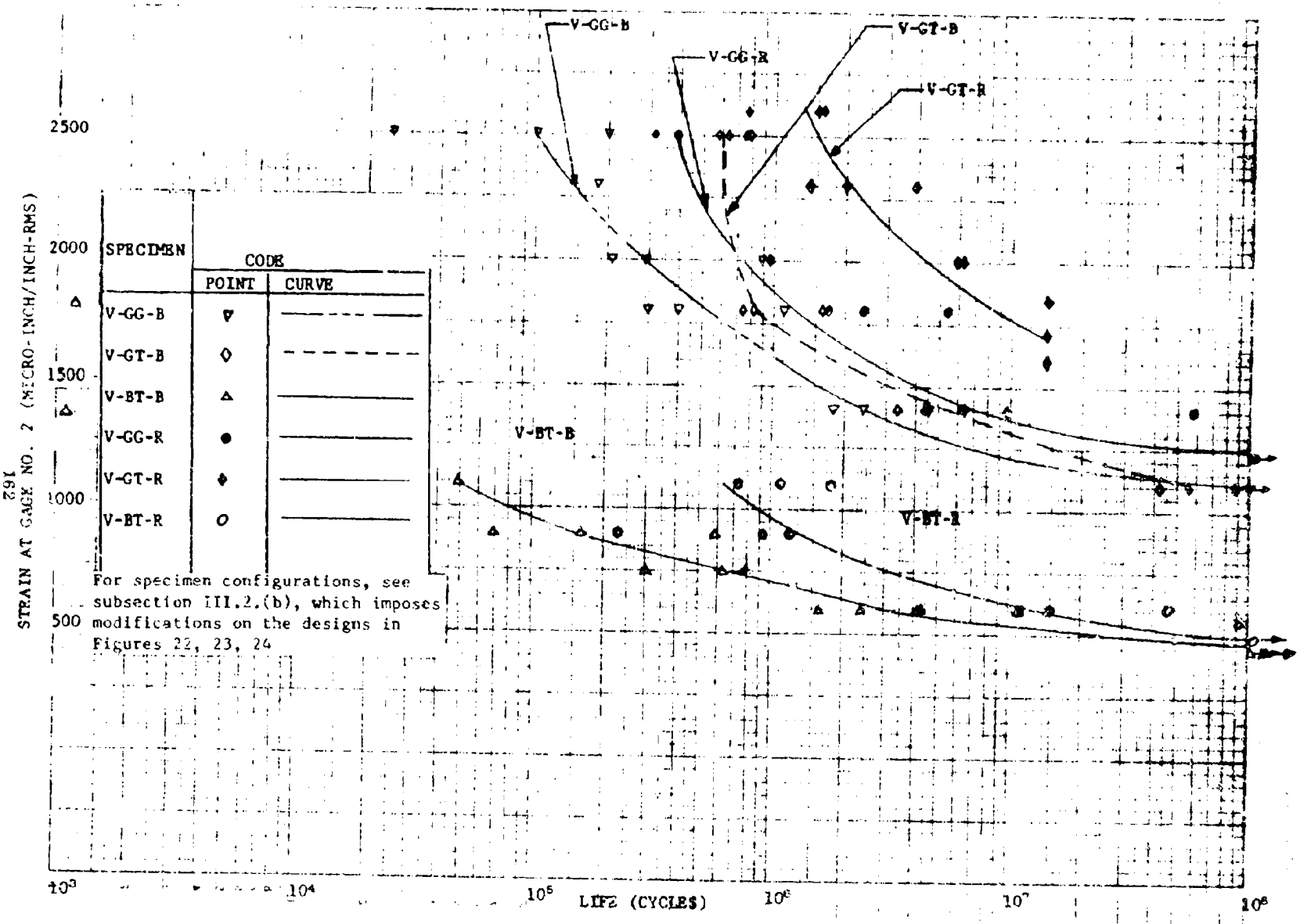

FIGURE 98. SUMMARY OF SHAKER S-N DATA AND PRELIMINARY S-N CURVES

VII. THEORY OF ORTHOTROPIC PANEL RESPONSE TO ACOUSTIC EXCITATION

In this section are given (1) the general theory for predicting the natural modes and response of an orthotropic plate to acoustic excitation, and (2) a simplified theory for predicting both the fundamental mode of an orthotropic plate of uniform thickness that is fully clamped on all four edges and the response of the plate to acoustic excitation.

The simplified theory can be used in the design of individual bays of cross-stiffened orthotropic plates in cases when each of the bays respond principally in its fundamental mode as though it were clamped on all four edges. The main limitation of the simplified theory is that the stiffeners around the periphery of a bay are assumed to be rigid. Therefore, neither the design and/or analysis of the internal structure of the cross-stiffened panel can be investigated with the simplified theory nor has a criterion yet been developed for determining when the simplified theory can be applied in the design of the skin. However, it appears that in many cases when the critical acoustic fatigue location in a cross-stiffened panel is in the skin at the joint with the internal structure, the simplified theory can be applied in the acoustic design.

Applications of the general theory and the simplified theory in the prediction of the response of unstiffened and stiffened plates to acoustic excitation are presented in Section VIII. Also in Section VIII is a comparison of experimental results with numerical results obtained with the general and simplified theories.

The equations of the general theory that are developed below are similar in form to the equations in Reference 10. The development of the simplified theory in Section VII.2 follows the approach given in References 7 and 11 for isotropic plate response analysis.

VII.1 GENERAL THEORY

The general theory, described below, is in matrix form. Hence, the general theory is suitable for programming for digital computer calculations using the finite element technique. Most aerospace firms have digital computer programs (e.g., Reference 12) that to some degree or another perform the calculations required by the general theory that is presented in this section. Northrop used its REDYN (REdundant DYNamics) digital computer program to perform many of the calculations required by the general theory. A drawback in attempting to apply the general theory is that the number of finite elements and node points may be prohibitive in a single computer run computation of several natural frequencies, modal shapes, and stresses at critical locations (of complex structures) where acoustic fatigue failures seem likely to occur. Thus major problems may arise when the equations of the general theory are applied in detailed stress analyses of advanced-composite panels of non-uniform thickness and with attachments such as stringers, ribs, frames, etc.

VII. 1. (a) Equations of Motion

In matrix form, the equations of motion in the time domain are

$$[K]\{d\} + [C]\{\dot{d}\} + [M]\{\ddot{d}\} = \{f(t)\} \tag{5}$$

where

$[K]$ = stiffness matrix

$[C]$ = damping matrix

$[M]$ = mass matrix

$\{d(t)\}$ = nodal deflection matrix

$\{f(t)\}$ = nodal force matrix

The equations of motion in the frequency domain are obtained by taking a Fourier transform of equation (5) and are

$$\left[[K] + i\omega[C] - \omega^2[M]\right]\{S_d(\omega)\} = \{S_f(\omega)\} \tag{6}$$

where

ω = frequency

$S_d(\omega)$ = Fourier transform of d(t)

$S_f(\omega)$ = Fourier transform of f(t)

VII. 1.(b) Eigenvalue Solutions

The eigenvalue solutions for natural frequencies are obtained from

$$[K]\{q^{(i)}\} = \bar{\omega}_i^2[M]\{q^{(i)}\} \tag{7}$$

where

$\{q^{(i)}\}$ = the ith mode shape, the eigenvector

$\bar{\omega}^{(i)}$ = the ith natural frequency

Let

$$[Q] = \left[\{q^{(1)}\}, \quad \{q^{(2)}\}, \quad \ldots\right] \tag{8}$$

Then, $[Q]$ satisfies the following orthogonality conditions:

$$[Q]^t [K] [Q] = \lceil \bar{\omega}^2 \rfloor \lceil M_i \rfloor \tag{9}$$

$$[Q]^t [M] [Q] = \lceil M_i \rfloor \tag{10}$$

with $\lceil M_i \rfloor$ being the matrix of generalized masses, and M_i being the generalized mass of the ith mode. Each eigenvector may be normalized according to equation (10) with M_i being a generalized mass of unit magnitude.

VII. 1. (c) Modal Amplitudes

In order to determine the modal response in the frequency domain, first let

$$\{S_d(\omega)\} = [Q] \{S_\xi(\omega)\} \tag{11}$$

where

$S_\xi(\omega)$ = i^{th} modal amplitude in the frequency domain

Then, substitute equation (11) into equation (6), premultiply the resulting equation by $[Q]^t$, and use equations (9) and (10) to simplify and obtain

$$\{S_\xi(\omega)\} = \lceil Z(\omega) \rfloor^{-1} [Q]^t \{S_f(\omega)\} \tag{12}$$

where

$$Z_j = \left(\bar{\omega}_j^2 - \omega^2 + 2i \gamma_j \omega\bar{\omega}_j\right) M_j \tag{13}$$

and the damping matrix $[C]$ is assumed to satisfy

$$[Q]^t [C] [Q] = 2 \lceil \gamma \rfloor \lceil \bar{\omega} \rfloor \lceil M_i \rfloor \tag{14}$$

VII. 1. (d) Deflection Spectral Density

The deflection and stress responses to random loading are obtained with the use of their spectral densities. By definition, the cross power spectral density of deflections at degrees of freedom i and j

$$\Phi_{d_i d_j}(\omega) \equiv \Phi_{d_{ij}}(\omega) = \lim_{T\to\infty} \frac{1}{T} S_{d_i} S_{d_j}^* \tag{15}$$

where the asterisk denotes the complex conjugate.

From the definition of $\Phi_{d_{ij}}(\omega)$, one may show that $\Phi_{d_{ji}}(\omega)$ is the complex conjugate of $\Phi_{d_{ij}}(\omega)$, i.e.,

$$\Phi_{d_{ji}}(\omega) = \lim_{T\to\infty} \frac{1}{T} S_{d_j} S_{d_i}^* = \Phi_{d_{ij}}^*(\omega) \tag{16}$$

The insertion of equations (11) and (12) into equation (15) produces

$$[\Phi_d(\omega)] = [Q] \left[Z(\omega)\right]^{-1} [Q]^t [\Phi_f(\omega)] [Q] \left[Z\right]^{-1*} [Q]^t \tag{17}$$

where $[\Phi_f(\omega)]$ is a complex matrix whose elements $\Phi_{f_{ij}}$ are defined by

$$\Phi_{f_{ij}}(\omega) = \lim_{T\to\infty} \frac{1}{T} S_{f_i}(\omega) S_{f_j}{}^*(\omega) = \Phi_{f_{ji}}{}^*(\omega) \tag{18}$$

Alternately, $\Phi_{f_{ij}}(\omega)$ may be expressed as the Fourier transform of the cross correlation function $R_{f_i f_j}$ with

$$\Phi_{f_{ij}}(\omega) = \frac{1}{\pi} \int_{-\infty}^{\infty} R_{f_i f_j}(\tau) e^{-i\omega\tau} d\tau \tag{19}$$

and

$$\Phi_{f_{ij}}(\omega) = \Phi_{f_{ji}}{}^*(\omega) \tag{20}$$

where the cross correlation function is defined by

$$R_{f_i f_j}(\tau) = \lim_{T\to\infty} \frac{1}{2T} \int_{-\infty}^{\infty} f_i(t) f_j(t+\tau) dt \tag{21}$$

VII. 1. (e) Stresses under Arbitrary Excitation

The stress-deflection, moment-deflection, or shear-deflection relationship is defined

$$\sigma = [B] \{d\} \tag{22}$$

where $[B]$ is called the stress matrix when σ is a stress.

After taking a Fourier transform of σ, one may show that the power spectral density of a stress, moment, or shear is

$$\Phi_\sigma(\omega) = [B] [\Phi_d] [B]^t \tag{23}$$

and $[\Phi_d]$ may be substituted into equation (23) from equation (17).

The mean square value of σ is

$$\bar{\sigma}^2 = \int_0^{\infty} \Phi_\sigma(\omega) d\omega \tag{24}$$

VII. 1. (f) Stresses under White Noise Excitation

Under white noise excitation, the spectral density of the force is

$$\left[\phi_f\right] = \left[A\right]\left[\phi_P\right]\left[A\right] \tag{25}$$

where

A_{ii} - the area (under pressure) associated with joint i

and

$[\phi_P]$ - the power spectral density matrix of the applied pressure

In the following, it is demonstrated that $\bar{\sigma}^2$ is a function of real components and not imaginary components of elements of the spectral density matrix, $[\phi]_f$

Let

$$[B'] = [B]\,[Q] \tag{26}$$

$$[E] = [Q]^t\,[\phi_f]\,[Q] \tag{27}$$

$$[X] = \int_0^\infty \left[Z(\omega)\right]^{-1} [E] \left[Z^*\right]^{-1} d\omega \tag{28}$$

$$X_{ij} = E_{ij}C_{ij} + E_{ji}^*C_{ji} = X_{ji}^* \tag{29}$$

and

$$C_{ji} = C_{ij} = \frac{2\pi(\gamma_i\bar{\omega}_i + \gamma_j\bar{\omega}_j)/M_i M_j}{\left[(\bar{\omega}_i^2 - \bar{\omega}_j^2)\right]^2 + 4\bar{\omega}_i\bar{\omega}_j\left[(\gamma_i^2 + \gamma_j^2)\bar{\omega}_i\bar{\omega}_j + \gamma_i\gamma_j(\bar{\omega}_i^2 + \bar{\omega}_j^2)\right]} \tag{30}$$

The derivation of equation (30) is in Reference 13. In equation (29), $E_{ij}C_{ij} = E_{ji}^*C_{ji}$ because $\phi_{f_{ij}} = \phi_{f_{ji}}^*$ (see equation (18).

Then

$$\bar{\sigma}^2 = [B']\,[X]\,[B']^t = \sum_i\sum_j B_i' X_{ij} B_j' \tag{31}$$

Alternate forms of equation (31) are

$$\bar{\sigma}^2 = \sum_i\sum_j B_j' X_{ji} B_i' = \sum_i\sum_j B_i' X_{ij}^* B_j' \tag{32}$$

Since the final expression in equations (31) and (32) are equal, $\bar{\sigma}^2$ does not depend on the imaginary components of X_{ij}. Hence

$$\bar{\sigma}^2 = \sum_i \sum_j B'_i \, \mathrm{Re}\,(X_{ij}) \, B'_j = \lfloor B' \rfloor \left[\mathrm{Re}\, X \right] \lfloor B' \rfloor^t \tag{33}$$

VII. 1. (g) Method of Applying the General Theory

Natural frequencies and modal shapes can be obtained from equation (7). In several computations discussed in Section VII, 49 nodes and 36 finite elements have been used in modal calculations using one quadrant of a panel. (Other combinations used in the calculations were 9 nodes and 4 finite elements, 16 nodes and 9 finite elements, 25 nodes and 16 finite elements, and 36 nodes and 25 finite elements.) By properly choosing boundary conditions of a quadrant of a panel that is symmetrical about both of its center lines, only the quadrant itself rather than the full panel is needed in the modal analysis. Since only those modes that are symmetric about both centerlines of the full panel are excited in many test and service conditions, the analysis of only one quadrant of a panel is adequate in many practical cases.

The damping factors that are needed as input for the response calculations may be obtained in resonance tests under discrete frequency excitation.

The pressure cross-spectral density, $\Phi_{f_{ij}}(\omega)$, is defined by equation (18) and may be obtained from the analysis of test data or from equation (19) after some theoretical cross-correlation function $R_{f_i f_j}(\tau)$ is assumed. The former approach may be carried out by making a record on tape of pressure signals at locations i and j on the panel and then using standard data analysis equipment to obtain the real and imaginary parts of the cross-spectral density of the pressure.

In equation (21), $\bar{\sigma}$ may be an rms stress, moment or shear. The amount of computation in the use of using equation (21) for the prediction of moments, shears, stresses may be reduced by ignoring modal coupling and computing the deflection, moment, and shear response of one mode at a time. It is shown in Reference 13 that the modal coupling may be relatively unimportant.

VII. 2 SIMPLIFIED THEORY

For the bending of anisotropic plates, Timoshenko (Reference 14) uses the equation

$$D_{xx} \frac{\partial^4 w}{\partial x^4} + 2H \frac{\partial^4 w}{\partial x^2 \partial y^2} + D_{yy} \frac{\partial^4 w}{\partial y^4} = q \tag{34}$$

that neglects the twist-pull coupling phenomenon. Equation (34) shall be the basis for the following simplified analysis for the prediction of strain at the center of the edges of a rectangular plate of uniform thickness (Figure 99) that is fully clamped on all four edges.

In the dynamic case, replace q in equation (34) with $p(t) - M_0 \frac{\partial^2 w}{\partial t^2}$ in order to include the plate inertia force.

The analysis that follows uses the approach in References 7 and 11. It is assumed that the lateral deflection of the plate is unimodal and can be expressed in terms of the clamped-clamped beam functions (for the 1-1 mode) of Reference 15. Thus the lateral deflection is

$$w(x, y, t) = \phi(\beta x)\, \psi(\gamma y)\, \eta(t) \tag{35}$$

with

$$\phi(\beta x) = \cosh \beta x - \cos \beta x - \alpha (\sinh \beta x - \sin \beta x) \tag{36}$$

and

$$\psi(\gamma y) = \cosh \gamma y - \cos \gamma y - \theta (\sinh \gamma y - \sin \gamma y) \tag{37}$$

In the case of spatially uniform, time harmonic loading the pressure is

$$p(t) = p_o e^{i \Omega_o t} \tag{38}$$

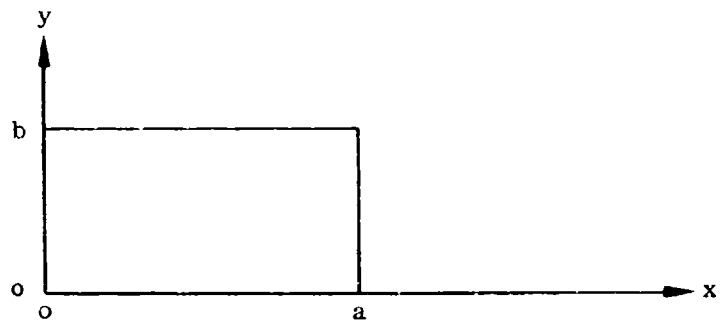

FIGURE 99. GEOMETRY AND COORDINATE SYSTEM OF RECTANGULAR PLATE

Substitute equations (35) and (38) into equation (34), multiply by $\phi\psi$, and integrate over the plate to obtain

$$\iint \left[D_{xx} \psi^2 \phi \frac{d^4\phi}{dx^4} + 2H \phi\psi \frac{d^2\phi}{dx^2} \frac{d^2\psi}{dy^2} + D_{yy} \phi^2 \psi \frac{d^4\psi}{dy^4} \right] \eta \, dx\, dy$$

$$= \iint \left[\phi\psi p_o e^{i \Omega_o t} - M_o \phi^2 \psi^2 \frac{d^2\eta}{dt^2} \right] dx\, dy \tag{39}$$

The integrals can be evaluated with the use of equations A7 c ·ference 7 and these integrals are repeated below:

$$\int_o^a \phi \, dx = \frac{4\alpha}{\beta}$$

$$\int_0^b \psi \, dy = \frac{4\theta}{\gamma}$$

$$\int_0^a \phi^2 \, dx = a$$

$$\int_0^b \psi^2 \, dy = b$$

$$\int_0^a \phi \frac{d^2\phi}{dx^2} \, dx = \alpha\beta \, (2 - \alpha\beta a)$$

$$\int_0^b \psi \frac{d^2\psi}{dy^2} \, dy = \theta\gamma \, (2 - \theta\gamma b)$$

$$\int_0^a \phi \frac{d^4\phi}{dx^4} \, dx = \beta^4 a$$

$$\int_0^b \psi \frac{d^4\psi}{dy^4} \, dy = \gamma^4 b$$

$$\alpha = \theta = .983$$

and

$$\beta a = \gamma b = 4.73 \tag{40}$$

Carrying out the integration in equation (39) produces

$$\left[D_{xx} b \beta^4 a + 2H \alpha\beta\theta\gamma (2 - \alpha\beta a)(2 - \theta\gamma b) + D_{yy} a \gamma^4 b\right]\eta$$

$$= \frac{16\alpha\theta}{\beta\gamma} p_o e^{i\Omega_o t} - a b M_o \frac{d^2\eta}{dt^2} \tag{41}$$

An alternate form of equation (41) is

$$K\eta + M \frac{d^2\eta}{dt^2} = \Gamma p_o e^{i\Omega_o t} \tag{42}$$

with

$$K = D_{xx} b \beta^4 a + 2 H \alpha \beta \theta \gamma (2 - \alpha \beta a)(2 - \theta \gamma b) + D_{yy} a \gamma^4 b \tag{43}$$

$$M = a b M_o \tag{44}$$

$$\Gamma = \frac{16 \alpha \theta}{\beta \gamma} \tag{45}$$

and

$$\omega^2 = \frac{K}{M} \tag{46}$$

where ω is the natural circular frequency.

The natural frequency expressed in Hz is

$$f = \frac{\omega}{2\pi} \tag{47}$$

Using the sign conventions of Reference 14 and assuming cross sections remain plane, the strains are

$$e_x = -z \frac{\partial^2 w}{\partial x^2}$$

$$e_y = -z \frac{\partial^2 w}{\partial y^2}$$

and

$$\gamma_{xy} = -2z \frac{\partial^2 w}{\partial x \partial y} \tag{48}$$

The derivation of the unimodal strain response to time harmonic and to time random loading that is spatially uniform follows.

An alternate form of equation (42) is

$$\ddot{\eta} + \omega^2 \eta = \frac{\Gamma}{M} p_o e^{i \Omega_o t} \tag{49}$$

with a steady state solution

$$\eta(t) = \frac{p_o \Gamma}{K} \frac{e^{i \Omega_o t}}{1 - \left(\frac{\Omega_o}{\omega}\right)^2} \tag{50}$$

Upon introducing viscous damping, equation (49) is modified to

$$\ddot{\eta} + 2\zeta\omega\dot{\eta} + \omega^2\eta = \frac{p_o\Gamma}{M} e^{i\Omega_o t} \tag{51}$$

with a steady state solution of absolute value

$$\left| \eta(t) \right| = \frac{p_o\Gamma}{K} \left| H(\Omega_o) \right| \tag{52}$$

with

$$\left| H(\Omega_o) \right| = \left\{ \left[1 - \left(\frac{\Omega_o}{\omega}\right)^2 \right]^2 + 4\zeta^2 \left(\frac{\Omega_o}{\omega}\right)^2 \right\}^{-\frac{1}{2}} \tag{53}$$

Therefore, the absolute strains at the upper and lower plate surfaces in the unimodal response are

$$\left| e_x \right| = \frac{h p_o \Gamma}{2K} \left| \psi \frac{d^2\phi}{dx^2} \quad H(\Omega_o) \right| \tag{54}$$

and

$$\left| e_y \right| = \frac{h p_o \Gamma}{2K} \left| \phi \frac{d^2\psi}{dy^2} \quad H(\Omega_o) \right| \tag{55}$$

Under harmonic excitation at the fundamental frequency

$$\left| e_x \right| = \frac{h p_o \Gamma}{4K\zeta} \left| \psi \frac{d^2\phi}{dx^2} \right| \tag{56}$$

and

$$\left| e_y \right| = \frac{h p_o \Gamma}{4K\zeta} \left| \phi \frac{d^2\psi}{dy^2} \right| \tag{57}$$

To determine the unimodal rms strain response to spatially uniform, time random loading, replace $p_o e^{i\Omega_o t}$ by $p(t)$ in equation (51) to obtain

$$\ddot{\eta}(t) + 2\zeta\omega\dot{\eta}(t) + \omega^2\eta(t) = \frac{\Gamma}{M} p(t) \tag{58}$$

Upon taking a Fourier transform of equation (35) and (58), one obtains the Fourier transform, denoted by the asterisk, of the deflection

$$w^*(x, y, \Omega) = \phi\psi \frac{\Gamma H(\Omega)}{K} p^*(\Omega) \tag{59}$$

with

$$H(\Omega) = \left[1 - \left(\frac{\Omega}{\omega}\right)^2 + \frac{2i\zeta\Omega}{\omega}\right]^{-1} \tag{60}$$

The spectral densities of the deflection and loading are respectively

$$S_w = \frac{|w^*|^2}{T_1} \tag{61}$$

and

$$S_p = \frac{|p^*|^2}{T_1} \tag{62}$$

The deflection spectral density in terms of the loading spectral density is

$$S_w = \left| \frac{\phi\psi\Gamma H(\Omega)}{K} \right|^2 S_f \tag{63}$$

With the definition of mean square response

$$\overline{w^2} = \int_0^\infty S_w \, d\Omega \tag{64}$$

for unimodal response, one obtains

$$\overline{w^2} = \frac{\phi^2\psi^2\Gamma^2}{K^2} \int_0^\infty \left| H(\Omega) \right|^2 S_p(\Omega) \, d\Omega \tag{65}$$

For constant spectral density of the applied pressure (i.e., white noise)

$$\int_0^\infty S_f \left| H(\Omega) \right|^2 d\Omega = \frac{\pi\omega S_p}{4\zeta} \tag{66}$$

The mean square strains at the surface with white noise excitation are

$$\overline{e_x^2} = \frac{h^2\Gamma^2\psi^2}{4K^2} \left(\frac{d^2\varphi}{dx^2}\right)^2 \frac{\pi\omega S_p}{4\zeta} \tag{67}$$

and

$$\overline{e_y^2} = \frac{h^2\Gamma^2\phi^2}{4K^2} \left(\frac{d^2\psi}{dy^2}\right)^2 \frac{\pi\omega S_p}{4\zeta} \tag{68}$$

For strain calculations at the center of an edge of the plate, the beam functions and the appropriate derivatives are given in Table XV.

TABLE XV. BEAM FUNCTIONS AND SECOND DERIVATIVES AT THE CENTERS OF THE EDGES

Location	ϕ	ψ	$\frac{d^2\phi}{dx^2}$	$\frac{d^2\psi}{dy^2}$
$x = \frac{a}{2},\ y = 0$	1.588	0	$-1.216\beta^2$	$2.00\gamma^2$
$x = 0,\ y = \frac{b}{2}$	0	1.588	$2.00\beta^2$	$-1.216\gamma^2$

To obtain the ratio of rms strains at the centers of the edges of the plate, let

$$e_1 = \left| (e_x)_{x = o,\ y = \frac{b}{2}} \right| \tag{69}$$

and

$$e_2 = \left| (e_y)_{y = o,\ x = \frac{a}{2}} \right| \tag{70}$$

Upon dividing equation (69) by equation (70), one obtains

$$\frac{e_1}{e_2} = \frac{\beta^2}{\gamma^2} \tag{71}$$

which implies that the strain is larger at the center of the long edge than at the center of short edge as is the case for isotropic plates of uniform thickness.

VII.3 DEFINITIONS OF PSD

This subsection has been included in order to prevent the misuse of theoretical equations and/or computer programs for the prediction of deflection and stress response to acoustic excitation, which is expressed in terms of the PSD of the pressure.

Miles (Reference 16) defined the mean square value of a random function F(t) with a power spectral density f (ω)

$$\overline{F(t)^2} = \int_o^\infty f(\omega)\, d\omega \tag{72}$$

Thus, $\overline{F(t)^2}$ could be calculated if the average f (ω) in each of an infinite number of small frequency bands dω were obtained (e.g. experimentally obtain the average pressure in each of the frequency bands dω) and summed over all the frequency bands.

On the other hand Hurty and Rubinstein (Reference 17) state that

$$\overline{y^2(t)} = \frac{1}{2\pi} \int_0^{\infty} y(\Omega)\, d\Omega \tag{73}$$

It is obvious that if

$$\overline{y^2(t)} = \overline{F(t)^2} \tag{74}$$

then the power spectral densities $y(\Omega)$ and $f(\omega)$ cannot be equal to each other if each of equations (72) and (73) are correct.

A proof of equation (73) and the reason for $y(\Omega) \neq f(\omega)$ even though both are called power spectral density of the same process follows.

Assume that $y(t)$ is almost stationary for $-T < t < T$. Then the spectral density is defined

$$y(\Omega) = \frac{|y^*|^2}{T} \tag{75}$$

with the use of the Fourier transform

$$y^*(\Omega) = \int_{-\infty}^{\infty} y(t)\, e^{-i\Omega t}\, dt \tag{76}$$

Because

$$e^{-i\Omega t} = \cos \Omega t - i \sin \Omega t \tag{77}$$

then

$$2 \int_0^{\infty} y(\Omega)\, d\Omega = \int_{-\infty}^{\infty} y(\Omega)\, d\Omega \tag{78}$$

Note that $y(t)$ and $y^*(\Omega)$ are a Fourier transform pair and because of equation (76)

$$y(t) = \frac{1}{2\pi} \int_{-\infty}^{\infty} y^*(\Omega)\, e^{i\Omega t}\, d\Omega \tag{79}$$

Another Fourier transform pair ($y^*_{c.c.}$ and y) to be used in the following are defined by

$$y^*_{c.c.}(\Omega) = \int_{-\infty}^{\infty} y(t)\, e^{i\Omega t}\, dt \tag{80}$$

and

$$y(t) = \frac{1}{2\pi}\int_{-\infty}^{\infty} y^*_{c.c.}\, e^{-i\Omega t}\, d\Omega \tag{81}$$

A substitution of equation (75) into equation (78) yields

$$2\int_{0}^{\infty} y\,(\Omega)\, d\Omega = \int_{-\infty}^{\infty} \frac{|y^*|^2}{T}\, d\Omega \tag{82}$$

The right side of equation (82) is

$$\int_{-\infty}^{\infty} \frac{1}{T}\; y^*_{c.c.}\,(\Omega)\, y^*\,(\Omega)\, d\Omega = \frac{1}{T}\int_{-\infty}^{\infty} y^*_{c.c.}(\Omega)\left[\int_{-\infty}^{\infty} y(t)\, e^{-i\Omega t}\, dt\right] d\Omega \tag{83}$$

Upon changing the order of integration in the right side of equation (83), one obtains

$$\frac{1}{T}\int_{-\infty}^{\infty} y(t)\left[\int_{-\infty}^{\infty} y^*_{c.c.}\,(\Omega)\, e^{-i\Omega t}\, d\Omega\right] dt = \frac{2\pi}{T}\int_{-\infty}^{\infty} y^2\,(t)\, dt \tag{84}$$

because of equation (81).

But since y^2 (t) is a real number,

$$\frac{2\pi}{T}\int_{-\infty}^{\infty} y^2\,(t)\, dt = \frac{4\pi}{T}\int_{0}^{\infty} y^2\,(t)\, dt \tag{85}$$

Since the left side of equation (82) equals the right side of equation (85) as a result of the development of equations (83), (84), and (85), then

$$\int_{0}^{\infty} \frac{y^2\,(t)}{T}\, dt = \frac{1}{2\pi}\int_{0}^{\infty} y\,(\Omega)\, d\Omega \tag{86}$$

But the left side of equation (86) is the mean square value of y(t). Hence equation (73) is proved, namely,

$$\overline{y^2\,(t)} = \frac{1}{2\pi}\int_{0}^{\infty} y\,(\Omega)\, d\Omega \tag{87}$$

In the equations developed in section VII.2 and in their application in Section VIII, the approach of Miles rather than that of Hurty and Rubinstein was used for establishing PSD.

VIII. APPLICATIONS OF STRESS ANALYSIS METHODS

This section is divided into four subsections. In the first subsection is an analytic investigation (and some comparison with experiments) of the free vibrations and dynamic stress analysis of unstiffened and cross-stiffened, isotropic panels using the theoretical approaches discussed in Section VII. The procedures and results in subsection VIII.1 are used as a guide in an analytic investigation (in subsection VIII.2) of the free vibrations and stress/strain response of unstiffened and cross-stiffened advanced-composite panels that are subjected to random, acoustic excitation. In subsection VIII.3 is a static stress analysis of the bonded joint assemblies of the acoustic test panels and the shaker test specimens. The results in subsection VIII.3 were used in selecting the design of the shaker test specimens. In Section VIII.4 is an investigation of residual stresses (and their effect on buckling) in panel A-GG-P 1 resulting from the cooling from the 250F bonding temperature. The results in subsection VIII.4 were used in establishing the design of acoustic test panels A-GG-B-2 and A-GG-B-3.

The methods presented in subsections VIII.1 and VIII.2 are methods which can be applied to the design of skins and possibly to the design of internal structure of panels subjected to acoustic loading. The method presented in subsection VIII.3 is shown to be applicable to the detail design of bonded joint assemblies of panels subjected to acoustic excitation and appears to be applicable when the bonded joint assemblies are replaced by riveted joint assemblies. The analysis in subsection VIII.4 is useful in investigating the possibility of buckling of the thin-skinned, cross-stiffened panels when a cool down from a boundary temperature introduces residual stresses in the panel.

VIII.1 FREE VIBRATIONS AND DYNAMIC STRESS ANALYSIS OF ISOTROPIC PLATES AND BEAMS

An objective of the analytic effort was to develop an analytic procedure to predict the natural modes and the strain/stress response of flat, cross-stiffened, advanced-composite panels subjected to random, acoustic excitation; and equations for these predictions have been given in Sections VII. Moreover, the contractor had available at the outset of the effort, the REDYN (REdundant DYNamic) digital computer program to perform calculations required by the general theory (presented in section VII.1). The methods of utilizing REDYN that are described in this report can be used by the various aerospace companies, universities, etc., that have digital computer programs that can perform the calculations of stress response to acoustic excitation.

It was deemed unwise merely to conduct an analytic investigation on cross-stiffened, advanced-composite panels since there were not enough experimental data to assess the validity of a multitude of calculations. Therefore, the analytic approach that was taken in this program was to investigate analytically several problems that could be posed for both isotropic panels and advanced-composite panels by first conducting the investigation (which is in this subsection) with isotropic panels. Then with the results and methods of this section to serve as a guide, an analytic investigation (which is presented in subsection VIII.2) was conducted on the free vibrations and the

dynamic strain/stress response of advanced-composite panels subjected to random, acoustic excitation. The results of these analytic investigations indicate that the methods of analysis presented in Section VII can be used in the design of skins of either isotropic or orthotropic cross-stiffened panels. No check of the theory was made for the design and/or stress analysis of the internal structure. The stress analysis of a joint assembly itself is given in subsection VIII.3.

VIII.1.(a) Unstiffened Square Plate

An unstiffened, flat, rectangular aluminum alloy plate, clamped on all four edges, with dimensions 21.00 x 21.00 x 0.10 inch was chosen as the model for the calculations with Young's modulus of 10.6×10^6 psi, Poisson's ratio of 0.34 and a density of 0.10 lb/in^3. Deflections and stresses resulting from fully correlated acoustic loading and natural frequencies and modal shapes are reported in the following.

1. Natural Frequency and Modal Shape

Fundamental frequencies were obtained by different methods and are given in Table XVI. In some calculations with REDYN, the grid points were at the intersections of equally spaced grid lines (parallel to the plate edges) throughout the plate; in other cases when symmetry conditions about both center lines of the plate were used, the grid points were at the intersections of equally spaced grid lines only in one quadrant of the plate (e.g., Figure 100). The closest agreement to the fundamental frequency obtained with beam functions (i.e., the simplified theory) occurred with the rectangular finite elements and implies that the rectangular option of REDYN is preferable to the triangular option.

When 36 nodes and 49 square elements were used with REDYN and when the distance between nodes was reduced by 50 percent, the fundamental frequency was increased approximately three percent; i.e., the frequency was increased from 77.7 Hz to 79.7 Hz (see Table XVI). In other words, by utilizing the conditions of symmetry and using the same number of nodes for the eigenvalue problem, a three percent change in natural frequency occurred. Therefore, the fundamental frequencies that were obtained with REDYN (even where conditions of symmetry are nonexistent and impose a full plate analysis with 49 nodes) were considered satisfactory for the acoustic design of the plate.

The mode shapes along a center line of the plate were calculated using (i) the clamped-clamped beam function approach and (ii) REDYN with triangular and with rectangular elements when only one quadrant of the plate and conditions of symmetry were used with REDYN. The results are presented in Table XVII and are normalized to unity at the center of the plate.

The finite-element approach and the beam function approach are both approximate analytical methods. Convergence of the lowest frequency and modal shape has not been shown because of limitations on the storage capacity of computers. However, the close agreement between the results (natural frequency in Table XVI, modal shape in Table XVII, and stress and deflection response to acoustic loading that are reported upon subsequently) obtained with the beam function method and the rectangular finite element (REDYN) method indicates that both methods give good results.

TABLE XVI. FUNDAMENTAL FREQUENCIES

	REDYN					Beam Functions	Experimental[4]
Elements[1]	Δ	Δ	□	□	□		
Quadrants[2]	1	1	1	4	4		
Nodes	36	49	36	49	36		
Fundamental Frequency, Hz	76.1	77.0	79.7	78.4	77.7	80.7	76.0[3]

(1) Δ = Triangular elements, □ = square elements (the rectangular option of REDYN)

(2) Either one quadrant and conditions of symmetry were used in the finite element analysis or all four quadrants were used.

(3) The average fundamental frequency of three plates, with edge dimensions approximately 21.0 x 21.0 inch at the junction of the unsupported plate area and the supports, was 76 Hz when excited at 139 db SPL. The supports were to simulate theoretical clamped boundary conditions. The experimental fundamental frequency may differ from the predicted frequency based on fully clamped boundary conditions because the ideal boundary conditions were not obtained experimentally and/or nonlinearities due to the excitation level existed.

(4) The experiments are reported in Reference 18.

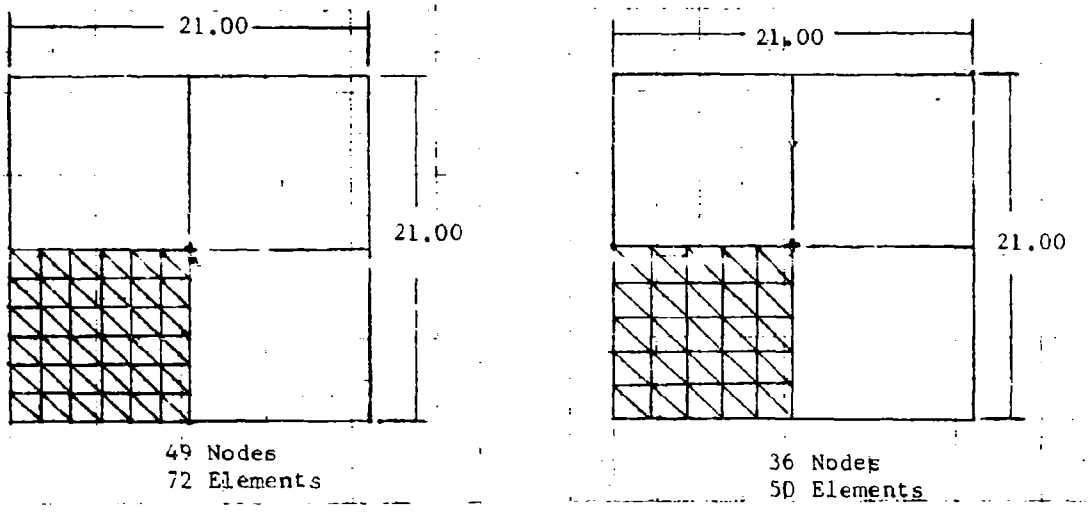

(Figure 100.a) (Figure 100.b)

FIGURE 100. FINITE ELEMENT MODELS

TABLE XVII. THEORETICAL MODE SHAPES

LOCATION	DEFLECTION		
	Beam Functions	REDYN, 36 Nodes, Triangular Elements, One Quadrant	REDYN, 36 Nodes, Rectangular Elements, One Quadrant
	(in.)	(in.)	(in.)
0.0	.00	.00	.00
0.1	.14	.12	.13
0.2	.43	.39	.41
0.3	.67	.69	.71
0.4	.94	.97	.92
0.5	1.00	1.00	1.00

2. Theoretical Dynamic Deflections and Stresses

As a check on the calculations performed using REDYN (with triangular finite elements in one quadrant of the panel), a comparison was made of the free vibration modal shape and the rms deflection response to fully correlated, white noise pressure loading for a case of unimodal response. The comparison showed the single mode response shape was the same as the free vibration modal shape; and, hence, a necessary condition for the accuracy of the finite element method was satisfied.

RMS deflection, strain, and stress response to fully correlated, white noise exciting only the fundamental mode was calculated with the clamped-clamped beam function method and with REDYN with triangular and with rectangular elements. Since the bending moments that are calculated by REDYN are for centroids of the elements rather than for the nodes, the bending moments from REDYN were extrapolated by hand to the center of the plate. The results in Table XVIII were based on fully correlated, white noise, acoustic pressure with a spectral density of 30.0×10^{-6} psi^2/Hz. A damping factor of 0.017 was used in the calculations.

In Table XVIII, the theoretical results obtained with the clamped-clamped beam function method and the rectangular finite element method with extrapolations show good agreement. Extrapolations were necessary when the calculated quantities were not at the desired locations. As expected, the agreement improved as the mesh size in the finite element calculations decreased.

TABLE XVIII. DEFLECTIONS AND STRESSES AT THE CENTER OF THE PLATE

	REDYN							CLAMPED-CLAMPED BEAM FUNCTIONS
Elements[4]	Δ	□	□	□	□	□	□	
Quadrants[5]	1	1	1	4	4	4	4	
Nodes	49	36	36	49	49	36	36	
Deflection, in.-rms	0.061[1]	0.057[1]	0.057[1]	0.059[1]	0.059[1]	0.050[3]	0.062[2]	.056
Principal Strain, micro-inch/inch-rms	85.[2]	96.[2]	106.[3]	85.2[2]	98.5[3]	96.5[1]	96.5[1]	110.
Principal Stress, ksi-rms	1.37[2]	1.54[2]	1.71[3]	1.37[3]	1.58[3]	1.55[1]	1.55[1]	1.77

(1) Deflections or stress and strain at the center of plate and no extrapolation necessary.

(2) Deflections, strains or stresses near the center of the plate but not extrapolated to the center of the plate. These strains and stresses were obtained at centroids of elements that included the center of the plate.

(3) These stresses and strains were extrapolated (by hand) from centroids of the finite elements to the plate center. The deflections were extrapolated along a center line to the plate center.

(4) Δ = triangular finite elements; □ = square finite elements (the rectangular option of REDYN).

(5) When only one quadrant was used with REDYN, symmetry conditions were used.

VIII. 1. (b) Unstiffened Beam

A beam, simply supported on both ends and 21.00 in. long x 1.00 in. wide x 0.10 in. thick, was chosen as the model for the calculations. For the beam, Young's modulus of 10.6×10^6 psi, Poisson's ratio of 0.34, and a weight density of 0.10 lb/in.^{3} were assumed. The fundamental frequency and mode shape (Table XIX) and the deflection and stress (Table XX) at the beam center were calculated with REDYN and by hand with the use of Young and Felger's beam functions and are reported below. The computations with REDYN were with 6 finite elements and 7 node points. The results in Tables XIX and XX show good agreement even for the few elements used with REDYN and imply that the finite element method can be successfully used for the dynamic analysis of panels with beams as stiffeners.

TABLE XIX. THEORETICAL MODE SHAPE

LOCATION(1)	DEFLECTION	
x/L	BEAM FUNCTION in.	REDYN in.
0.00	0.00	0.00
0.17	0.50	0.50
0.33	0.87	0.87
0.50	1.00	1.00
0.67	0.87	0.87
0.83	0.50	0.50
1.00	0.00	0.00

(1) The left end of the end beam corresponds to x = 0, and the length of the beam equals L.

TABLE XX. NATURAL FREQUENCY AND STRESS AT THE CENTER OF BEAM, SIMPLY SUPPORTED AT BOTH ENDS

ITEM(1)	BEAM FUNCTION	REDYN
Deflection, in.-rms	0.323	0.321
Principal Stress, ksi-rms	3.82	3.74
Fundamental Frequency, Hz	20.7	20.3

(1) The predicted deflections, strains, and stresses are based on fully correlated, white noise, with a spectral density of 30.0×10^{-6} psi^2/Hz. The discrepancy between results in using REDYN and the beam function methods is due to a slight difference in beam stiffness as input to REDYN and to the beam function calculations. A damping factor of 0.017 was used.

VIII. 1. (c) Effect of Node Locations on Stress Predictions of Cross-Stiffened Panels

Two mathematical models (Figure 101) were used to investigate with REDYN the effect of the finite element node locations on predictions of natural frequencies and stresses resulting from acoustic loading of cross-stiffened panels. The method of locating nodes is especially important when stresses are predicted since local rms stresses are wanted and not average stresses in large finite elements.

Model M-1 of Figure 101 has relatively uniform spacing; i.e., each of the nine bays of the complete panel is presented by four finite elements. Model M-2 of Figure 101 consists of only one quadrant of the complete panel and the central bay has 16 finite elements, the end bay has 4 finite elements, and the other two bays have 8 finite elements each. The intent in constructing model M-2 is to have fine finite elements at the center of the central bay and at the center of the edges of the central bay since these are locations of high stress in the skin of an experimental or service panel.

Computer runs were made with REDYN for the mathematical models of Figure 101 with the data of Table XXI. In Table XXI, the material chosen for the skin and stiffening elements was an aluminum alloy.

The nominal bay dimensions of the panel in Figure 101 and the geometry in Table XXI of the I-beams, tee sections, and skin was the geometry used in the design of the cross-stiffened, graphite-epoxy panels of the acoustic test program.

The lowest four natural frequencies of models M-1 and M-2 are in Table XXII. The agreement of the natural frequencies is excellent.

The results of several dynamic analyses are in Table XXIII. Results from REDYN with both a single mode solution and a four mode solution with model M-2 are included in Table XXIII. Also in Table XXIII are the hand calculation results of a one mode solution using clamped-clamped beam functions for a rectangular aluminum alloy plate clamped on all four edges and of dimensions 10.00 x 7.00 x 0.025 inches. The 10 x 7 inch rectangular plate was chosen to simulate the central bay of the cross-stiffened models M-1 and M-2.

The deflection and stress in Table XXIII resulted from a spatially uniform, white noise, acoustic loading of 30×10^{-6} psi^2/Hz. A damping factor of 0.017 was used.

The close agreement of natural frequency and deflection in the last three columns of Table XXIII indicate that in the fundamental mode the central bay of the cross-stiffened panel behaves somewhat as though it were clamped on all four edges. However, the deflection of the stiffeners on the four edges of the central bay tends to shift the stress distribution in the skin from the stresses calculated with the clamped-clamped beam functions. There is no experimental data for comparison with the theoretical data of Table XXIII; hence, the only conclusion that is drawn from the data of Table XXIII is that the finite element analysis (and also the simplified theory using beam functions) may be used for the dynamic analysis of cross-stiffened panels.

It is interesting to note that the deflection (in Table XXIII) increased substantially when multi-modal response is considered whereas the stress did not change significantly.

In Table XXIII, no stresses are reported for Model M-1, since those computed stresses are averages for large finite element areas and are useless.

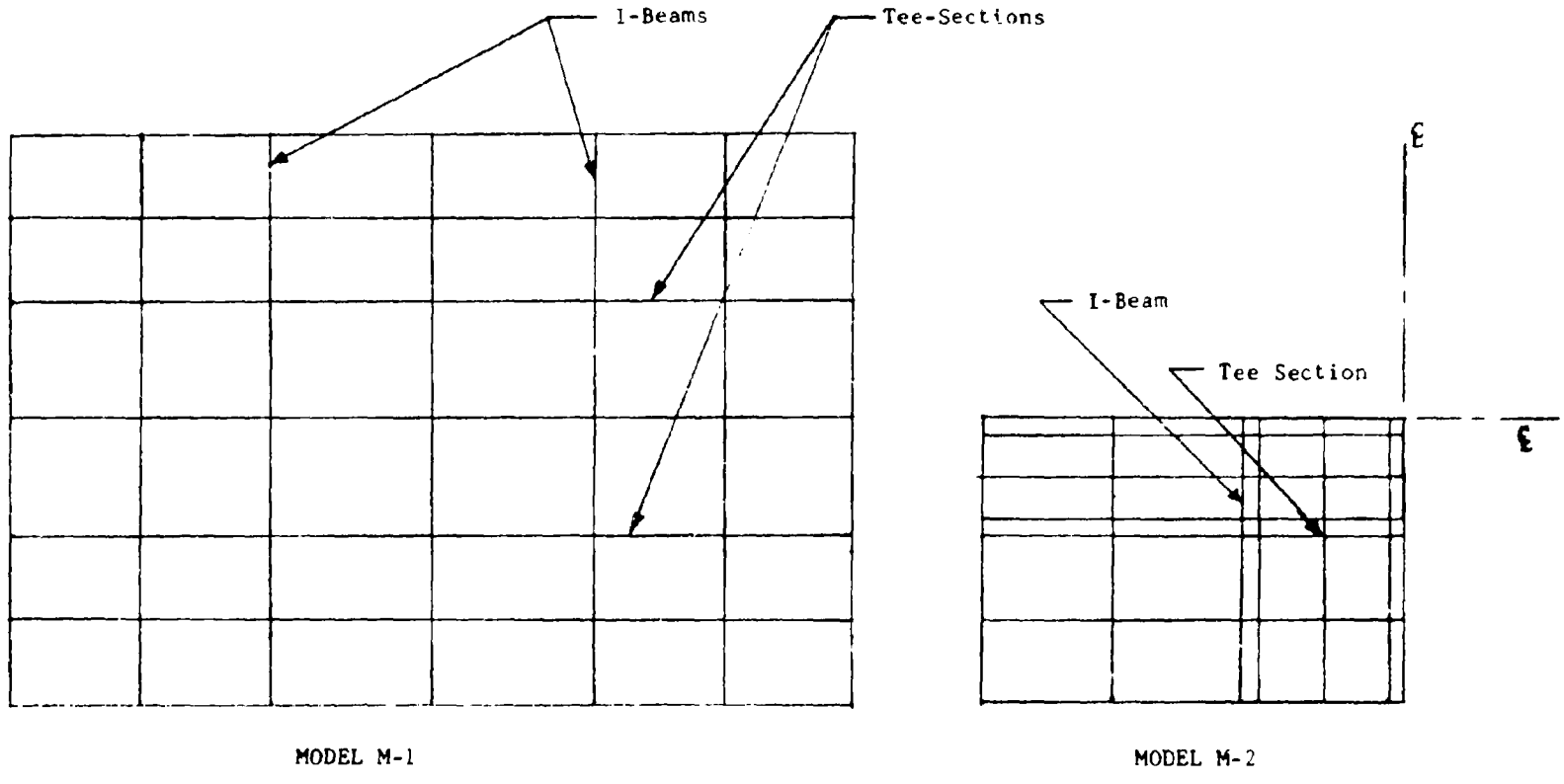

Scale: 1 in. = 5 in.

FIGURE 101. MATHEMATICAL MODELS

TABLE XXI. MODEL TO INVESTIGATE THE EFFECT OF NODE LOCATIONS

Overall length, in.	26.0
Overall width, in.	17.0
Spacing of central I-sections, in.	10.0
Spacing of central tee-sections, in.	7.0
Shear modulus, psi	3.95×10^6
Young's modulus, psi	10.5×10^6
Poisson's ratio	0.34
Area of I-sections, $in.^2$	0.1238
Bending inertia of I-beam about axis normal to plate, $in.^4$	.1625
Bending inertia of I-beam about the other principal axis, $in.^4$	.00417
Torsional constant of I-beam, $in.^4$	.00003
Offset of centroid of I-beam to plate midplane, in.	1.5125
Area of tee-sections, $in.^2$	.00434
Bending inertia of tee-section about axis normal to plate, $in.^4$	.0034
Bending inertia of tee-section about the other principal axis, $in.^4$	.00142
Torsional constant of tee-section, $in.^4$	.00001
Offset of centroid of tee-section to plate midplane, in.	0.465
Damping factor of fundamental mode	0.017
Damping factor of other modes	0.017
Weight density, $lb/in.^3$	0.100
Thickness of skin, in.	0.025

TABLE XXII. NATURAL FREQUENCIES

	Model M-1	Model M-2
Lowest Frequency, Hz	130	129
First Harmonic Frequency, Hz	154[1]	154
Second Harmonic Frequency, Hz	227	227
Third Harmonic Frequency, Hz	---	249

[1] A repeated root because of symmetry about both center lines.

TABLE XXIII. THEORETICAL FREQUENCY AND RESPONSE DATA

	REDYN[1]			Clamped-Clamped Beam Functions 1 Mode
	Model M-2 4 Modes	Model M-1 1 Mode	Model M-2 1 Mode	
Fundamental Frequency, Hz	129	130	129	128
Deflection at the Center of the Central Bay, in.-rms	0.420	0.165	0.157	0.175[2]
Stress at the Panel Center[3] ksi-rms	8.0	---	7.9	10.7
Stress in the Skin at the Center of the Long Edge of the Central Bay, ksi-rms	11.7	---	11.6	15.1[4]

(1) All REDYN calculations for Model M-2 are based on symmetry about both center lines of Model M-1.

(2) Deflections at the panel center.

(3) The maximum extensional stress; i.e., the stress in the width direction.

(4) The stress at the center of the long edge of the plate.

VIII. 1. (d) Warning on Use of the Simplified Theory (of Section VII. 2)

It was just shown that with the stiffener and rib spacing that produced a 10.0 x 7.0 inch central bay of a (nine-bay) cross-stiffened panel, the cross-stiffened panel could have been modeled (for the purpose of obtaining the principal dynamic characteristics of the fundamental mode) by a rectangular plate that was clamped on all four edges and that had the geometrical, elastic, and physical properties of the central bay of the cross-stiffened plate. However, this modeling procedure may produce unsatisfactory dynamic characteristics of the fundamental mode of some cross-stiffened plates.

To demonstrate a case when unsatisfactory results are produced by this modeling procedure, calculations were performed with REDYN for nine-bay, cross-stiffened panels with a central bay of 21.0 x 21.0 x 0.10 inches. The length and width of the cross-stiffened panels are included in the discussion of the computed frequencies in the next paragraph. The choice of a central bay with dimensions of 21.0 x 21.0 x 0.10 inches was made in order to obtain data for comparison with data presented in Section VIII.1.(a) for a 21.0 x 21.0 x 0.10 inch plate, that is clamped on all four edges. The stiffeners and ribs of these cross-stiffened panels have the properties reported in Table XXI.

The lowest natural frequency computed with REDYN is 63.8 Hz for a plate with the 37.0 x 37.0 x 0.10 inch overall skin dimensions and a 21.0 x 21.0 inch central bay and is 57.0 Hz for a plate with the 23.0 x 23.0 x 0.10 inch overall skin dimensions and a 21.0 x 21.0 inch central bay. In the REDYN calculations for the fundamental frequency of the cross-stiffened plates with overall dimensions of 37 x 37 and 23 x 23 inch dimensions, the finite element model consisted of only a quarter of the panel.

From Section VIII. 1. (a), the lowest natural frequency obtained with the clamped-clamped beam function for a 21.0 x 21.0 x 0.10 inch plate clamped on all four edges is 80.7 Hz; and the fundamental frequency of a 21.0 x 21.0 x 0.10 inch aluminum alloy plate that is simply supported on all four edges is 44.1 Hz when obtained using the beam function approach. Hence, the calculated fundamental frequency of neither the 37 x 37 nor the 23 x 23 inch cross-stiffened plates compares favorably with the fundamental frequency of the unstiffened 21 x 21 inch plate, regardless of whether the unstiffened plate is simply supported on all four edges or is fully clamped on all four edges.

Some easy-to-apply theory is needed to determine when the simplified theory is applicable for the prediction of the fundamental frequency of a cross-stiffened plate. Until such a criterion is developed, it appears that the simplified theory produces an upper bound on the fundamental frequency of a cross-stiffened plate.

VIII. 1. (e) Effect of Flanges of Stiffeners on Dynamic Characteristics of Stiffened Panels

The calculations with REDYN are based on a certain set of inputs to characterize the skin and stiffeners. The cross-sectional area, the bending rigidities about the principal axes, and the torsional rigidity of the stiffeners are computed by hand and submitted as input to REDYN. The stiffeners are then identified by REDYN as lines with no thickness but with extensional, bending, and torsional rigidities. Hence, the total effect of a stiffener's flange that is bonded or riveted to the skin is not automatically taken into account by this procedure with REDYN, since the local stiffening around the periphery of a bay of a multi-bay panel may not be adequately defined.

For example, when the flange thickness of the stiffener that is attached to the skin is approximately as thick as the skin or is thicker than the skin, the flange may stiffen the periphery of a bay considerably, as demonstrated below.

A 10.0 x 7.0 x 0.025 inch aluminum alloy plate has been chosen as a model. The plate is clamped on all four edges. The fundamental frequency is 139 Hz when computed by REDYN (using 49 nodes in one quadrant of the panel). When the thickness of the 10 x 7 inch plate is altered so that the thickness is 0.025 inch within the 9.0 x 6.0 inch central section and 0.050 inch around the periphery then the frequency as computed by REDYN increases to 174 Hz. (In this computation of 174 Hz, the 9.0 x 6.0 inch central section is symmetric about both centerlines of the plate.)

For comparison, the fundamental frequency of a 9.0 x 6.0 x 0.025 inch aluminum alloy plate that is clamped on all four edges is 184 Hz when computed by REDYN with the use of 49 nodes in one quadrant. Hence the 10 x 7 inch plate (of the preceding paragraph) with the two thicknesses has a fundamental frequency much closer to that of a 9 x 6 inch plate than to a 10 x 7 inch plate.

The implication from this investigation is that to predict accurately the fundamental frequency of the multi-bay panels with bonded stiffeners, the portion of the flange that is bonded to the central bay must be considered part of the central bay.

VIII.2 FREE VIBRATIONS AND DYNAMIC STRESS ANALYSIS OF ADVANCED-COMPOSITE PANELS

The method of predicting the free vibrations and the strain/stress response of advanced-composite panels subjected to random, acoustic excitation is presented in this subsection. The method and results of the investigation (subsection VIII.1) on the free vibrations and the strain/stress response of isotropic panels served as a guide to the analysis in this subsection.

VIII.2.(a) Material Properties

Material properties of the Fothergill/Harvey Courtaulds 4617/HT-S graphite-epoxy system are given in Appendix A and are summarized here.

In tension and compression tests of unidirectional laminates of 0.025 inch average thickness and 62.8 percent average fiber volume, the average elastic moduli of

$$E_1 = 22.7 \times 10^6 \text{ psi}$$

$$E_2 = 1.53 \times 10^6 \text{ psi}$$

and

$$\nu_1 = 0.34$$

were obtained.

In rail shear tests of rectangular cross-plied laminates (with the fibers parallel or perpendicular to the specimen edges) with an average fiber volume of 57.8 percent, a shear modulus of $G = 1.0 \times 10^6$ psi was obtained.

The principal reason for obtaining the numerical values of E_1, E_2, ν_1, and G that were given above was to utilize those parameters in calculations of the bending

and torsional rigidities of the six-ply $[0/\pm45]_S$ skin and the $[\pm45/0]_S$ internal structure of the acoustic test panels.

Since the average fiber volume of the six-ply $[0/\pm45]_S$ skin of panel A-GG-B-1 was 56.1 percent, whereas in the tests reported above the average fiber volume was 62.8 and 57.8 percent, it became necessary to modify E_1, E_2 and G by reducing them in proportion to the decrease in fiber volume.

The reduction resulted in $E_1 = 20.2 \times 10^6$ psi, $E_2 = 1.53 \times 10^6$ psi, $\nu_1 = 0.34$, and $G = 0.974 \times 10^6$ psi.

However in the coupon tests (reported in Data Sheets 6, 7, and 8) with material used in fabricating skins of the acoustic test panel, A-GG-B-3, it was noted that the average skin thickness was 0.027 inch. Therefore to compensate for the eight percent increase in the thickness of 0.025 inch in the initial coupon tests, the elastic moduli were reduced eight percent more to reach final values that were subsequently used in analysis of

$$E_1 = 18.6 \times 10^6 \text{ psi}$$

$$E_2 = 1.26 \times 10^6 \text{ psi}$$

and

$$G = .895 \times 10^6 \text{ psi}$$

with

$$\nu_1 = 0.34$$

These latter values were used as input to the SQ5 advanced-composite computer program developed under Contract F33615-69-C-1494 to obtain the elements of the A, B, and D matrices in the equation

$$\begin{Bmatrix} N \\ M \end{Bmatrix} = \begin{bmatrix} A & B \\ B^t & D \end{bmatrix} \begin{Bmatrix} \epsilon \\ \kappa \end{Bmatrix} \tag{88}$$

and to obtain the average inplane elastic constants. However, only elements of the D matrix were used in the stress analysis. With the 0 degree direction of the six-ply $[0/\pm45]_S$ skin of 0.027 inch thickness coinciding with the x-axis of Figure 99, the computed bending and twisting rigidities were

$$D_{xx} = 24.6 \text{ lb in.}$$

$$D_{xy} = 2.60 \text{ lb in.}$$

$$D_{yy} = 4.44 \text{ lb in.}$$

$$D_{xz} = 1.59 \text{ lb in.}$$

$$D_{zz} = 3.36 \text{ lb in.}$$

and the average in-plane elastic properties were

$$E_{x\text{-}av} = 8.29 \times 10^6 \text{ psi}$$

$$E_{y\text{-}av} = 3.61 \times 10^6 \text{ psi}$$

$$\nu_{xy\text{-}av} = 0.672$$

$$G_{xy\text{-}av} = 3.49 \times 10^6 \text{ psi}$$

VIII. 2. (b) Unstiffened Plate

The simplified, unimodal theory (the beam function approach) and the finite element approach with REDYN were used to calculate the fundamental frequency and the strain at the center of the long edge and at the center of the short edge of an orthotropic plate that was clamped on all four edges and that possessed the following properties:

a = 9.0 inch length

b = 6.0 inch width

h = 0.027 inch thickness

γ_c = 0.0504 lb/in^3 density

D_{xx} = 24.6 lb in. rigidity

D_{yy} = 4.44 lb in. rigidity

D_{zz} = 3.36 lb in. rigidity

D_{xy} = 2.60 lb in. rigidity

The model above was intended to simulate the central bay of the cross-stiffened, graphite-epoxy test panels. D_{xz} and D_{yz} were assumed zero for a variety of reasons including (1) in a thin-skinned, advanced-composite plate D_{xz} and D_{yz} are relatively small compared to D_{xx}, and (2) the finite element computer program (REDYN) did not include the D_{xz} and D_{yz} terms.

The choice of the 9.0 x 6.0 inch edge dimension was based on the fact that the I-beam and tee section details of acoustic test panels supported the nominal 10.0 x 7.0 inch central bay approximately 0.5 inch around the periphery, thereby reducing the unsupported area of the central bay to 9.0 x 6.0 inch. The effect of flanges of stiffeners on dynamic characteristics of plates was discussed in detail under subsection VIII. 1. (e). The computations of fundamental frequency and the unimodal strain response at the center of the long and short edge of the plate to fully correlated, white noise are given in Table XXIV. The computations are based on a pressure PSD of 1.21×10^{-6} psi ^{2}/Hz which from Figure XXI appears to be a reasonable estimate of the acoustic excitation during the 139 db SPL test for panel A-GG-B-3. The strain gage No. 2 and No. 7 response

during the 139 db test runs for panels A-GG-B-2 and A-GG-B-3 are also in Table XXIV. No data on panel A-GG-B-1 are considered because the initial curvature would invalidate the flat plate analysis.

TABLE XXIV. COMPARISON OF EXPERIMENTAL RESULTS OF CROSS-STIFFENED PANELS WITH RESULTS USING UNSTIFFENED PLATE THEORY

Approach	Method	Fundamental Frequency	Strain at $x = 0,\ y = \frac{b}{2}$	Strain at $x = \frac{a}{2},\ y = 0$
		(Hz)	(micro-inch/inch-rms)	(micro-inch/inch-rms)
Analytic	Simplified theory (Beam Functions)	182	180(2)	406(2)
Analytic	Finite Element (REDYN)	180	180(2)	348(2)
Experimental	Test Panel A-GG-B-2	187(1)	96(3)	160(3)
Experimental	Test Panel A-GG-B-3	170(1)	74(4)	164(4)

(1) Obtained during damping factor determination under loudspeaker excitation

(2) Strain response to fully correlated, white noise excitation of 1.2×10^{-6} psi ^{2}/Hz

(3) Strain gage No. 2 reading during 139 db run

(4) Strain gage No. 7 reading during 139 db run

The agreement between the frequency and strain predictions in Table XXIV using the beam function approach and the finite element approach is satisfactory. The agreement between the predicted and experimental fundamental frequencies is also satisfactory. The disagreement between theoretical and experimental strains, while not desirable, is of the same order of magnitude as discrepancies between theoretical and experimental stresses reported in Reference 11 in a review of many investigations of the dynamic behavior of isotropic panels. A partial explanation for the theoretical strains being higher (approximately by a factor of two) than the experimental strains is the nonlinear strain-pressure relationship that is implied by the fact that the fundamental resonance in the 139 db run is at a higher frequency (at approximately 200 Hz) than the resonance (178 Hz ±9 Hz) under loudspeaker excitation when the damping factors were obtained. Another explanation is that the local strain at the periphery of the cross-stiffened panel may be significantly influenced by the local geometry that has not been modeled in the dynamic analysis by a fine grid. A third explanation is that acoustic pressure may not be considered spatially uniform. The important observation that is drawn from the results in Table XXIV is that since the theory overestimates the measured strains, the effect of the finite element grid size is the least important of the three proposed explanations for the particular panel design.

VIII.2.(c) Cross-Stiffened Panels

The linear, finite element program REDYN was also used to predict the fundamental frequency and strain response at acoustic fatigue sensitive locations near strain gage No. 2 and No. 7 (Figure 31), in the skin in the central bay of the acoustic test panels, A-GG-B-2 and A-GG-B-3. The finite element model M-3 (Figure 102) was designed for the analysis, and represents only one quadrant of the cross-stiffened panel being analyzed. The region of the acoustic test panels that included the -41 graphite-epoxy doubler was considered to have an insignificant effect on the lowest frequency of the panel and on the acoustic response of the fundamental mode in the central bay; and therefore the portion of the test panels that included the -41 doubler was not a part of Model M-3. The boundary conditions of Model M-3 that were used in the computer run were chosen to produce symmetrical response about the panel centerlines and neither deflection nor slope at the other two edges.

In Model M-3, the finite elements that have an edge dimension of 0.50 inch simulate a portion of the skin that is supported either by an I-beam on tee section detail; and the finite elements that have an edge dimension of 0.25 inch were designed to refine the grid in the acoustic fatigue sensitive zones (that include strain gages No. 2 and No. 7) where the computed strains are of interest.

In the computations with REDYN, the elastic properties of the skin were the same as used in the analysis of the unstiffened, graphite-epoxy plates of the previous subsection; the elastic properties of the I-beam and tee section details were 9.01×10^6 psi and $G = 3.79 \times 10^6$ psi (these stiffeners are considered as isotropic beams in REDYN); the damping factor was 0.017 (which was used in all theoretical response calculations in this report); and the acoustic pressure was characterized as fully correlated, white noise with a PSD of 1.21×10^6 psi ^{2}/Hz. The pressure PSD was estimated from the data analysis of the pressure applied to panel A-GG-B-3 during the 139 db SPL run.

The calculations obtained with the use of REDYN included a fundamental frequency (of panels A-GG-B-2 and A-GG-B-3) of 165 Hz and strains, some of which are in Table XXV. The theoretical strains in Table XXV were at the centroids of elements (with the .25 inch edge dimension) that included the locations of strain gages No. 2 and No. 7.

TABLE XXV. COMPARISON OF NATURAL FREQUENCIES AND STRAINS OF CROSS-STIFFENED, GRAPHITE-EPOXY PANELS USING FINITE ELEMENT ANALYTIC RESULTS AND EXPERIMENTAL DATA

Method	Fundamental Frequency (Hz)	Strains: Strain Gage No. 2 (micro-inch/inch-rms)	Strains: Strain Gage No. 7 (micro-inch/inch-rms)
Theoretical (REDYN)	165	304	168
Experimental (Panel A-GG-B-3)	170(1) 177(1)	164	74

(1) Different values were obtained for the fundamental frequency during tests to obtain the panel damping factor.

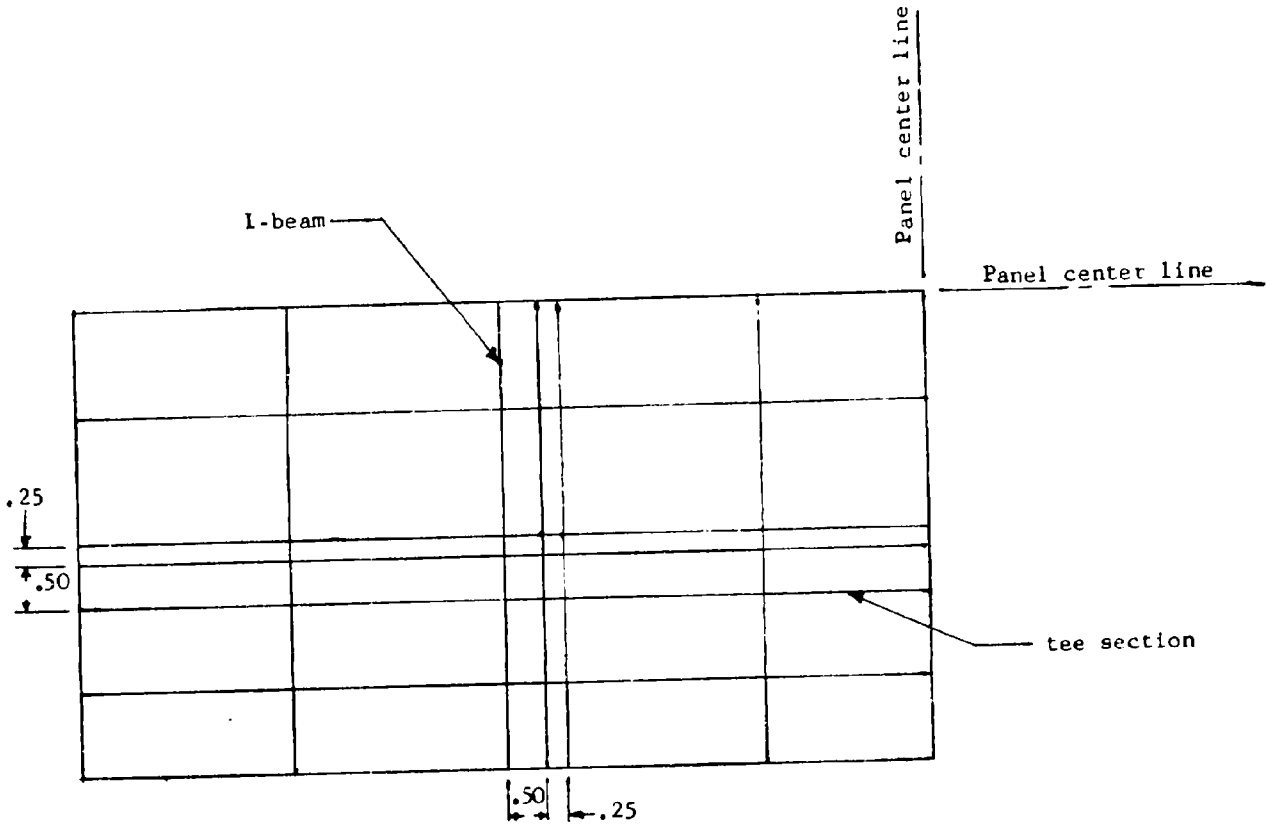

SCALE = 1 inch = 2 inch

FIGURE 102. FINITE ELEMENT MODEL M-3 REPRESENTING LOWER LEFT QUADRANT OF ACOUSTIC TEST PANELS A-GG-B-2 AND A-GG-B-3

There is satisfactory agreement between the theoretical and experimental frequencies in Table XXV. The differences in Table XXV between the theoretical and experimental strains is not unusual (see the preceding subsection) when viewed as part of a collection of data from many programs that have been conducted over a span of several years.

It is believed that the differences between the theoretical and experimental strains can be reduced in a future program by using a finer grid in the finite element analysis (a substantially finer finite element grid could not be used in the present version of REDYN because of limitations on core storage) and by accounting in the finite element analysis for the deviations from the theoretical, fully correlated loading conditions (finite element computer programs including REDYN have the capability of accounting for arbitrary pressure correlations).

VIII.3 DETAILED STRESS ANALYSIS OF BONDED JOINTS

The selection of the shaker test specimen design (i.e., the choice between the Candidate A-1 and Candidate A-2 type shaker test specimens) was to be based on the location of the first acoustic fatigue failure of a joint assembly of a cross-stiffened acoustic test panel. Specifically, it was necessary to predict whether the initial acoustic fatigue failure of a cross-stiffened test panel would occur at a joint assembly with the internal structure being an I-beam detail or a tee section.

VIII.3.(a) Analytic Approach

Two cases were investigated in the detailed stress analysis, that is summarized below, leading to the choice of Candidate A-2 type shaker specimen. The analytic problem that was formulated in each of the two cases was to predict stresses (at the individual ply level at the edges of the joint assembly) in a beam that was clamped at both ends and loaded by a uniform unit static pressure. In Case 1, the beam was of unit width with geometrical and elastic properties of a section between the tee section details (i.e., parallel to the I-beam details) of the nominal 10.0 x 7.0 inch central bay of the acoustic test panels. In Case 2, the beam was of unit width with geometrical and elastic properties of a section between the I-beam details (i.e., parallel to the tee section details) of the nominal 10.0 x 7.0 inch central bay of the acoustic test panels. The length of the beam in Case 1 is 7 inches and the length of the beam in Case 2 is 10 inches. The clamped-clamped beam boundary conditions were chosen to represent closely the expected boundary condition of a strip in the central bay of the cross-stiffened, test panels.

Because of symmetry, only one-half the cross-section was used in the analysis, and it is shown in Figure 103. A stress analysis was performed at the individual ply level by considering finite-elements in the individual plies. With this approach, stresses developed in individual plies and the bonding material were obtained. The detailed finite-element set-up is shown in Figure 104. A finer mesh was taken near the edge of the adhesive because of the expected stress concentration effects in this region. The linear, finite-element program SAAS-II (see pa[illegible] 5) was used with the plane-strain option.

The computed stresses in the bonding material and the individual panel plies for the two cases are presented in Figures 105 and 106. The following observations were made from these results:

1. High shear stresses were developed in the bond at the corner point.

2. The ratios of yield stresses to developed stresses show that for Case 1 the first fatigue failure is expected to occur in the 90 degree ply of the skin and for Case 2 the first fatigue failure is expected to occur in the bond (see the discussion below).

Based on these results and the assumption that the material stress-strain curves were linear to the ultimate stress, it was concluded that for the acoustic test panels, the initial acoustic fatigue failure should be expected at or near the tee section stiffeners rather than at or near the I-beam stiffeners, since the most severely stressed (relative to yield stresses) finite element was in the 90 degree ply of the skin adjacent to the adhesive bond (see Figure 104 with the ratio $\frac{\sigma_{yield}}{\sigma_{z\,max}} = 0.49$ being the critical stress ratio). The results of this bonded joint analysis was a key factor in the selection of the Candidate A-2 type shaker specimen. Subsequently, in the fatigue tests of the shaker test specimens, the fatigue failures did occur in the skin of the 90 degree plies (Figure 87 and 88) as predicted by the analysis in this subsection.

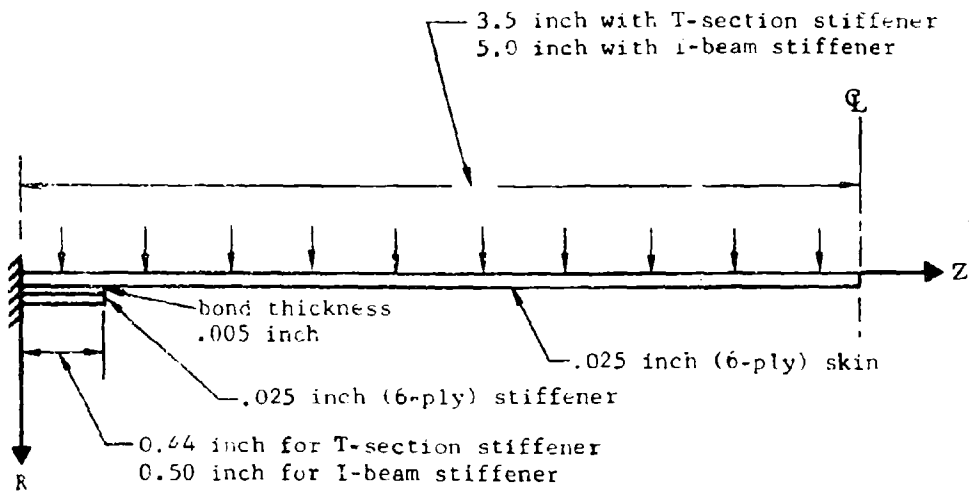

FIGURE 103. CROSS-SECTION USED FOR STRESS ANALYSIS

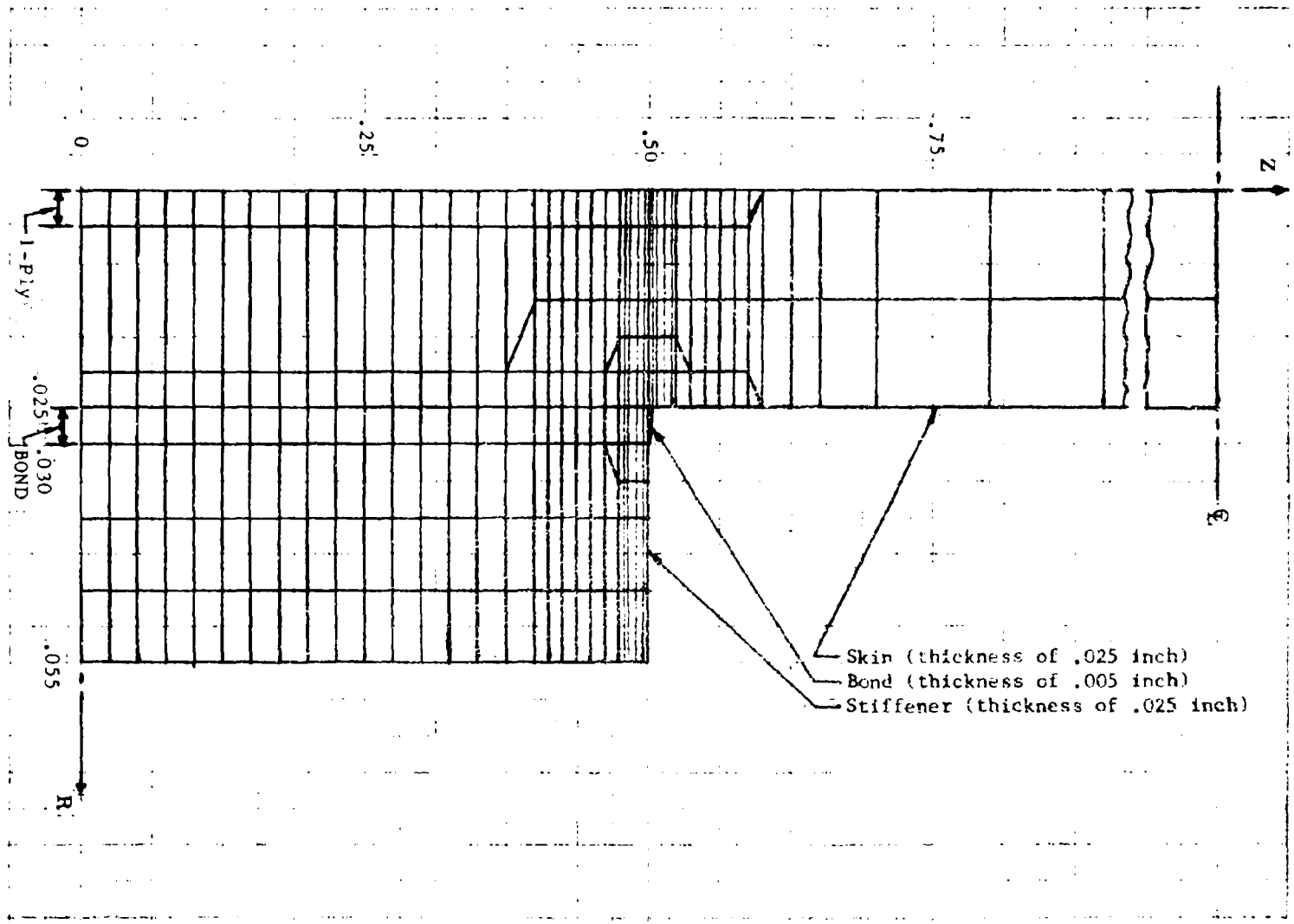

FIGURE 7-3. FINITE ELEMENTS IN BONDED JOINT ANALYSIS

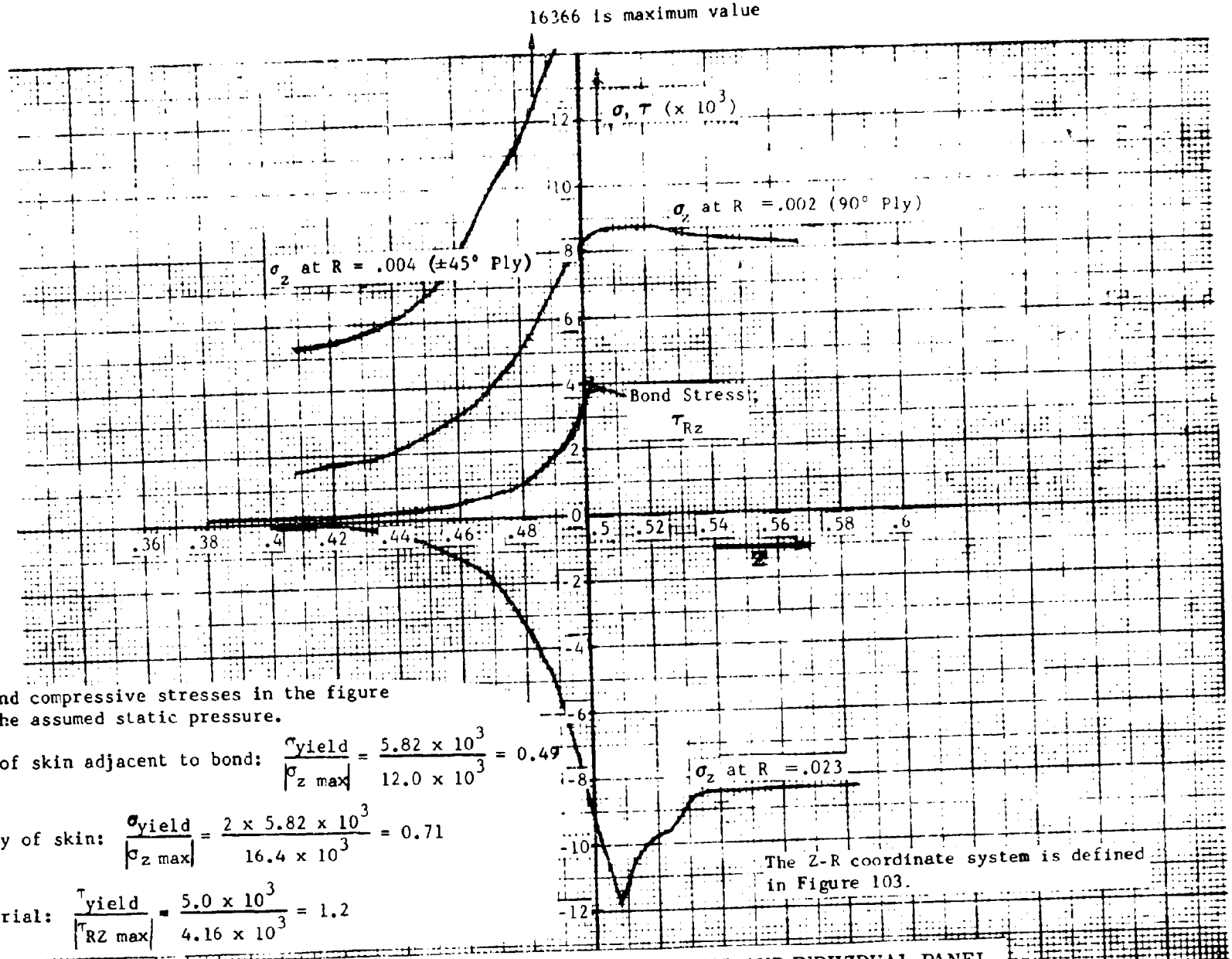

Tensile and compressive stresses in the figure are for the assumed static pressure.

90° - ply of skin adjacent to bond: $\frac{\sigma_{yield}}{|\sigma_{z\ max}|} = \frac{5.82 \times 10^3}{12.0 \times 10^3} = 0.49$

±45° - ply of skin: $\frac{\sigma_{yield}}{|\sigma_{z\ max}|} = \frac{2 \times 5.82 \times 10^3}{16.4 \times 10^3} = 0.71$

Bond material: $\frac{\tau_{yield}}{|\tau_{RZ\ max}|} = \frac{5.0 \times 10^3}{4.16 \times 10^3} = 1.2$

The Z-R coordinate system is defined in Figure 103.

FIGURE 105. STRESSES IN THE BONDING MATERIAL AND INDIVIDUAL PANEL PLIES FOR CASE 1

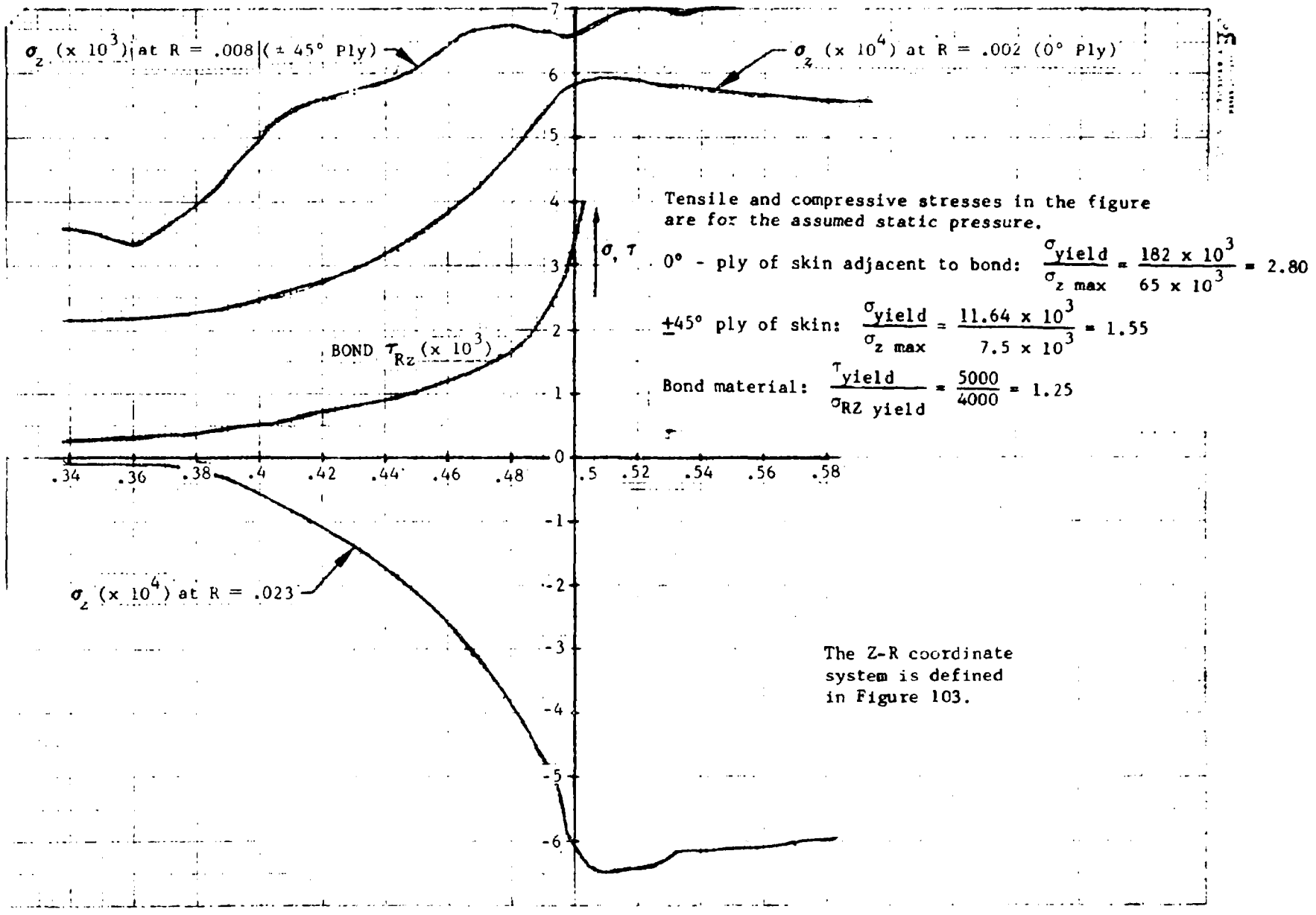

FIGURE 106. STRESSES IN THE BONDING MATERIAL AND INDIVIDUAL PANEL PLIES FOR CASE 2

VIII. 3. (b) Elastic Constants

In the previous subsection, results of a detailed stress analysis of two sections of the cross-stiffened acoustic panels under a static, uniform pressure load were presented. The stress analysis was performed at the individual ply level by considering finite-elements in the individual plies. The individual ply material properties used for stress analysis were computed by using orthotropic ply properties and ply orientations. These elastic properties for all the skin and adhesive plies are presented in Table XXVI. The coordinate system used is shown in Figure 107. The individual plies are parallel to the Z-θ coordinate plane and the R-coordinate is normal to the ply plane. The analytic methods for computing Poisson's ratios ν_{ZR}, $\nu_{\theta Z}$ and the shear modulus G_{RZ} for the plies other than 0° and 90° are described below.

TABLE XXVI. ELASTIC CONSTANTS FOR BONDED JOINT ANALYSIS

PLY ORIENTATION	MATERIAL NO.	E_R (psi)	E_Z (psi)	E_θ (psi)	ν_{ZR}	$\nu_{\theta R}$	$\nu_{\theta Z}$	G_{RZ} (psi)
	Case 1 - Skin, Adhesive, tee section							
Skin 90°	1	1.37×10^6	1.37×10^6	20.2×10^6	0.34	0.34	0.34	194,000
Skin 45°	2	1.37×10^6	3.32×10^6	3.32×10^6	0.442	0.442	0.706	324,000
Adhesive	3	0.30×10^6	0.30×10^6	0.30×10^6	0.30	0.30	0.30	100,000
Skin 90°, ± 45°	4	1.37×10^6	2.92×10^6	16.2×10^6	0.41	0.672	0.672	281,000
	Case 2 - Skin, Adhesive, I-beam							
Skin 0°	1	1.37×10^6	20.2×10^6	1.37×10^6	0.34	0.34	0.0231	974,000
Skin 45°	2	1.37×10^6	3.32×10^6	3.32×10^6	0.442	0.442	0.706	324,000
Adhesive	3	0.30×10^6	0.30×10^6	0.30×10^6	0.30	0.30	0.30	100,000
Skin 0°, ± 45°	4	1.37×10^6	16.2×10^6	2.92×10^6	0.41	0.41	0.1215	541,000

1. Poisson's Ratio

Consider a simplified coordinate system (α, β, Z) shown in Figure 108. The principal orthotropic properties of a ply are along the (1, 2) coordinate directions at an angle θ to the (α, β) coordinates. Coordinate Z is normal to the ply plane.

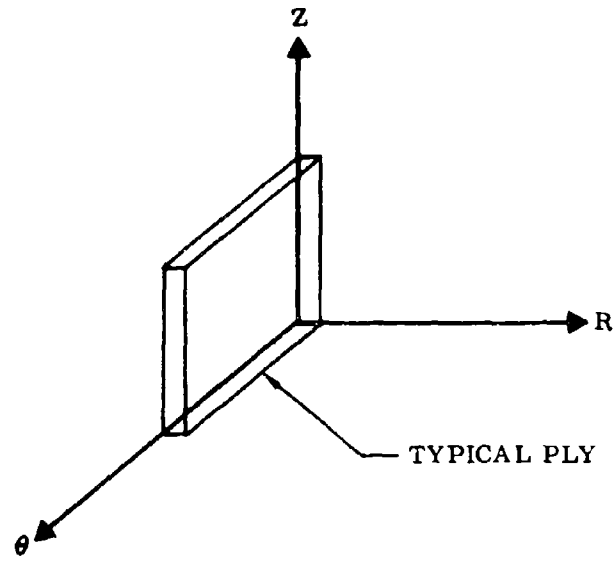

FIGURE 107. COORDINATE SYSTEM FOR BONDED JOINT ANALYSIS

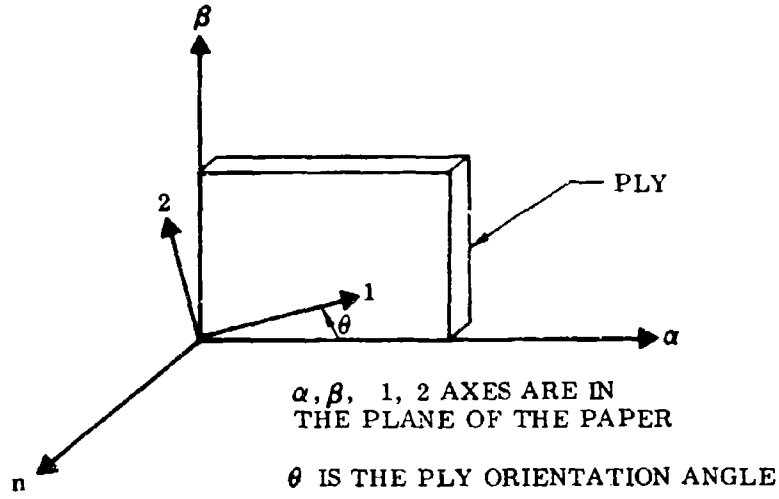

FIGURE 108. ALTERNATE COORDINATE SYSTEM FOR BONDED JOINT ANALYSIS

Consider the case when the uniaxial stress s is applied. The stress components along the (1, 2) directions are

$$s_1 = \cos^2\theta \; s_\alpha \tag{89}$$

$$s_2 = \sin^2\theta \; s_\alpha$$

$$s_{12} = -(\sin\theta \cos\theta) \; s_\alpha$$

The strain component in the thickness direction is given by

$$e_n = -\left(\frac{\nu_{13}}{E_1} s_1 + \frac{\nu_{23}}{E_2} s_2\right) \tag{90}$$

Substituting s_1 and s_2 from equations (89) into (90), one obtains

$$e_n = -\left(\frac{\nu_{13}}{E_1}\cos^2\theta + \frac{\nu_{23}}{E_2}\sin^2\theta\right) s_\alpha \tag{91}$$

Assuming that

$$\nu_{13} = \nu_{23} = \nu_{12} \quad ,$$

$$e_n = \frac{-\nu_{12}}{E_2}\left(\frac{E_2}{E_1}\cos^2\theta + \sin^2\theta\right) s_\alpha \tag{92}$$

By definition of $\nu_{\alpha n}$, one obtains for uniaxial loading

$$e_n = -\frac{\nu_{\alpha n}}{E_\alpha} s_\alpha \tag{93}$$

Equating the two expressions for e_n from equation (92) and (93),

$$\nu_{\alpha n} = \frac{\nu_{12}}{E_2}\cdot\left(\frac{E_2}{E_1}\cos^2\theta + \sin^2\theta\right) E_\alpha \tag{94}$$

This expression was used to compute numerical values of ν_{ZR} and given in Table XXVI, by allowing α to assume values of Z or θ, and allowing n to assume the value R.

2. Thickness Shear Modulus

For the single ply shown in Figure 107, consider the case when only shear stress component $s_{\alpha N}$ is applied. The shear stress components along the (1, 2) coordinate directions are

$$s_{1n} = \cos\theta \; s_{\alpha n}$$

$$s_{2n} = \sin\theta \; s_{\alpha n}$$

The corresponding shear strain components are

$$e_{1n} = \frac{1}{2G_{1n}} s_{1n} \tag{95}$$

$$e_{2n} = \frac{1}{2G_{2n}} s_{2n}$$

The resultant of these shear strain components $e_{\alpha n}$ is obtained by using strain transformation relations. Thus

$$e_{\alpha n} = \sin\theta \, e_{2n} + \cos\theta \, e_{1n} \tag{96}$$

Substituting from equations (94) and (95) into equation (96), one obtains,

$$e_{\alpha n} = \frac{1}{2}\left(\frac{\sin^2\theta}{G_{2n}} + \frac{\cos^2\theta}{G_{1n}}\right) s_{\alpha n} \tag{97}$$

With the definition of $G_{\alpha Z}$ and the use of equation (97)

$$G_{\alpha n} = \left(\frac{\sin^2\theta}{G_{2n}} + \frac{\cos^2\theta}{G_{1n}}\right)^{-1} \tag{98}$$

This expression was used to compute numerical values of G_{RZ} given in Table XXVI by letting α assume the value Z and letting n assume the value R.

VIII.4 SUPPORTING CALCULATIONS FOR THE DESIGN OF ACOUSTIC PANEL A-GG-B-2

Calculations that were conducted in changing the acoustic panel design following the manufacturing and testing of panel A-GG-B-1 in order to obtain flat, as-manufactured panels are presented in this subsection.

VIII. 4. (a) Thermal Stress Analysis of Acoustic Panel A-GG-B-1

A simplified thermal stress analysis was performed by considering only the in-plane thermal deformations for various structural members of Figure 109. Consider the thermal expansion of structural members from a reference temperature.

Let δ_i^T = free thermal expansion of ith member.

and δ_i = actual expansion of the ith member. Then

$$\delta_i^T = \alpha_i (\Delta T) L_i \tag{99}$$

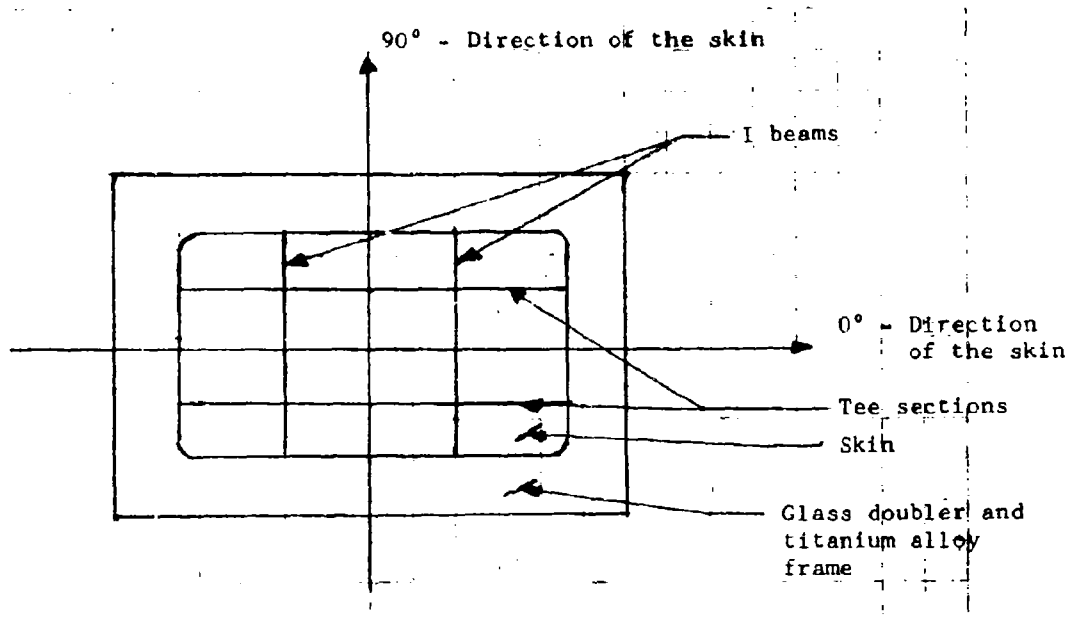

FIGURE 109. SCHEMATIC DRAWING OF NINE-BAY, CROSS-STIFFENED PANEL A-GG-B-1

The built-up structure is in equilibrium. Therefore, the sum of all the force resultants at any cross-section is zero. Thus

$$\sum_i (s_i A_i) = 0 \tag{100}$$

where

$$s_i = E_i e_i = E_i \left(\frac{\delta - \delta_i^T}{L_i} \right) \tag{101}$$

Hence,

$$\sum \frac{\delta - \delta_i^T}{L_i} E_i A_i = 0 \tag{102}$$

and

$$\delta \sum \frac{E_i A_i}{L_i} = \sum \delta_i^T \frac{E_i A_i}{L_i} \tag{103}$$

Substituting from equation (99) for δ_i^T,

$$\delta = \Delta T \frac{\sum \alpha_i E_i A_i}{\sum \frac{E_i A_i}{L_i}} \tag{104}$$

Assuming the same length for all structural members, $L_i = L$. Thus

$$\delta = L\Delta T \frac{\sum \alpha_i E_i A_i}{\sum E_i A_i} = K_o L \Delta T \tag{105}$$

where

$$K_o = \frac{\sum \alpha_i E_i A_i}{\sum E_i A_i} \tag{106}$$

Therefore,

$$s_i = E_i (K_o - \alpha_i) \Delta T \tag{107}$$

Using equations (106) and (107), the average thermal stresses in any one of the structural member can be readily computed.

Numerical Results:

Elastic and thermal properties of the structural members of Figure 109 (that simulates acoustic panel A-GG-B-1) are tabulated below.

TABLE XXVII. DATA FOR THERMAL ANALYSIS

Structural Member	Elastic Modulus (psi)	Thermal Coefficient (in/in/F)	Cross-Section (in^2)
Skin, 0°	9.0×10^6	1×10^{-6}	0.52
Skin, 90°	3.9×10^6	10×10^{-6}	0.75
T-section	9.0×10^6	1×10^{-6}	0.104
I-beam	9.0×10^6	1×10^{-6}	0.250
Glass Doubler	3.5×10^6	5×10^{-6}	1.04
Titanium Frame	16×10^6	5×10^{-6}	.85

Using the aforementioned elastic and thermal properties in equations (106) and (107), the following average stresses in the skin were obtained.

Along 0° direction: $s_{skin} = -4620$ psi (compressive stress)

Along 90° direction: $s_{skin} = +3160$ psi (tensile stress)

Upon comparing the above -4,620 compressive stress with the critical buckling stress for the 10 inch x 7 inch plate (simulating the central bay of panel A-GG-B-1), it is determined that the thermal stresses induced in cooling panel A-GG-B-1 from

250F were sufficient to produce buckling and oil canning. The critical buckling stress of the central bay is determined in the next subsection.

The use of equations (106) and (107) with the glass doubler being replaced by a graphite/epoxy doubler (see Section I.C.4) resulted in a thermally induced stress in the skin of -3,080 psi of the titanium alloy frame if bonded to the skin at 250F at the same time that the skin is bonded to the I-beam and tee sections details. Because the -3,080 psi stress was still high relative to the predicted skin buckling stress, a room temperature curing adhesive was used in bonding the titanium alloy frame to the skin in panels A-GG-B-2 and A-GG-B-3.

VII.4.(b) Critical Buckling Stresses

A buckling stress analysis of rectangular composite 6-ply plates was performed using the RA-5 computer program (developed under Contract AF33(615)-5257). The computed buckling stresses for the skin and stem of the tee section are given below:

10- x 7-inch plate - simply supported (simulating the central bay of panel A-GG-B-1) - 265 psi.

10- x 0.708-inch plate - simply supported on 3-sides, free on one long side (simulating the vertical leg of the tee sections of panel A-GG-B-1) - 5480 psi.

The large ratio of 4620 psi to 265 psi is not an exact ratio of the thermally induced compressive stress (in cooling the panel from 250F to 80F) to the critical stress of the central bay since the analysis in equations (99) thru (107) overlooks stabilizing effects of tensile stresses in the panel cross section. Furthermore, the thermal coefficients of 1×10^{-6} and 10×10^{-6} in/in/F of the graphite-epoxy skin and stiffeners are estimates based on data from different graphite-epoxy systems. However, the conclusion of this brief analysis was that changes from the design of bonded A-GG-B-1 were needed to obtain flat, as manufactured, panels A-GG-B-2 and A-GG-B-3.

Upon comparing the 5,480 psi critical stress in the stem of the tee section with the experimental strain data of acoustic panel A-GG-B-1, no change was made in the tee sections of the acoustic test panels.

IX. SUMMARY AND CONCLUSIONS

Two useful methods of analysis were developed for predicting the linear, strain response to acoustic excitation. One method (using a simplified theory) was developed for hand calculation predictions of the unimodal response at the fundamental frequency of a flat, rectangular, orthotropic plate (of constant thickness) subjected to fully correlated, white noise excitation and clamped on all four edges. The plate was used to simulate the central bay of the acoustic test panels for which the predicted fundamental frequency and strain response in acoustic fatigue critical locations in the skin was in satisfactory agreement with experimental values. A drawback in applying the simplified theory in the design of skins of cross-stiffened, advanced-composite panels is that there is now no criterion indicating when the simplified theory is applicable. The development of a simple criterion would be quite useful.

The second method of analysis that was developed consisted of applying an available, linear, finite element, dynamic stress analysis computer program for predicting the natural frequencies and the multi-modal, stress response in the skin and internal structure of orthotropic plates subjected to broad-band acoustic pressure excitation. This method of analysis provided satisfactory agreement between predicted and experimental fundamental frequencies and strain response in the skin of the acoustic test panels at low excitation levels (for which the use of linear theory is appropriate). It appears that this second method which is more general than the simplified method described in the preceding paragraph, can be developed further and utilized in the design of both the internal structure and skin of thin-skinned, cross-stiffened, advanced-composite and metallic panels.

Several conclusions that were drawn from the overall program which contained three distinct, yet interrelated, phases (namely, an analytic investigation, an acoustic test program, and a shaker test program) are discussed below.

1. It was demonstrated in the acoustic test program that high quality, thin-skinned (a 0.027 inch average skin thickness and a 6 ply, $[0/\pm 45]_S$ layup), cross-stiffened panels (with the largest bay of 10.0 x 7.0 inch nominal edge dimensions) with graphite-epoxy skins bonded to graphite-epoxy internal structure can be designed, manufactured, and tested in a high intensity broad-band, noise environment (166 db SPL) at ambient temperature for an extended period of time (100 hours) without experiencing major acoustic fatigue failures. Based on these acoustic test results, it appears that thin-skinned cross-stiffened panels with advanced-composite skins attached to advanced-composite or metallic internal structure are attractive for use in high intensity, noise environments.

Preceding page blank

2. Analytic methods were developed to predict the fundamental frequency of flat, rectangular, cross-stiffened, thin-skinned, advanced-composite panels and the strain response (at sufficiently low, broad-band, acoustic excitation levels where linear strain versus pressure relations are approximately correct) at acoustic fatigue sensitive locations. A comparison of the predicted fundamental frequencies and the strains in the panel skins at low excitation levels (e.g. 139 db SPL) with the experimental fundamental frequency and strains in the skins of the flat, acoustic test panels showed satisfactory agreement in the sense that percentage differences between predicted and experimental values were approximately the same as the differences that have been documented during acoustic fatigue investigations conducted with metallic panels during the last several years. Furthermore, it is believed that the percentage differences between the predicted and experimental fundamental frequency and strains in the linear response range can be reduced when a finer finite element grid and experimentally available pressure correlation data are used in the analytic prediction process.

3. In the experimental program, it was demonstrated that as the sound pressure level with a broad-band spectrum was increased, the nonlinear effects (as evidenced by rms strain readings and fundamental frequency observations) became increasingly more significant. Furthermore, at the highest excitation SPL, the strain response of the fundamental mode relative to the overall rms response was significantly less than at lower excitation levels. Since there is no generally accepted theory that is available for predicting the nonlinear strain-pressure relation, it is still necessary to resort to empirical methods of predicting strains when the response is nonlinear. Neither an analytic nor empirical study of nonlinear response relations was conducted in this investigation.

4. A linear, static, finite element stress analysis method for predicting the weakest member of a (skin/adhesive/internal structure) joint assembly was presented. The location of the fatigued component (the skin in all experimental cases) of the shaker specimens confirmed the predictions. The two satisfactorily manufactured acoustic test panels, A-GG-B-2 and A-GG-B-3, did not experience an acoustic fatigue failure in the joint assemblies and, hence, no comparison of predicted and experimental failure location could be made for the acoustic test panels.

5. The overall rms strain level at acoustic fatigue critical locations was the parameter used in predicting the life of the acoustically loaded panels. With this method, the average response frequency based on the spectrum of the response was calculated for the flat, acoustic test panels; the overall rms strain was obtained experimentally under the acoustic loading; and then the panel life under the acoustic loading was predicted on the basis of an S-N curve obtained in the shaker test program. For the acoustic test panels, the absence of an acoustic fatigue failure at the joint assemblies was predicted based on the experimental overall rms strains, and the absence of an acoustic fatigue failure was verified in the acoustic tests of panels A-GG-B-2 and A-GG-B-3. In general, when the location of failure is at a joint assembly in a thin skin and possibly in the joint attachment of an acoustically loaded panel, it appears that the stress at the failure location results from simple bending and therefore the use of S-N curves obtained under essentially simple bending conditions (such as the shaker test program) appears feasible in the prediction of the panel life.

6. The data analysis of strain response and the broad-band pressure in the acoustic tests of panels A-GG-B-2 and A-GG-B-3 indicated that both the strain response and the acoustic loading were repeatable to within acceptable tolerances. This repeatability provided evidence of a satisfactory manufacturing and testing procedure.

7. Six S-N curves for shaker specimens with different material systems (one system utilized graphite-epoxy skins in the shaker specimens and the other system utilized boron-epoxy skins), different attachments (i.e., bonded and riveted), and different stiffeners (either graphite-epoxy or titanium alloy) were obtained in the test program. The approach of conducting shaker tests to obtain S-N data for acoustic fatigue application appears promising since (1) it appears that the strain at the failure location in the shaker specimens and the cross-stiffened, thin-skinned, acoustic panels results from simple bending and therefore the S-N data obtained under less expensive shaker testing can be substituted for S-N data obtained under more expensive acoustic panel tests; and (2) it appears practical to conduct a series of shaker tests and vary important items such as the method of attachment, the orientation of plies in advanced-composite skins, and the stacking sequence of the plies in order to obtain experimental S-N data to compare advantages and disadvantages of various types of joint assemblies.

8. Care must be taken in the design of bonded, cross-stiffened, advanced-composite panels to avoid high, residual stresses (such as were experienced by the first acoustic test panel) resulting from the cooling from the bonding temperature.

9. The manufacturing processes that were developed for the graphite-epoxy, I-beam and tee section details that were developed in this program appear to be satisfactory for other stacking sequences, configurations, and advanced-composite material systems.

REFERENCES

1. M.J. Jacobson, "Acoustic Fatigue Design Information for Fiber Reinforced Structures," Technical Report AFFDL-TR-68-107, October 1968.
2. J.R. Ballentine, et.al, "Refinement of Sonic Fatigue Structural Design Criteria," Technical Report AFFDL-TR-67-156, January 1968.
3. "Data Sheets on Fatigue: Sheets No. 66012-66022," The Royal Aeronautical Society, 1966.
4. "Structural Design for Acoustic Fatigue," Technical Documentary Report No. ASD-TDR-63-820, October 1963.
5. E.J. Richards and D.J. Mead, Noise and Acoustic Fatigue in Aeronautics, John Wiley and Sons, Ltd., New York, 1968.
6. T.F. Nelson, "An Investigation of the Effects of Surrounding Structure on Sonic Fatigue," NASA CR-1536, May 1970.
7. M.J. Jacobson, "Acoustic Fatigue Design Information for Skin-Stiffened Metallic Panels," Northrop Report NOR 69-111, August 1969.
8. M.J. Jacobson, "Dynamic Response and Acoustic Fatigue Characteristics of Flat Skin-Stringer Aluminum Alloy Panels," Northrop Report NOR 70-22, February 1970.
9. H.G. Harris, I.U. Ojalvo, R.E. Hooson, "Stress and Deflection Analysis of Mechanically Fastened Joints," Technical Report AFFDL-TR-70-49, May 1970.
10. L.D. Jacobs and D.R. Lagerquist, "Finite-Element Analysis of Complex Panel Response to Random Loads," Technical Report AFFDL-TR-68-44, October 1968.
11. N. Arcus, "Prediction of Stress and Fatigue Life of Acoustically Excited Structures."The Shock and Vibration Bulletin, January 1969, pp 87-97.
12. R.N. Yurkovich, J.H. Schmidt, A.R. Zok, "Dynamic Analysis of Stiffened Panel Structures," J. Aircraft, Vol. 8, No. 3, March 1971, pp 149-155.
13. M.J. Jacobson, "Stress and Deflection of Honeycomb Panels Loaded by Spatially Uniform White Noise," AIAA J., Vol. 6, No. 8, August 1968, pp 1503-1510.
14. S. Timoshenko and S. Woinowsky-Kieger, "Theory of Plates and Shells," McGraw-Hill Book Co., New York, 1959, p. 365.
15. D. Young and R.P. Felgar, Jr., "Table of Characteristic Functions Representing Normal Modes of Vibration of a Beam," The University of Texas, Austin, Texas, Engineering Research Series No. 44, 1949, pp 12-14.
16. J.W. Miles, "On Structural Fatigue Under Random Loading," Journal of the Aeronautical Sciences, November 1954, p. 754.
17. W.C. Hurty and M.F. Rubinstein, "Dynamics of Structures," Prentice Hall, Inc., Englewood Cliffs, New Jersey, 1964, p. 389.
18. M.J. Jacobson, "Linear and Nonlinear Aluminum Plate Response to Acoustic Loading," Northrop Report 69-37, February 1969.

Preceding page blank

APPENDIX A

ADVANCED-COMPOSITE MATERIALS

The Fothergill/Harvey Courtaulds HT-S/4617 graphite-epoxy system and the Narmco 5505 boron-epoxy system were chosen for the test program. These systems are expected to be among the prominent advanced-composite systems to be used in hardware applications during the next several years.

The reinforcements and epoxy resins met or exceeded the requirements of the contractor procurement specifications:

1. Northrop Specification, NAI-1302 - "Prepreg for Structural Composites, Boron-Epoxy, High Strength, High Modulus"

2. Northrop Specification, NAI-1318 - "Unidirectional Graphite Prepreg for Structural Composites, High Modulus, High Strength."

The scope of the specifications establishes the requirements for the resin-impregnated multifilament prepreg tapes and cloth products made from high strength and high modulus boron and graphite filaments. The specifications include physical property requirements for material acceptance (flow, resin content, and volatiles). Physical appearance such as fiber spacing, broken fibers, surface condition, and material uniformity are specified. The prepreg shelf life, room temperature requirement, and additional mechanical property acceptance levels also are specified.

The Fothergill/Harvey Courtauld HT-S/4617 graphite-epoxy system was purchased in sheets with nominal dimensions of 48-inch by 12-inch by 0.005-inch and resin content of 40 percent by weight. The Narmco 5505 boron-epoxy system was purchased in three-inch wide tapes with a thickness of 0.005-inch and 40 percent resin by weight.

The subsequent fabrication procedures applied to the advanced-composite materials were compatible with the Northrop Process Specifications PL-35 and PL-36.

At the beginning of the experimental program, tests were conducted to obtain physical and mechanical properties of the Fothergill/Harvey Courtaulds HT-S/4617 graphite-epoxy material. The test results for the uniaxial loading of parallel plied specimens with the load parallel or transverse to the fibers are given in Figures A-1 thru A-4 and in Data Sheets 1 thru 4. The results of the rail shear test of cross-plied specimens are given in Figure A-5 and Data Sheet 5. The test results on a portion of the laminate that was prepared for acoustic panel A-GC-B-1 are given in Figure A-6 and Data Sheet 6.

After shaker specimens had been fabricated and fatigue failures were obtained in the specimen skins during the shaker test program, six-ply $[90/\pm45]_S$, graphite-epoxy and boron-epoxy specimens were fabricated for static tests with the principal objective being to obtain static ultimate strains for comparison with the rms fatigue

strains that were obtained in the shaker test program. To complete the static test program, six-ply $[0/\pm45]_S$ graphite-epoxy and boron-epoxy specimens were also fabricated for tests to obtain strength and stiffness data, which are in Figures A-7 thru A-10 and Data Sheets 7 thru 10. The graphite-epoxy test specimens in Data Sheets 7 and 8 were sectioned from a center section that had been removed from a six-ply component of the graphite-epoxy doubler of panel A-GG-B-3. (The skins of several graphite-epoxy shaker specimens were obtained from center sections of graphite-epoxy doublers of acoustic panels A-GG-B-2 and A-GG-B-3.) The weight density of the graphite-epoxy laminates was 0.0504 lb/in^3.

A summary of the various tests to obtain physical and mechanical properties is in Table A-1. Results from tests reported in Figures A-6 thru A-10 are in Table A-2.

TABLE A-1. LOCATION OF TEST SUMMARIES

Figure	Data Sheet	No. of Specimens	Loading		Laminate Description
			Force	Orientation	
A-1	1	5	Uniaxial tensile	Parallel to fibers	8 parallel plies, graphite-epoxy
A-2	2	3	Uniaxial tensile	Transverse to fibers	8 parallel plies, graphite-epoxy
A-3	3	5	Uniaxial compressive	Parallel to fibers	16 parallel plies, graphite-epoxy
A-4	4	3	Uniaxial compressive	Transverse to fibers	16 parallel plies, graphite-epoxy
A-5	5	3	Rail shear	Parallel & transverse to fibers	$[(0/90)_4]_S$, graphite-epoxy
A-6	6	4	Uniaxial tensile	Parallel to laminate 0 degree direction	$[0/\pm45]_S$, graphite-epoxy
A-7	7	5	Uniaxial tensile	Parallel to laminate 0 degree direction	$[0/\pm45]_S$, graphite-epoxy
A-8	8	5	Uniaxial tensile	Parallel to laminate 90 degree direction	$[90/\pm45]_S$, graphite-epoxy
A-9	9	5	Uniaxial tensile	Parallel to laminate 0 degree direction	$[0/\pm45]_S$, boron-epoxy
A-10	10	5	Uniaxial tensile	Parallel to laminate 90 degree direction	$[90/\pm45]_S$, boron-epoxy

TABLE A-2. SIX-PLY SPECIMEN UNIAXIAL TEST RESULTS

Item	Figure	Material	Ply Lay-up	Load Direction	Average Tensile Modulus	Average Ultimate Strain	Average Thickness	Poisson's Ratio(1)
			(degree)	(degree)	(psi)	(micro-inch per inch)	(inch)	
1	A-6	Graphite-epoxy	$[0/\pm45]_S$	0	9.0×10^6	7,900	0.028	0.63
2	A-7	Graphite-epoxy	$[0/\pm45]_S$	0	9.4×10^6	6,800	0.027	0.64
3	A-8	Graphite-epoxy	$[90/\pm45]_S$	0	3.4×10^6	9,300	0.027	0.23
4	A-9	Boron-epoxy	$[0/\pm45]_S$	0	10.6×10^6	6,500	-	0.67
5	A-10	Boron-epoxy	$[90/\pm45]_S$	0	4.5×10^6	4,100	-	0.29

(1) The Poisson's ratio is the induced strain that is 90° from the load direction resulting from an applied strain in the load direction.

For Figures A-1 thru A-5, s is the standard deviation of the ultimate strengths, v is the ratio of s to the average ultimate strength, $\bar{\sigma}_{avg}$ is the average ultimate strength, and a solid circle denotes the ultimate stress and strain.

The average of the stiffness properties from Figures A-1 thru A-5 are summarized below with E_1, E_2, G, and ν_1 describing the elastic properties of the parallel-plied orthotropic laminates. The 1 and 2 direction are the principal elastic directions.

E_1 = 23,000,000 psi (tension)

E_1 = 22,400,000 psi (compression)

E_2 = 1,460,000 psi (tension)

E_2 = 1,600,000 psi (compression)

G = 1,000,000 psi (rail shear)

ν_1 = 0.34

The averages of the ultimate strengths from Figures A-1 thru A-5 are summarized below:

σ_1 = 182,100 psi (tensile ultimate)

σ_1 = 147,700 psi (compressive ultimate)

σ_2 = 5,820 psi (tensile ultimate)

σ_2 = 37,700 psi (compressive ultimate)

τ = 19,700 psi (rail shear ultimate)

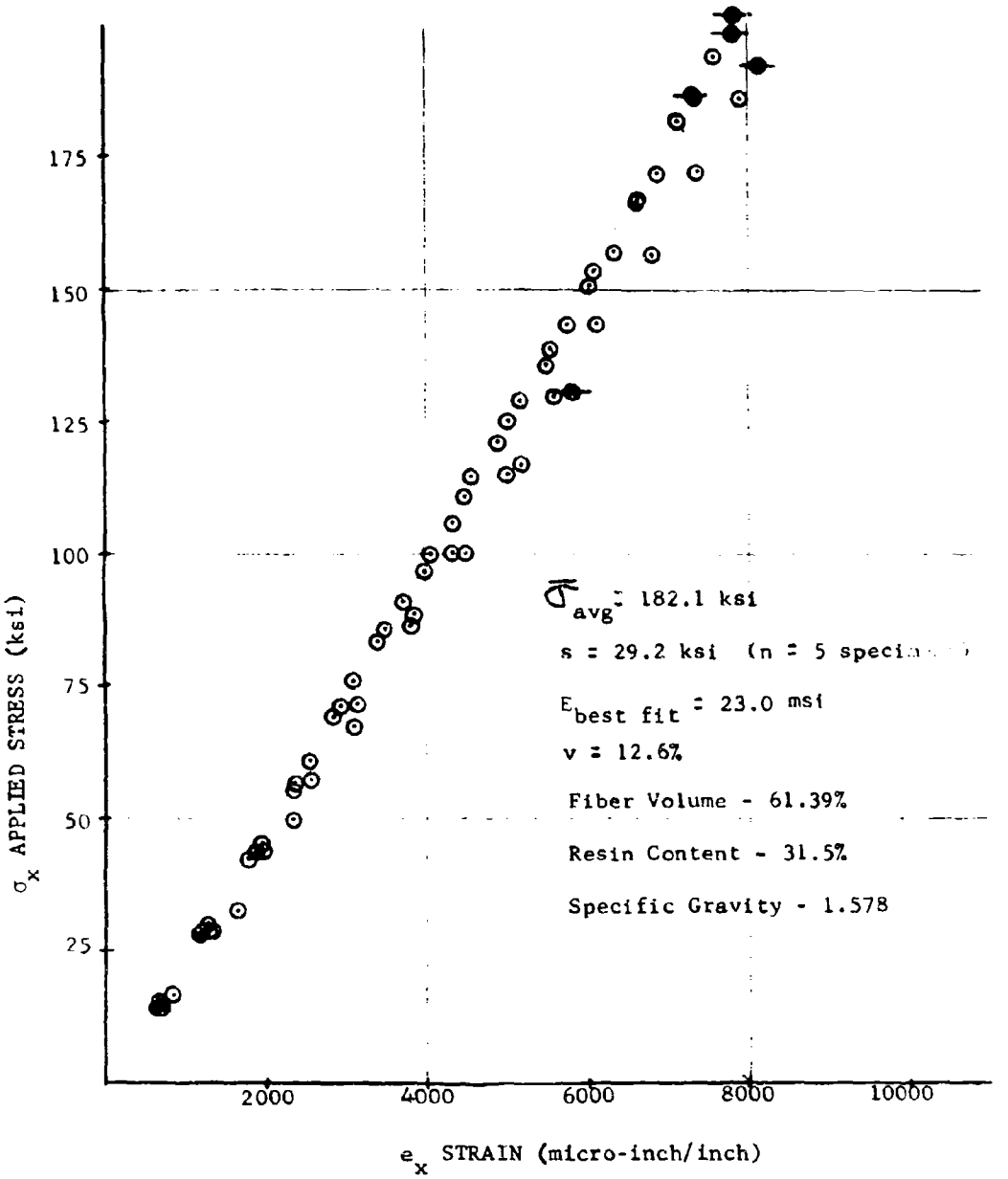

Stress-Strain data for 0° applied tension loading.
Fothergill/Harvey Courtaulds HT-S/4617.
Unidirectional $(0^{\circ})_{8T}$ Laminate fiber orientation.

FIGURE A-1. LONGITUDINAL TENSILE STRESS-STRAIN DATA - UNIDIRECTIONAL LAMINATE

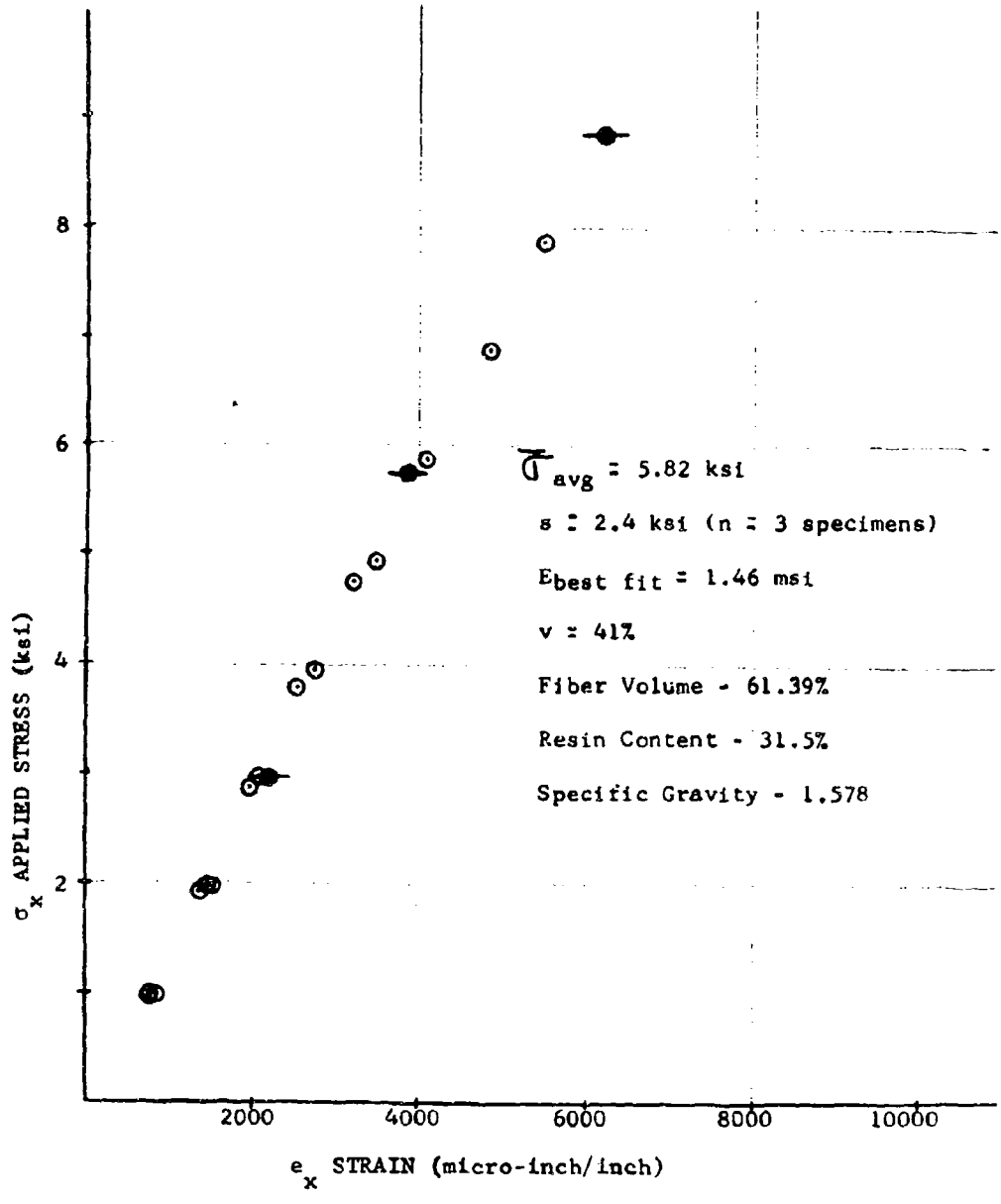

Stress-Strain data for 0° applied tension loading.
Fothergill/Harvey Courtaulds HT-S/4617.
Transverse $(90°)_{8T}$ Laminate fiber orientation.

FIGURE A-2. TRANSVERSE TENSILE STRESS-STRAIN DATA - UNIDIRECTIONAL LAMINATE

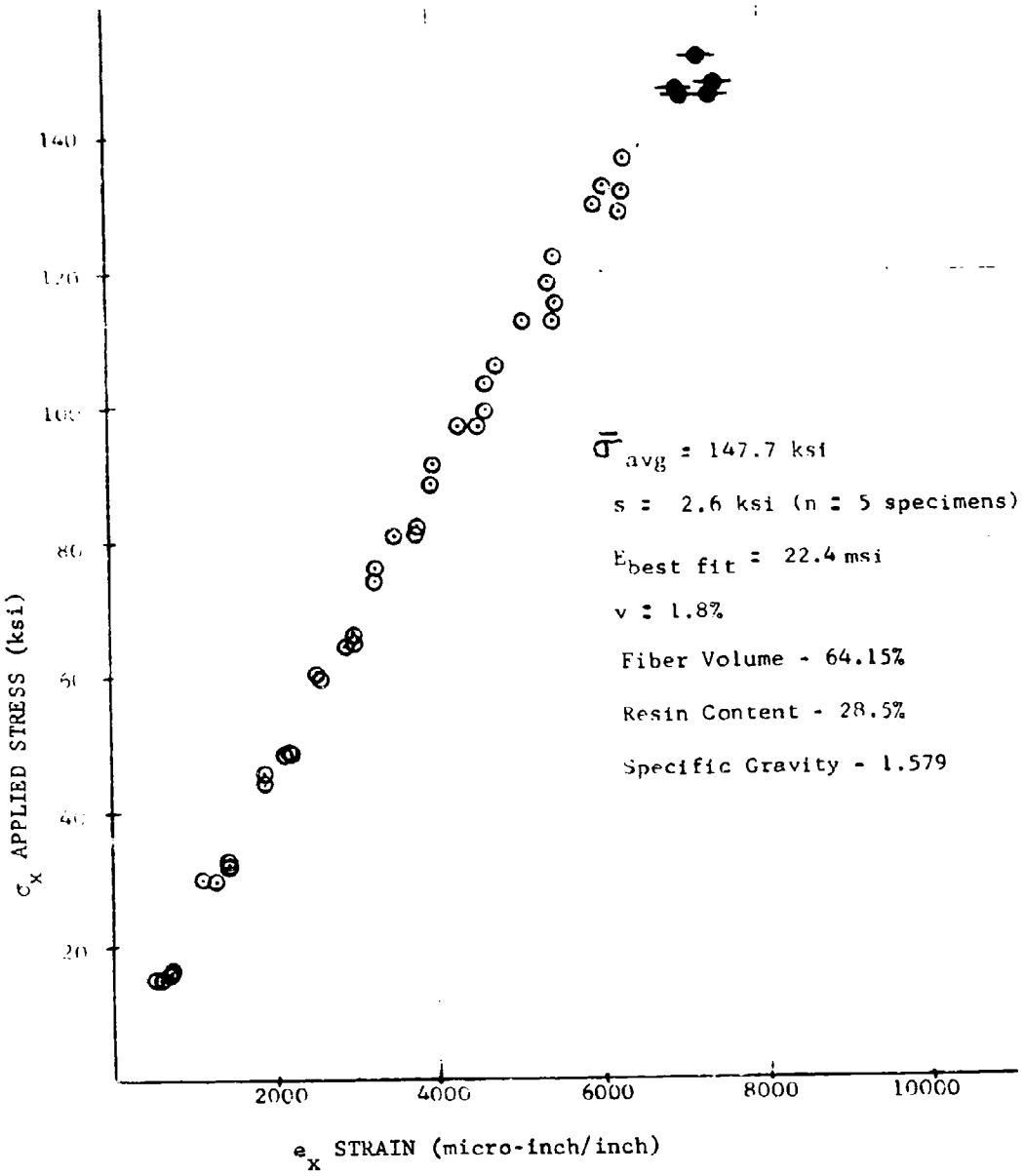

Stress-Strain data for 0° applied compression loading.
Fothergill/Harvey Courtaulds HT-S/4617.
Unidirectional $(0^{\circ})_{16T}$ Laminate fiber orientation.

FIGURE A-3. LONGITUDINAL COMPRESSIVE STRESS-STRAIN DATA - UNIDIRECTIONAL LAMINATE

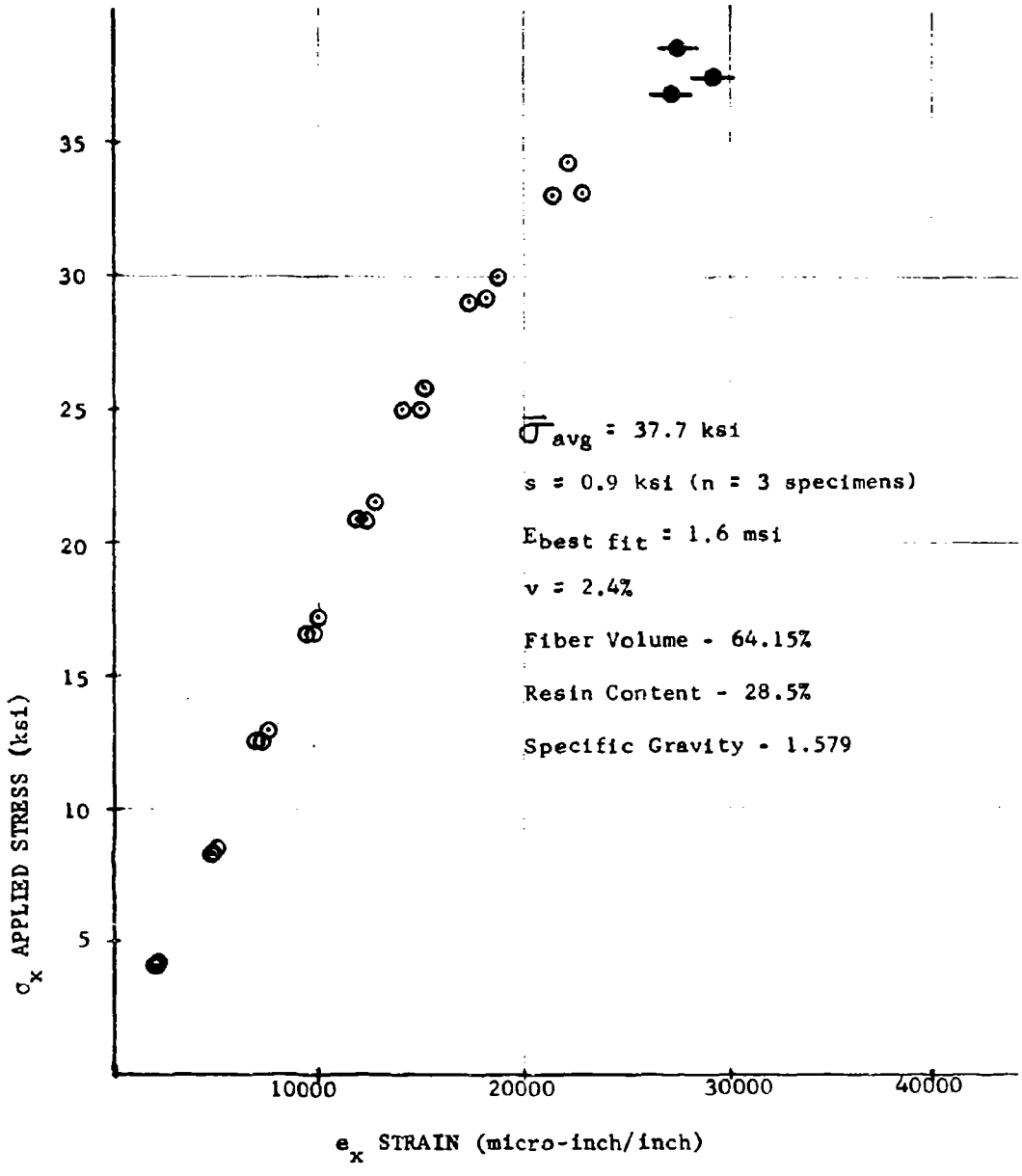

Stress-Strain data for 0° applied compression loading.
Fothergill/Harvey Courtaulds HT-S/4617.
Transverse $(90^o)_{16T}$ Laminate fiber orientation.

FIGURE A-4. TRANSVERSE COMPRESSIVE STRESS-STRAIN DATA - UNIDIRECTIONAL LAMINATE

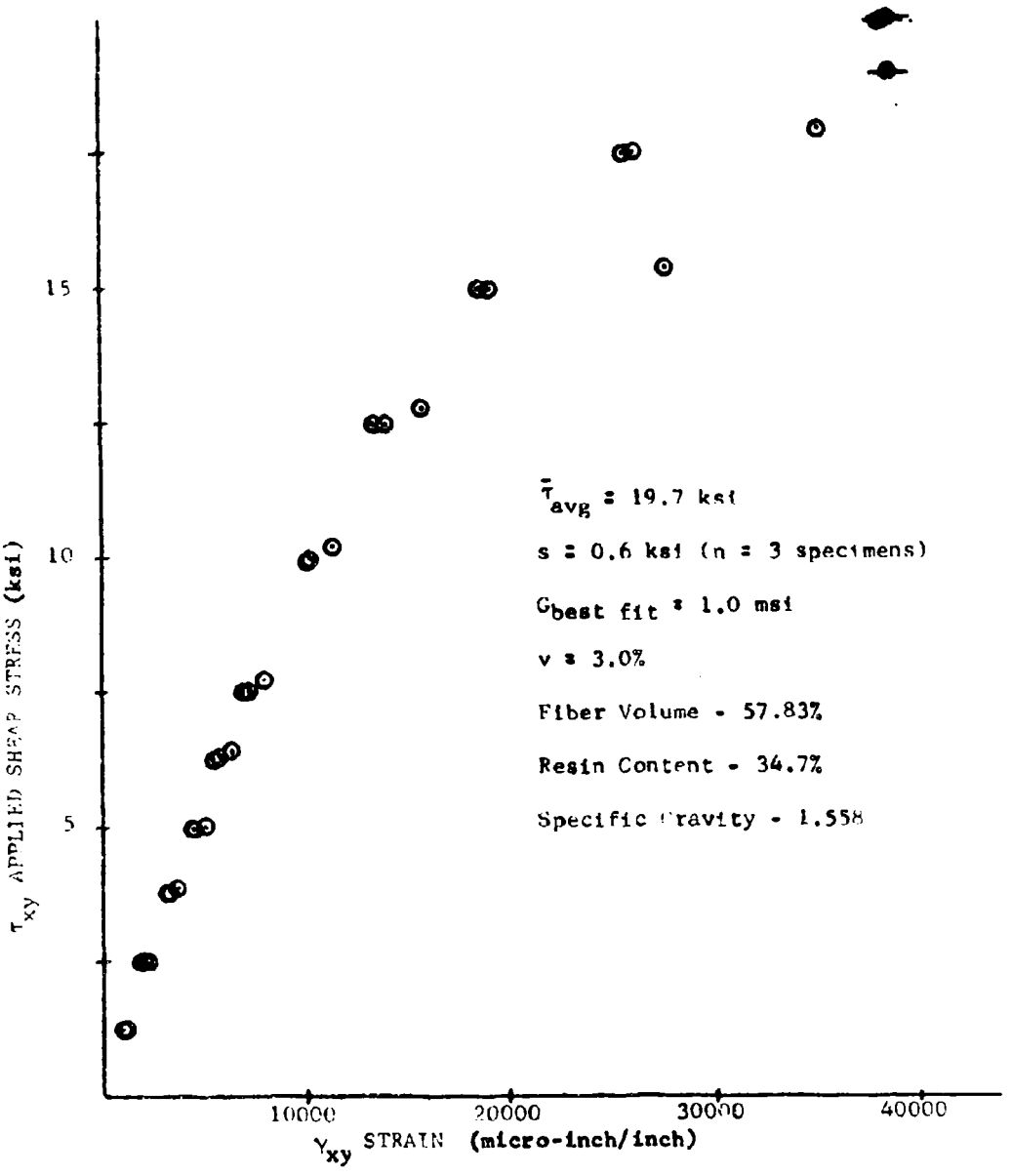

Shear Stress-Strain data for rail shear applied loading.
Fothergill/Harvey Courtaulds HT-S/4617.
$[(0/90)_4]_S$ laminate fiber orientation

FIGURE A-5. RAIL SHEAR STRESS-STRAIN DATA

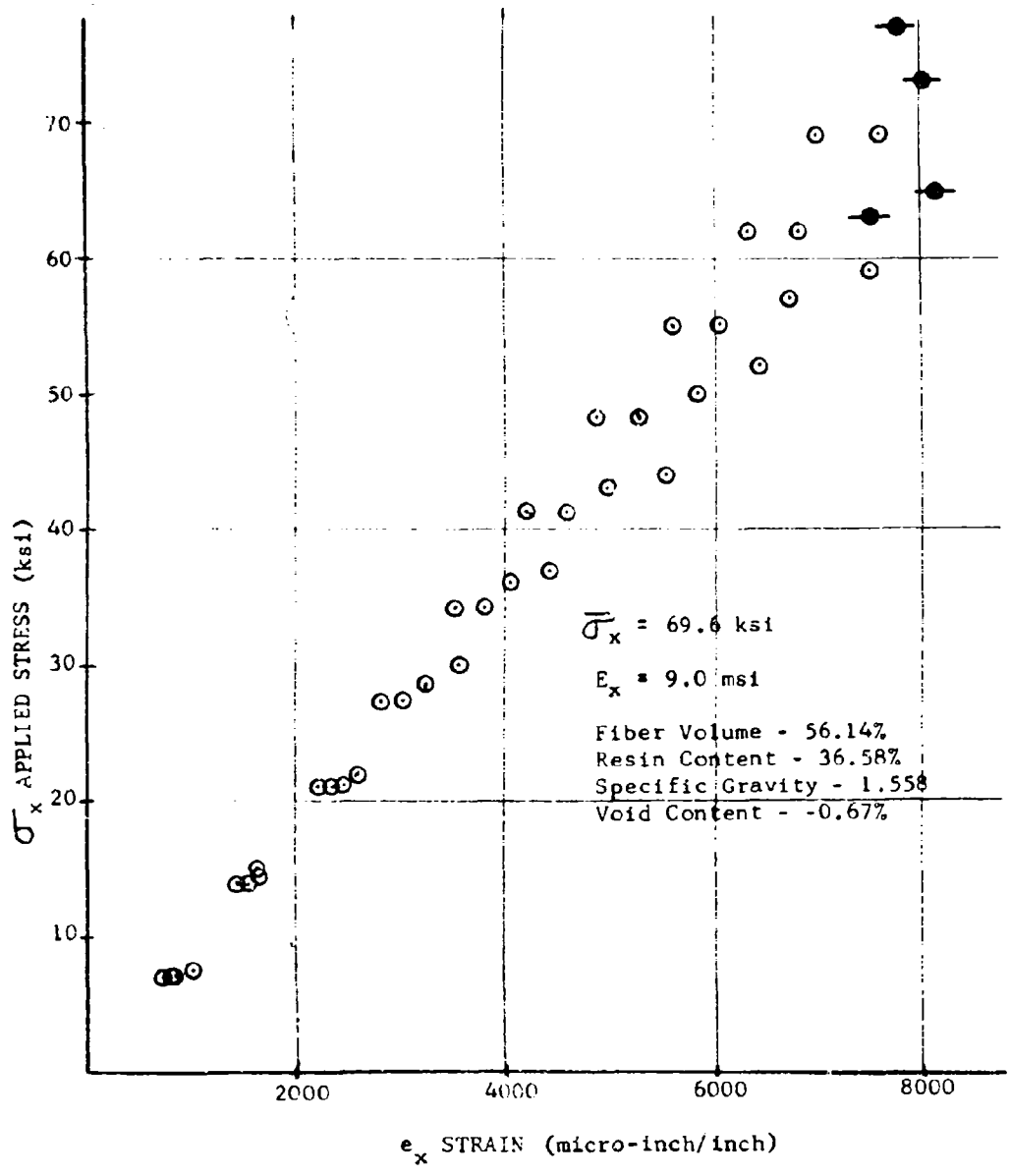

0° Applied Tension Stress-Strain Curve Data.
Courtaulds HT-S/4617 (Fothergill-Harvey).
Orientation - $[0/\pm45]_S$ 6-ply Laminate.

FIGURE A-6. LONGITUDINAL TENSILE STRESS-STRAIN DATA OF 6-PLY LAMINATE

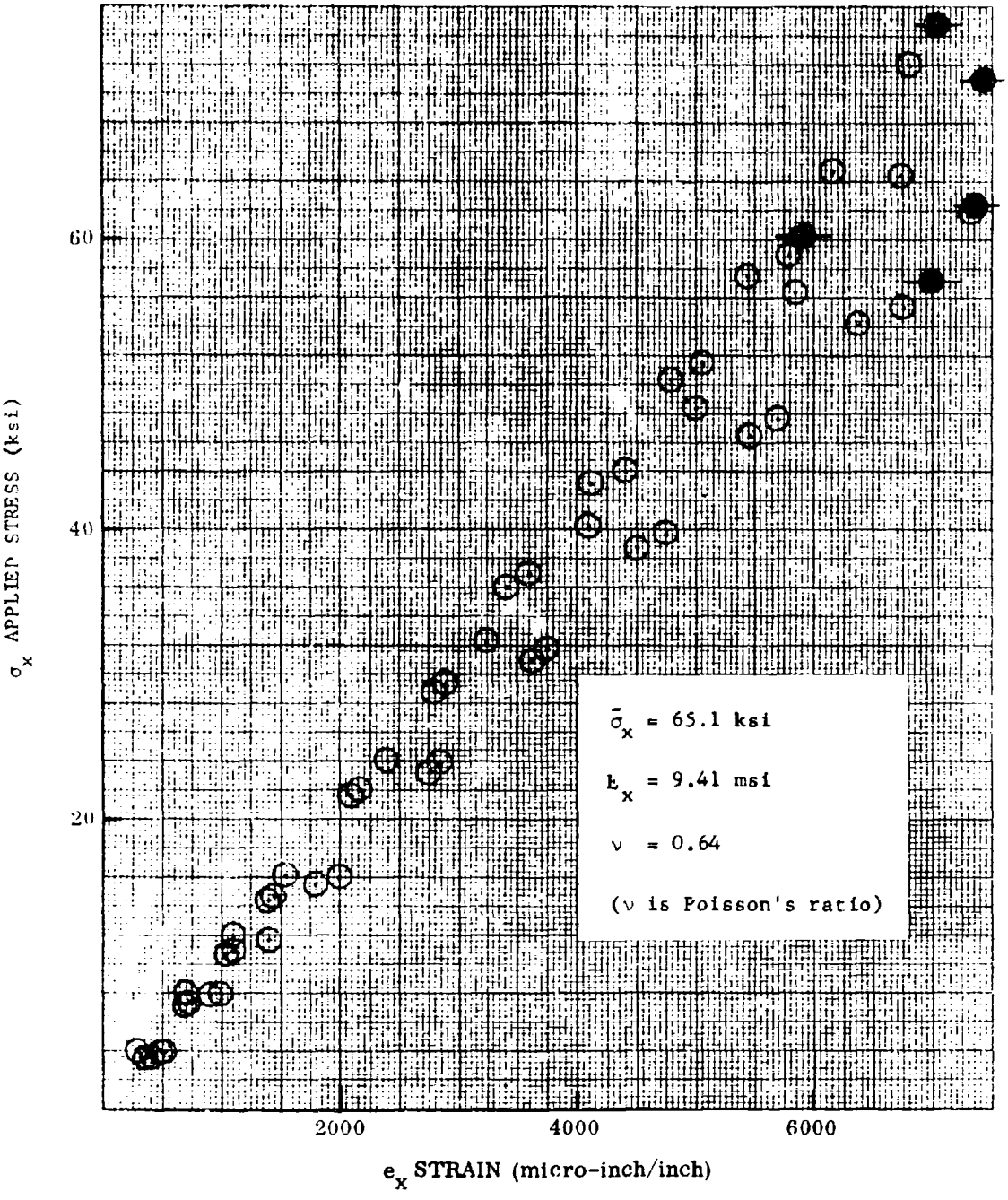

0° Applied Tension Stress-Strain Curve Data.
Courtaulds HT-S/4617 (Fothergill-Harvey).
Orientation - $[0/\pm45]_S$ 6-ply Laminate.

FIGURE A-7. LONGITUDINAL TENSILE STRESS-STRAIN DATA OF SIX-PLY LAMINATE

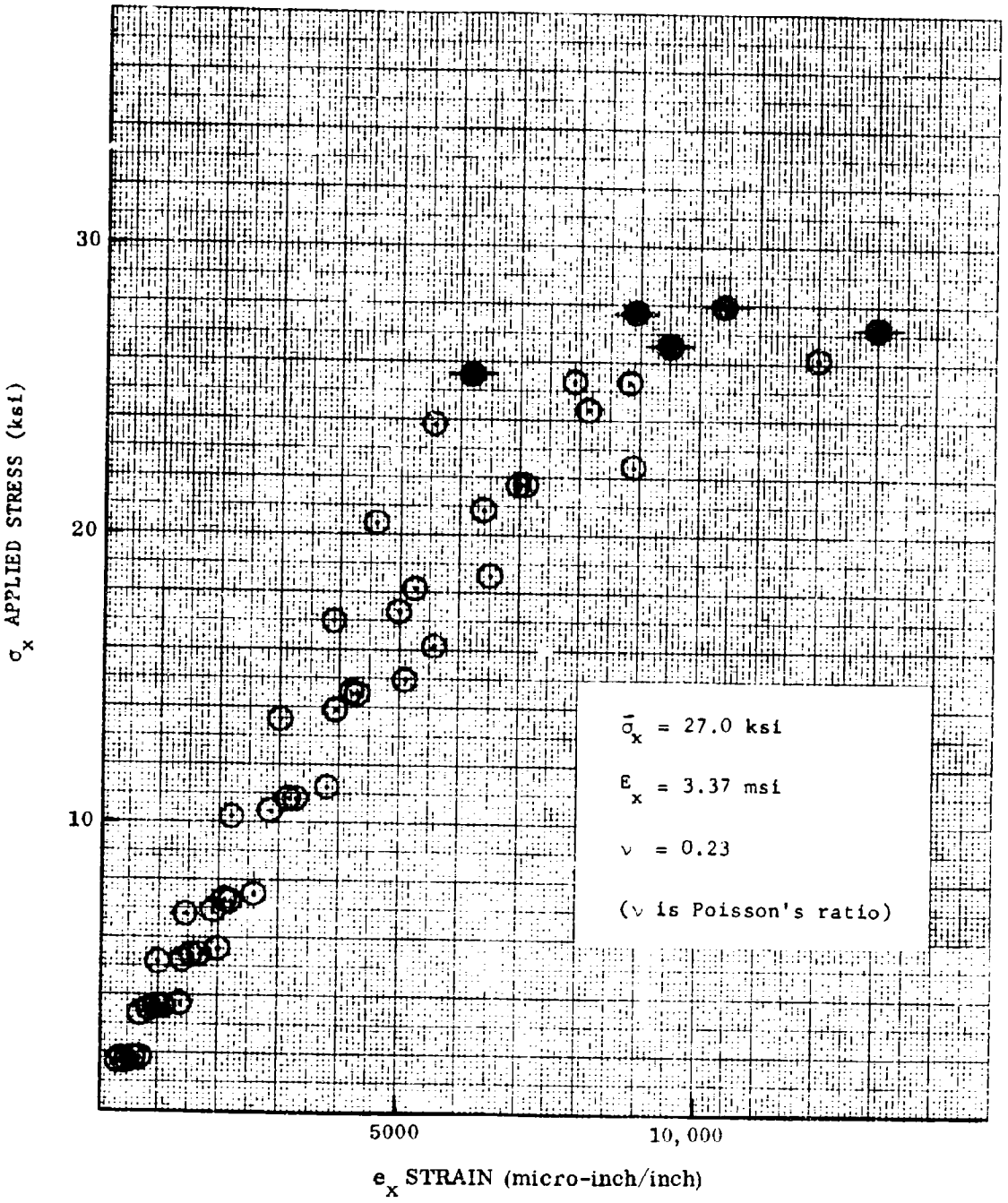

0° Applied Tension Stress-Strain Curve Data.
Courtaulds HT-S/4617 (Fothergill-Harvey).
Orientation - $[90/\pm45]_S$ 6-ply Laminate.

FIGURE A-8. TRANSVERSE TENSILE STRESS-STRAIN DATA OF SIX-PLY LAMINATE

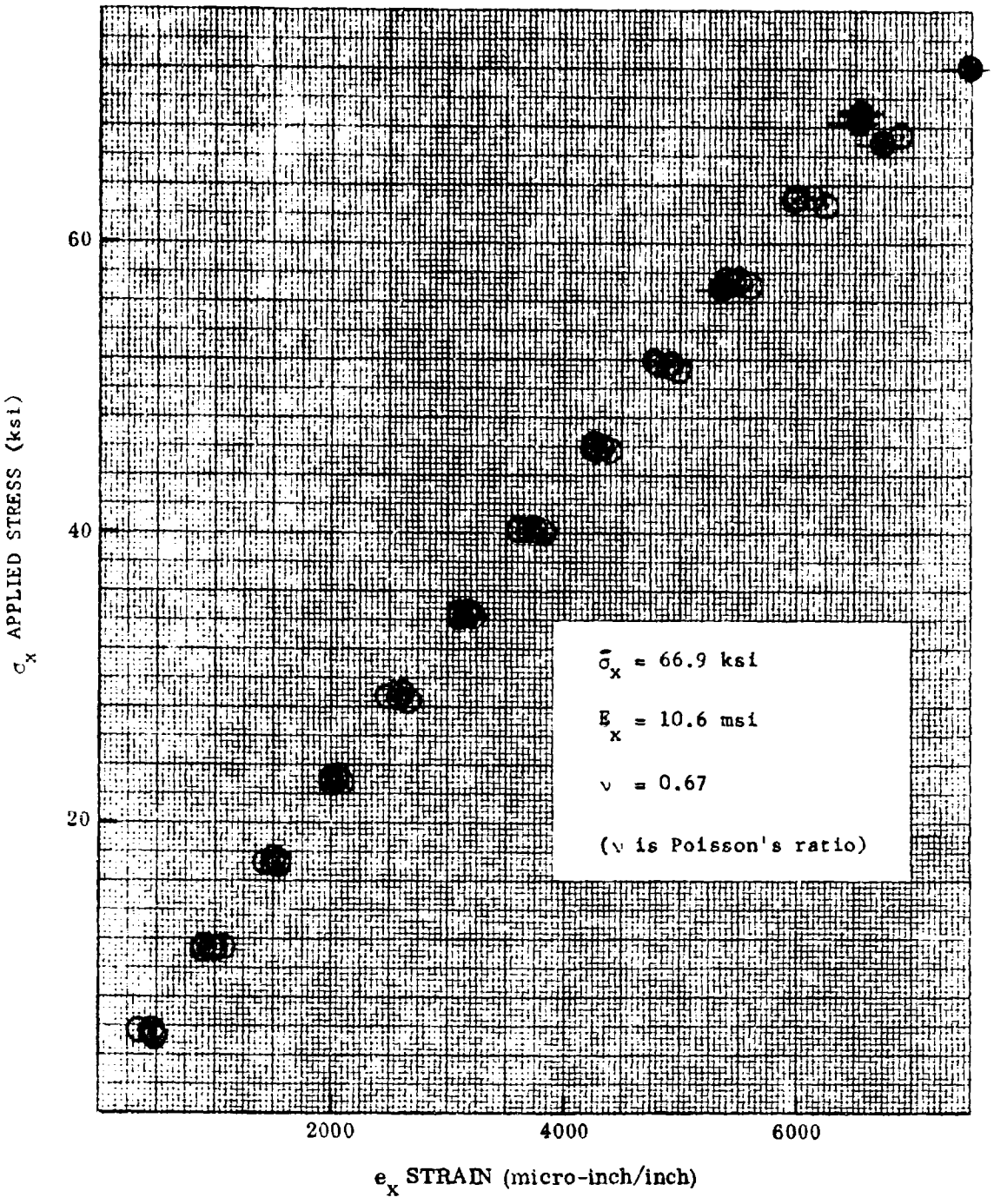

0° Applied Tension Stress-Strain Curve Data.
Narmco 5505 Boron-epoxy System.
Orientation - $[0/\pm45]_S$ 6-ply Laminate.

FIGURE A-9. LONGITUDINAL TENSILE STRESS-STRAIN DATA OF SIX-PLY LAMINATE

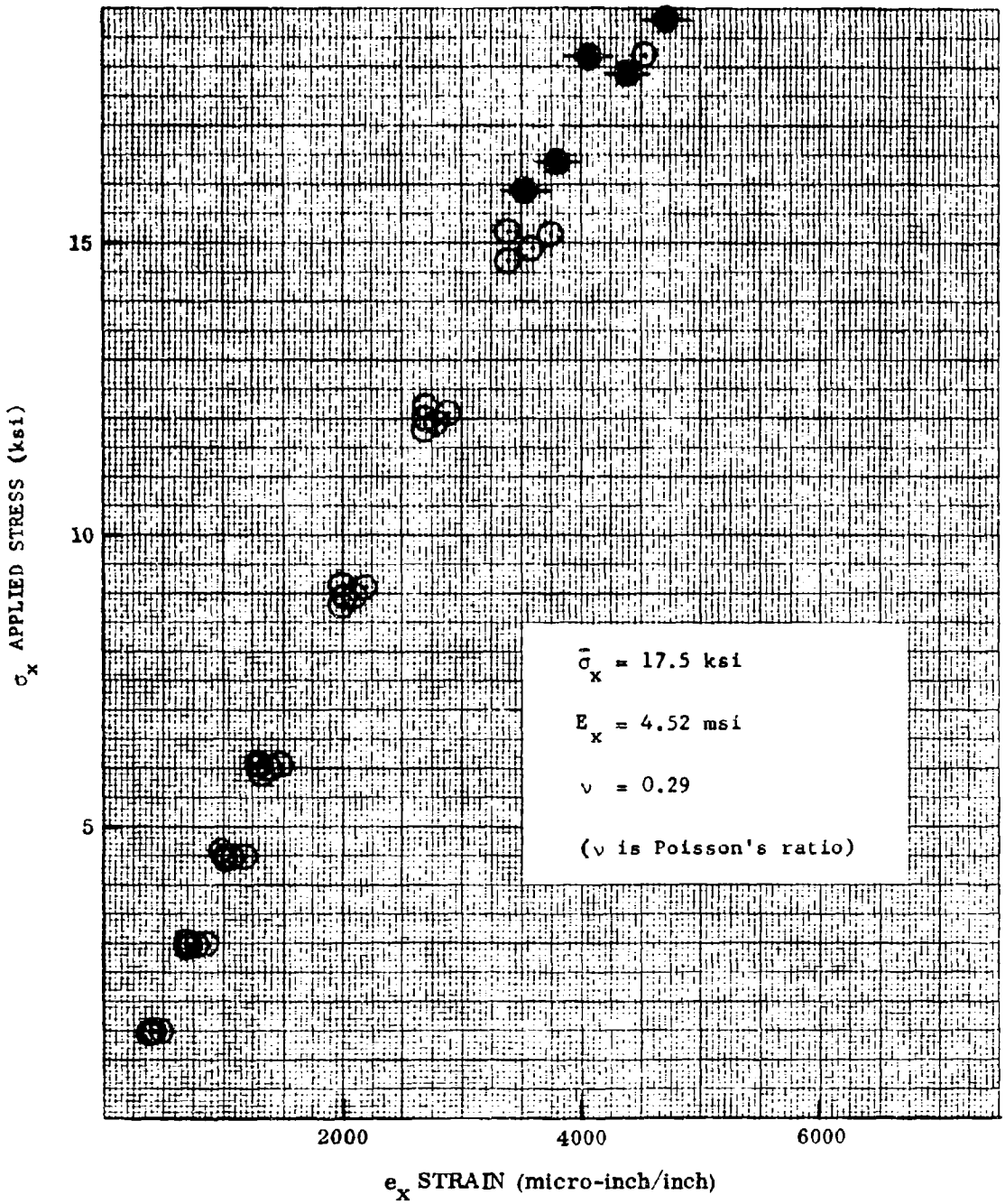

0° Applied Tension Stress-Strain Curve Data.
Narmco 5505 Boron-epoxy System.
Orientation - $[90/\pm45]_S$ 6-ply Laminate.

FIGURE A-10. TRANSVERSE TENSILE STRESS-STRAIN DATA OF SIX-PLY LAMINATE

DATA SHEET 1

FILAMENTARY LAMINATE STATIC PROPERTY DATA

Material System: Courtaulds HT-S/4617 Laminate Orientation: $(0_4)_S$

Loading Orientation: 0° Type Loading: Tension Number of Plies: 8

Test Specimen Description: 1/2 X 8 per IT-58 Specification Applicable Specification: IT-58

Testing Temperature: R/T ^oF Soak at _____ ^oF for _____ Hrs. minimum.

PROPERTY	Batch No.		SF-X						
	Spec. Ident.		SF-1	SF-2	SF-3	SF-4	SF-5		Avg.
STRESS LEVEL (ksi)	F_{pl}		85	85	97	75	95		
	F_{ult}		187.3	198.3	202.2	192.0	130.7		182.1
	$F_{2/3\ \varepsilon ult}$		123.5	130.9	132.5	125.1	86.2		
MODULUS (msi)	E or G (initial)		23.8	24.4	24.3	22.0	22.2		*23.0
Strain Levels μ in/in	Proport. Limit Strain	ε_1	3600	3500	4000	3400	4300		3800
		ε_2	-720	-1300	-1750	-	-		-1250
		ε_{45}							
	Failure Strain		7400	7900	7950	8200	5830		7450
Specimen Thickness (in.) Exper. measurement req'd			0.033	0.035	0.036	0.035	0.030		

Laminate Fiber Volume: 61.39 % Resin Content 31.5 % Void Fraction _____ Sp.G. 1.548

LAMINATE: Tape or Matrix Description Fothergill/Harvey Courtaulds HT-S/4617 48" X 12" tapes (3 hrs @ 350°F)

Manufacturer Fothergill/Harvey Cure Spec PL-36

Date of Test 8/3/70 Date of Reduction 9/14/70 Org'n 3772

Comments: *Modulus determined by least-squares best fit of experimental data.

DATA SHEET 2

FILAMENTARY LAMINATE STATIC PROPERTY DATA

Material System: Courtaulds HT-S/4617 Laminate Orientation: $(90_4)_S$

Loading Orientation: 0° Type Loading: Tension Number of Plies: 8

Test Specimen Description: 3/4" X 5" No tabs Applicable Specification: IT-58

Testing Temperature: R/T °F Soak at ____ °F for ____ Hrs. minimum.

PROPERTY	Batch No.		SF-2						Avg.
	Spec. Ident.		2-1	2-2	2-3	2-4			
STRESS LEVEL (ksi)	F_{pl}		none	none	none				
	F_{ult}		8.82	5.70	2.94				
	$F_{2/3\ \varepsilon_{ult}}$		N/A	N/A	N/A	N/A denotes that the stress-strain curve is linear			
MODULUS (msi)	E or G (initial)		1.42	1.59	1.40				
Strain Levels μ in/in	Proport. Limit Strain	ε_1	N/A	N/A	N/A				
		ε_2							
		ε_{45}							
	Failure Strain		6200	3900	2200				
Specimen Thickness (in.) Exper. measurement req'd			0.034	0.035	0.034				

Laminate Fiber Volume: 61.39 % Resin Content 31.5 % Void Fraction ____ Sp.G. 1.578

LAMINATE: Tape or Matrix Description Courtaulds HT-S/4617 48" X 12" prepreg tapes

Manufacturer Fothergill/Harvey Cure Spec PL-36

Date of Test 8/3/70 Date of Reduction 9/14/70 Org'n 3772

Comments: The large spread in data can be attributed to the high fiber volume which results in low transverse strengths.

DATA SHEET 3

FILAMENTARY LAMINATE STATIC PROPERTY DATA

Material System: Courtaulds HT-S/4617 Laminate Orientation: $(0_8)_S$

Loading Orientation: 0° Type Loading: Compression Number of Plies: 16

Test Specimen Description: 1/2" X 4-1/2" No tabs Applicable Specification: IT-58

Testing Temperature: R/T °F Soak at _____ °F for _____ Hrs. minimum.

PROPERTY	Batch No.		SF-3						
	Spec. Ident.		3-1	3-2	3-3	3-4	3-5		Avg.
STRESS LEVEL (ksi)	F_{pl}		80	80	76	70	65		
	F_{ult}		145.6	145.6	152.0	148.0	147.5		147.7
	$F_{2/3\ \varepsilon_{ult}}$		100.0	98.5	107.0	102.3	103.0		
MODULUS (msi)	E or G (initial)		21.4	23.0	22.9	21.4	23.0		*22.4
Strain Levels μ in/in	Proport. Limit Strain	ε_1	3700	3500	3300	3300	2800		3300
		ε_2	-	-	-	-	-		
		ε_{45}							
	Failure Strain		7000	6600	7000	7100	6900		6900
Specimen Thickness (in.) Exper. measurement req'd			0.062	0.062	0.066	0.061	0.068		

Laminate Fiber Volume: 64.15 % Resin Content 28.5 % Void Fraction _____ Sp.G. 1.579

LAMINATE: Tape or Matrix Description Fothergill/Harvey Courtaulds HT-S/4617 48" X 12" tapes

Manufacturer Fothergill/Harvey Cure Spec PL-36

Date of Test 8/3/70 Date of Reduction 9/14/70 Org'n 3772

Comments: *Modulus determined by least-squares best fit of experimental data

DATA SHEET 4

FILAMENTARY LAMINATE STATIC PROPERTY DATA

Material System: Courtaulds HT-S/4617 Laminate Orientation: $(90_8)_S$

Loading Orientation: 0° Type Loading: Compression Number of Plies: 16

Test Specimen Description: 1/2" X 4-1/2" No tabs Applicable Specification: IT-58

Testing Temperature: R/T °F Soak at ____ °F for ____ Hrs. minimum.

PROPERTY	Batch No.		SF-3						
	Spec. Ident.		3-11	3-12	3-13				Avg.
STRESS LEVEL (ksi)	F_{pl}		21.5	22.0	17.5				
	F_{ult}		38.6	36.9	37.5				37.7
	$F_{2/3\ \varepsilon_{ult}}$		30	30	30				
MODULUS (msi)	E or G (initial)		1.7	1.7	1.5				*1.6
Strain Levels μ in/in	Proport. Limit Strain	ε_1	13000	12500	11500				12300
		ε_2							
		ε_{45}							
	Failure Strain		27500	27000	29000				27800
Specimen Thickness (in.) Exper. measurement req'd			0.062	0.064	0.064				

Laminate Fiber Volume: 64.15 % Resin Content 28.5 % Void Fraction ____ Sp.G. 1.579

LAMINATE: Tape or Matrix Description Fothergill/Harvey Courtaulds HT-S/4617 48"X12" tapes

Manufacturer Fothergill/Harvey Cure Spec PL-36

Date of Test 8/3/70 Date of Reduction 9/14/70 Org'n 3772

Comments: *Modulus determined by least-squares best fit of experimental data

DATA SHEET 5

FILAMENTARY LAMINATE STATIC PROPERTY DATA

Material System: Courtaulds HT-S/4617 Laminate Orientation: $[(0/90)_4]_S$

Loading Orientation: N/A Type Loading: Rail Shear Number of Plies: 16

Test Specimen Description: 3" X 6" (3 element gage used) Applicable Specification: IT-58

Testing Temperature: R/T °F Soak at ____ °F for ____ Hrs. minimum.

PROPERTY	Batch No.	SF-4						
	Spec. Ident.	4-1	4-2	4-3				Avg.
STRESS LEVEL (ksi)	F_{pl}	5.0	4.5	5.2				
	F_{ult}	20.1	20.0	19.0				19.7
	$F_{2/3\ \epsilon_{ult}}$	17.7	17.5	15.0				
MODULUS (msi)	E or G (initial)	1.1	1.0	1.0				*1.0
Strain Levels μ in/in	Proport. Limit Strain ϵ_{45}	4600	4400	5200				4700
	[redacted]							
	[redacted]							
	Failure Strain	38500	39000	39000				39000
Specimen Thickness (in.) Exper. measurement req'd		0.066	0.067	0.065				

Laminate Fiber Volume: 57.83 % Resin Content 34.7 % Void Fraction ____ Sp.G. 1.558

LAMINATE: Tape or Matrix Description Courtaulds HT-S/4617 48" X 12" prepreg tapes

Manufacturer Fothergill/Harvey Cure Spec PL-36

Date of Test 8/3/70 Date of Reduction 9/14/70 Org'n 3772

Comments: *Modulus determined by least squares best fit of experimental data.

DATA SHEET 6

FILAMENTARY LAMINATE STATIC PROPERTY DATA

Material System: Courtaulds HT-S/4617 Laminate Orientation: $[0/\pm 45]_S$

Loading Orientation: 0° Type Loading: Tension Number of Plies: 6

Test Specimen Description: 1/2" X 8" with 2-1/2" X 3/4" Taper Applicable Specification: IT-58

Testing Temperature: R/T °F Soak at ____ °F for ____ Hrs. minimum.

PROPERTY	Batch No.		SF-5						
	Spec. Ident.		1	2	3	4			Avg.
STRESS LEVEL (ksi)	F_{pl}		Not Apparent From Stress-Strain Curve						
	F_{ult}		77.2	73.1	62.9	65.2			69.6
	$F_{2/3\ \varepsilon ult}$		51.1	49.2	42.9	41.3			46.1
MODULUS (msi)	E or G (initial)		9.6	9.1	8.9	7.8			*9.0
Strain Levels μ in/in	Proport. Limit Strain	ε_1	P.R. = .65	PR = .60	-	-			
		ε_2							
		ε_{45}							
	Failure Strain		7800	8100	7500	8200			7850
Specimen Thickness (in.) Exper. measurement req'd			0.029	0.029	0.028	0.027			0.028

Laminate Fiber Volume: 56.14% Resin Content 36.58% Void Fraction -0.67 Sp.G. 1.558

LAMINATE: Tape or Matrix Description Fothergill/Harvey CHT-S/4617 12" X 48" tapes

Manufacturer Fothergill/Harvey Cure Spec PL-36

Date of Test 9/23/70 Date of Reduction 10/2/70 Org'n 3772

Comments: *Modulus was calculated using best-fit least-squares method on data.

DATA SHEET 7

FILAMENTARY LAMINATE STATIC PROPERTY DATA

Material System: Courtaulds HT-S/4617 Laminate Orientation: $[0/\pm45]_s$

Loading Orientation: 0° Type Loading: Tension Number of Plies: 6

Test Specimen Description: ½" X 8" Applicable Specification: IT-58

Testing Temperature: R/T °F Soak at ____ °F for ____ Hrs. minimum.

PROPERTY	Batch No. / Spec. Ident.		SF-4G 1	2	3	4	5		Avg.
STRESS LEVEL (ksi)	F_{pl}		N/A						
	F_{ult}		57.1	62.4	71.1	74.8	60.3		65.1
	$F_{2/3\ \varepsilon ult}$		N/A						
MODULUS (msi)	E or G (initial)		8.50	8.65	9.85	10.61	10.02		* 9.41
Strain Levels μ in/in	Proport. Limit Strain	ε_1							
		ε_2							
		ε_{45}							
	Failure Strain		6916	7380	7439	7113	5979		6965
Specimen Thickness (in.) Exper. measurement req'd			.025	.025	.024	.027	.027		

Laminate Fiber Volume: ____ % Resin Content ____ % Void Fraction ____ Sp.G. ____

LAMINATE: Tape or Matrix Description ____

Manufacturer ____ Cure Spec ____

Date of Test 6/17/71 Date of Reduction 7/1/71 Org'n 3772

Comments: *Best fit - least squares

DATA SHEET 8

FILAMENTARY LAMINATE STATIC PROPERTY DATA

Material System: Courtaulds HT-S/4617

Laminate Orientation: $[90/\pm 45]_s$

Loading Orientation: 0°

Type Loading: Tension

Number of Plies: 6

Test Specimen Description: 1" X 8"

Applicable Specification: IT-58

Testing Temperature: R/T °F Soak at ____ °F for ____ Hrs. minimum.

PROPERTY	Batch No.		SF-46						
	Spec. Ident.		6	7	8	9	10		Avg.
STRESS LEVEL (ksi)	F_{pl}								
	F_{ult}		27.2	26.6	27.9	25.5	27.8		27.0
	$F_{2/3\ \varepsilon_{ult}}$								
MODULUS (msi)	E or G (initial)		2.98	3.43	3.08	4.49	3.37		* 3.37
Strain Levels μ in/in	Proport. Limit Strain	ε_1							
		ε_2							
		ε_{45}							
	Failure Strain		12080	9350	9800	6260	9010		9300
Specimen Thickness (in.) Exper. measurement req'd			.026	.028	.027	.029	.027		

Laminate Fiber Volume: ____ % Resin Content ____ % Void Fraction ____ Sp.G. ____

LAMINATE: Tape or Matrix Description ____

Manufacturer ____ Cure Spec ____

Date of Test 6/17/71 Date of Poduction 7/1/71 Org'n 3772

Comments: * Best fit - least squares

DATA SHEET 9

FILAMENTARY LAMINATE STATIC PROPERTY DATA

Material System: Narmco 5505

Laminate Orientation: $[0/\pm45]_s$

Loading Orientation: 0°

Type Loading: Tension

Number of Plies: 6

Test Specimen Description: ½" X 8"

Applicable Specification: IT-58

Testing Temperature: R/T °F Soak at ____ °F for ____ Hrs. minimum.

PROPERTY	Batch No.		SF-4B						
	Spec. Ident.		1	2	3	4	5		Avg.
STRESS LEVEL (ksi)	F_{pl}								
	F_{ult}		68.4	66.9	68.7	56.9	73.6		66.9
	$F_{2/3\ \varepsilon_{ult}}$								
MODULUS (msi)	E or G (initial)		11.11	10.37	11.34	10.12	10.80		* 10.60
Strain Levels μin/in	Proport. Limit Strain	ε_1							
		ε_2							
		ε_{45}							
	Failure Strain		6519	6709	6538	5449	7278		6499
Specimen Thickness (in.) Exper. measurement req'd			.034	.035	.034	.034	.034		

Laminate Fiber Volume: ____ % Resin Content ____ % Void Fraction ____ Sp.G. ____

LAMINATE: Tape or Matrix Description ____

Manufacturer ____ Cure Spec ____

Date of Test 6/18/71 Date of Reduction 7/1/71 Org'n 3772

Comments: * Best fit - least squares

DATA SHEET 10

FILAMENTARY LAMINATE STATIC PROPERTY DATA

Material System: Narmco 5505 Laminate Orientation: $[90/\pm45]_s$

Loading Orientation: 0° Type Loading: Tension Number of Plies: 6

Test Specimen Description: ½" X 8" (No tabs) Applicable Specification: LT-58

Testing Temperature: R/T °F Soak at ____ °F for ____ Hrs. minimum.

PROPERTY	Batch No.		SF-4B						
	Spec. Ident.		6	7	8	9	10		Avg.
STRESS LEVEL (ksi)	F_{pl}								
	F_{ult}		18.18	18.85	15.91	16.35	17.86		17.5
	$F_{2/3\ \varepsilon_{ult}}$								
MODULUS (msi)	E or G (initial)		4.48	4.44	4.83	4.59	4.55		* 4.52
Strain Levels μ in/in	Proport. Limit Strain	ε_1							
		ε_2							
		ε_{45}							
	Failure Strain		4079	4798	3810	3810	4427		4185
Specimen Thickness (in.) Exper. measurement req'd			.032	.032	.032	.033	.033		

Laminate Fiber Volume: ____ % Resin Content ____ % Void Fraction ____ Sp.G. ____

LAMINATE: Tape or Matrix Description ____

Manufacturer ____ Cure Spec ____

Date of Test 6/18/71 Date of Reduction 7/1/71 Org'n 3772

Comments: * Best fit - least squares

UNCLASSIFIED

Security Classification

DOCUMENT CONTROL DATA - R & D

(Security classification of title, body of abstract and indexing annotation must be entered when the overall report is classified)

1. ORIGINATING ACTIVITY (Corporate author)

NORTHROP CORPORATION
AIRCRAFT DIVISION
HAWTHORNE, CALIFORNIA 90250

2a. REPORT SECURITY CLASSIFICATION

Unclassified

2b. GROUP

3. REPORT TITLE

ADVANCED COMPOSITE JOINTS; DESIGN AND ACOUSTIC FATIGUE CHARACTERISTICS

4. DESCRIPTIVE NOTES (Type of report and inclusive dates)

FINAL - APRIL 1970 TO JULY 1971

5. AUTHOR(S) (First name, middle initial, last name)

MARCUS J. JACOBSON

6. REPORT DATE

JULY 1971

7a. TOTAL NO. OF PAGES

258

7b. NO. OF REFS

18

8a. CONTRACT OR GRANT NO.

F33615-70-C-1463

b. PROJECT NO.

1471

c. Task No. 147101

d.

9a. ORIGINATOR'S REPORT NUMBER(S)

NOR 71-114

9b. OTHER REPORT NO(S) (Any other numbers that may be assigned this report)

AFFDL-TR-71-126

10. DISTRIBUTION STATEMENT

Distribution limited to U.S. Government agencies only; test and evaluation statement applied August 1971. Other requests for this document must be referred to AF Flight Dynamics Laboratory (FY), Wright-Patterson AFB, Ohio 45433.

11. SUPPLEMENTARY NOTES

12. SPONSORING MILITARY ACTIVITY

AIR FORCE FLIGHT DYNAMICS LAB
WRIGHT-PATTERSON, AFB
OHIO 45433

13. ABSTRACT

The results of an interrelated analytic investigation, acoustic test program, and shaker test program to develop information on the design and acoustic fatigue characteristics of joints with advanced-composite materials are presented. Three nine-bay, cross-stiffened, graphite-epoxy panels with a six-ply skin and a central bay with nominal dimensions of 10.0 x 7.0 x 0.03 inch were designed and manufactured. The panels were tested to obtain response and acoustic fatigue data. The final two of the three tested panels survived 100 hours (the planned runout point) of exposure in a broad-band 166 db SPL acoustic environment; the first panel experienced a premature acoustic fatigue failure that was attributed to a design and manufacturing deficiency that was corrected for the other two panels. Six S-N curves were developed in the shaker test program and included data obtained with two joint configurations, either bonded or riveted, and three material combinations with six-ply skins, namely, graphite-epoxy skin to a graphite-epoxy stiffener, boron-epoxy skin to a titanium alloy stiffener, and graphite-epoxy skin to a titanium alloy stiffener. The lamina stacking sequence was the same for all the shaker specimens. A simplified theory for hand calculation predictions of dynamic stresses in an unstiffened orthotropic plate subjected to a spatially uniform, white noise environment was developed and successfully applied in the dynamic analysis of the cross-stiffened, graphite-epoxy test panels. Other principal items in the analytic investigation included the use of a finite-element computer program for the prediction of the cross-stiffened panel response to acoustic excitation and another finite-element computer program for the static stress analysis of bonded-joint assemblies to determine the acoustic fatigue critical component of the joint assemblies. The effect of the experimental multimodal response of the acoustic test panels was considered in predicting the absence of an acoustic fatigue failure in the two acoustic test panels that survived the 100 hours of acoustic exposure.

DD FORM 1 NOV 65 1473

UNCLASSIFIED

Security Classification

14 KEY WORDS	LINK A ROLE	LINK A WT	LINK B ROLE	LINK B WT	LINK C ROLE	LINK C WT
ACOUSTIC FATIGUE						
GRAPHITE-EPOXY PANELS						
CROSS-STIFFENED PANELS						
ADVANCED-COMPOSITE PANELS						
DYNAMIC RESPONSE						
GRAPHITE-EPOXY BEAMS						
BORON-EPOXY BEAMS						
S-N CURVES						
ADVANCED-COMPOSITE FATIGUE DATA						
STRUCTURAL DESIGN						